

https://dspace.org/

Simulating the influence of blast geometry and rock geology on rock fragmentation

Lijojo, Lebohang

2021

https://hdl.handle.net/10539/33348

Downloaded from a DSpace repository. https://dspace.org/

Simulating the Influence of Blast Geometry and Rock Geology on Rock Fragmentation

Lebohang Lijojo

A dissertation submitted to the Faculty of Engineering and the Built Environment, University of the Witwatersrand, in fulfilment of the requirements of the degree of Master of Science in Engineering.

Johannesburg, 2021

DECLARATION

I declare that this research report is my own, unaided work. I read the University Policy on Plagiarism and hereby confirm that no plagiarism exists in this report. I also confirm that there is no copying nor is there any copyright infringement. I willingly submit to any investigation in this regard by the School of Mining Engineering, and I undertake to abide by the decision of any such investigation.

Name: Lebohang Lijojo

Signed: 

Date: 07 June 2021

ABSTRACT

Drill and blast is a critical process in the size reduction of rock. The process uses explosive energy to reduce rock into manageable fragment size before the rock fragments are transferred to other mining activities. The size reduction of rock by mechanical energy is generally accepted as a relatively expensive process due to the cost of energy required to break the rock. For this reason, it is essential to reduce the energy requirements in the plant by sending optimal blast fragments. However, rock geology, blast design geometry and explosives properties can influence the degree to which optimal fragment size would be achieved.

This study aimed to determine the degree to which these parameters influence the blast fragment size and the associated blasting costs by simulating various blast conditions. The objective of the study was to implement a blasting simulation model at Ruashi mine to solve the challenges experienced with blast fragmentation and blasting in general. Based on a review of diverse literature and theories on blasting, the Kuz- Ram model was chosen as the basis for the study. Three test sites of varying geological conditions were selected, and different blast design patterns and simulation conditions were used to answer the research questions. Image analysis was utilised to compare actual fragment results against simulated fragment size results to refine the model and ensure the simulation model can better predict the fragment size.

Analysis of the findings indicated that the Blastability Index, which is a measure of the difficulty in blasting rock, for the rock types encountered in the mine ranged between 4 and 8 which indicated weak to moderately competent rockmass. This index was primarily influenced by rock density and joint dip angle. The higher the rock density, the greater the difficulty was in blasting rock. Also, the steeper the joint sets (joint spacing less than 0.1m), the more difficult it was to blast the rockmass.

The Uniformity Index, which measures the uniform nature of the blast fragmentation distribution, was found to range between 0.9 and 1.5 for South-East and South-West. This index value indicated that muck piles in these areas were mostly non- uniform. This result was expected given that the rockmass in these areas was less competent and relatively more fractured while the South blast Uniformity Index was between 1.5 and 2.2 which depicted a more uniform muckpile achieved from competent rockmass.

The burden and spacing were the influential parameters on the Uniformity Index value in a variable blast pattern design. While in a fixed burden and spacing pattern, the index value depended mainly on the change in the stemming length.

In a fixed blast pattern design, the blasting costs were mainly influenced by the change in the stemming length. The higher the stemming length, the lower the unit blasting costs. Also, the higher the Blastability Index, the greater the blasting costs. The uniform nature of the muckpile was found not to have an impact on the blasting costs.

Two standard blast patterns were chosen for ore and waste material. Firstly, for waste blasting, final blasting pattern of 2.5m by 2.5m was selected together with a powder factor of 0.35 kg/Bcm. Secondly, for ore blasting, a 2m by 2m blast pattern was chosen along with the powder factor of 0.35 kg/Bcm. These selected parameters were found to produce reasonably good results in terms of fragmentation size and blasting costs for the rock types encountered in the mine.

Due to the cross-sectional nature of the study and limited resources such as blasting software, mill data and digging data, the study was restricted to cover only the blasting operations by utilising the Kuz-Ram model. Further studies on the comminution system would be necessary to quantify the overall impact of the fragment size on total mining costs. One other important recommendation from the study is that the mine needs to establish the blasting department to deal with issues of performance, quality assurance, and control, and the development of blasting standards. This is key given that the mine does not have technical capability for extensive blasting operations that will be required as a consequence of working in hard strata.

ACKNOWLEDGEMENTS

I want to thank my supervisor, Professor Rudrajit Mitra, for his patience, academic guidance and for proofreading the report.

Thank you to all my colleagues at Ruashi mine for assisting me in conducting test blasts and collecting results.

A special thank you to my dear mother, Makatseng Lijojo, and late father, Masalio Lijojo, for their endless love, teachings, and discipline they have imparted on me.

Finally, I want to take this opportunity to express my eternal appreciation to my wife, Mukondeleli Lijojo, for her endless love, encouragement, and support. Thank you for being my pillar of strength.

Contents page

DECLARATION I

ABSTRACT II

ACKNOWLEDGEMENTS IV

LIST OF FIGURES XI

LIST OF TABLES XIV

TERMINOLOGY XV

CHAPTER 1 1

Introduction 1

1.1 Introduction 1

1.2 Background and Problem 2

1.3 Research Questions 6

1.4 Research Objectives 6

1.5 Purpose of the Study 6

1.6 Research Design and Methodology 7

1.7 Research Limitations 7

1.8 Report Structure 8

1.9 Chapter Summary 8

CHAPTER 2 9

Literature Review 9

2.0 Introduction 9

2.1 Review of theory 9

A. Blasting costs 9

B. Fragmentation modelling 10

2.2 Rock Blasting Theory 12

2.3 Uncontrollable Factors 14

2.3.1 Blastability Index 14

2.4 Controllable Factors 16

2.4.1 Stemming Length and Material Type 17

2.4.2 Bench Stiffness Ratio 18

2.4.3 Spacing to Burden Ratio 20

2.4.4 Powder Factor 21

2.4.5 Explosives Strength 22

2.5 Fragmentation Modelling 23

2.5.1 The Kuznetsov Function 23

2.5.2 Rosin-Rammler Function 24

2.5.3 The Uniformity Index Function 26

2.6 Blast Efficiency 27

2.7 Cost Modelling 27

2.7.1 Drilling Costs 28

a) Direct Costs: 29

b) Indirect Costs 30

2.7.2 Single Blast Hole Cost 31

2 .8 Chapter Summary 31

CHAPTER 3 32

Research Methodology 32

3.1 Introduction 32
3.2 Data Collection 32
3.2.1 Pre Blasting Data Collection 33
3.2.2 Post Blast Data Collection 33
3.3 Rockmass Properties Data for Test Sites 34
3.4 Blast Design Process 37
3.5 The Kuz-Ram Model population 39
3.6 Monte Carlo Model Simulation 43
3.7 Application of the Simulator to the Study 46
3.8 Scaled Image Analysis by Wipfrag 47
3.9 Regression Analysis 50
3.10 Model Validation 51
3.11 Blasting Costs Calculation 52
3.12 Chapter Summary 55
CHAPTER 4 56
Results and Discussions 56
4.1 Introduction 56
4.2 Blastability Index Results. 56
4.2.1 Blastability Index Frequency Distribution 56
4.2.2 Blastability Index Sensitivity 58
4.2.3 Blastability Index Scatter Plots 60
4.3 Uniformity Index Results 63
4.3.1 Uniformity Index Frequency Distribution 63

4.3.2 Uniformity Index Sensitivity 65
4.3.3 Uniformity Index Scatter Plots 67
4.4 Mean Fragment Size Results 69
4.4.1 The Mean Fragment Size Frequency Distribution 70
4.4.2 Mean Fragment Size Sensitivity 73
4.4.3 Mean Fragment Size Scatter Plots 75
4.5 Fragment Size Distribution from Simulation 80
4.6 Fragmentation Size Distribution Results from Image Analysis 85
4.7 Results Comparison for Single Particle Size Distributions 87
4.8 Blasting Costs 91
4.9 Chapter Summary 98
CHAPTER 5 99
Conclusions and Recommendations 99
5.1 Introduction 99
5.2 Conclusions 100
5.2.1 Blastability Index 100
5.2.2 Uniformity Index 100
5.2.3 Mean Fragment Size 102
5.2.4 Suggested Blast Pattern 103
5.2.5 Blasting Costs 103
5.3 Recommendations 103
REFERENCES 105
APPENDICES 111

Appendix A 111

Table A1: Ruashi Explosive Prices for January 2018 111

Appendix B 112

Table B 1: Rock Mass Classification from the Core in Pit 3 113

Figure B 1: Relationship between Weathering and RMR 108

Figure B 4: Friction Angle vs Density 109

Figure B 5: Moisture Content vs Density 110

Table B 2: Triaxial Strength Test Database 111

Appendix C 112

Table C 1: Drill and Blast Costs 113

Appendix D 114

Table D 1: South-West Kuz-Ram Model 115

Figure D 1: South-West Blastability Index Report 116

Figure D 2: South-West Uniformity Index Report 117

Figure D 3: South-West Mean Fragment Size Report 118

Figure D 4: South-West Actual Fragment Report (image analysis) 119

Table D 2: South-East Kuz-Ram Model 120

Figure D 5: South-East Blastability Index Report 121

Figure D 6: South-East Uniformity Index Report 122

Figure D 7: South-East Mean Fragment Size Report 123

Figure D 8: South-East Actual Fragment Report (image analysis) 124

Table D 3: South Kuz-Ram Model 125

Figure D 9: South Blastability Index Report 126

Figure D 10: South Uniformity Index Report (Pf 0.35 kg/Bcm) 127

Figure D 11: South Uniformity Index Report (Pf 0.65 kg/Bcm) 128

Figure D 12: South Mean Fragment Size Report (Pf 0.35 kg/Bcm) 129

Figure D 13: South Mean Fragment Size Report (Pf 0.65 kg/Bcm) 130

Figure D 14: South Actual Fragment Report (image analysis) 131

Appendix D15: South-East blast simulation results (PF=0.65kg/Bcm) 132

Appendix D16: South-West blast simulation results (PF=0.30kg/Bcm) 133

Appendix D17: South blast simulation results (PF=0.35kg/Bcm) 134

LIST OF FIGURES

Figure 1.1: Zambia DRC Copperbelt (Ruashi, 2015) 2
Figure 1.2: Schematic diagram of geotechnical zones (Ruashi, 2015) 3
Figure 1.3: Blasting challenges at the mine 3
Figure 1.4: Proximity of mine operations to Ruashi community 5

Figure 2.1: Physical phenomena in rock blasting (Atlas Powder Company, 1987) 12
Figure 2.2: Factors affecting fragmentation, adapted from Scott (2015) 13
Figure 2.3: Key design features in bench blasting (Tucker, 2015) 17
Figure 2.4: Mechanism of breakage by flexion (Rai et al., 2005) 19
Figure 2.5: Example of a fragmentation distribution curve (Solomon, 2015) 25

Figure 3.1: Geotechnical boreholes relative to Ruashi-3 design (brown) 34
Figure 3.2: Core samples from boreholes RGT6 and RGT8 35
Figure 3.3: Blast site locations relative to different weathering domains 36
Figure 3.4: Blast plan process flowsheet 37
Figure 3.5: Cumulative percentage passing graph 43
Figure 3.6: Monte Carlo simulation process (Thornton et al., 2001) 44
Figure 3.7: Input parameters with respective statistical distributions 45
Figure 3.8: Rock specific gravity distribution 46
Figure 3.9: Blast fragment image with a net 48
Figure 3.10: Blast image with a heat map 49
Figure 3.11: Cumulative particle size distribution curve 49
Figure 3.12: Blastability Index vs rock specific gravity 50
Figure 3.13: Sensitivity analysis of the mean fragment size 51
Figure 3.14: Blast-hole drilling 52
Figure 3.15: Drilling costs (Adapted from Table 2.4) 53
Figure 3.16: Blast tie-up plan 55

Figure 4.1: South-West Blastability Index distribution 57
Figure 4.2: South Blastability Index distribution 57
Figure 4.3: South-East Blastability Index distribution 58

Figure 4.4: South-West sensitivity analysis 59
Figure 4.5: South sensitivity analysis 59
Figure 4.6: South-East sensitivity analysis 60
Figure 4.7: South-West Blastability Index vs specific gravity 61
Figure 4.8: South-East Blastability Index vs specific gravity 61
Figure 4.9: South Blastability Index vs rock specific gravity 62
Figure 4.10: South Blastability Index vs joint dip angle 62
Figure 4.11: South-West Uniformity Index 63
Figure 4.12: South Uniformity Index 64
Figure 4.13: South-East Uniformity Index 64
Figure 4.14: South-East Uniformity Index sensitivity analysis 65
Figure 4.15: South Uniformity Index sensitivity analysis 66
Figure 4.16: South–West Uniformity Index sensitivity analysis 66
Figure 4.17: South-West Uniformity Index vs stemming length 67
Figure 4.18: South-East Uniformity Index vs burden 67
Figure 4.19: South-East Uniformity Index vs spacing 68
Figure 4.20: South Uniformity Index vs burden 68
Figure 4.21: South Uniformity Index vs spacing 69
Figure 4.22: South-West mean fragment size distribution (PF = 0.30 kg/m^3) 70
Figure 4.23: South-East mean fragment size distribution (PF = 0.65 kg/m^3) 71
Figure 4.24: South mean fragment size distribution (PF = 0.35 kg/m^3) 72
Figure 4.25: South mean fragment size distribution (PF = 0.65 kg/m^3) 72
Figure 4.26: South-West mean fragment size sensitivity analysis 73
Figure 4.27: South-East mean fragment size sensitivity analysis 74
Figure 4.28: South mean fragment size sensitivity analysis 75
Figure 4.29: South-West mean fragment size vs stemming 76
Figure 4.30: South-West mean fragment size vs charge density 77
Figure 4.31: South-West charge density vs stemming length 77
Figure 4.32: South-East mean fragment size vs stemming length 78
Figure 4.33: South-East mean fragment size vs explosives strength 78
Figure 4.34: South mean fragment size vs dip angle 79
Figure 4.35: South mean fragment size vs rock specific gravity 79
Figure 4.36: South mean fragment size vs stemming length 80
Figure 4.37: South-East blast fragmentation distribution (PF = 0.65 kg/m^3) 81

Figure 4.38: South-East simulation output results (PF = 0.65 kg/m^3)..... 81
Figure 4.39: South-West blast fragmentation distribution (PF = 0.30 kg/m^3) 82
Figure 4.40: South-West simulation output results (PF = 0.30 kg/m^3)..... 83
Figure 4.41: South blast fragmentation distribution (PF = 0.35 kg/m^3)..... 84
Figure 4.42: South simulation output results (PF = 0.35 kg/m^3)..... 84
Figure 4.43: South blast fragmentation distribution (PF = 0.65 kg/m^3)..... 85
Figure 4.44: South-West blast fragmentation distribution 86
Figure 4.45: South blast fragmentation distribution..... 86
Figure 4.46: South-East blast fragmentation distribution 87
Figure 4.47: South-West blast actual fragmentation vs predicted..... 88
Figure 4.48: South-West blast actual fragmentation vs predicted vs adjusted..... 89
Figure 4.49: South blast actual fragmentation vs predicted 89
Figure 4.50: South-East blast actual fragmentation vs predicted..... 90
Figure 4.51: South-East blast actual fragmentation vs predicted vs adjusted..... 91
Figure 4.52: Unit drilling and blasting costs 92
Figure 4.53: Total drilling and blasting costs for 400 blast holes..... 92
Figure 4.54: Comparison of actual costs vs planned costs 93
Figure 4.55: Powder factor and the fragment size 94
Figure 4.56: Unit drill and blast costs vs charge length..... 95
Figure 4.57: Unit costs vs stemming length 95
Figure 4.58: Powder factor vs charge per hole. 96
Figure 4.59: Unit costs and Blastability Index 97
Figure 4.60: Uniformity Index and unit costs..... 97

LIST OF TABLES

Table 2.1: Ratings for Lilly's rock factor parameters. Adapted from Lilly (1986) 15
Table 2.2: The potential problems associated with stiffness ratio. 20
Table 2.3: Typical technical powder factor for different rock type. 22

Table 3.1: Ruashi rock properties 35
Table 3.2: Summary of rockmass conditions 36
Table 3.3: Blast patterns with simulation conditions 38
Table 3.4: Burden to stiffness ratio 38
Table 3.5: Burden to spacing ratio 39
Table 3.6: Kuz-Ram model 41
Table 3.7: Drilling costs. Adapted from Ruashi Mining Contract (2018) 53
Table 3. 8: Explosives and accessories costs. 54

Table 4.1: Blasting Efficiency using single particle size distribution 88

TERMINOLOGY

South Blast: Refers to blast scenarios undertaken in the south area of Ruashi pit 3.

Southeast Blast: Refers to blast scenarios undertaken in the southeast area of Ruashi pit 3.

Southwest Blast: Refers to blast scenarios undertaken in the southwest area of Ruashi pit 3

CHAPTER 1

Introduction

1.1 Introduction

Blast rock fragmentation is an essential component of the mine to mill optimisation philosophy. A variety of empirical models are used to predict the fragment size of blasted rock materials. These models depend on elements such as the drillhole diameter, burden, spacing, bench height, rockmass conditions, and the explosive properties amongst others to predict the fragment size. The Kuz-Ram model is popularly used in predicting the size fragmentation distribution of blasted rock material.

Various literature shows that sub-optimal or poor fragmentation size distribution of the blasted material can have adverse consequences on the following mining operations such as loading, hauling, and processing operations. Thus, leading to a loss of value in the entire mining value chain. Mackenzie (1966) defined optimum blast as “the blasting practice, which gives the blast results necessary to obtain the lowest overall costs for drilling, loading, hauling, and crushing.”

The costs of both drilling and blasting operations are a vital component in the overall scheme for achieving lower operating costs. However, to achieve a higher value (profitability), the mine to mill optimisation process requires that, the entire value chain rather than at a unit level optimisation approach be carried out. It is essential to specify the ideal ROM (run of mine) size fragment required by the plant as this will influence the drill and blast design pattern and overall costs involved (Mackenzie, 1966). It might be necessary to increase the blasting energy, thus decreasing the fragment size to ensure that lower mechanical energy input in the comminution circuit is achieved.

It is, therefore, essential that the relationship between the rockmass parameters, blast design parameters, and the explosive energy required to achieve the desired fragment size distribution be well understood.

1.2 Background and Problem

Ruashi Mine is an open-cast copper and cobalt mine situated 10km northeast of the town of Lubumbashi in the province of Katanga in the Democratic Republic of Congo (Ruashi, 2015). Figure 1.1 shows the geographic location of the Ruashi mine.

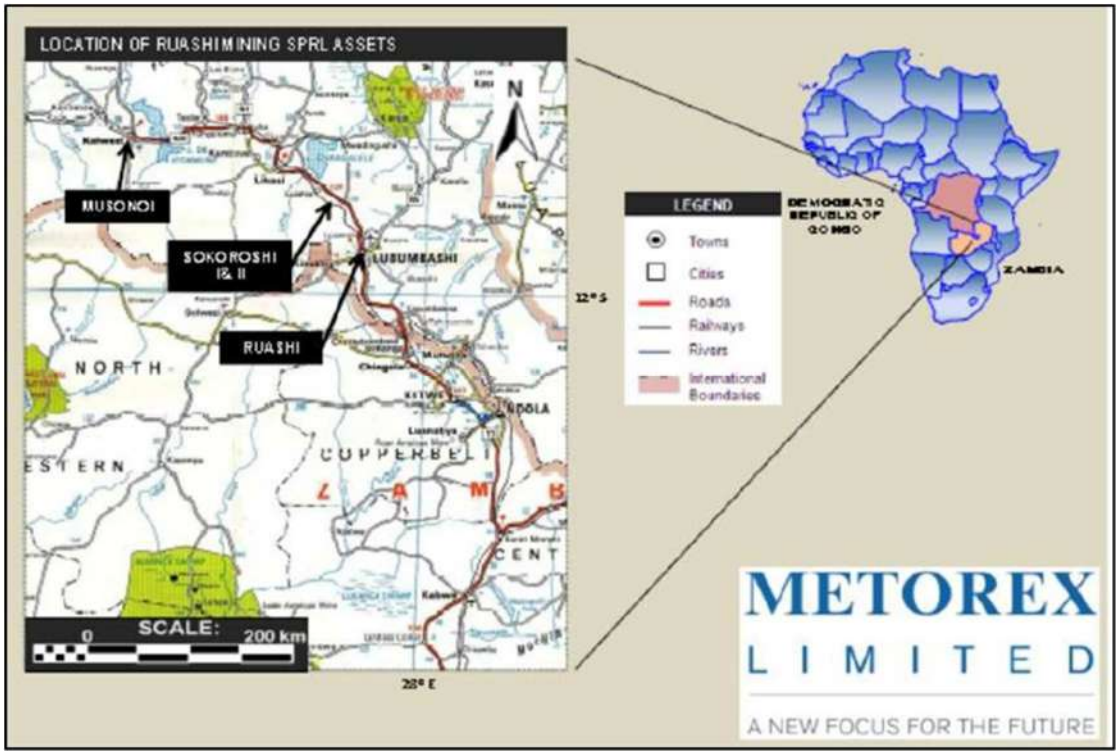

Figure 1.1: Zambia DRC Copperbelt (Ruashi, 2015)

The mine was established in 1919 and mining took place sporadically up to 2003. The disruptions to mining operations were due to the turbulent political history of the country. During 2004 and 2005, Metorex took over the mining permit, and operational control to Ruashi mine and the operation has experienced stable production to date. The mine currently produces 36000 metric tonnes of copper cathode and 4800 metric tonnes of cobalt concentrate per year. The total material mined per year is around 11 million tonnes.

The mining production mentioned above came from easy to mine oxide domains which allowed for free digging operations. However, over the past few years, a significant part of the oxide material has been depleted. Presently, the mine operates in the harder strata of the transition and fresh material domains in some parts of the pits, thus, requiring a formalised blasting program. Figure 1.2 depicts the depth of the mining areas relative to competent material domains.

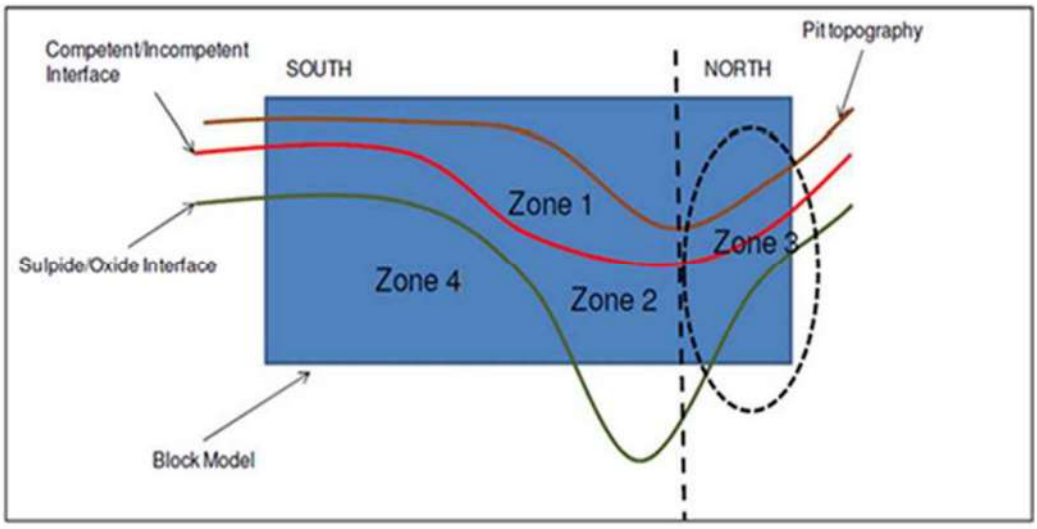

Figure 1.2: Schematic diagram of geotechnical zones (Ruashi, 2015)

The problem: The mine has never had a formalised blasting unit established in the mining department. Many challenges concerning the performance of blasting operations can be attributed to the lack of standards, experience, and expertise in blasting operations. The consequence of not having a blasting division was now apparent to mine management. Figure 1.3 depicts a range of challenges encountered from the blasting operations.



Figure 1.3: Blasting challenges at the mine

Discussing briefly the problems depicted by Figure 1.3 (in a clockwise direction) starting with:

- Top-right image, excessive pinnacles were formed (especially on the second mining flitch) after holes that collapsed were not redrilled, and the amount of explosive placed in the standing holes varied tremendously across the pattern. These are typical quality assurance and control issues. In some of these cases, the entire area had to be blasted for the second time to correct the situation, thus incurring high costs.

- Bottom-right image, huge boulders were common and frequent across all blasted areas. These boulders presented safety issues to people and equipment, especially when operators attempted to load them into trucks or push them down the mining faces to the lower working areas. Digging and loading were extremely difficult and slow in such circumstances.

- Bottom-left image, poor fragment size distribution emanating from poor burden and spacing for the rockmass encountered coupled with an ineffective explosive charge (poor powder factor). These areas are a challenge to mine and result in low digging rates and frequent damage to bucket's teeth.

- Top-left image, this situation occurred when the burden and spacing were excessive, and there was no interaction between the adjacent blast holes. This kind of blast results were commonly associated with flyrocks, excessive vibration, poor diggability, and boulder.

The problem, in general, is that the results of the blasting operations are shamefully inappropriate, characterised with poor fragmentation. Further, the bench turnaround times are excessive and impacting on the mine planning schedule and plant feed due to planned ore being locked up in benches. High-grade ore areas from the Minerais Verts formations continuously required redrilling and blasting to get the fragmentation size to match the plant requirements. The ore from the MV formation was essential in ensuring a stable head grade to the plant. Delays in exposing and mining these areas resulted in lower copper recovery due to delays caused by blasting.

Another issue of significance was the safety of the neighbouring communities. The mining lease area was not adequately secured, and illegal settlements overtime took place inside the mining concession. The only form of barrier between the community

and the mine was a water trench established to serve two purposes, one, stop further community encroachment and second, to divert water away from the pits. It is common to find kids playing near open mining faces and illegal miners coming down into the pits to steal ore. During blasting operations, it is a mission to clear both employees and community members to a safe distance away from the blast.

Frequent claims of injury and damage to property were being raised against the mine with compensation demanded whenever blasting took place. Sometimes, the communities would close accesses to the mine in protest to blasting operations. The government intervened and set the following blasting conditions: a maximum of 800 blast holes per blast, a maximum of four blasts per week, and the mine to establish a joint committee comprised of mine management and community leaders to facilitate community evacuations and damage assessment. Therefore, this study aims to resolve all these problems by proposing a blast pattern that would deliver optimal fragment size safely. Figure 1.4 shows the proximity of mining operations to the community.

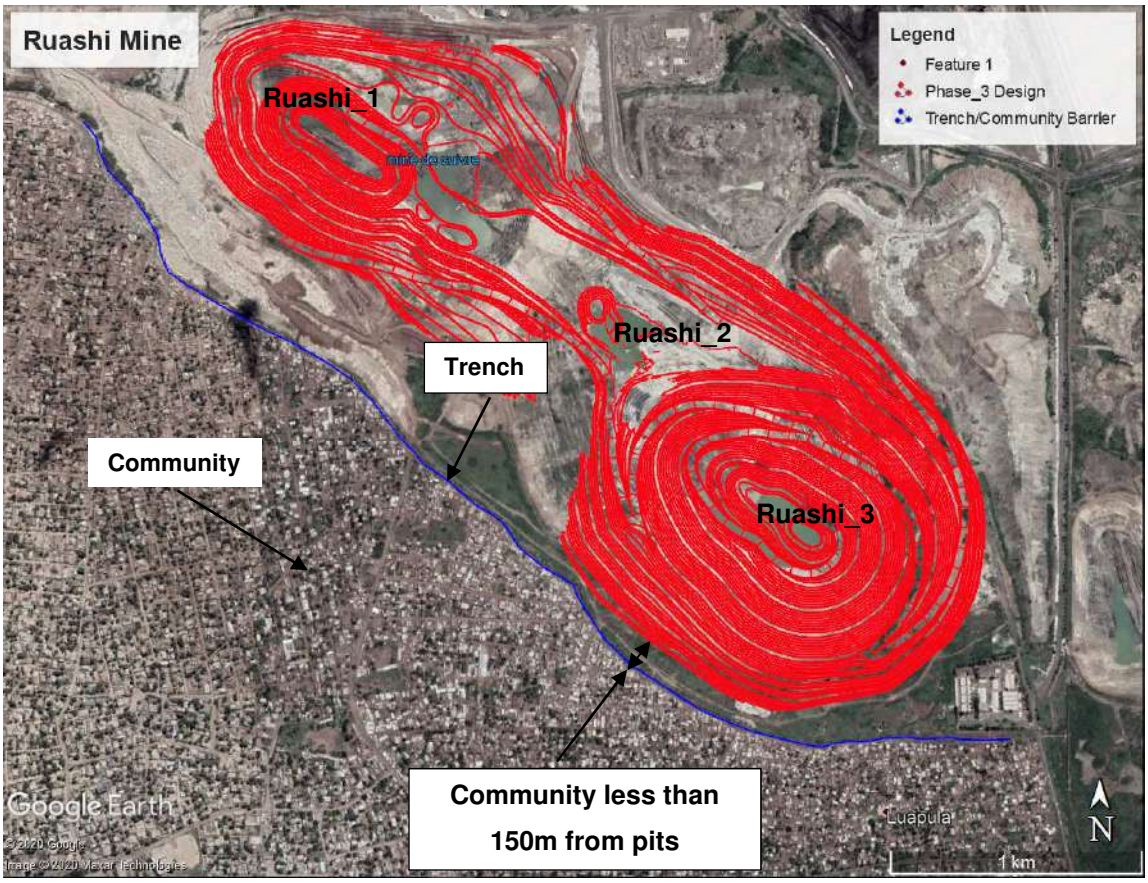

Figure 1.4: Proximity of mine operations to Ruashi community

1.3 Research Questions

The study sought to investigate factors that influence blast fragmentation by answering the following research questions (RQ):

RQ1: How does rockmass characteristics impact on blast rock fragmentation size?

RQ2: What is the impact of blast design parameters on blast rock fragmentation size?

RQ3: What is the influence of a blast design pattern on mine blasting costs?

1.4 Research Objectives

The objectives (RO) of the study are:

RO1: To explore the role of rockmass conditions on blast rock fragmentation size.

RO2: To explore the role of blast design parameters on blast rock fragmentation size

RO3: To determine a drill and blast pattern that will produce optimal fragmentation size at the lowest cost possible.

1.5 Purpose of the Study

The purpose of this descriptive, quantitative study was to explore the impact of rockmass characteristics and blast design parameters on the resultant fragmentation size. This was done by running various Blastability Index and Uniformity Index parameter simulations using the Kuz-Ram model in order to identify the simulation conditions and parameters that produce the best fragmentation results when compared with the actual fragmentation size to adopt those conditions as the blast design parameters for the mine. This study applied existing blasting theories and models to address the challenges at the mine and in this way, added to the current body of knowledge by successfully resolving the mines blasting challenges.

1.6 Research Design and Methodology

The research approach to the study was a positivistic, deductive approach wherein the study began with an in-depth review of the theories and models that govern the topic. Scientific methods were used to explain the causal relationships between the different variables in the study. The research design of this study used a case study, quantitative, simulation approach (Rensburg, 2017). The simulation approach involved the construction of artificial environments wherein data and information were generated. The simulation approach allowed for observations of the dynamic behavior of the system under controlled conditions.

Research methods are specific techniques selected by the researcher for conducting the actual research (Rensburg, 2017). It includes techniques for developing the research instruments, as well as collecting and analysing data (Rensburg, 2017). An applied research methodology was used wherein data was collected from the test sites. The data consisted of both numerical and descriptive data.

Test sites were chosen based on their geological properties. Pre-blast data such as rockmass condition, explosives properties and environmental condition were recorded in Microsoft Excel software. Post blast data such as rock fragment size, heave, and bench conditions were also recorded in Microsoft Excel, and images were taken and imported into Wipfrag software. @Risk software was used for data analysis, and simulation runs with the actual blast results analysed on Wipfrag software. The results from Wipfrag were compared with the @Risk simulation runs to determine the optimal blast pattern.

1.7 Research Limitations

The study had a number of limitations, firstly; resources. The author did not have the necessary blast design software such as JKSimblast as the mine had not procured such software. Blast designs were done on Surpac software and Microsoft Excel Kuz-Ram model. As such, sophisticated and advanced analysis of blast results could not be performed.

The second limitation was time. The study had to be completed within twelve months to comply with the University requirements for research studies. This meant the study had to be narrowed down and focused on a particular issue that could be studied within this period. Also, from the mines point of view, the author was given two months

to conduct the test blast studies. This meant that time was very much constrained to conduct an in-depth study.

The third limitation was financing. To resolve finance issues, test blasts were conducted as part of the standard mining production to avoid additional cost being incurred to conduct this study. Also, existing software on the mine was used to conduct the study to ensure expenses were minimised.

1.8 Report Structure

The research report consists of five chapters. Chapter one contextualises the problem and provides the motivation and purpose for conducting the research study at Ruashi mining. It further highlights the scope and objectives of the research. The chapter also outlined the geological and geographic setting of the mine.

Chapter two outlines the theoretical work of the research report—the principles and theories of blast design, explosives energy, and fragmentation size distribution. The chapter also highlights the relationship between mining cost and blast fragment size. This chapter essentially grounds the study by highlighting the relevant theories applied in the study.

Chapter three outlines the process followed in collecting and storing data along with the equipment and software that were used to analyse the data. The chapter further describes the application of the Monte Carlo simulation technique in the implementation of the Kuz-Ram blast fragmentation model.

Chapter four deals with the presentation and interpretation of the results achieved from the study, while Chapter five deals with the conclusions drawn from the results and the recommendation.

1.9 Chapter Summary

This chapter presented the background to the problems experienced by Ruashi mine. It further outlined the research questions and objectives of the study. The chapter also described the research design and methodology used in conducting the study. In conclusion, this chapter aimed to present the motivation for conducting the study to resolve the challenges of poor fragmentation.

CHAPTER 2

Literature Review

2.0 Introduction

This chapter presents the theories that form the foundation for the study, highlights the developments in drilling and blasting concepts and fragmentation estimation models over the decades. The chapter also outlines the basis for having used the Kuz-Ram model together with Monte Carlo simulation to predict the relationship between various parameters that govern the fragmentation size distribution. The chapter also outlines the equations that are used to estimate the cost of drilling and blasting. In summary, this chapter brings together drilling and blasting parameters to target fragmentation size distribution and the total drilling and blasting costs.

2.1 Review of theory

A. Blasting costs

Some of the earliest research into the optimisation and evaluation blasting performance on surface mines was performed by Mackenzie (1967). Mackenzie (1967) showed understanding the various relationships between fragmentation size, hauling costs, digging costs and drilling costs could be beneficial to the mining operations. Mackenzie's (1967) primary focus was on achieving two objectives, minimum cost, and blast efficiency during blasting operations. His papers demonstrated that that improving the fragmentation achieved by the blasting had a positive effect on downstream mining operations such as loading, hauling and crushing.

Studies have shown that good fragmentation had tremendous benefits to the grinding circuits because most of the energy was consumed by crushing and grinding (McKee et al., 1995). In a study conducted by Moody et al. (1996), their results indicated that the power consumption at the crusher was more sensitive to rock fragmentation size than the throughput. Meanwhile, Fernberg (2005) presented a breakdown of the costs associated with drilling and blasting, loading and hauling, and crushing as follows: drilling and blasting accounted for 25%, loading and hauling was 25% and crushing accounted for 50%. The findings of this study showed a 10% reduction in energy

consumed in the grinding system, which was achieved by improving the blast pattern together with the explosives consumption in the blasting process (Fernberg, 2005).

Ash (1963, 1990) makes the point that the burden and spacing are critical parameters for achieving a good fragmentation. Kojovic et al. (1995), in their studies, demonstrated that the powder factor was also an essential parameter in achieving good fragmentation. Their results showed that a powder factor increase from 0.52 to 0.61 kg/m^3 improved loading productivity by 25% and resulted in savings of 0.40 USD/tonne, and in the crushing and grinding system the savings were 0.30 USD/tonne. However, when one intends to improve blasting operations, they must understand the relationship between rockmass characteristics, blast pattern design and fragmentation size distribution.

B. Fragmentation modelling

Kanchibotla et al. (1998) indicated that blast modelling and simulation were the most cost-effective ways to evaluate blasting and comminution strategies. The Kuznetsov equation has been reliable and accurate over the years for predicting the average fragment size (Chung and Katsabanis, 2000). The primary role of fragmentation modelling was to be able to predict the entire fragmentation distribution to obtain the 80% passing size (Demenegas, 2008).

Gaudin-Schumann or the Rosin-Rammler distributions are often used to represent fragmentation size distributions despite the fact that these models underestimate the fines material in fragment size distribution (Kecojevi & Komljenovic, 2016). The original intent of the Rosin-Rammler model was to be a tool to predict reasonable changes when blast design parameters are modified (Kecojevi & Komljenovic, 2016). However, despite the model's shortcomings, operators continue to use and place a great amount of confidence in these model’s predictions due to the familiar properties of the model and the ease of use. Also, the Kuz-Ram model is able to accurately and reasonably predict the relatively coarse part of the fragment size distribution (fragments with size greater than 50 mm) (Djordjevic, 1998).

Attempts have been made over the years to correct the Kuz Ram model drawbacks (Hall & Brunton, 2001). The corrections were based on the modification of the Rosin – Rammler fragmentation distribution. Various models have been used to predict blast rock fragmentation, ranging from empirical models to numerical models. Two of

the latest models used to predict fragmentation sizes are the Julius Kruttschnitt Mineral Research Centre (JKMRC) prediction model and the KCO model (Swebrec function). The JKMRC model uses a 'Two-Component Model' (TCM) and the 'Crushed Zone Model' (CZM) developed by Djordjevic (1998) and Kanchibotla (1998). The JKMRC model represents a modified version of the Kuz-Ram model to predict the coarse and fines end of the distribution (Kojovic et al., 1995)

The KCO model is the latest model amongst the two that is used in the prediction of fines and in improving the prediction of the fragment size distribution (Ouchterlony, 2006). The model replaces the Rosin-Rammler function used to describe the fragmentation curve in the Kuz-Ram model by the Swebrec function (Ouchterlony, 2006). Both the JKMRC and KCO models are more accurate in the estimation of the fine materials (<100 mm) than the Kuz-Ram model (Hall & Brunton, 2001). Fine fragment size can be a problem to mines where the price received for products (iron ore and coal) is affected by the percentage of fines or where the throughput is affected by the fines (-25mm) (Kanchibotla, Valery & Morrell, 1999). In the case of the copper mines, fines are not a problem as they do not affect the price received for the product. In such a scenario, Kuz-Ram model can be reasonably applied.

Whatever prediction model one choses, it is important to understand that various blast parameters have an influence on the fragmentation size distribution. These are parameters such as rock strength, the explosive velocity of detonation and powder factor. Thornton et al. (2002) developed a stochastic technique to identify the parameters that have the most significant influence on various fragment size distributions. Thorton et al (2002) stated that "the technique takes the input variables as statistical distributions rather than constants and through several thousand iterations, generates a statistical representation of the expected fragmentation resulting from a poduction blast"

This study will thus focus on the theories used to develop the Kuzram model, and the application of simulation techniques to explore paramters with the greatest influence of the blast fragmentation size distribution.

2.2 Rock Blasting Theory

When an explosive charge is loaded within a blast hole and detonated, the shock pressure is transmitted to the surrounding rockmass causing the blast hole diameter and volume to expand (Doucet, 1995). The increase or expansion in the rockmass results from the pressure that is induced in the drillhole, the rate of explosive energy released and the expansion rate (Doucet, 1995). The pressure in the rockmass directly surrounding the blast hole is 1.5 to 2 times greater than the rock compressive strength, thus crushing of the rockmass in this zone will occur (Doucet, 1995).

Outside the crushed zone, the crack will propagate radially from the blasthole and continue to extend as long as the stresses exceed the rock strength, which is a function of the Poisson's ratio, Young's Modulus, and the surface tension coefficient. Figure 2.1 illustrates the physical phenomena in rock blasting.

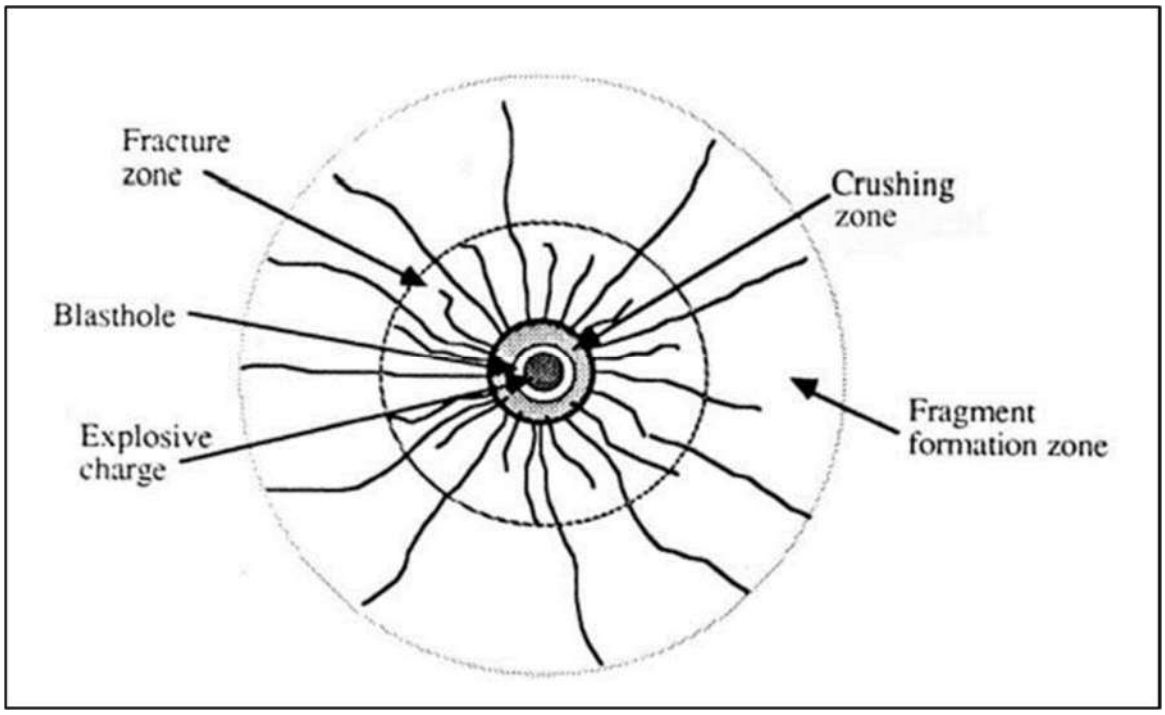

Figure 2.1: Physical phenomena in rock blasting (Atlas Powder Company, 1987)

Although cracks stop propagating some distance away from the detonated blasthole, the pressure pulse continues until it reaches a free face. At this point, the compressive wave reflects as a tensile wave (Doucet, 1995). In cases where the tensile strength of the rock is exceeded, the tensile wave will add additional cracks by expanding and extending the existing cracks (Doucet, 1995). Doucet (1995) stated that "The total work of the shock energy becomes completed when the tensile wave dissipates into

the rock. At this point, gas energy continues the fragmentation process". Fragmentation is thus a product of shock energy and gas energy acting upon the rockmass. The rate of energy release and rock properties influence the amount of shock energy transmitted to the rockmass

Having understood the process of rock fragmentation, one then focuses on the blast design aspect of rock fragmentation. There are mainly two aspects that influence the performance of any blast, namely the uncontrollable variables and controllable variables. Researchers and mine practitioners alike have long observed that rock geology does affect the blast results. However, the extent of the influence is poorly understood. The performance of the blast results has mostly depended on the expertise of the blasting practitioner. The rockmass properties are difficult to study individually and separately, hence the challenge in quantifying their influence on blast results (Doucet, 1995).

The uncontrollable factors are mostly geological issues such as joint condition, rock hardness, rock strength, and so on. The controllable aspects are the design geometry and choice of explosive. Figure 2.2 shows the controllable and non-controllable factors.

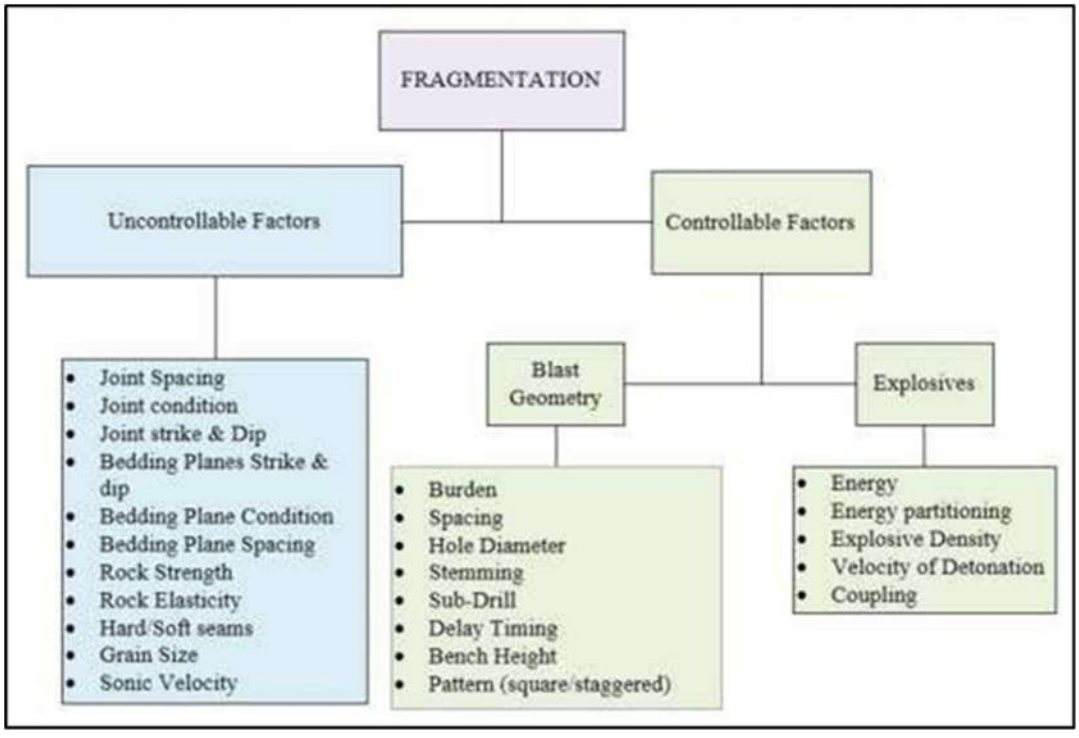

Figure 2.2: Factors affecting fragmentation, adapted from Scott (2015)

2.3 Uncontrollable Factors

The geological structures and the rockmass characteristics of the rock to be blasted have a significant influence on how the energy of the explosives will interact with the rockmass, and as a result, the kind of blast results achieved post-blast. There is a general acceptance that, there is some degree of difficulty in the effort to quantify the rockmass characteristics. Researchers such as Tandanand (1973) and Hustrulid (1999) identified the following parameters to consider when quantifying the rockmass properties:

- "Geology of the deposit: Lithology, chemical composition, and rock types;
- Structural geology: Faults, fissures, and inherent fractures;
- Water presence: The quantity and source of origin;
- Rock strength and properties: Physical properties and mechanical properties".

2.3.1 Blastability Index

Lilly (1986) defined a parameter called the Blastability Index (A) which was adopted by Cunningham (1987) to quantify the influence of rockmass on fragmentation by incorporating it into his Kuz Ram model which he developed in 1983. Cunningham (1987) mentioned that the assessment of any rock blastabilty should account for the rock strength, elastic properties, density and fracture formations inherent in the rock. The equation for the Blastability Index is then given by equation 1:

$$\mathbf{A = 0.06\ x\ (RMD + JF + RDI + HF)} \quad \ldots\ldots\ldots\ldots\ldots\ldots\ldots \mathbf{(1)}$$

Where A is the rock factor, RMD is the rock mass description, JF is the joint factor, RDI is the rock density influence, and HF is the hardness factor. Table 2.1 provides the ratings for Lilly's rock factors.

Table 2.1: Ratings for Lilly's rock factor parameters. Adapted from Lilly (1986)

Parameters		Rating
1. Rock Mass Description (RMD)	1.1 Powdery or Friable	10
	1.2 Blocky	20
	1.3 Massive	50
2. Joint Plane Spacing (JPS)	2.1 Close (< 0.1m)	10
	2.2 Intermediate (0.1 to MS)	20
	2.3 MS to DP	50
3. Joint Plane Orientation (JPO)	3.1 Horizontal	10
	3.2 Dip out of the Face	20
	3.3 Strike normal to Face	30
	3.4 Dip into the Face	40
4. Rock Density Influence (RDI)	SGI = 25dg -50 (where dg is in tonnes/cubic metre	
5. Hardness Factor (HF)	E/3 if E is less than 50 GPa UCS/5 if E is more than 50GPa	Units (GPa)
• E is the Young's Modulus • UCS is the Uniaxial compressive strength • JF = JPS + JPO • MS is the oversize material • DP is the drilling pattern size	Units (GPa) Units (Mpa) Units (m) Units (m)	

Lilly (1986) explains in detail the importance of the five different parameters that make up the Blastability Index equation. These parameters are summarised as follows:

a) Rock Mass Description: The rock mass is made up of the blocky ground, powdery ground and massive ground. When blasting blocky rockmass made up of multiple joints, one should already know that the fragmentation in this ground will be governed by the joints more than the explosives' energy (Lilly, 1986). In massive rock mass with minimal planes of weakness, the

fragmentation will be primarily controlled by the creation and intersection of the blast-induced fissures (Lilly, 1986).

b) Joint Planes: These are planes of weakness in the rock, e.g. fault planes, joint planes, bedding planes and mining-induced joint planes. The spacing of the joint set gives an indication of the blast fragment size that will be achieved after the blast. Closely spaced joint sets require less explosive energy than larger joint spacings (Lilly, 1986).

c) Joint Plane Orientation: Horizontal or vertical joint planes to the free face or the direction of the blast are critical to the fragment size, diggability of the muckpile, and bench floor conditions (Lilly, 1986). Joint planes that dip in the direction of the throw produce slabby muckpile with saw-toothed bench floor profile (Lilly, 1986).

d) Specific Gravity Influence: The heavier rock density rocks require more explosive energy to break than lighter rock mass (Lilly, 1986).

e) Hardness Factor: Harder rocks can be challenging to break than softer rocks (Lilly, 1986).

The Blastability Index is used to describe the ease of blasting, and it is also related to the powder factor and fragmentation. Low values of Blastability Index (less than 8) indicate medium to hard rock conditions. Values of Blastability Index between 8 to 10 indicate hard to highly fractured rocks, and values above 10 to 13 indicate hard, weakly fractured rocks (Gheibie et al., 2009).

2.4 Controllable Factors

Controllable factors can easily be manipulated and are wholly within the control of the blast engineer. These are factors such as:

- Choice of explosives,
- Blast geometry (hole diameter, burden, spacing),
- The initiation systems and
- The timing of the shot.

The following geometric parameters are part of the controllable factors:

- Diameter (D) and depth of drillhole (Dl),

- Bench Height (H),
- Burden (B) and Spacing (S),
- Stemming (T),
- Length of Charge (Le) and Sub-drill (J),
- Rock hardness.

For this study, the parameters that were considered to have a significant influence on the performance were: stemming length and material type, bench stiffness ratio, spacing to burden ratio and powder factor.

The list of investigated parameters is by no means exhaustive, and for this study and time duration, the stated parameters were the ones examined. Figure 2.3 depicts the geometric parameters of bench blasting.

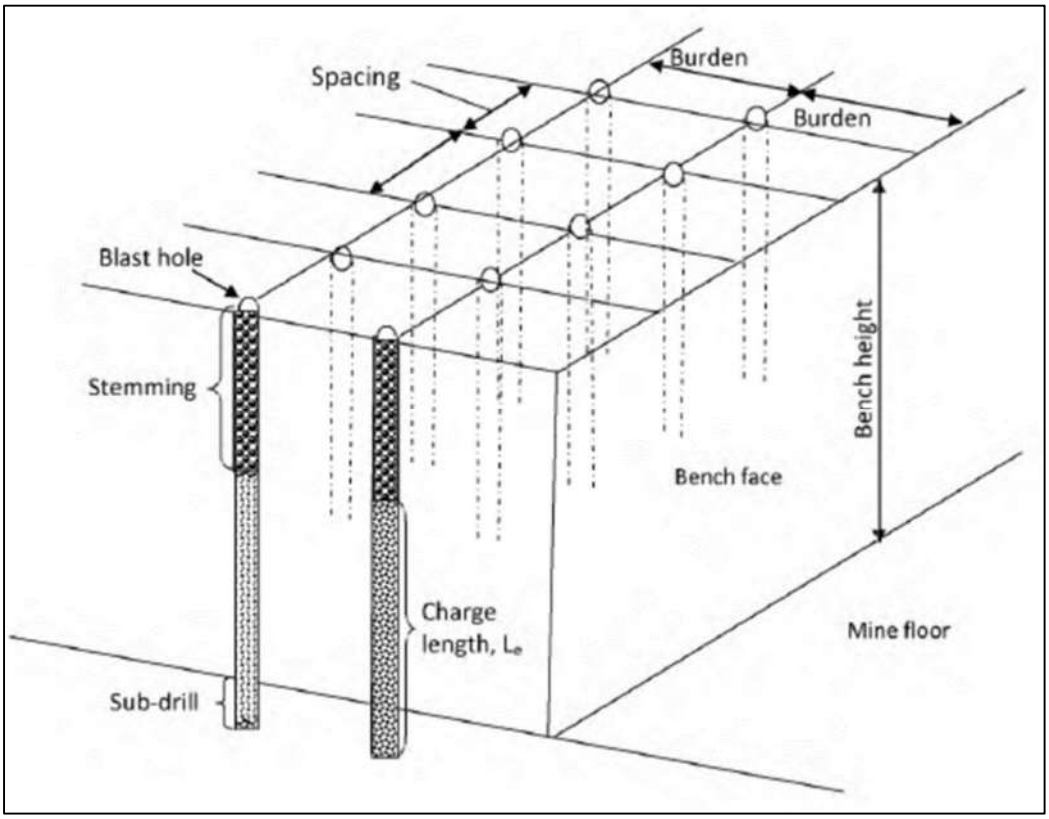

Figure 2.3: Key design features in bench blasting (Tucker, 2015)

2.4.1 Stemming Length and Material Type

The role of stemming is to retain the blast energy within the rockmass for sufficient time to promote adequate fracturing of the rock. In the event of insufficient stemming, early escape of gases into the atmosphere will occur together with an air blast and fly

rocks (Rajpot, 2009). Conversely, if the stemming is excessive, large boulders will be formed at the top part of the bench, also increased ground vibration and poor swelling of the muckpile will occur (Rajpot, 2009).

Rajpot (2009) proposed that “optimum length of the stemming increases as the quality and the competence of the rock decreases, varying between 20D and 60D, where D is the diameter of the blasthole.” To avoid problems with airblast, fly rock, overbreak and cutoffs, the recommended stemming length of 25D is maintained (Rajpot, 2009). Konya and Walter (1991) suggest that the stemming length should be 0.7 x Burden for stemming with crushed rock and 1.0 x Burden for drill cuttings, with the sub-drill being 0.3 x Burden.

The stemming material should never allow the gases to escape prematurely (blow out) to achieve maximum use of blasthole energy within the rockmass, (Rajpot, 2009). It is advised that the borehole diameter to stemming material size should be between D/10 to D/20 (D is the drill diameter in mm) for angular material with minimum fines. It is a typical practice to use drill cutting as stemming material due to their availability near the hole (Rajpot, 2009). However, it was observed that the crushed angular material is more effective as a stemming material due to the interlocking properties of the angular shapes and it is resistant to ejection and hence contains the explosive energy better within the blasthole (Rajpot, 2009).

2.4.2 Bench Stiffness Ratio

The bench stiffness ratio was introduced by Konya and Walter (1991) as a means to classify how benches will break relative to the burden. Konya and Walters (1991) stated that “The burden rock is more difficult to break by flexural failure when bench height approaches the burden dimensions in length.” Konya and Walters (1991) further stated that “when bench heights are many times the burden in length, the burden rock was easily broken.” In short, the stiffness ratio determines whether the rock crater upwards, or break parallel to the borehole.

In the fragmentation process of the rock mass by explosives, there are at least eight mechanisms of rock breakage involved. These are radial fracturing, crushing of rock, reflection breakage and spalling, gas extension fracturing, fracturing by release-of-load, fracturing along boundaries of modulus contrast of shear fracturing, breakage by flexion, and fracturing by in-flight collisions (Jimeno et al., 1995).

One of the rock breakage mechanism used to explain the bench stiffness ratio is the flexion mechanism. The phenomena resemble that of beam failure with pressure applied in the middle, and both endpoints fixed. In rock breakage by explosives, the stemming area and the sub-drill area act as fixed anchor points. While other mechanisms such as radial fracturing and spalling are taking place and the explosive gases apply pressure on the rockmass in front of the explosive column thus making the rockmass to act like a beam (Jimeno et al., 1995). Rock breakage by flexion mechanism is depicted in Figure 2.4.

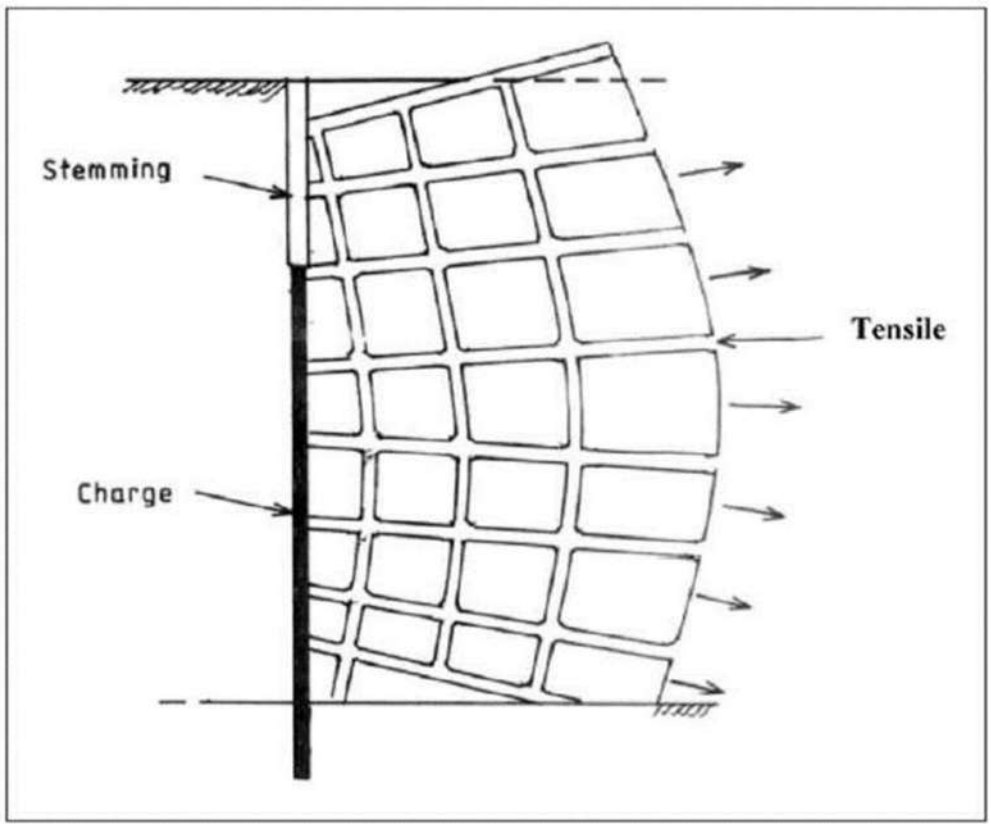

Figure 2.4: Mechanism of breakage by flexion (Rai et al., 2005)

The equation for the stiffness ratio is given by bench height divided by the burden, as shown in Equation 2:

SR = H/ ……... (2)

The blasthole diameter size and the burden distance are limited or controlled by the bench height (Ash, 1968). It is easy to deform and displace the rock material located in the middle of the bench when the bench height to burden ratio is large (Ash, 1968). If the stiffness ratio is below two, there is a high probability that the bench will crater and result in incidents of air-blast, high blast vibration and severe back break on the

benches. Table 2.2 depicts the potential problems associated with changes in the stiffness ratio.

Table 2.2: The potential problems associated with stiffness ratio.

Adapted from Konya and Walter (1991).

Stiffness Ratio Values	Fragmentation	Air Blast Results	Fly Rock Results	Ground Vibration Results
1	Poor	Severe	Severe	Severe
2	Fair	Fair	Fair	Fair
3	Good	Good	Good	Good
4	Excellent	Excellent	Excellent	Excellent

2.4.3 Spacing to Burden Ratio

The spacing to burden ratio has a direct impact on the size of fragments achieved in a blast. The larger the spacing to burden ratio, the less the energy interaction between the blast holes and the likely the chances of excessive vibration and fly rocks. Small burdens allow the explosive gases to escape prematurely and cause the blasted rock to be pushed out at high speeds posing a great danger of fly rocks. While, excessive burden creates resistance to explosion gases to penetrate the rock resulting in chocked blasts (Roy et al., 2016).

Small spacings result in extreme crushing between the holes, and large spacings result in inadequate fracturing between the blasthole thus leading to the creation of irregular faces with hard toes being formed (Roy et al., 2016). The standard spacing to burden ratio is between one and two with 1.15 considered to be the optimal burden to spacing for a staggered pattern and 1.25 ratio for the rectangular pattern (Roy et al., 2016). In situations where the attainment of an ideal spacing to burden is not possible, Roy et al. (2016) stated that “the spacing to burden ratio be adjusted by changing the detonation sequence through the different cut designs such as diagonal firing, V-cut and elongated V-cut.”

2.4.4 Powder Factor

The choice of explosives is one of the parameters that is influenced by the uncontrollable factors such as rock hardness, fractures, rock strength and environmental conditions such as the presence of water, infrastructures close to the blast and controllable factors. The mass of the explosives per metre of blast hole is dependent upon the square of the hole diameter and the average in-hole density of the explosive (School of Mining, 2019). The following equation gives the mass per metre:

$$\boldsymbol{M = \frac{P * D^2}{1273}} \quad \textbf{.....(3)}$$

Where M is the mass of explosives per metre of blast hole (kg/m), P is the average in- hole density of the explosive (g/cc), and D is the blasthole diameter (mm).

The methodology used to determine the blast pattern is dependent upon the powder factor (PF). The mass of explosives (energy) required to break one cubic metre of rock is called the powder factor (School of Mining, 2019). Differentiating between technical and actual powder factor is essential. The technical powder factor does not consider the sub-drill, as this part of the charged drill hole is not considered to contribute to the fragmentation of the rock (School of Mining, 2019). The actual powder factor will include the sub-drill, and it is essential when calculating the actual amount of explosives used (School of Mining, 2019). The equation for the powder factor is given by:

$$\mathbf{PF_{tech} = \frac{M * L_e}{B * S * H}} \quad \textbf{.....(4)}$$

Where M is the mass of explosives per metre of blast hole (kg/m), L_e is the charge length (m) above the grade level, S is the spacing (m), H is the bench height and B is the burden (m).

The objective of a blast design is to determine the variables of the blast pattern, which are spacing, burden, sub-drill and stemming length. To achieve a suitable interaction between the rows of holes, the spacing to burden ratio (**a = S/B**) must be between 1.0 and 1.5 with 1.15 being an equilateral triangle with a staggered pattern. Equation 4 can be manipulated to determine the burden when estimating the powder factor.

$$\mathbf{B} = \sqrt{\frac{\mathbf{M} * (\mathbf{H}-\mathbf{T})}{\mathbf{a} * \mathbf{PF}_{tech} * \mathbf{H}}} \quad \text{.....(5)}$$

Where a is the spacing to burden ratio (S/B), and T is the stemming length; thus, Le is the charge length given by H bench height minus the T stemming length. The sub-drill is only considered when calculating the actual powder factor, which is essential for calculating the exact amount of explosives used. Table 2.3 depicts the generally accepted powder factors for different rock types.

Table 2.3: Typical technical powder factor for different rock type.

Adapted from de Graaf (2010)

Blasting Category	Rock Type	Technical Powder Factor (kg/m^3)
Very hard	Norite	0.85 to 1.2
Hard	Granite	0.65 to 0.85
Medium	Sandstone	0.35 to 0.65
Soft	Shale	0.25 to 0.35
Very soft	Coal	0.15 to 0.25

2.4.5 Explosives Strength

Comparing explosives' energy from different manufacturers is difficult because, these manufacturers use different computer models such as Project, Fortran-BKW and Vixen to calculate the energy released by their explosives. A more comparable indication of the strength of the explosive is the relative weight strength 'RWS' (School of Mining, 2019). The RWS compares the calculated energy of a unit mass of explosive with the calculated energy of a unit mass of the ammonium nitrate fuel oil-based explosive (ANFO) at a density of 0.8 g/cc. The RWS value is calculated by:

$$\boldsymbol{RWS} = \frac{\textbf{Explosive Energy of Explosive}}{\textbf{Explosive Energy of equal mass of ANFO}} * \mathbf{100} \quad \text{..... (6)}$$

In the explosive's detonation theory, the amount of energy released by the explosive is calculated using Tidman's equation 7:

$$\mathbf{E_s} = \left(\frac{\mathbf{VoD_e}}{\mathbf{VoD_n}}\right)^{\mathbf{2}} * \mathbf{RWS} \quad \text{.....(7)}$$

Where Es is the effective power by relative mass of an explosive; VoD_e is the speed of the effective explosive detonation (measured in the field); VoD_n is the nominal velocity of the detonation of the explosive (m/s). All the components of the Tidman's equation are used in the explosive component of the blast fragmentation model

2.5 Fragmentation Modelling

The primary objective of any rock blasting activity is to deliver the size fragment that meets plant specifications, allows for efficient mining operations and delivers material that is safe to handle during load and haul operations.

2.5.1 The Kuznetsov Function

Cunningham (1983) proposed an empirical model named the Kuz-Ram model, which predict the distribution of the rock fragment size. The Kuz-Ram model was developed from the work concluded by Kuznetsov (1973) in estimating the mean fragment size (X_{50}) and the Uniformity Index (n). Rosin-Ramler (1933) developed the function which incorporates Uniformity Index (n) in the prediction of the blasted material size distribution around the Rosin-Ramler profile.

Rosin-Ramler (1933) function describes the particle size distribution over the entire fragmentation range (McKee, 2013). Kuznetsov (1973) formulated his equation based on field investigations and other published data that related the mean fragment size (X_{50}) to the volume of rock to be broken and the relative weight strength of explosives.

The mean fragment size related the applied energy per broken volume of rock over powder factor as a function of rock type (Kuznetsov, 1973). Kuznetsov equation expresses the mean fragment size as:

$$\mathbf{X_m} = \mathbf{A}\left(\frac{\mathbf{V_o}}{\mathbf{Q_T}}\right)^{\mathbf{0.8}} \mathbf{Q_T}^{\mathbf{1/6}} \text{.....(8)}$$

Where, Xm or X50 is the mean fragment size in centimetres (cm), A is the rock constant factor, VO is the volume of rock broken per hole [$\boldsymbol{Vo}$ = B x S x H (m3)], Q_T is the mass (kg) of TNT containing the energy equivalent to the explosive charge in the blast hole.

TNT is expressed as ANFO strength by using the relative weight strength of TNT compared to ANFO of 115. ANFO relative strength is 100. Equation 8 can be altered to:

$$\mathbf{X_m = A\left(\frac{V_o}{Q_e}\right)^{0.8} Q_e^{1/6}\left(\frac{S_{ANFO}}{115}\right)^{-19/30}} \text{.....(9)}$$

Where, Q_e is the mass of explosives used in (kg), $\mathbf{Q_e = M \times L_e}$ is the numerator in the powder factor Equation defined in Equation 5. S_{ANFO} is the weight strength of ANFO.

But: $\mathbf{\frac{V_o}{Q_e} = \frac{1}{K}}$

Where, K is the powder factor, $\mathbf{K = PF_{tech}}$ as defined by Equation 5. Then Equation 9 becomes:

$$\mathbf{X_m = A(K)^{-0.8} Q_e^{1/6}\left(\frac{115}{S_{ANFO}}\right)^{19/30}} \text{.....(10)}$$

Where now, the mean fragment size (X_m) is compared with the given powder factor. The Kuz-Ram model has since its introduction in 1983 been surpassed by a more complex model such as Swebrec function (McKee, 2013). The prediction of the blast size distribution from coarse to fine fragments was more accurate with the Swebrec function. However, the Kuz-Ram model remains popular due to its reasonable approximation of fragments size distribution and ease of application (McKee, 2013).

2.5.2 Rosin-Rammler Function

Rosin and Rammler (1933) developed an equation that characterised the particle size distribution of blasted material. The Kuz-Ram equation is accurate in predicting the average fragment size (X_m). However, it was essential to consider the entire fragment size distribution to obtain the 80% material pass. To achieve this, Cunningham (1983) used the Rosin-Rammler equation together with the Uniformity Index.

$$\mathbf{R = e^{-\left(\frac{x}{x_c}\right)^n}} \text{.....(11)}$$

Where R is the fraction of material larger than x (the screen size), x_c is the constant called the characteristic size, n is the Uniformity Index, and e is the base of a natural log = 2.7183.

The Uniformity Index values range between 0.6 and 2.2, where 0.6 represents a muck pile with no uniform distribution (fines and large boulders) and 2.2 represents a uniform muck pile with the bulk of material close to mean fragment size (Clark, 1987).

Given that the Kuznetsov equation accounts for explosive strength and rock mass properties, and that, the mean fragment size is related to the characteristic fragment size, the Rosin and Rammler equation can be modified. When there is 50 percent of the material passing through the sieve, R equals 0.5. The mean fragment size is expressed by x_m or x_{50} then:

$$\mathbf{x_C = \frac{X_m}{(0.693)^{1/n}}} \quad \textbf{.....(12)}$$

The above equation represents material retained on the sieve, and the equation can be modified to represent material passing given by:

$$\mathbf{R_m = 1 - e^{-0.693\left(\frac{x}{x_{50}}\right)^n}} \quad \textbf{.....(13)}$$

Where R_m is the percentage passing, x is the mesh sieve size, and the only unknown in the equation is the uniformity index (n). Figure 2.5 depicts a typical fragmentation size distribution curve

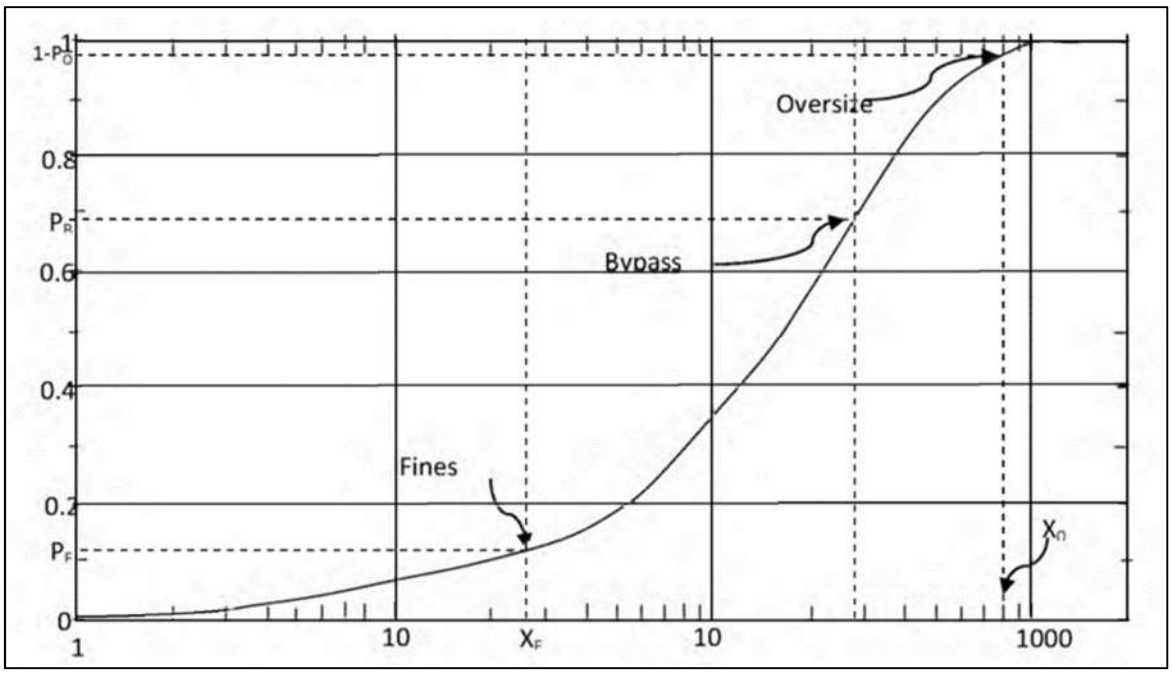

Figure 2.5: Example of a fragmentation distribution curve (Solomon, 2015)

2.5.3 The Uniformity Index Function

Cunningham (1983) determined the range of values of the Uniformity Index by observing the impact the blast design parameter had on the value of the index using a square blast pattern. The exponent (n) in the Rosin and Rammler equation is expressed by:

$$\mathbf{n} = \left(\mathbf{2.2} - \mathbf{14}\frac{\mathbf{B}}{\mathbf{D}}\right)\left[\frac{\mathbf{1}+\frac{\mathbf{S}}{\mathbf{B}}}{\mathbf{2}}\right]^{\mathbf{0.5}}\left(\mathbf{1} - \frac{\mathbf{W}}{\mathbf{B}}\right)\left(\frac{\mathbf{L}}{\mathbf{H}}\right) \quad \textbf{.....(14)}$$

Where, B is the burden (m), D is the diameter of the blast hole (mm), S is the spacing (m), W is the standard hole deviation (m), L is the charge length (m), H is the bench height (m).

Cunningham (1987) observed that there was a 10 percent increase in the value of 'n' when using a staggered pattern. When desiring uniform fragmentation, high values of 'n' are preferred (Cunningham, 1987).

Cunningham (1987), as cited in Tucker (2015), observed the following results when determining the Uniformity Index:

- "The normal range of 'n' for blasting fragmentation in the reasonably competent ground is from 0.75 to 1.5, with the average being around 1.0. The more competent rocks have higher values of Uniformity Index.
- Values of 'n' below 0.75 represent a situation of "dust and boulders" which, if it occurs on a wide scale in practice, indicates that the rock conditions are conducive to control fragmentation through changes in blasting. Cunningham (1983, 1987) observed that "dust and boulders" typically happen when stripping overburden in the weathered ground.
- For values below 1.0, variations in the Uniformity Index 'n' are more critical to oversize and fines. For n = 1.5 and higher, muck pile texture does not change much, and errors in the judgment are less punitive.
- The rock at a given site will tend to break into a particular shape. These shapes may be loosely termed "cubes," "plates," or "shards." The shape factor has an essential influence on the results of the sieving test, as the mesh used is generally square, and will retain the majority of fragments having dimensions higher than the mesh size."

2.6 Blast Efficiency

Blast efficiency is the percentage ratio that relates to the expected mean fragmentation results from the Kuz-Ram model to the actual mean fragmentation result achieved. The actual fragmentation size results are obtained from the analysis of a series of blast fragmentation images (Kulula et al., 2017). The equation used to calculate the blasting efficiency ratio is expressed as:

$$\textbf{Blasting effeciency} = \frac{\mathbf{AF}}{\mathbf{EF}} * \mathbf{100} \quad \textbf{.....(15)}$$

Where, AF = Actual mean block fragmentation from the scaled image analysis. EF = expected mean fragmentation from the Kuz- Ram model.

The blast efficiency equation is used to compare the actual fragmentation results against the predicted fragment results; the difference between the two represents the error between the two results. Knowing this error is essential because one could then adjust the Blastability Index (equation 1) by introducing Lilly's correction factor 'C(A)' for the index. Equation 16 would then give the final Blastability Index equation

$$\mathbf{A = 0.06\ x\ (RMD + JF + RDI + HF)} \textbf{ * C(A) .....(16)}$$

The correction factor C(A) would normally be between 0.5 to 2 (Cunnignham, 2015). The other alternative is to use the Uniformity Index parameters such as burden, spacing or powder factor to narrow the difference between the predicted results and actual results, thus refining the prediction model for the next blast. The adjustment is made by choosing one parameter at a time, and changing the value and assessing the fit of the curve with the actual fragmentation curve.

2.7 Cost Modelling

Costs are an integral component of any business venture. A variety of activities in a business generates associated costs. For companies to create value, they must be able to identify and optimise their costs, improve their efficiency and increase their productivity. There are different types of expenses that any business will incur. Types of costs discussed are:

- Direct costs: These costs, by definition, are the expenses that any company can easily connect to a specific cost element. These are labour costs, supervision, power, fuel, equipment replacement, maintenance, and consumables (Anon, 2018).

- Indirect costs are also known as owning costs; these costs are not related to production units. They are composed of investments and depreciation as governed by the host country's tax policies and regulation (Anon, 2018).

Several methods are used to calculate costs, such as the actual costs/actual output, average costs, first in first out, and specific identification (Anon, 2018). The most common and natural of the methods to apply is the actual cost/actual output method. This method is the ratio between actual costs and actual production, resulting in unit cost.

The costs discussed in this research focus only on drilling and blasting costs using the actual costs/actual output method. The reasons for preferring this particular method was that, first, mining activities are contracted out, and the contractor provides unit mining rates. Secondly, there was no access to the contractor financial data to compute the individual elements of the unit cost. As such, the theory behind the calculation of drilling costs was provided for academic purposes

2.7.1 Drilling Costs

The drilling costs are made up of a combination of different costs components. These components are both the direct costs and the indirect costs. The costs of drilling are in cost per metre drilled ($/m). Jimeno et al. (1995) as cited by Rajpot (2009) developed the equation to relate both the direct and indirect costs components. The drilling costs are given by:

$$C_{TD} = \frac{C_A + C_i + C_M + C_O + C_E + C_L + C_B}{P_R} \quad \text{.....(17)}$$

Where Indirect costs components are C_A and C_i, C_A is the depreciation rate ($/h), C_i is the insurance and interest rate. The remaining elements of the equation are direct costs. C_M is the Repair and maintenance ($/h), C_O is the labour ($/h), C_E is the energy or fuel ($/Kwh) or ($/L), C_L is the oil, grease, and filters ($/h), C_B is the rods, bits, and

shanks ($/h) and the P_R is the productivity (m/h) (Rajpot, 2009). When developing drilling cost rates, it is imperative to deconstruct the equation into its components of direct and indirect costs.

a) Direct Costs:

Maintenance costs (C_M): The maintenance costs consist of two components: preventative maintenance and repairs. The maintenance costs are made up of the total costs of lubricants, filters, labour and grease (Rajpot, 2009). These costs are usually between 15% to 20% of the power costs of the machine and are expressed as mechanical availability (Rajpot, 2009). The mechanical availability was given by operating hours divided by total operating hours plus the maintenance hours.

The repair costs are calculated by multiplying the delivered price of the machine and the interpolation factor, then divided by the useful life of the machine (Rajpot, 2009). Therefore, the costs of preventative maintenance and repairs is given by:

$$\mathbf{C_M = [purchase\ price/1000] * F_r}\ (\%) \quad \textbf{.....(18)}$$

Where, FR is the reparation factor (given by manufacturers) and must include the cost of spares and maintenance (Rajpot, 2009).

Operating Costs (C_O): These costs are made up of direct labour costs of drillers and their helpers, and it includes their fringe benefits (Rajpot, 2009).

Fuel and Energy Costs (C_E): These costs depend on the type of energy source used by the machine. These sources of power are either electric or fossil fuel (Rajpot, 2009).

$$\mathbf{C_E = Power\ hp\ x \left(\frac{litres}{Hp}\right) * \$/L} \quad \textbf{.....(19)}$$

$$\mathbf{C_E = Power\ Kwh * \$/Kwh} \quad \textbf{.....(20)}$$

Costs of Consumables (C_M): The nature of the rock being drilled through influences the cost of consumables such as sleeves, bits, shanks and hammers. Harder rocks have a greater impact on costs. The consumption of the consumables mentioned above usually costs between 15 to 40 percent of the total drilling costs (Rajpot, 2009).

The cost of the pipes are calculated by Equation 21.

$$\mathbf{L_m = d_l * \left[\frac{d_l + L_p}{2L_p}\right]} \quad \textbf{.....(21)}$$

Where L_m is the length of pipe in metre, d_l is the length of blasthole and L_p is the length of the pipe in metres. The cost of the bits and hammer is calculated as a total cost divided by the useful life of the consumable. The tricone bit life is given by (rotary drill machine):

$$\mathbf{Life(m) = \frac{28.14 * d^{1.55} * E_d^{-1.67}}{N_r} * 3V_d} \quad \textbf{.....(22)}$$

Wher d is the diameter (inches), E_d is the pull-down force on the bit (kN), N_r is the rotary speed (r/min), and V_d is the penetration rate (m/h)

b) Indirect Costs

Insurance and interest rate cost (C_i): Jemeno (1995) developed an equation for calculating this cost and is given by:

$$\mathbf{C_I = \frac{\frac{N+1}{2N} * P_p * (I + I_n + T)\%}{W_h}} \quad \textbf{.....(23)}$$

Where N is the service life years, P_p is the purchase price; I is the interest rate, I_n is the insurance, T is the taxes and W_h is the work hours per year.

Depreciation Cost (C_A): Garrison (1991) as cited by Rajpot (2009) defines depreciation as "deterioration produced by use and due to ageing and loss of value. Depreciation is closely tied to the useful life of an asset, with year by year depreciation deductions typically computed by a variety of method." Salvage value is subtracted from the asset cost, and only the remainder is depreciated (Rajpot, 2009). Wagner (1987) developed the equation for calculating machine depreciation costs, as shown by Equation 24.

$$\textbf{Hourly depreciation cost} = \mathbf{\frac{Total\ delivered\ price}{Total\ useful\ hours}} \quad \textbf{.....(24)}$$

This equation does not account for resale or salvage value. Therefore the total ownership costs are given by:

Total hourly owning costs = Hourly investment cost (CI) + Hourly depreciation cost ……. (25)

The author was assured by the contractor representatives that the cost equations stated in section 2.6 are indeed correct and that they are using them in determining the drilling rates to be charged to Ruashi mine.

2.7.2 Single Blast Hole Cost

When calculating the cost of one blast hole, the cost equation must incorporate both the explosives and accessories cost per hole and the drilling cost per hole drilled. The cost equation per hole is thus given by Equation 26

$$\textbf{Cost per blast hole} = \{[(\mathbf{M} * \mathbf{L_e}) * \textbf{unit cost explosives}] + \textbf{accessories cost per hole}\}$$

$$+ [\textbf{drilling cost per meter} * \textbf{hole length}] \ldots\ldots\ldots\ldots\ldots\ldots\textbf{(26)}$$

Where M is the mass of explosives per metre, L_e is the length of charge.

The total cost of drilling and blasting is, thus, the cost per blast hole multiplied by the number of holes to get the total cost per blast polygon. Depending on the pattern used and the drill hole diameter used, the total cost per polygon is expected to vary.

2 .8 Chapter Summary

This chapter outlined the different fundamental theories applied in drill and blast operations. In particular, the application of theories such as the Kuz-Ram model in determining the blast fragmentation size distribution based on the influence of the different parameters such as rockmass condition, blast design geometry, and explosive properties. The chapter further provided the foundation for modelling the drilling costs and explosives cost, which, when combined form the overall drill and blast costs model for any size fragment distribution.

CHAPTER 3

Research Methodology

3.1 Introduction

This particular section of the report will focus on the data collection methods, data tools, analysis tools that were used in the application of the Kuz-Ram fragmentation on the three test sites selected in Ruashi mine. Three test sites were chosen based on the different rockmass condition from massive to friable conditions, with varying hardness factors and density. The Monte Carlo Simulation technique was used to determine the optimal blast size distribution given the varying blast geometric patterns and the different rockmass characteristics. Image analysis was used to compare and validate the blast design properties based on the actual results received.

3.2 Data Collection

Data collection is the process of gathering specific information that is required to answer the research questions (Babbie, 2004). There are several issues associated with data collection, including the use of primary or secondary data, research design, sampling (Babbie, 2004). Data can be primary or secondary, and whether one or both are used, and which is used, depends largely on the research question and the availability of these data sources (Davies, 2004). Primary data refers to the first-hand physical collection of data the researcher will collect to answer the research question. In contrast, secondary data would be data gathered from others or other studies.

Naturally, a descriptive quantitative study involves measuring one or more variables in some way (Leedy, 2015). The collection of data is essential in ensuring that the data is captured correctly, and the information can be used to answer the research question. The data collected for blast fragmentation modelling had three main categories: rock mass characteristics, blast design geometry, and explosives properties. These three listed categories, within them, contain some variable inputs parameters that can influence the blast fragmentation process. The data collected in both the pre blasting stage and the post blasting stages will differ in both nature and purpose.

3.2.1 Pre Blasting Data Collection

The data collected at this stage is used to design an effective and efficient blast for the prevailing rock conditions. Information gathered concerning the rockmass includes geological mapping, rockmass characteristics such as rock type, rock density, uniaxial compressive strength, joint spacing, and joint orientation. Data is collected using joint mapping and geotechnical data logging.

The explosive properties contain information such as; the type of explosives to use (emulsion or ANFO), density, explosives strength and the velocity of detonation. The overall pit environmental conditions (wet or dry) is also an essential factor to consider in determining the type of explosives to be used. The proximity of Ruashi pits to community settlements necessitate for the establishment of additional safety precautions to reduce and prevent fly rocks, excessive ground vibration, noise, and dust from impacting the community.

To this end, the establishment of a safe blast zone is critical to the operations. Before any blast can be conducted, an evacuation notice and blast plan are circulated within the community and spotters made up of members from the community are allocated and stationed at various predetermined locations in the settlement.

3.2.2 Post Blast Data Collection

Concerning the blast result, data collected at this stage consist of information such as heave height, throw distance, diggability of material, fragment size distribution, back break extension on the bench and pit floor condition. In adhering to community safety obligations, pictures of damaged infrastructure and reports of any safety incidents are recorded together with data received from a blast monitoring system.

Methods used to collect some of the data used in the post-blast analysis consist of a video recording of the blast, images of fragmentation size distribution, recordings from the vibration monitoring system and records of actual costs incurred.

3.3 Rockmass Properties Data for Test Sites

Ruashi mine commissioned a geotechnical study in 2011 to investigate the influence of rockmass properties and weathering on the pit slope design. The geotechnical drilling focused on the southern side of Ruashi-3 and Ruashi-2. The analysis of geotechnical information recovered from boreholes RGT3 to RGT9 (drilled in Ruashi-3) showed some of the following results (see Appendix B for details):

- The rock mass rating (RMR) improved with depth from the surface.
- Weathering is extensive at shallow elevations above 1200 mRL (reduced metre level).
- The transition zone is highly fractured and slightly weathered
- The moisture content decreased with an increase in rock density.
- The friction angle of the rock increased with increasing density of the rock

Figure 3.1 depicts the position of the geotechnical holes relative to Ruashi-3 and weathering zone.

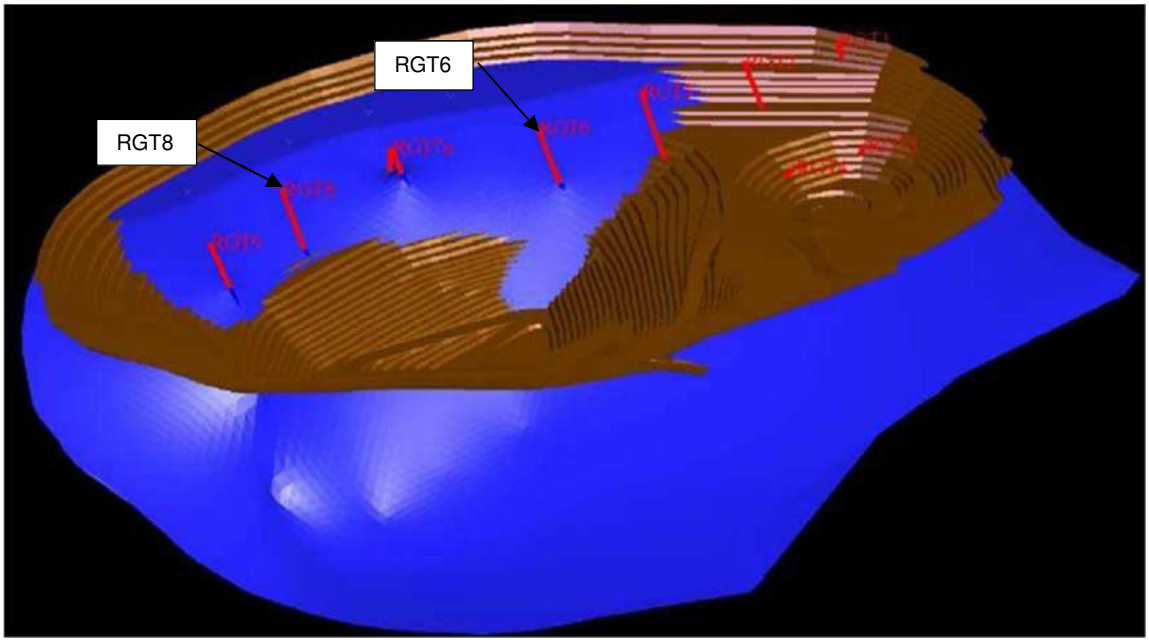

Figure 3.1: Geotechnical boreholes relative to Ruashi-3 design (brown) and the fresh-weathered contact (blue)

The most common rock types encountered in the Ruashi pits are dolomite, siltstone, shale, sandstone, and breccia. Figure 3.2 provides a visual depiction of the rock

quality from cores recovered from the transition zone (sample-A: from RGT6) and fresh domains (sample-B: from RGT8) carried out in Ruashi-3.

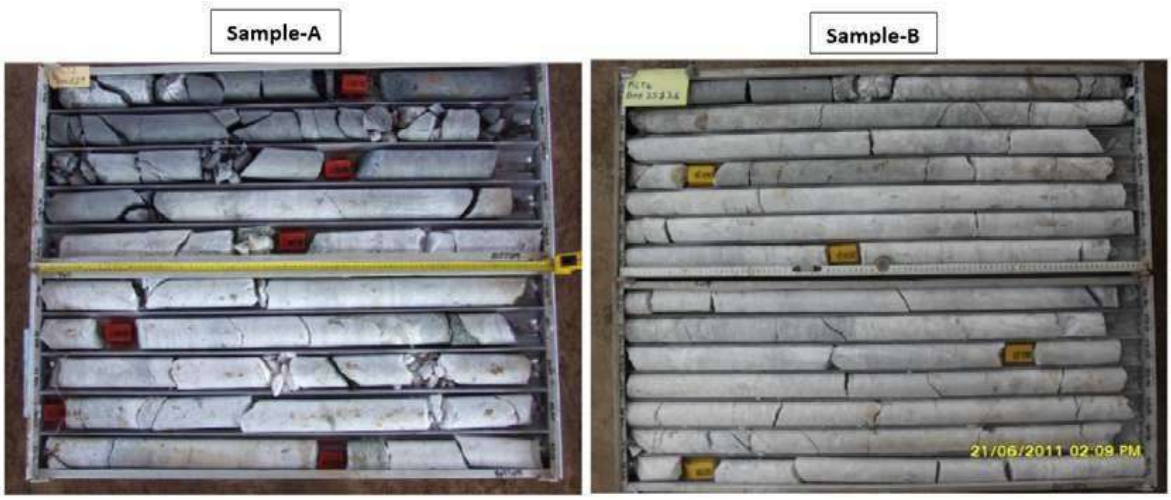

Figure 3.2: Core samples from boreholes RGT6 and RGT8

A summary of the rock strengths and densities of the different rock types is outlined in Table 3.1 (for detailed results see Appendix B, Table B2).

Table 3.1: Ruashi rock properties

Rock Types	UCS (MPa)	Elastic Modulus (GPa)	Density (kg/m^3)
Shale	42	35	2.31
Siltstone	63	14	2.66
Sandstone	88	60	2.73
Breccia	82	55	2.42
Dolomite	79	53	2.71

Given the results of the geotechnical study report as summarized earlier, three test sites were chosen, namely Pit3_South-East, Pit3_South, and Pit3_South-West. Table 3.2 provides a summary of the rockmass data for each test site selected for the study.

Table 3.2: Summary of rockmass conditions

Ruashi_3	South-East	South	South-West
Rock-type	Sandstone & Dolomite	Sandstone & Siltstone	Shale & Breccia
Density (Kg/m^3)	2.70 to 2.73	2.66 to 2.73	2.31 to 2.42
Average UCS (MPa)	84	76	62
Average Elasticity (GPa)	56	38	45
RMD	Solid / Massive	Slightly fractured to Massive	Fractured and Blocky
JPS	Closed	Intermediate	Moderate Separation
JPO	Horizontal	Out of Face	Normal to Face
Blastability Category	Medium	Medium	Soft

There were no test sites planned for the northern side of the Ruashi_3 because areas in this part of the pit were mainly free dig areas. Figure 3.3 depicts the position of the blasting areas in Ruashi_3 relative to weathering domains as indicated by the legend.

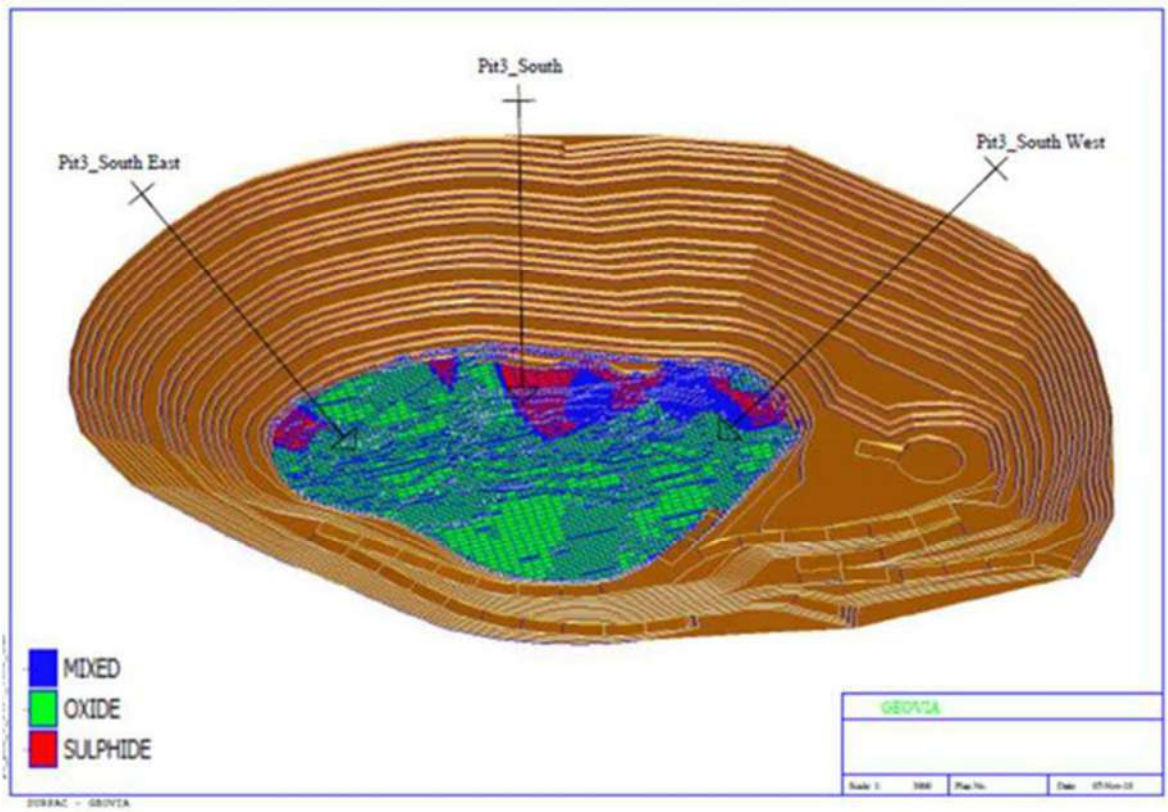

Figure 3.3: Blast site locations relative to different weathering domains

Each test location was planned to have a minimum of three blasts performed with a total of nine blasts. However, in the end, eleven tests were done for the entire study. The rationale to conduct test blasts in different rockmass characteristics and

weathering domains was to establish a suitable blast pattern that will cater to the prevailing and predominant rockmass conditions and deliver optimum blast fragment size.

The rockmass is not a homogeneous and isotropic piece of material. It contains some variabilities ranging from rock strength, joint spacing, hardness, elasticity, and joint orientation. Particular attention must be placed in understanding the interaction of variables such as joint spacing, rock hardness, and explosive energy. This relationship can have a significant effect on the blast size fragment distribution.

3.4 Blast Design Process

When constructing a blast design layout, it is imperative to consider the prevailing rock mass condition. This consideration is essential in assisting the design process in determining the choice of explosives to use, the burden and spacing requirements, and blast direction relative to the predominant joint sets.

Depending on the size of the blast area and the different types of lithology encountered, one could have different blast patterns for different rock mass conditions, or the blast pattern can be tailored to fit the hardest rocks encountered in the blast zone. Figure 3.4 outlines the general process followed in the design of the blast

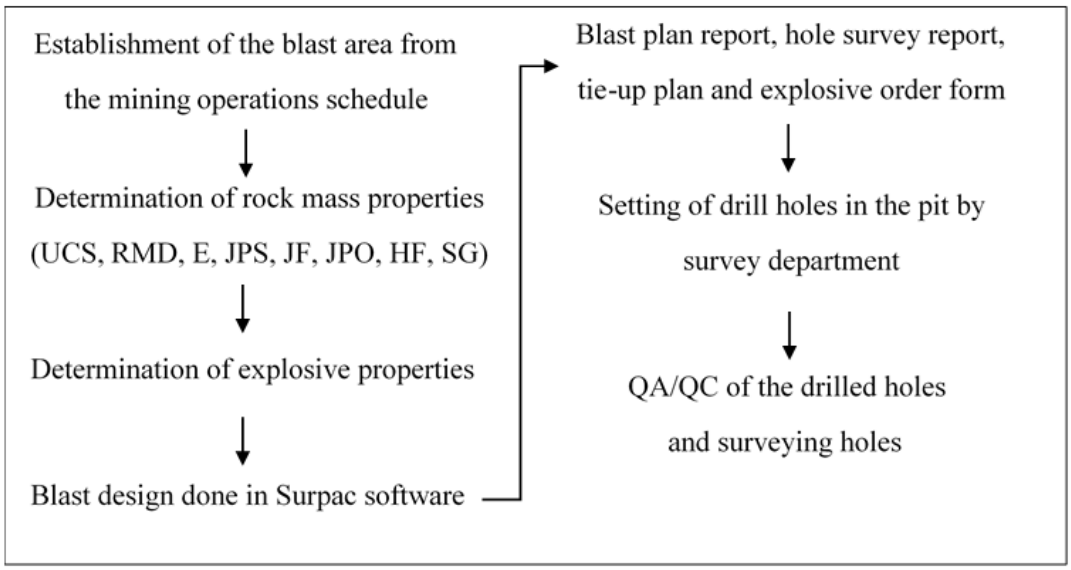

Figure 3.4: Blast plan process flowsheet

Table 3.3 represents the blast patterns together with the simulation conditions that were used for the respective simulation scenarios in each of those areas.

Table 3.3: Blast patterns with simulation conditions

Ruashi_3	South-East	South	South-West
Burden (m)	3	2.5	2
Spacing (m)	3	2.5	2
Bench height (m)	5	5	5
Powder factor (kg/Bcm)	0.65	0.35 to 0.65	0.30
Simulation condition	Dynamic burden, spacing and powder factor. Bench height fixed.	Fixed burden and spacing. Dynamic powder factor. Bench height fixed.	Fixed powder factor. Dynamic burden and spacing. Bench height fixed.
Number of actual blasts performed	3	4	3

To achieve fair to good blasting results that produce the desired blast fragment size with a minimum air blast, reduced fly rocks incidents and reasonable ground vibration, the value of the bench stiffness ratio should be between two and three. The restrictions placed upon the bench height in Ruashi mine meant that the 5m bench height could not be changed and will be maintained. The bench stiffness ratio (SR = H/B), as shown in Table 3.4 was used to design the geometric blast pattern for Ruashi mine.

Table 3.4: Burden to stiffness ratio

Burden, m	Bench Height, m	SR
1.0	5	5.0
1.5	5	3.3
2.0	5	2.5
2.5	5	2.0
3.0	5	1.7
3.5	5	1.4
4.0	5	1.3

Given that the bench height at the mine is 5m, the recommended burden range is between 1.5m to 2.5m. The blast pattern at mine generally alternates between staggered pattern (S/B = 1.1) and square pattern (S/B =1). Table 3.5 outlines the minimum and maximum spacing for both the square and staggered blast pattern.

Table 3.5: Burden to spacing ratio

Square Pattern		
Burden, m	**Pattern**	**Spacing, m**
1.5	1	1.5
2.0	1	2.0
2.5	1	2.5
Staggered Pattern		
1.5	1.1	1.65
2.0	1.1	2.20
2.5	1.1	2.75

The drill diameter used at the mine is 105mm and 127mm depending on the rockmass encountered. The stemming length depends on the nature of the stemming material used. The stemming material generally used is the drill chips. However, crushed rock may be used at times. The general rule for the stemming length is 0.7 times the burden for crushed rock and 1.2 times the burden for drill chips.

Stemming length, together with the stemming material, is crucial in the rock fragmentation process. Stemming ensures that the explosive energy is contained within the rockmass to have a maximum effect in breaking the rockmass. The geometric blast pattern parameters such as burden, spacing, stemming length, charge length can have a significant degree of variability, which could influence the blast results both positively or negatively.

3.5 The Kuz-Ram Model population

Cunningham (1983, 1987), Rosin and Ramler (1933), Kuznetsov (1973) and Lilly (1986) are some of the researchers who had a profound impact on the development of predictive blast fragmentation models used widely in the mining industry. Chapter 2 of this report outlines in detail the theories and equations used in the development of the Kuz-Ram model. In short, the model predicts fragmentation from blasting in terms of the mass percentage passing through the screen or mesh size.

The challenge the operators encounter in using any of the models (even latest models) generally consists of the following issues:

- Definition of the rockmass properties.

- Establishing relevant explosive's performance indices.
- Determination of actual blast fragmentation.

There are two essential equations which form the necessary foundations of the Kuz-Ram model. They are the modified Kuznetsov and the Rosin-Rammler equations (Denoted by Equation 10 and 13 respectively). The crucial parameters in determining the mean particle size by the Kuz-Ram model are rock factors and explosive's properties. The fragmentation distribution by Rosin-Ramler depends on both the mean fragment size and the blast pattern deployed in the blasting practice. Microsoft Excel was used to establish the Kuz-Ram model, as shown in Table 3.6.

Table 3.6: Kuz-Ram model

1. Intact Rock Properties		
Rock Type	Dolomite and Sandstone	
Rock Specific Gravity	2.72	SG
Elastic Modulus	56	GPa
UCS	83.5	MPa
2. Jointing		
Spacing	0.1	m
Dip	40	deg
Dip Direction	0	deg
In-situ block	0.3	m
3. Explosives		
Density	1.1	SG
RWS	100%	(% ANFO)
Nominal VOD	4800	m/s
Effective VOD	4500	m/s
Explosive Strength	0.88	
4. Pattern Design		
Hole Diameter	102	mm
Charge Length	2.5	m
Burden	2.5	m
Spacing	2.5	m
Drill Accuracy SD	0.1	m
Bench Height	5	m
Stemming length	3	m
Mass per Meter	8.98	kg/m
Broken Volume	34.38	m3
Powder Factor	0.65	kg/tonne
Charge Density	0.65	kg/m^3
Charge Weight per hole	22.46	kg/hole
5. Kuz-Ram Model		
Blastability Index, A	5.67	
Average Size of Material, X_{50}	16	cm
Uniformity Exponent, n	1.19	
Characteristic Size, Xc	0.22	m
6. Predicted Fragmentation		
Percent Oversize	6.7%	m
Percent In Range	60.3%	m
Percent Undersize	33.0%	m
7. Fragmentation Target Parameters		
Oversize	0.5	m
Optimum	0.3	m
Undersize	0.1	m

The model consists of seven sections. The first and second section contains rockmass parameters which have been collected from geological mappings and geotechnical report, as shown in Figure 3.2 and Table 3.2.

The third section contains explosive properties data provided by the manufacturer of the explosives. The velocity of detonation and explosives strength have a significant impact on the rock breaking process. These factors could be varied in the simulation work to determine their influence on the powder factor and the mean fragment size when maintaining a constant burden to spacing ratio.

The fourth section contains blast geometric parameters such as the burden, spacing, stemming and charge length and the resultant powder factor. The burden and spacing could be varied while maintaining a constant powder factor to determine the mean fragment size. The converse could be done by modifying the powder factor and keeping a constant burden to spacing ratio.

Section five deals with the Kuz-Ram parameters achieved by the blast pattern and the powder factor. These parameters then feed directly into the Rosin-Rammler size fragment distribution. A comparison of the predicted blast distribution results with the actual results achieved from image analysis was made to determine the relationship between the simulation and the actual results.

Section six deal with the proportion of the blasted material within the stipulated categories of minimum, maximum, and optimum size. While section seven allows for the target parameters to be specified. In this case, Ruashi mine specified that undersize material is <10cm, the optimal size is 30cm and oversize is >50cm. The objective was to ensure that 80% of the material is below 50cm, and at least 50% of the material is near 30cm (optimal size).

After determining the Rosin-Rammler parameters such as the Blastability Index (A) and the mean fragment size (x_{50}), it is now possible to construct a cumulative percentage graph of particle sizes passing through a predetermined mesh size. The Rosin-Rammler model produced a cumulative fragmentation size distribution, as depicted in Figure 3.5.

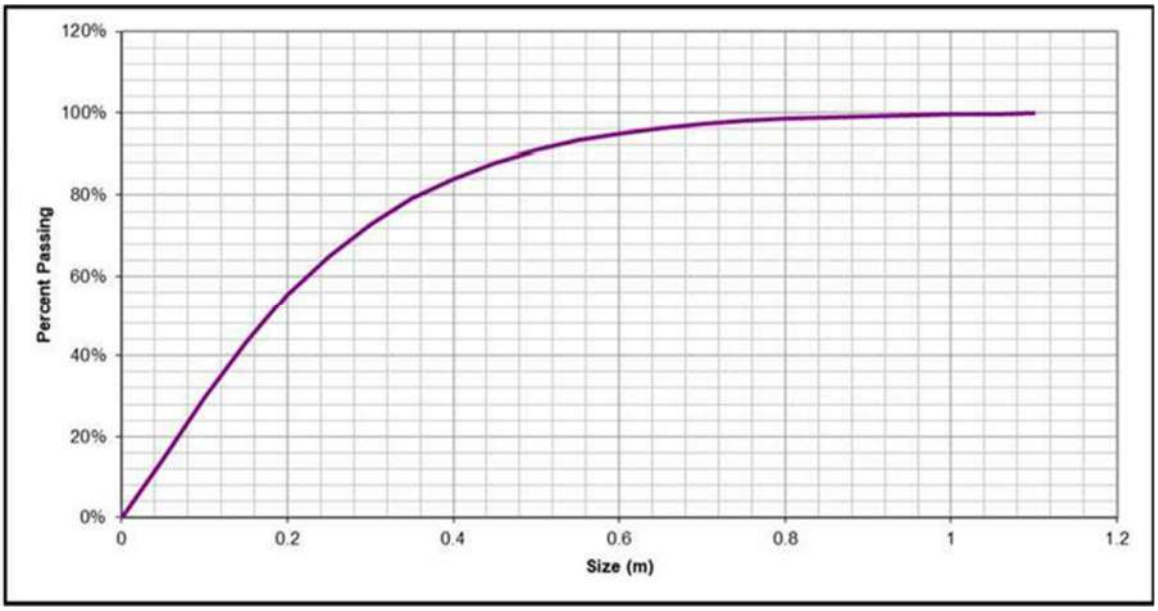

Figure 3.5: Cumulative percentage passing graph

The blasting engineer can choose to categorize his muckpile size distribution into three size fragment categories, undersize, optimum size, and oversize. The undersize fragment is the lower bound size or finer fragment size; the oversize is the upper bound or coarser part of the blasting, and the optimum size is the most likely fragment size.

3.6 Monte Carlo Model Simulation

Monte Carlo simulation is merely a mathematical technique that accounts for uncertainty or risk in the quantitative analysis and decision-making processes. The method ascribes a probabilistic distribution to input values. Thus, the results of any model or study that are based on probabilistic inputs are themselves a probabilistic distribution.

Natural materials such as rocks are neither homogenous nor isotropic and tend to display some variability in their properties, i.e. joint spacing, hardness, rock strength, and elasticity. There are two types of variability, namely systematic and random. Stochastic methods such as Monte Carlo simulation is not suited for systematic variabilities, and hence, the kind of variables analysed here are random.

The drilling process also introduces some degree of variability in the blast design. These variables are in the form of hole deviation, irregular spacing to burden ratios and non-uniform hole depths. The effect of these variations could result in non-uniform blast fragment size distribution resulting in the muckpile consisting of a significant proportion of boulders and fines.

Monte Carlo simulation packages such as @Risk are very efficient in conducting hundreds of what-if scenarios where input data is given an appropriate statistical distribution to assess and quantify the output distribution. Figure 3.6 depicts the Monte Carlo Simulation process.

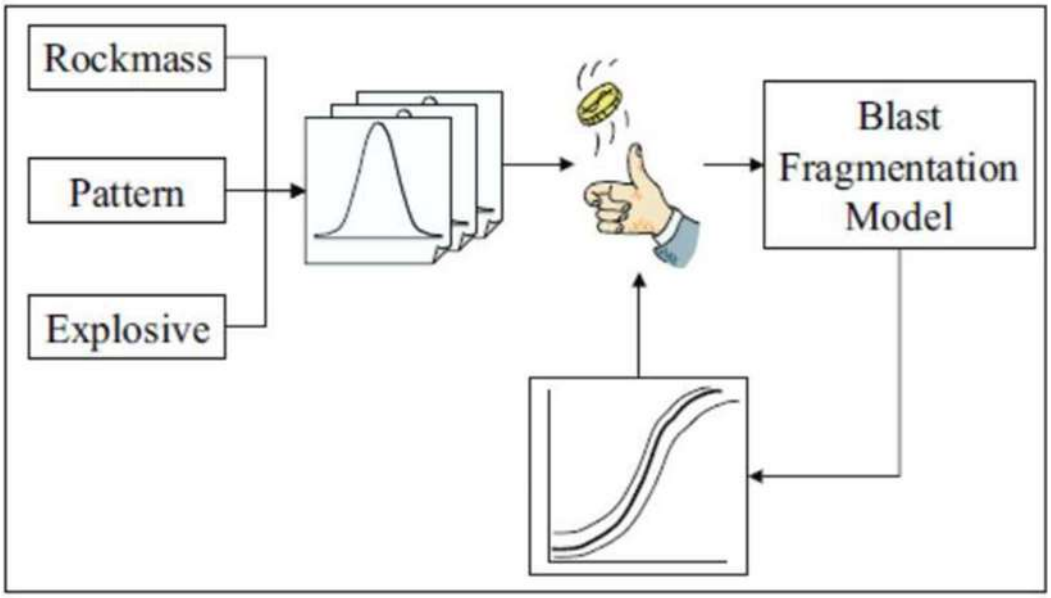

Figure 3.6: Monte Carlo simulation process (Thornton et al., 2001)

The blast fragment simulation process is as follows:

- The input data for explosives parameters, blast design parameters and rockmass characteristics were collected from a variety of sources such as lab reports, mappings and geotechnical reports.
- A suitable statistical distribution that carefully describes the variability is assigned, such as the triangular or normal distribution. For example, rockmass data and explosive data was assigned normal distribution or lognormal distribution, and the blast pattern design data was assigned triangular.
- A simulator is then run to determine a range of possible fragmentation size outcomes.
- The mean and confidence interval of the output results are provided at the end of the simulation work.
- A sensitivity analysis of inputs with a major influence on the outcome can be determined, and this assists in the decision-making processes.

Figure 3.7 depicts the input parameters that were assigned statistical distribution from Table 3.6 in order to perform the Monte Carlo Simulation process.

@RISK Model Inputs
Performed By: Lijojo
Date: Wednesday, 04 September 2019 13:10:39

Name	Worksheet	Cell	Graph	Function	Min	Mean	Max
Category: Burden							
Burden / 4. Pattern Design	Pit3_South_Cons t Pf min 0,35	B30		RiskTriang(1,5;3;3,5;RiskStatic(3))	1,50	2,67	3,5
Burden / 4. Pattern Design	Pit3_South_Cons t Pf max 0,65	B30		RiskTriang(1,5;3;3,5;RiskStatic(3))	1,50	2,67	3,5
Category: Dip							
Dip / 2. Jointing	Pit3_South_Cons t Pf min 0,35	B17		RiskNormal(10;1;RiskStatic(10))	-∞	10	+∞
Dip / 2. Jointing	Pit3_South_Cons t Pf max 0,65	B17		RiskNormal(10;1;RiskStatic(10))	-∞	10	+∞
Category: Dip Direction							
Dip Direction / 2. Jointing	Pit3_South_Cons t Pf min 0,35	B18		RiskNormal(207;20,7;RiskStatic(207))	-∞	207	+∞
Dip Direction / 2. Jointing	Pit3_South_Cons t Pf max 0,65	B18		RiskNormal(207;20,7;RiskStatic(207))	-∞	207	+∞
Category: Elastic Modulus							
Elastic Modulus / Dolomite	Pit3_South_Cons t Pf min 0,35	B13		RiskNormal(53;5,3;RiskStatic(53))	-∞	53,00	+∞
Elastic Modulus / Dolomite	Pit3_South_Cons t Pf max 0,65	B13		RiskNormal(53;5,3;RiskStatic(53))	-∞	53,00	+∞
Category: Explosive Strength							
Explosive Strength / 3. Explosives	Pit3_South_Cons t Pf min 0,35	B25		RiskNormal(0,88;0,088;RiskStatic(0,88))	-∞	0,88	+∞
Explosive Strength / 3. Explosives	Pit3_South_Cons t Pf max 0,65	B25		RiskNormal(0,88;0,088;RiskStatic(0,88))	-∞	0,88	+∞
Category: Hole Diameter							
Hole Diameter / 4. Pattern Design	Pit3_South_Cons t Pf min 0,35	B28		RiskTriang(95;105;127;RiskStatic(105))	95,00	109,00	127
Hole Diameter / 4. Pattern Design	Pit3_South_Cons t Pf max 0,65	B28		RiskTriang(95;105;127;RiskStatic(105))	95,00	109,00	127
Category: In-situ block							
In-situ block / 2. Jointing	Pit3_South_Cons t Pf min 0,35	B19		RiskLognorm(0,07;0,07;RiskShift(0,7);RiskStatic(0,7))	0,7	0,77	+∞
In-situ block / 2. Jointing	Pit3_South_Cons t Pf max 0,65	B19		RiskLognorm(0,07;0,07;RiskShift(0,7);RiskStatic(0,7))	0,7	0,77	+∞
Category: Rock Specific Gravity							
Rock Specific Gravity / Dolomite	Pit3_South_Cons t Pf min 0,35	B12		RiskNormal(2,71;0,271;RiskStatic(2,71))	-∞	2,71	+∞
Rock Specific Gravity / Dolomite	Pit3_South_Cons t Pf max 0,65	B12		RiskNormal(2,71;0,271;RiskStatic(2,71))	-∞	2,71	+∞
Category: Spacing							
Spacing / 2. Jointing	Pit3_South_Cons t Pf min 0,35	B16		RiskLognorm(0,005;0,005;RiskShift(0,05);RiskStatic(0,05))	0,05	0,06	+∞
Spacing / 4. Pattern Design	Pit3_South_Cons t Pf min 0,35	B31		RiskTriang(2;3;3,5;RiskStatic(3))	2,00	2,83	3,5
Spacing / 2. Jointing	Pit3_South_Cons t Pf max 0,65	B16		RiskLognorm(0,005;0,005;RiskShift(0,05);RiskStatic(0,05))	0,05	0,06	+∞
Spacing / 4. Pattern Design	Pit3_South_Cons t Pf max 0,65	B31		RiskTriang(2;3;3,5;RiskStatic(3))	2,00	2,83	3,5
Category: Stemming length							
Stemming length / 4. Pattern Design	Pit3_South_Cons t Pf min 0,35	B35		RiskTriang(1;1,2;4;RiskStatic(1,2))	1,00	2,07	4
Stemming length / 4. Pattern Design	Pit3_South_Cons t Pf max 0,65	B35		RiskTriang(1;1,2;4;RiskStatic(1,2))	1,00	2,07	4
Category: UCS							
UCS / Dolomite	Pit3_South_Cons t Pf min 0,35	B14		RiskNormal(79;7,9;RiskStatic(79))	-∞	79,00	+∞
UCS / Dolomite	Pit3_South_Cons t Pf max 0,65	B14		RiskNormal(79;7,9;RiskStatic(79))	-∞	79,00	+∞

Figure 3.7: Input parameters with respective statistical distributions

3.7 Application of the Simulator to the Study

One of the critical aspects of simulation is the knowledge or understanding of the kind of distribution the input data represent. There are three commonly used distribution, namely the normal distribution, pert distribution and triangular distribution. The pert and normal distribution have the mean (most likely value) and the standard deviation. Whereas the triangular distribution has the minimum value, most likely value and the maximum value.

The distribution to use or apply depends on the knowledge of the user and his intuition (very subjective), expert opinion or industry data. The rockmass and explosive parameters were assigned the normal and lognormal distribution. The author believed these statistical distributions best suited the input parameter data set. The triangular distribution was assigned to the blast design pattern because the minimum and maximum limits were known for parameters such as the burden, spacing, stemming and drill bit size. Figure 3.8 depicts the rock specific gravity results with normal distribution applied to them.

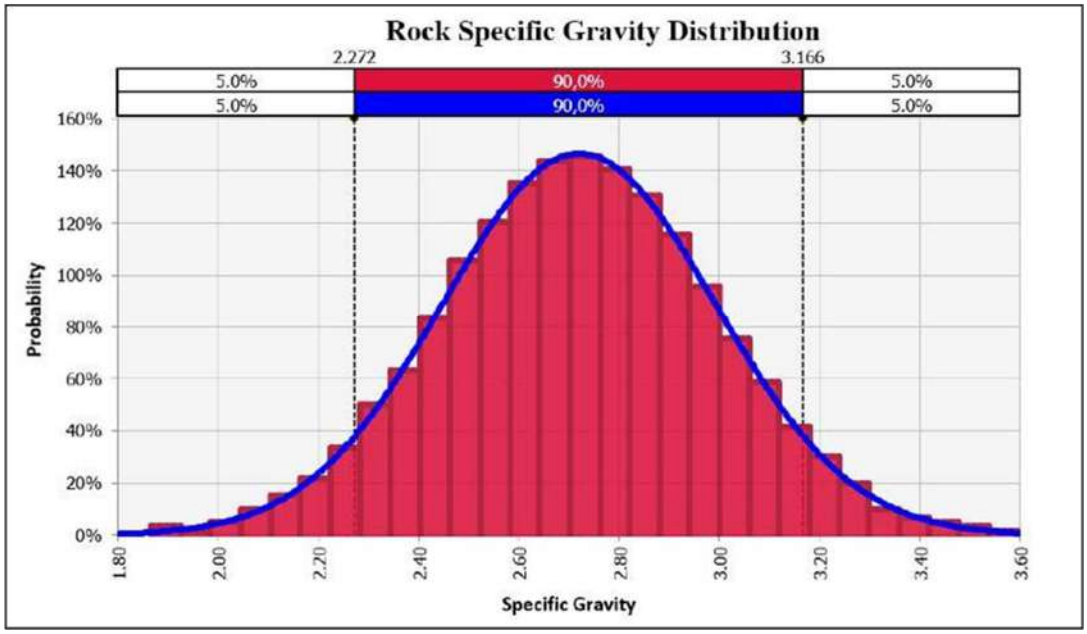

Figure 3.8: Rock specific gravity distribution

The output results that the study assessed are, the Mean fragment size (X_{50}), the Characteristic size (X_C), Blastability Index (A), and the Uniformity Index (n). The simulation process follows the process as described in Section 3.6 with minor differences in the study:

- In the first run of the simulation, all the essential input parameters are assigned various distributions and allowed to run without placing restrictions to any parameter. The sensitivity analysis of the results will then show the influence of all the inputs parameters relative to the output results.
- In the second simulation run, restrictions or constraints are placed on the burden, spacing, drill diameter, hole length, and the powder factor is allowed to be dynamic and unrestricted. A sensitivity analysis study was performed on the output results to determine the input parameters with the major influence on the output results.
- On the third run, the powder factor is constant or restricted, and the blast design parameters are dynamic. Sensitivity analysis studies are also conducted to determine the influence of the input parameters. For all the simulation runs, the rockmass parameters are left to be dynamic.
- Different relationship graphs are plotted to determine the relationships between the input parameters and the output results.
- The mean fragment size results from the different simulations are compared with the actual mean fragmentation size obtained from the image analysis to determine the simulation results, which best represents the actual results.
- The costs of the actual blast results are plotted against the simulation output results. The actual results achieved are then also compared against these costs to determine the blast efficiency and reliability of the simulation.

3.8 Scaled Image Analysis by Wipfrag

In this phase of the study, the objective was to analyze the fragment size distributions achieved by blast design. The analyzed mean fragment size (x_{50}) from the image analysis was compared with the Kuz-Ram model (x_{50}) value. Image analysis is the most effective and efficient way to study blast fragmentation results. Several image analysis software products are available in the market, such as Split software and Wipfrag.

The image analysis process begins with the acquisition of a clear evenly lit image. The image quality is essential in image analysis. Good quality pictures reduce the amount of editing required and give optimized results. The scaled image of unconsolidated material or broken rock is converted into a “net” of fragments as depicted in Figure 3.9.



Figure 3.9: Blast fragment image with a net

Wipfrag software allows comparisons of the resultant nets against the blast fragmentation images to manually correct errors in the net. There are generally two types of errors found in image analysis, fusion and disintegration. Fusion error occurs when the net combines small particles giving them the appearance of one uniform large size particle. Disintegration occurs when large nets of large rocks are broken up into smaller particles, giving the effect of large particles appearing as small particles.

Heat maps are used by the software to indicate fragments of different sizes, ranging from large (red/hot colour) to small (blue or cold colour). The areas with warm colours indicate large size (Xc, D80, and D95) with small sphericity (sph) and lower Uniformity Index value. Whereas, cold colours indicate the areas with small size (Xc), larger sphericity and larger Uniformity Index value. The images were scaled using two 65cm reference sticks. Each blast site location had three best images of the muckpile taken from different directions to cover as much of the muckpile as possible. Figure 3.10 depicted the heat map of varying fragment sizes.

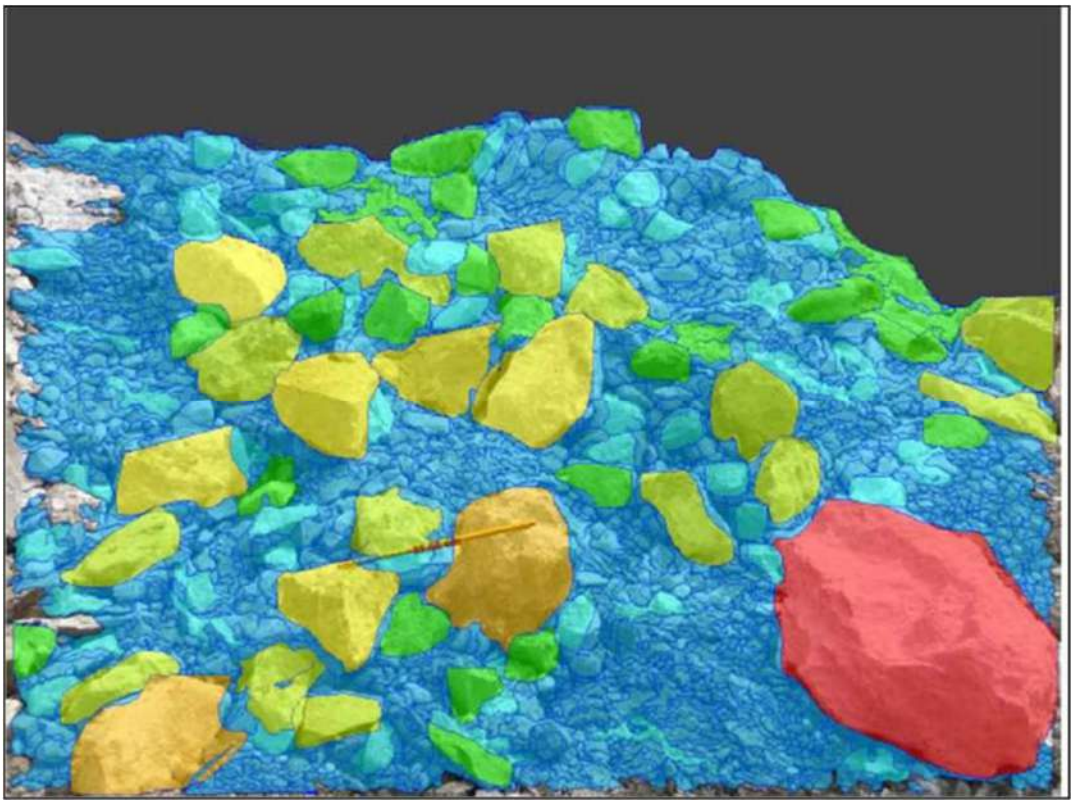

Figure 3.10: Blast image with a heat map

The scaled images are then analyzed individually and then combined to give the overall representative fragmentation statistics. The results then represent the actual blast fragmentation and are used for comparison purposes with Kuz-Ram simulation results. Wipfrag measures the 'nets', displays and plots the fragmentation statistics and produces the graphs as depicted in Figure 3.11.

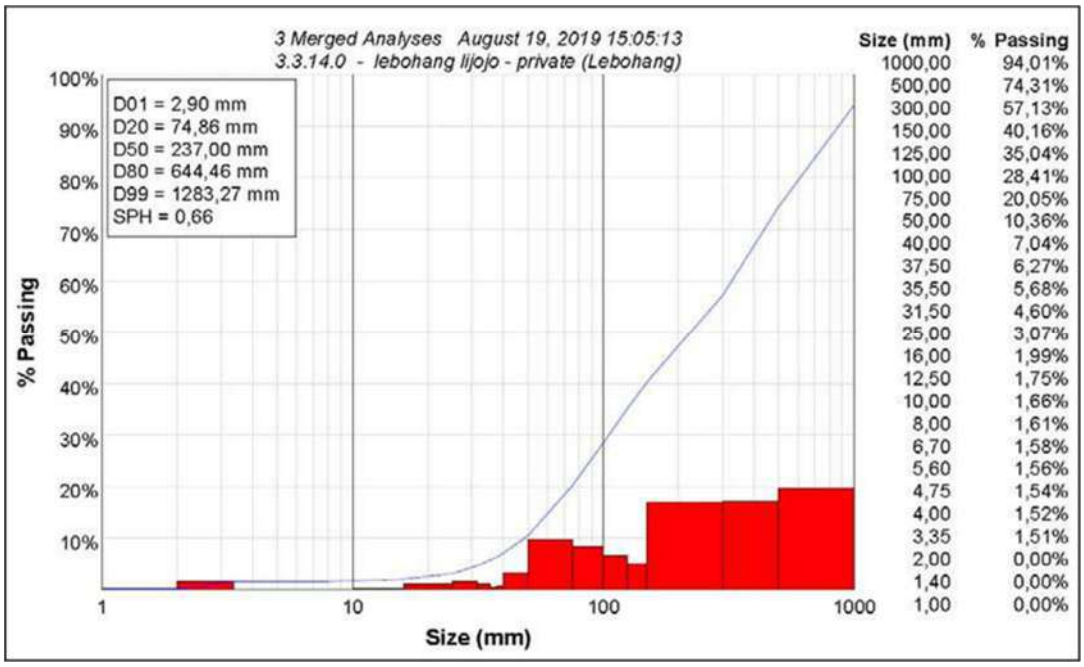

Figure 3.11: Cumulative particle size distribution curve

3.9 Regression Analysis

Quantitative data analysis techniques such as calculation of statistics, constructing of summary tables, creating graphs and employing advanced statistical analysis techniques will help to explore, describe, present and examine relationships and trends within data (Renseburg, 2017). Regression analysis is a form of predictive modelling techniques which investigates the relationships between a dependent (target) and independent variables (predictors). The method is used for forecasting, time series modelling, and finding the causal effect relationship between the variables (Renseburg, 2017). Figure 3.12 depicts the relationships between the Blastability Index and specific rock gravity.

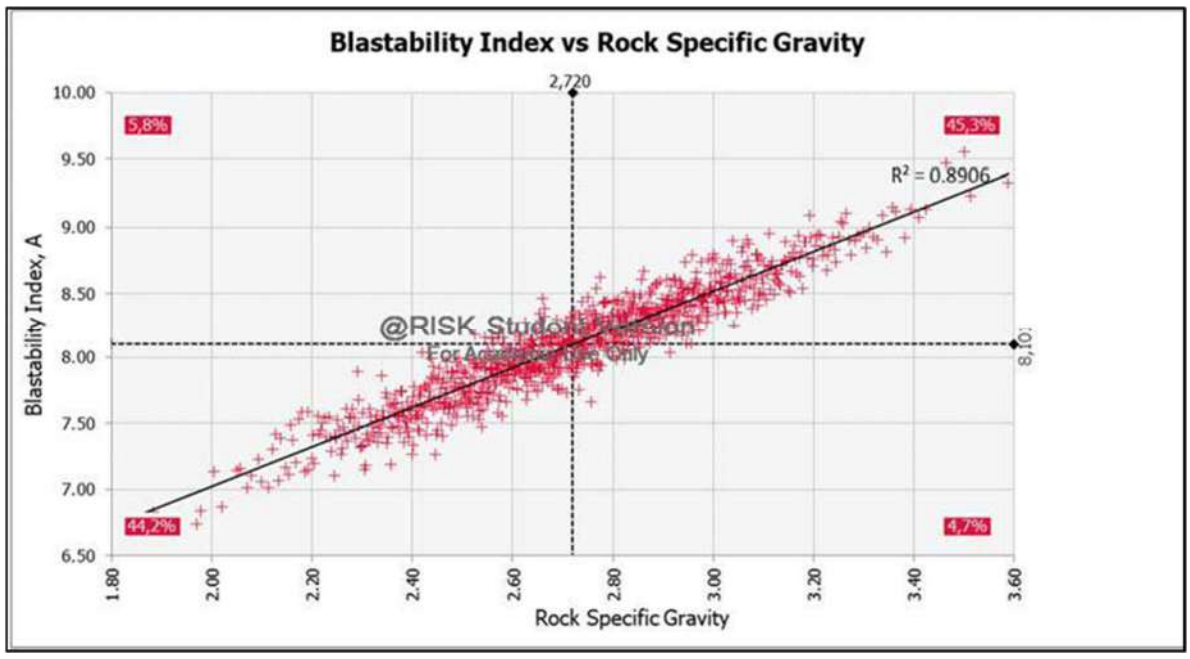

Figure 3.12: Blastability Index vs rock specific gravity

The benefits of using regression analysis are:

- It indicates the significant correlations between dependent and independent variables.
- It indicates the strength of the impact of the multiple independent variables on a dependent variable.
- Allows for the effect of variables measured on different scales to be studied. Thus, assisting in evaluating the best set of variables to be used for building predictive models.

Several regression techniques could be used, such as linear regression, logistic regression and polynomial regression. The regression technique to use depends on

the independent and dependent variables, dimensionality in the data and other characteristics. In this study, linear regression was used to study the causal effect between variables measured on different scales.

After plotting the various relationship graphs of the input parameters against the output parameters (Blastability Index, mean fragment, and Uniformity Index), a sensitivity analysis of the outcome results is conducted to determine the inputs with the most significant impact of the output results. The causal relationships of the prominent input parameters against parameters such as mean fragment size and blast pattern geometry are then determined.

The identified significant input parameters become the prominent factors that are focused upon in designing a blast plan that will deliver optimal fragmentation size. Figure 3.13 depicts the tornado graph of the inputs with the most significant impact on the mean fragment size.

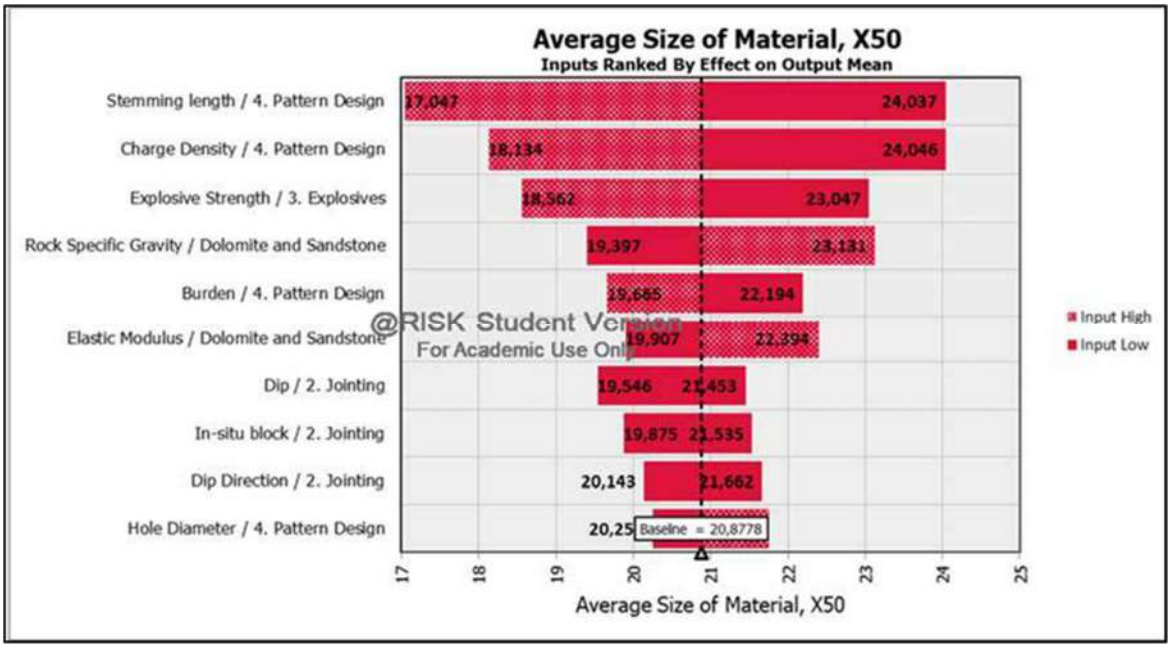

Figure 3.13: Sensitivity analysis of the mean fragment size

3.10 Model Validation

To ensure that the results obtained from the blast simulation work performed in Microsoft Excel are reasonable and accurate, a validation process is undertaken. The actual results achieved from image analysis are compared with the simulation results from Microsoft Excel to determine the degree of variability between the actual fragmentation distribution and the expected fragmentation distribution from the simulation.

The simulation results should be within the 20% error region of the actual fragmentation distribution to be declared reasonable. If the error is significant, the outcome results of the simulation are adjusted by a factor to bring them in line with the actual results. On the next blast simulation for a new blast polygon, the adjusted input parameters are then used to run the simulation.

Once, the simulation results are declared reasonable; the blast efficiency can be calculated as stated in Chapter 2, section 2.6. The ideal outcome is that the actual mean fragmentation size results should be between +20% to -20% of the expected/predicted mean fragmentation size.

3.11 Blasting Costs Calculation

The blasting cost consists of two components, drilling cost and explosives cost. The mine usually blasts between 400 holes to 800 holes per blast. In December 2018, eleven blasts took place. Figure 3.14 depicts the drilling operations in Ruashi south-west polygon.



Figure 3.14: Blast-hole drilling

The mine utilizes SANDVIK model DX900i (Top Hammer) which can manage hole diameters from 89mm to maximum 140mm. Figure 3.15 graphically illustrates the increase in drilling costs relative to the increase in hole diameter, and this graph is developed from the information provided in Table 3.7.

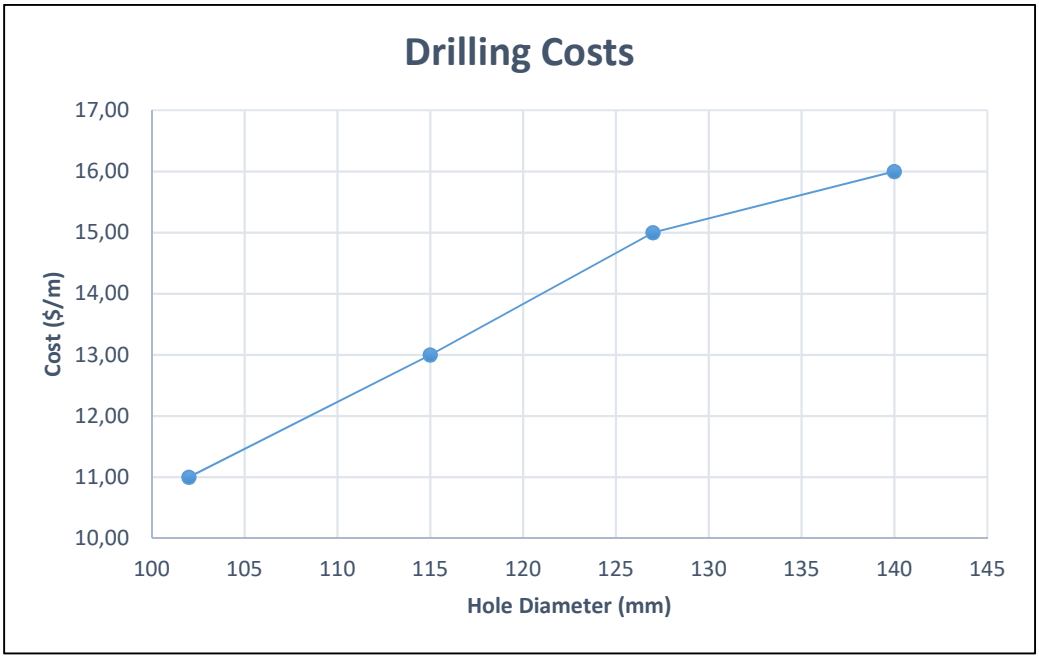

Figure 3.15: Drilling costs (Adapted from Table 2.4)

Table 3.7: Drilling costs. Adapted from Ruashi Mining Contract (2018)

Diameter (mm)	USD/m
102	11.00
115	13.00
127	15.00
140	16.00

The bigger the drill bit diameter, the costlier it is to drill per metre. In Ruashi mine, both the grade control holes and blast holes are drilled using a 102mm bit. To determine the blasting costs of a single blast hole, it is essential to quantify the accessories and explosives consumed per hole. Other costs such as the delivery of explosives to the site are waivered against Ruashi mine (due to a contractual agreement which saw the supplier establishing a distribution magazine on Ruashi Site). The explosives costs are variable and depend on the amount consumed per hole. To quantify the total cost involved in the blasting process, the individual cost items that make up the blasting costs are derived from the number of drilled holes to be blasted. The unit costs of the explosives items used were derived from Table 3.8

Table 3. 8: Explosives and accessories costs.

Adapted from Ruashi Mine Explosives Prices List (2018)

Initiation Systems				
Item	Units/Box	USD/Unit	Cost/Unit or kg	Cost/Unit or kg
Cordtex 10 gm/m (2 x 350m)	700	690.00	0.99	0.99
Explosives				
Item	Units	Kg/Unit	USD/Unit	USD/kg
Anfex	Bags	25	71.66	2.87
P100 Emulsion	Bags	1000	1614.66	1.62
Pentolite Booster 150gm	Pack	120	642.95	5.36
Detonators				
Item	Units/Box	USD/Box	Cost/Unit	Cost/Unit or kg
Benchmaster 7.5m-500ms	150	735.36	4.90	4.90
Handite 7.5m-0ms	150	735.36	4.90	4.90
Handite 7.5m-17ms	150	735.36	4.90	4.90
Handite 7.5m-25ms	150	735.36	4.90	4.90
Handite 7.5m-42ms	150	735.36	4.90	4.90
IED	1000	1243.00	1.24	1.24

Ruashi mine uses one detonator with a booster placed at the bottom of the blasthole. Table 3.8 above outlined price list of explosives and accessories that are used in the blasting process. The full price list is provided in Appendix A, Table A1.

The blast hole positions and hole depths are surveyed, before charging of the holes can take place. The volume of rockmass to be blasted and the explosive quantities required are calculated. The blast tie-up plan depicted in Figure 3.16 is developed in conjunction with the explosive supplier, and the explosive order is then placed after all the designs are approved.

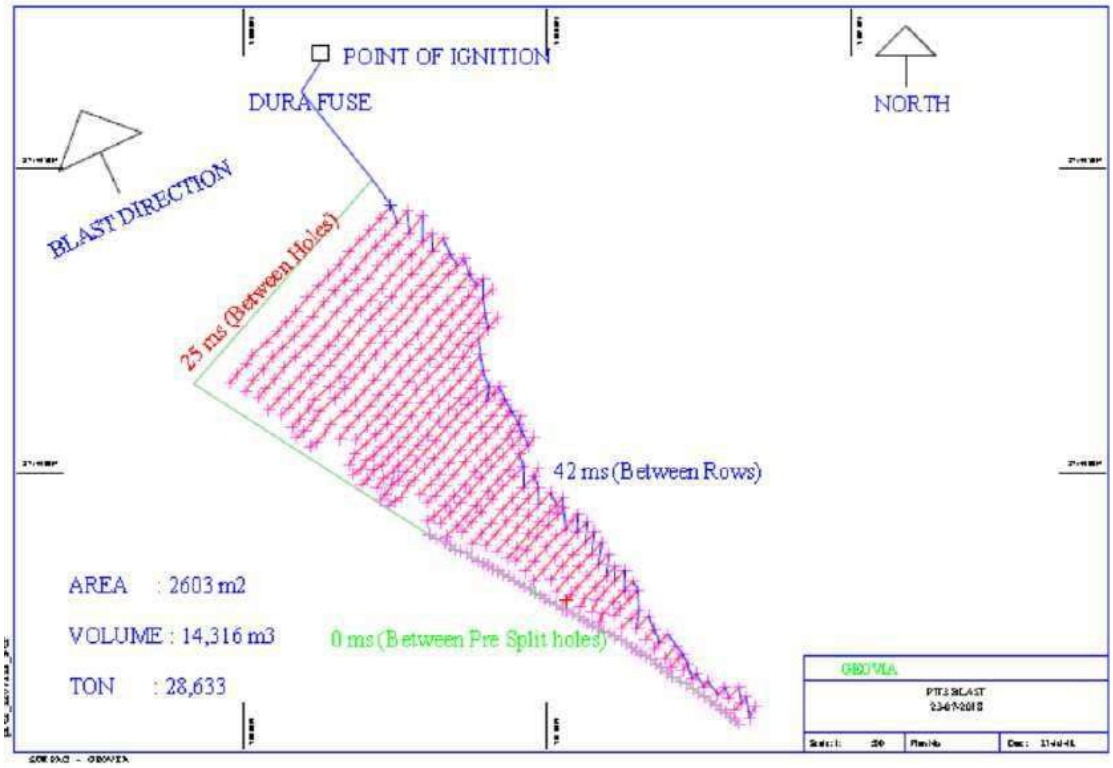

Figure 3.16: Blast tie-up plan

The kilogram of explosives and blasted volume are used to calculate the powder factor and cost per volume.

3.12 Chapter Summary

This chapter explains the methodology and application of the theoretical information provided in Chapter 2 of this study. Different methods were used to collect pre-blast input data and post-blast data such as mappings, geotechnical studies and image analysis of blasted material. The pre-blast data was used in the development of the Kuz- Ram model and the Rosin-Rammler distribution in Microsoft Excel. The @Risk software program was used to perform the Monte Carlo simulation studies on the polygon to be blasted.

The process of assigning statistical distributions and performing sensitivity analysis in @Risk software was also explained. Scaled image analysis was performed using the Wipfrag software. The results of these images were then, compared with the simulation results to determine their correlation and accuracy. The results of the simulation studies and image analysis were used to predict the expected blasting costs for a range of fragment size.

CHAPTER 4

Results and Discussions

4.1 Introduction

This chapter presents the results obtained from the eleven blasts undertaken in Ruashi _3. The three test sites were assigned different simulation conditions in order to study the effects of the geotechnical and geometric blast design parameters on rock fragmentation. The South-East blast area parameters were allowed to be dynamic, the South blast area had a constant powder factor, and the South-West area had constant burden and spacing.

The results presented henceforth draw relationship patterns between Blastability Index, Uniformity Index, and mean fragment size with respect to rockmass conditions, explosives parameters, blast design parameters, and unit mining costs. The relationships thus highlight the parameters with the most significant impact on blast fragmentation. The results for each test blast area are presented together under one heading. For example, results for Blastability Index for all test blast will be discussed under the heading Blastability Index. Detailed results are contained in Appendix D for each respective blast area.

4.2 Blastability Index Results

Three different blast areas with varying rockmass conditions were studied to identify how the rockmass conditions affect the fragmentation results. Each of these areas indicated varying ranges of Blastability Index values. In general, the Blastability index for the Ruashi rockmass was less than ten. Section 4.2.1 presents the distribution of the Blastability Index values results for the tests.

4.2.1 Blastability Index Frequency Distribution

The graphical results presented in this section show the blastability distribution frequencies for the three test sites. Figures 4.1, 4.2 and 4.3 depict the Blastability Index results obtained from the respective test sites.

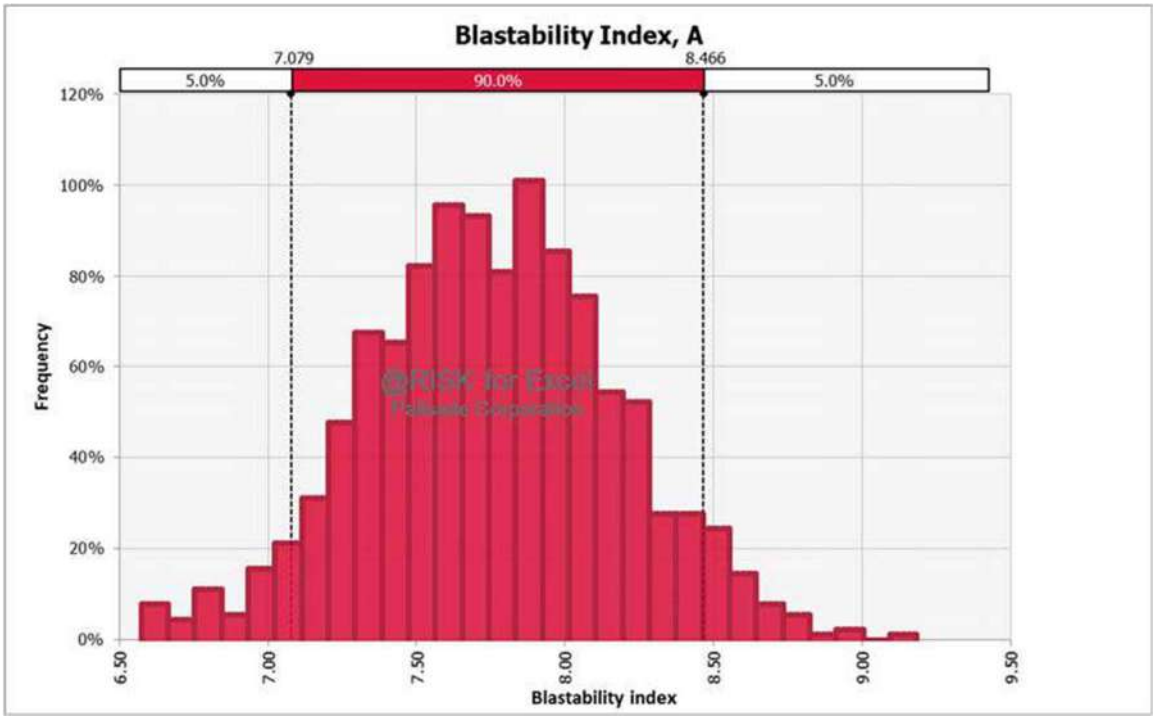

Figure 4.1: South-West Blastability Index distribution

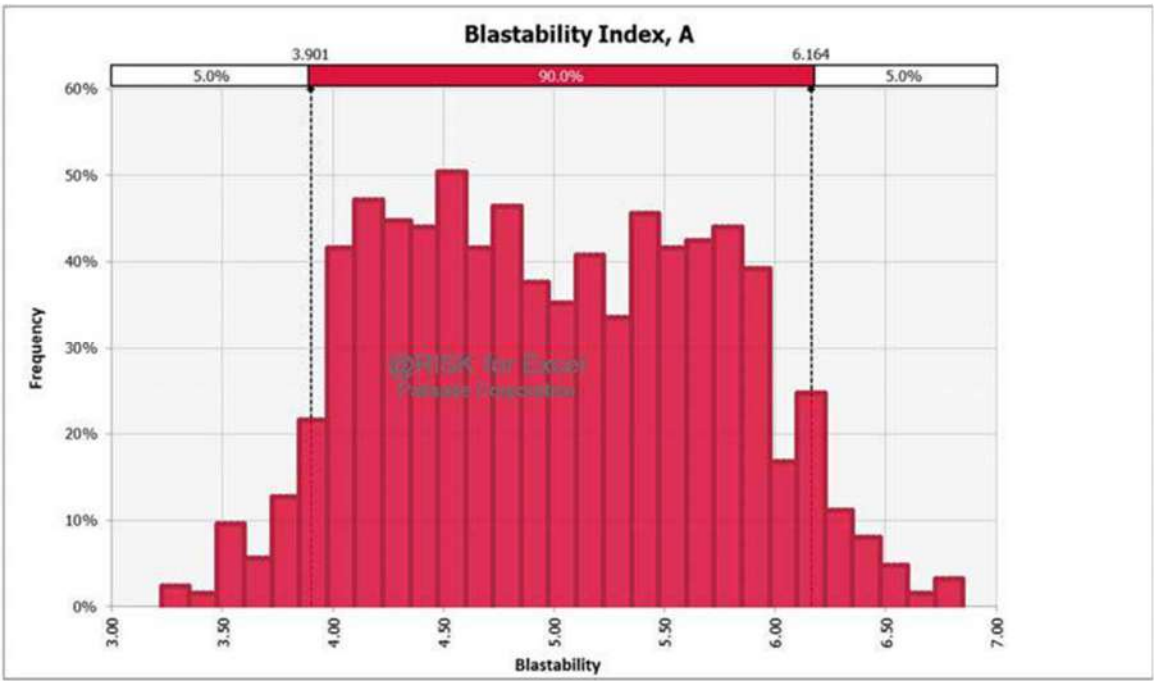

Figure 4.2: South Blastability Index distribution

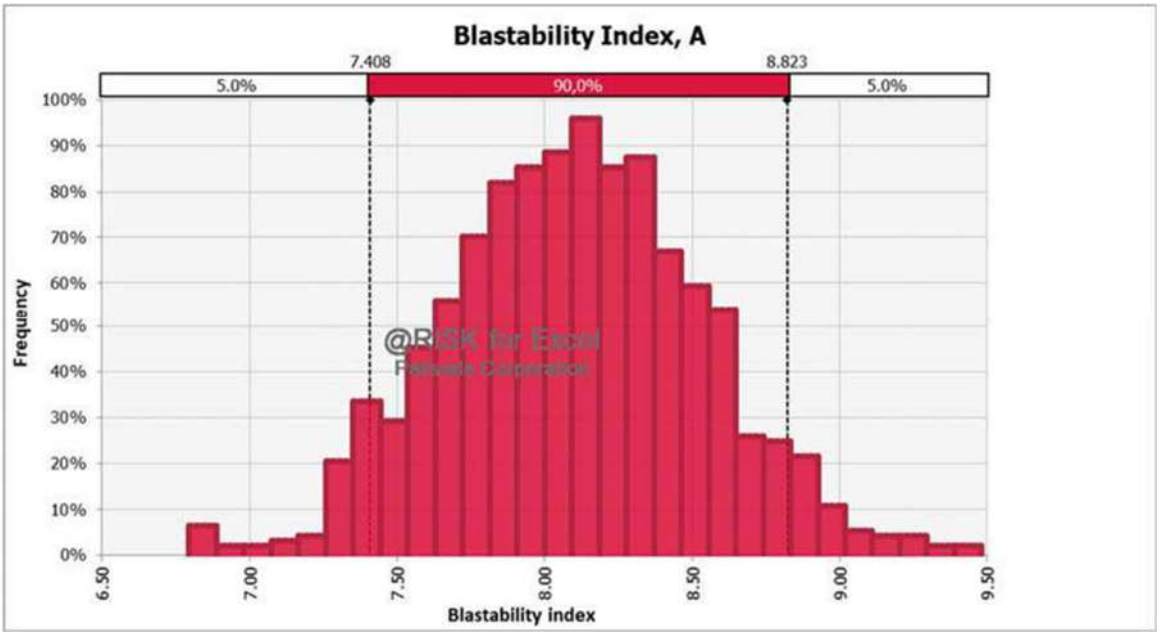

Figure 4.3: South-East Blastability Index distribution

In the South-West and South-East areas, the joint spacing was 0.1m and above, and the rock density varied between 2.62 and 2.71 tonnes/m^3. In these conditions, the Blastability Index distribution was found to be between 7 and 9 (Figures 4.1 and 4.3). In contrast with the results obtained for the South-West and South-East, the blast area in the South, where the joint spacing was less than 0.1m to none, the Blastability Index distribution was between 3 and 6, as depicted by Figure 4.2. The density in this area was 2.72 tonnes/m^3.

It was apparent from the Blastability Index results that rock density, joint spacing, and joint plane orientation influence the Blastability Index, as shown in Lilly's Blastability Index Equation 1. It was also evident from this equation that there is a linear relationship between Lilly's equation variables, of significance, was to determine which of these parameters have the most impact on the Blastability Index for the encountered rockmass. In order to establish the nature of the causal relationship between the different parameters, a sensitivity analysis was performed for each blast area, and their results are presented in Section 4.2.2.

4.2.2 Blastability Index Sensitivity

This section shows the sensitivity analysis of the Blastability Index results to determine influential parameters to the Blastability Index. Figures 4.4, 4.5, and 4.6 depict the results obtained from the sensitivity analysis.

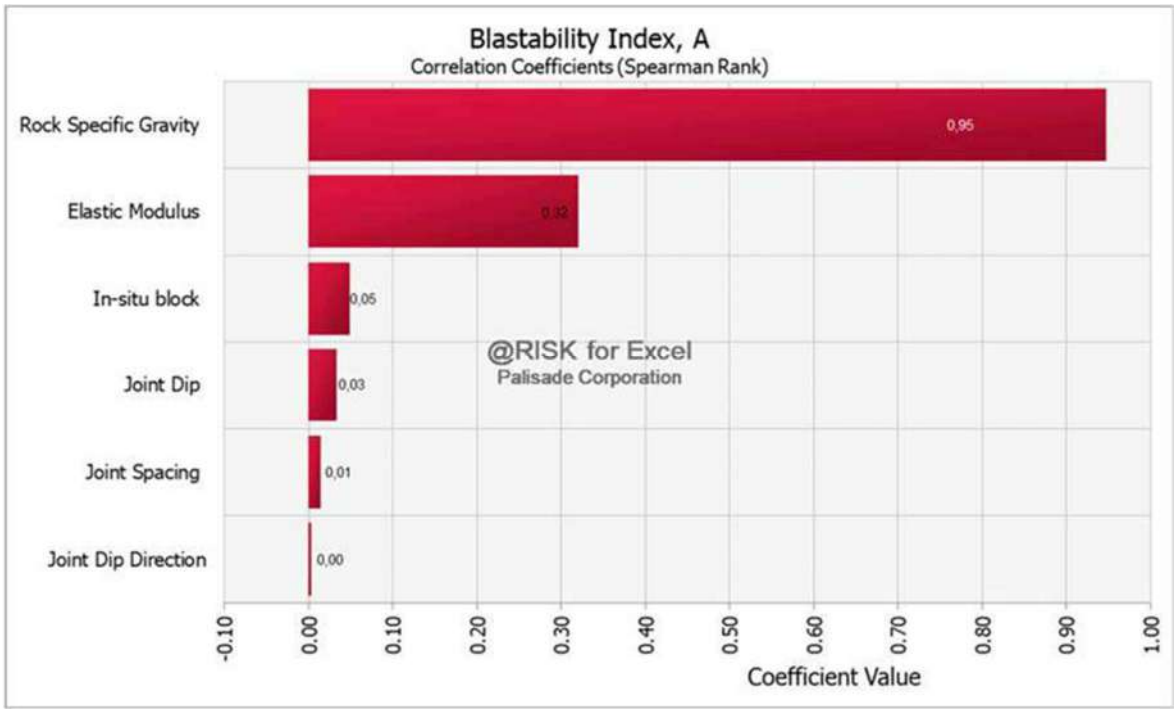

Figure 4.4: South-West sensitivity analysis

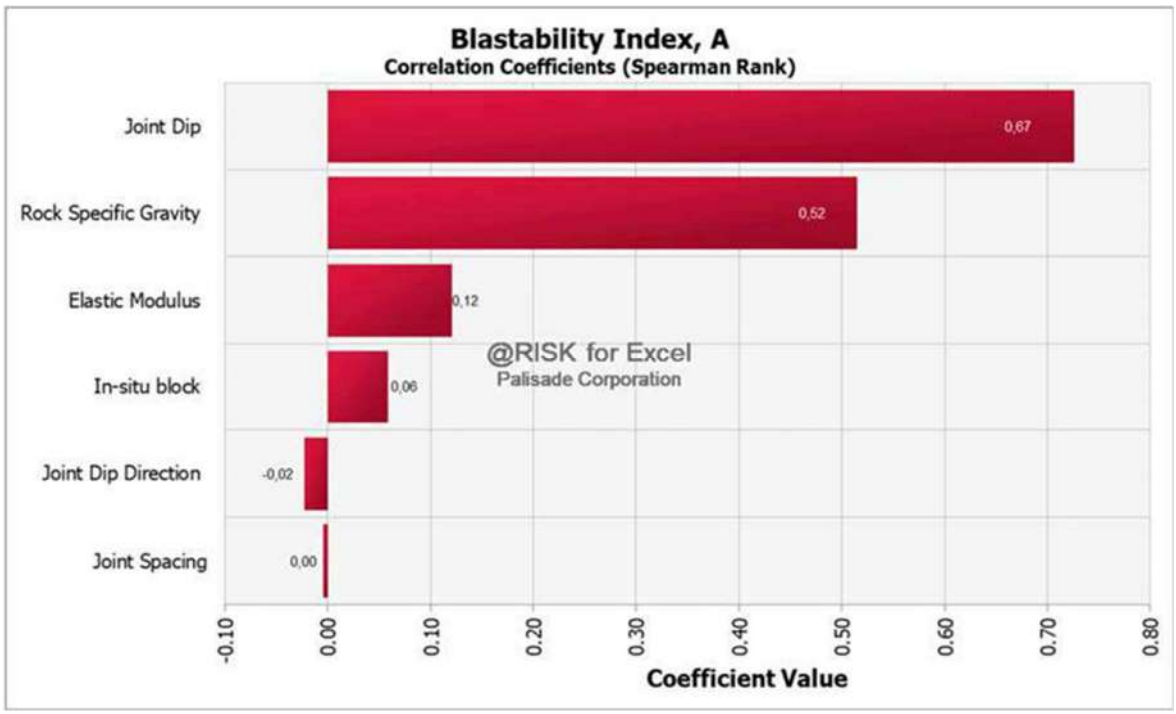

Figure 4.5: South sensitivity analysis

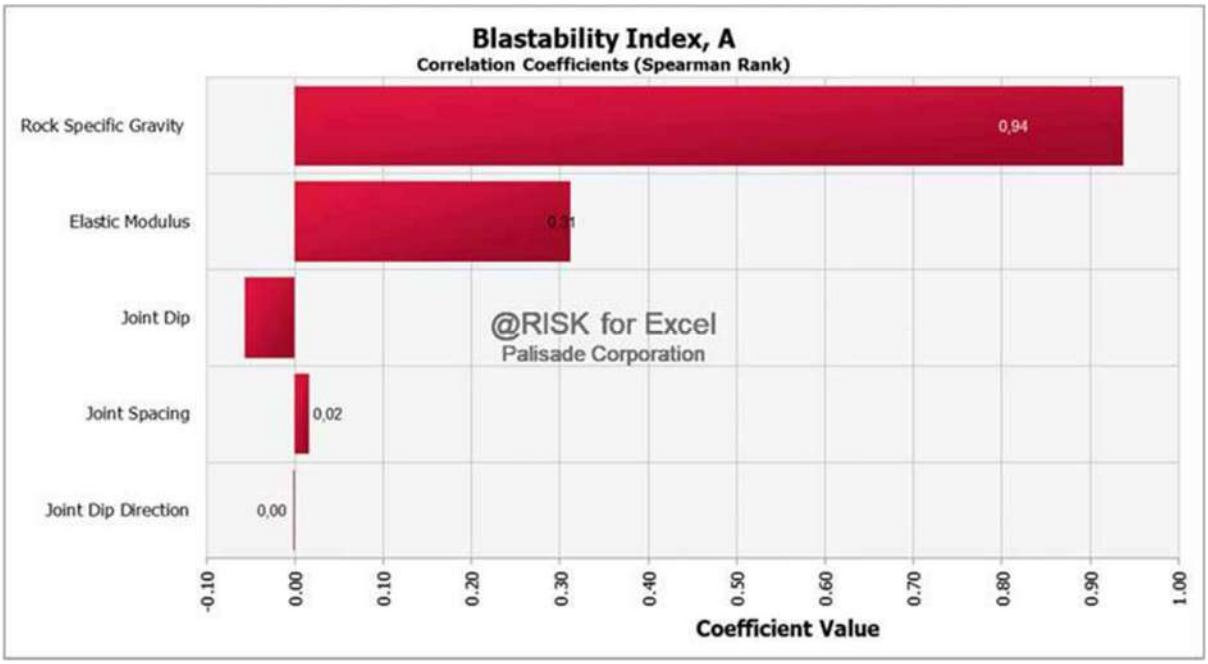

Figure 4.6: South-East sensitivity analysis

Figures 4.4 and 4.6 (South-West and South-East) indicate that the parameter with the strongest influence on the Blastability Index is the rock specific gravity with the correlation coefficient at 0.94 (94%) for both areas. Figure 4.5 (South) sensitivity results were different from Figures 4.4 and 4.6. The rockmass in the South had fewer joints (less than 0.1m) and flatter dipping joints. In this regard, the parameters that were observed to have a significant influence on the Blastability Index were rock specific gravity and joint dip angle.

Upon the conclusion of the sensitivity analysis work, parameters with the most substantial influence on the Blastability Index results for each respective blast area were identified. The scatter plot diagrams were drawn to depict the nature of the causal relationship between the influential parameters and the Blastability Index, and their results are presented in Section 4.2.3.

4.2.3 Blastability Index Scatter Plots

The scatter plots map the relationships between the various influential parameters. Figures 4.7 to 4.10 depict the nature of the relationship between rock specific gravity, joint dip, and Blastability Index. The focus is on determining the parameters with the highest degree of influence on Blastability Index. The regression coefficient indicates the strength of the relationships.

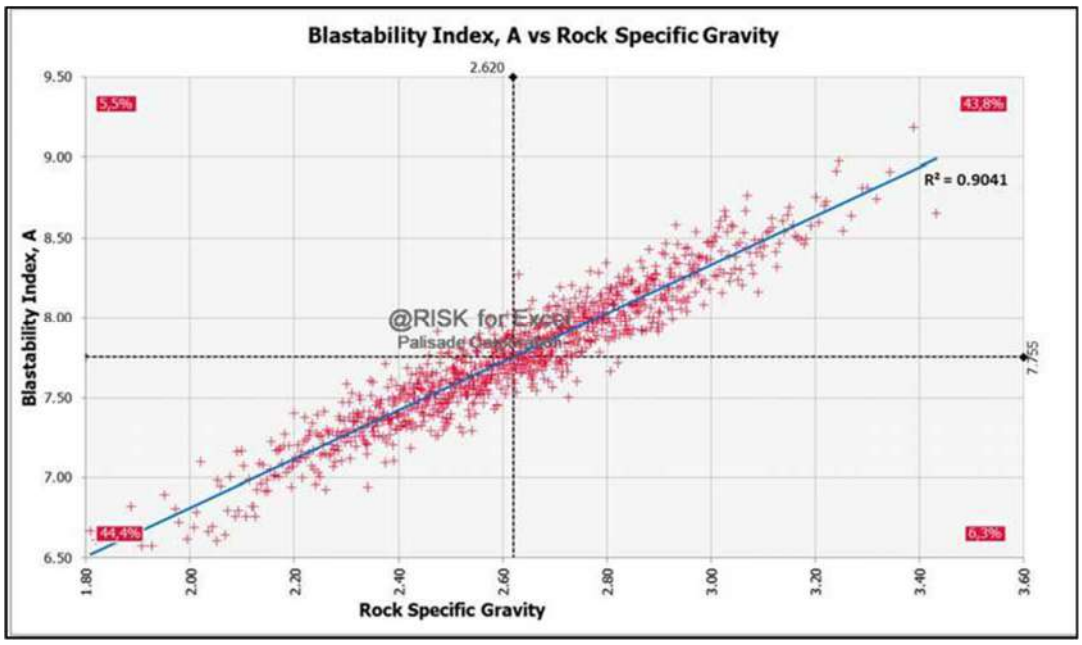

Figure 4.7: South-West Blastability Index vs specific gravity

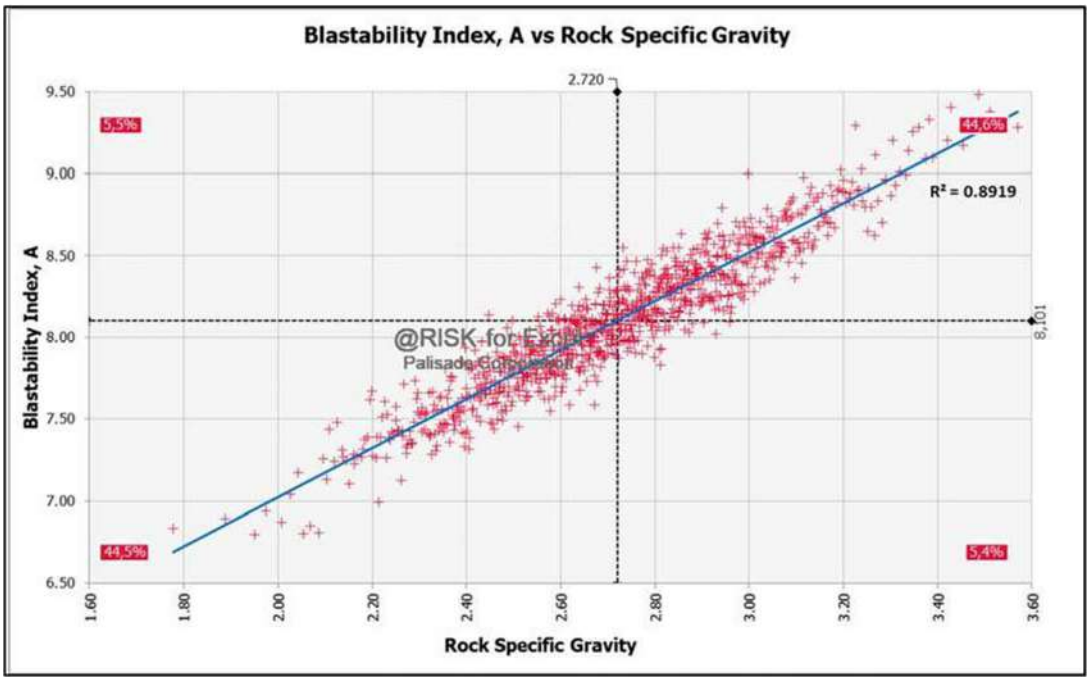

Figure 4.8: South-East Blastability Index vs specific gravity

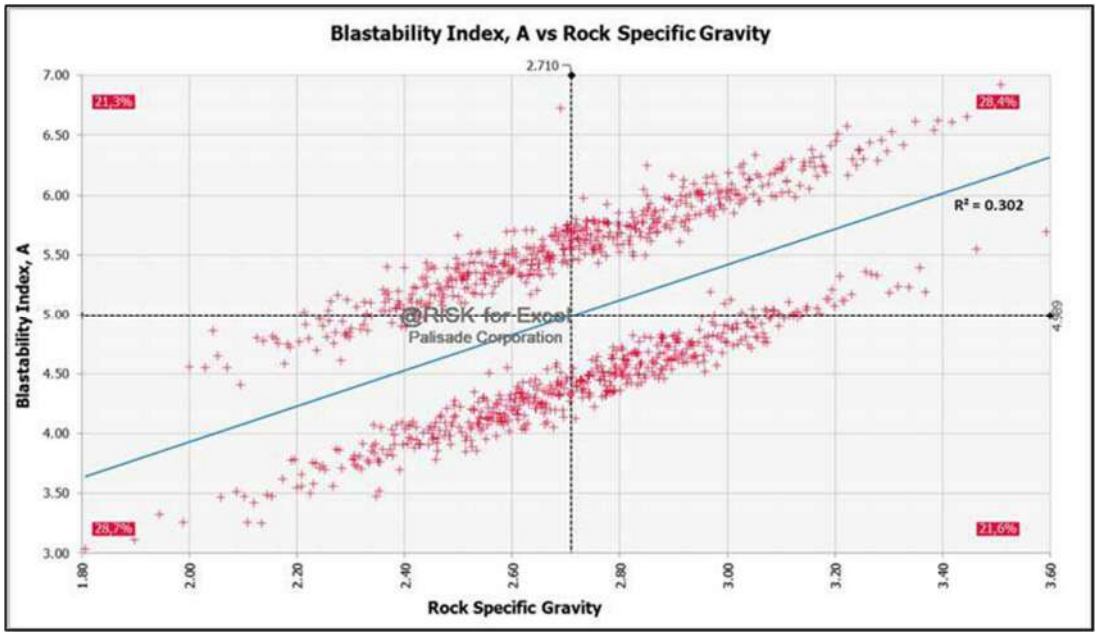

Figure 4.9: South Blastability Index vs rock specific gravity

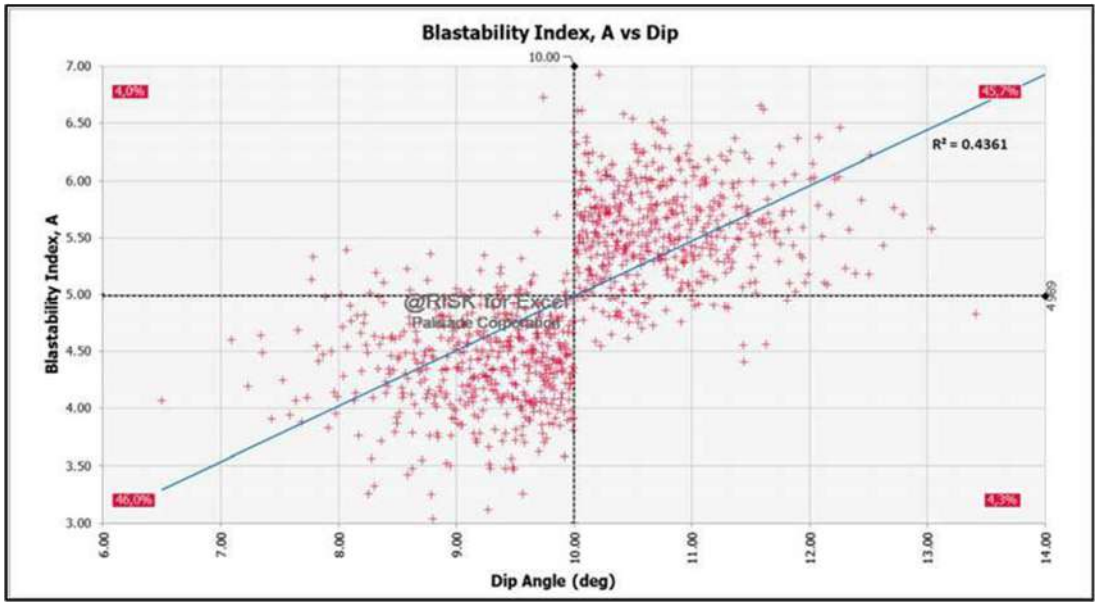

Figure 4.10: South Blastability Index vs joint dip angle

There was a positive relationship between rock density and Blastability Index, as shown by Figures 4.7 to 4.9. It was observed that the Blastability Index increased with the increase in rock density. Lower Blastability Index values were observed for the type of rock (sedimentary rock) encountered at Ruashi mine. Figure 4.9 shows the split in the data as a result of a bimodal distribution of the Blastability Index results, as depicted in Figure 4.2. Despite this split in the data, the trend was still consistent with the results obtained for the other blasted areas, which indicated a positive trend.

Figure 4.10 indicated that the Blastability Index was expected to increase with the increase in the joint dip. The steeper the joints, the higher the Blastability Index. This means that it is much easier to blast rocks with steep joints than those with flatter joints. It is also necessary to understand the direction of these joints relative to the blasting face (i.e. are these joints parallel to the face or perpendicular to the face) as this will influence the fragmentation size.

4.3 Uniformity Index Results

The Uniformity Index is mainly affected by the burden, spacing, bench height and drill hole diameter. The South-West blast was the only blast with constant burden and spacing, whereas the South and South-East areas had variable burden and spacing. The results of the Uniformity Index are presented in the following sections, starting with frequency distribution.

4.3.1 Uniformity Index Frequency Distribution

The section shows the Uniformity Index distributions results from the three test sites with varying drill and blast patterns. Figures 4.11 to 4.13 depict the spread of the Uniformity Index.

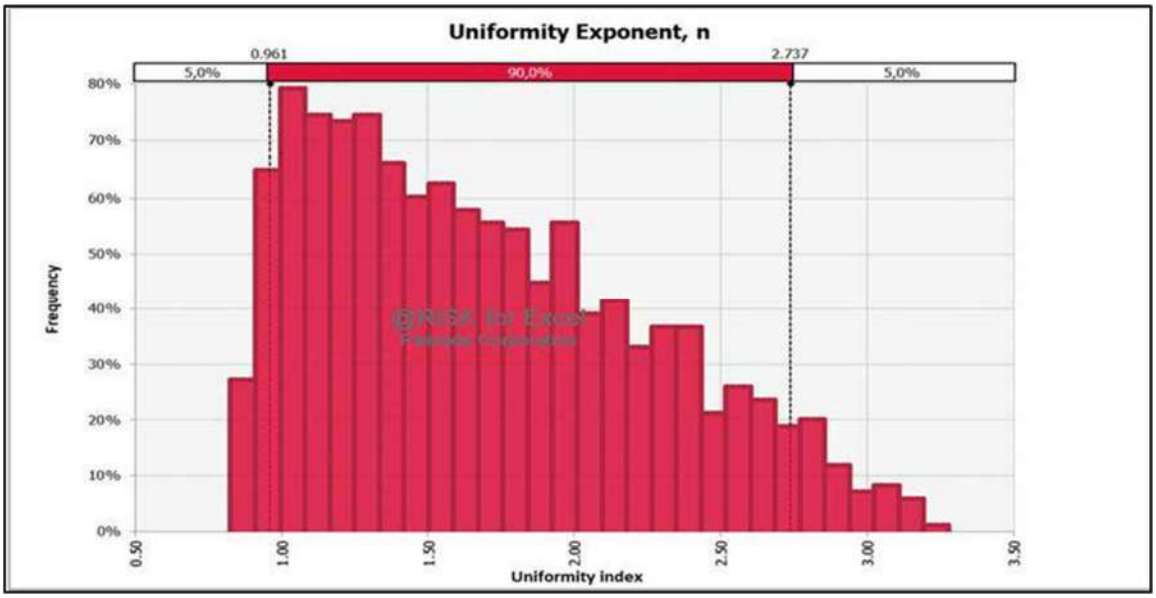

Figure 4.11: South-West Uniformity Index

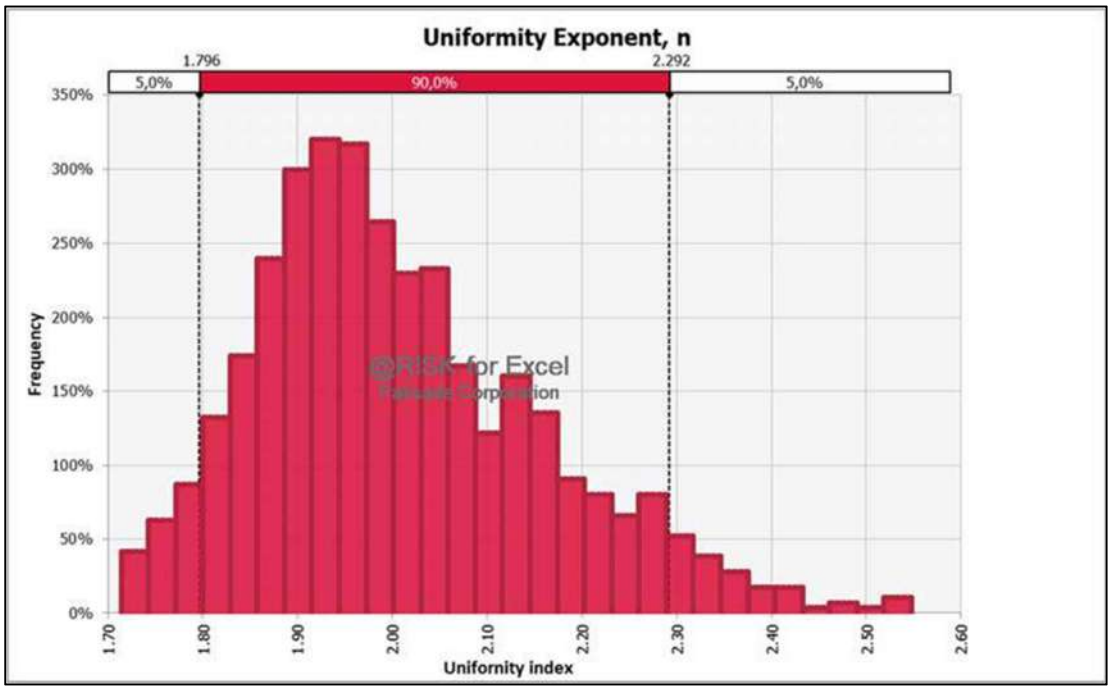

Figure 4.12: South Uniformity Index

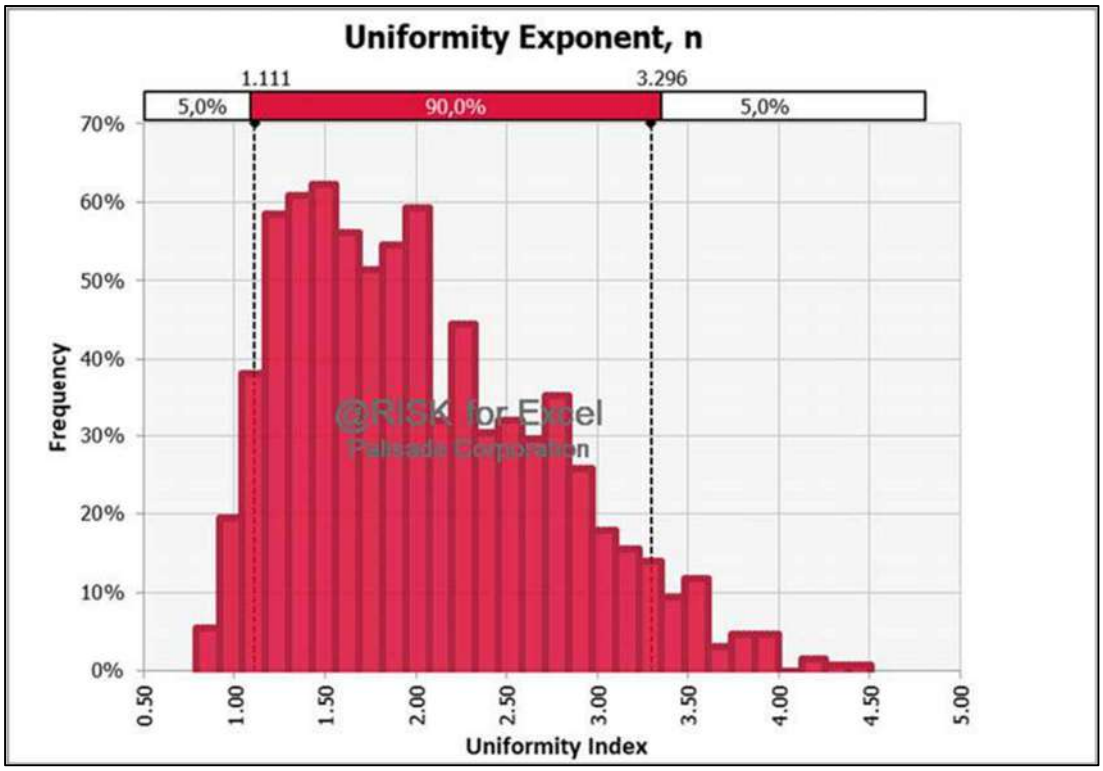

Figure 4.13: South-East Uniformity Index

The Uniformity Index values amongst the three test sites were low, which indicated that the muck piles were generally non-uniform in their size fragment distributions. The mine was generally not worried about fines; the biggest issue is having the majority of the muckpile comprising of larger blocks that are higher than 50cm max size limit. It is clear from this Uniformity Index distribution that the blasting geometry must be adjusted and a good pattern established to improve the Uniformity Index distribution.

4.3.2 Uniformity Index Sensitivity

The sensitivity analysis for the Uniformity Index results for the South-East and South blast areas were the same in terms of which parameters had a more significant influence on the Uniformity Index. These results were as expected, given that the blast geometric design elements (burden and spacing) were dynamic during the simulation runs. Figures 4.14 and 4.15 depict the parameters with the more significant influence of the index, which is the burden and spacing.

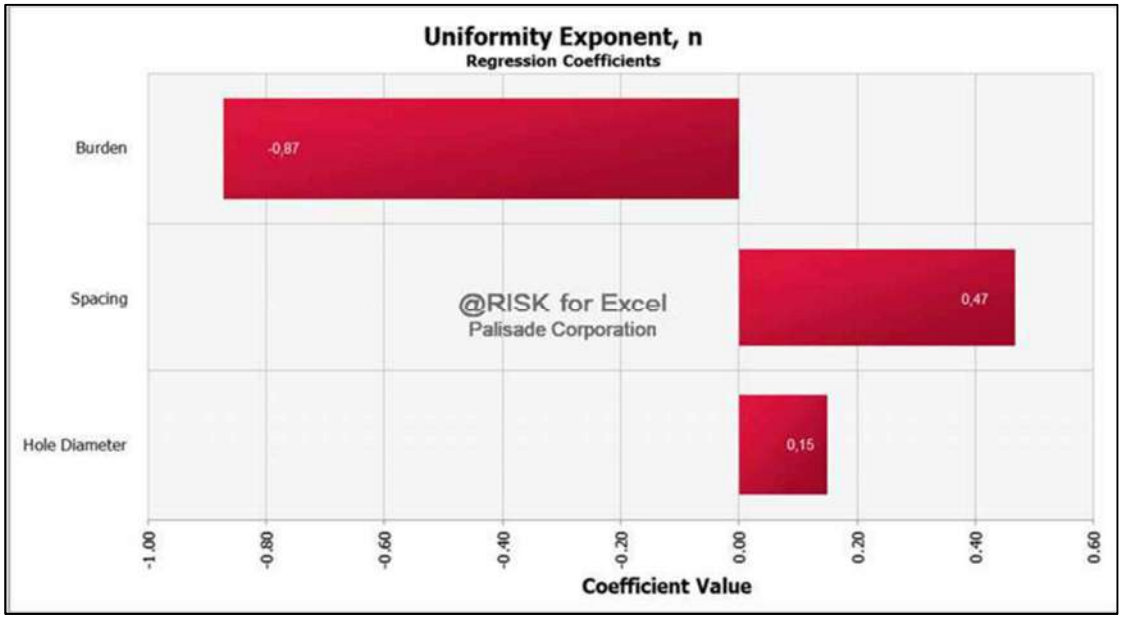

Figure 4.14: South-East Uniformity Index sensitivity analysis

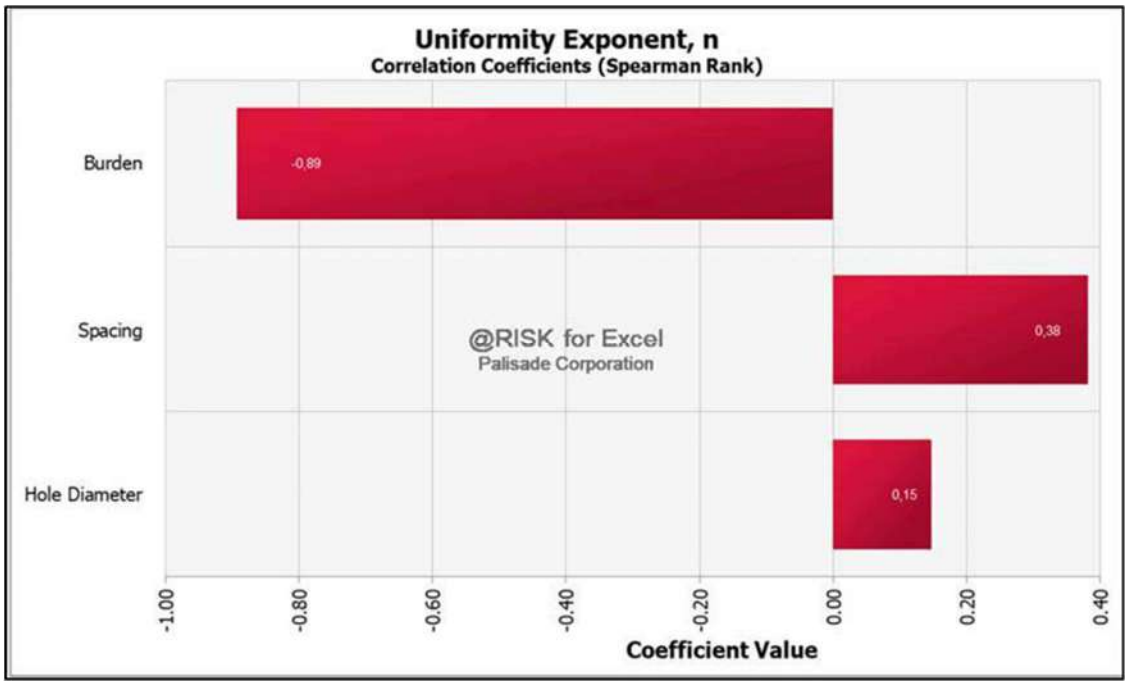

Figure 4.15: South Uniformity Index sensitivity analysis

However, the sensitivity analysis results for South–West area indicated that the only parameter that affected the Uniformity Index results was the stemming length when the burden and spacing were constant. Figure 4.16 depicts the influence of the stemming length on the Uniformity Index for constant burden and spacing (South-West).

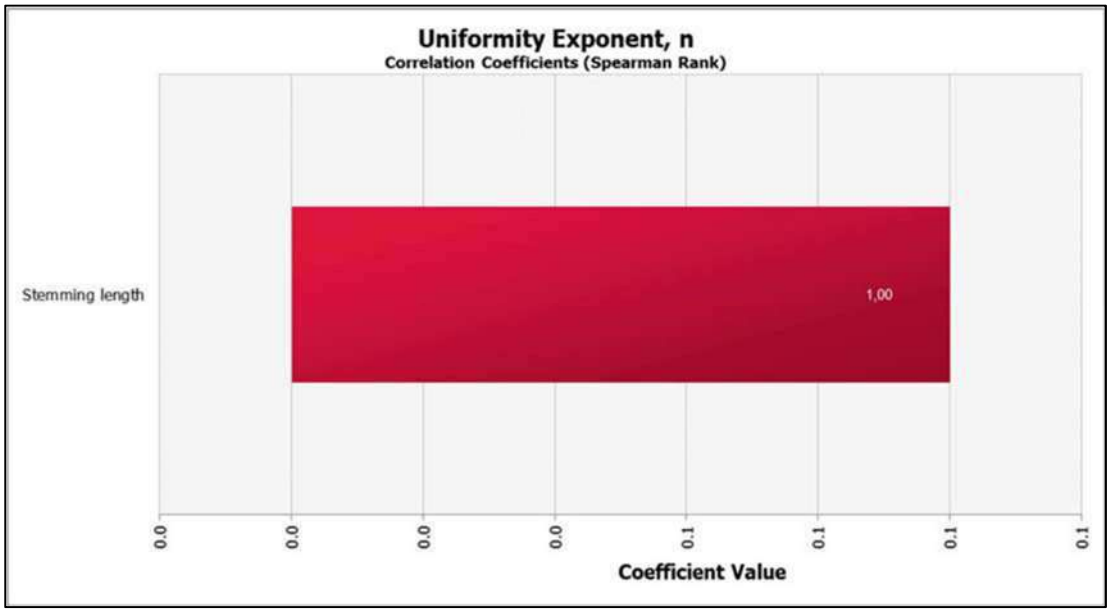

Figure 4.16: South–West Uniformity Index sensitivity analysis

4.3.3 Uniformity Index Scatter Plots

Figures 4.17 to 4.21 depict the relationship between the stemming, burden, spacing, and Uniformity Index for the South, South-East, and South-West blast areas.

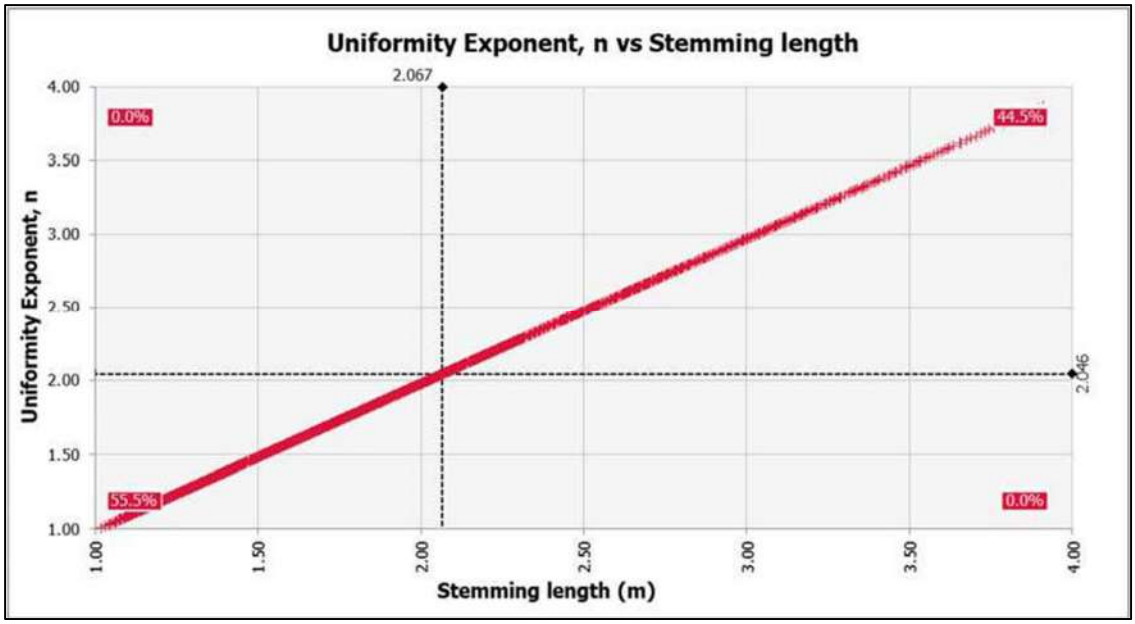

Figure 4.17: South-West Uniformity Index vs stemming length

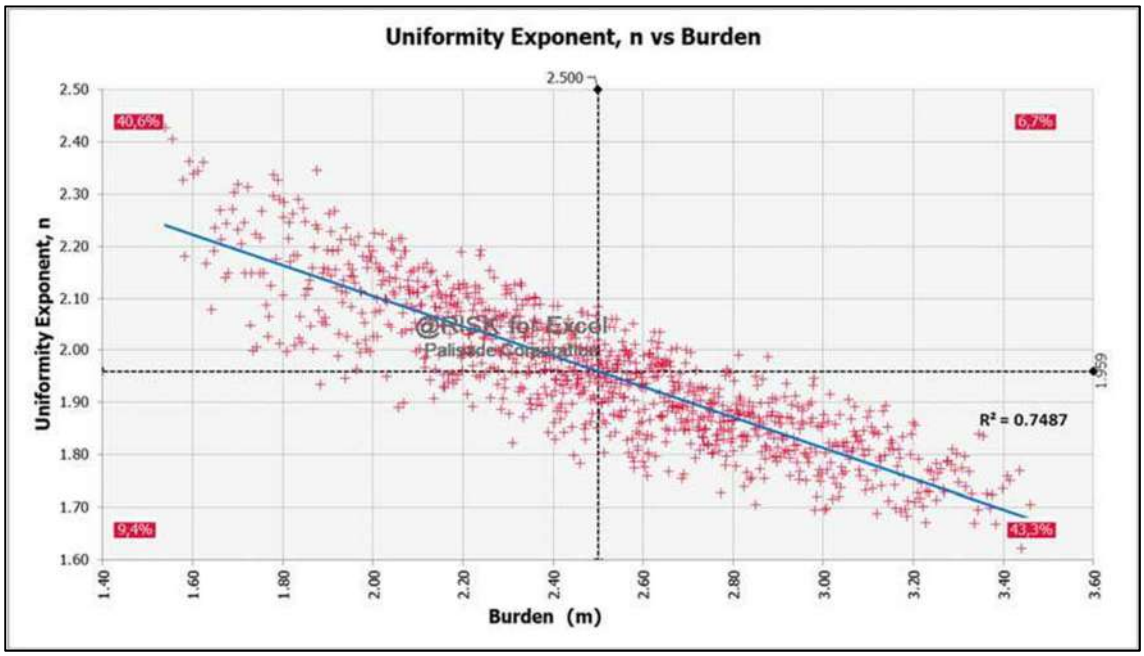

Figure 4.18: South-East Uniformity Index vs burden

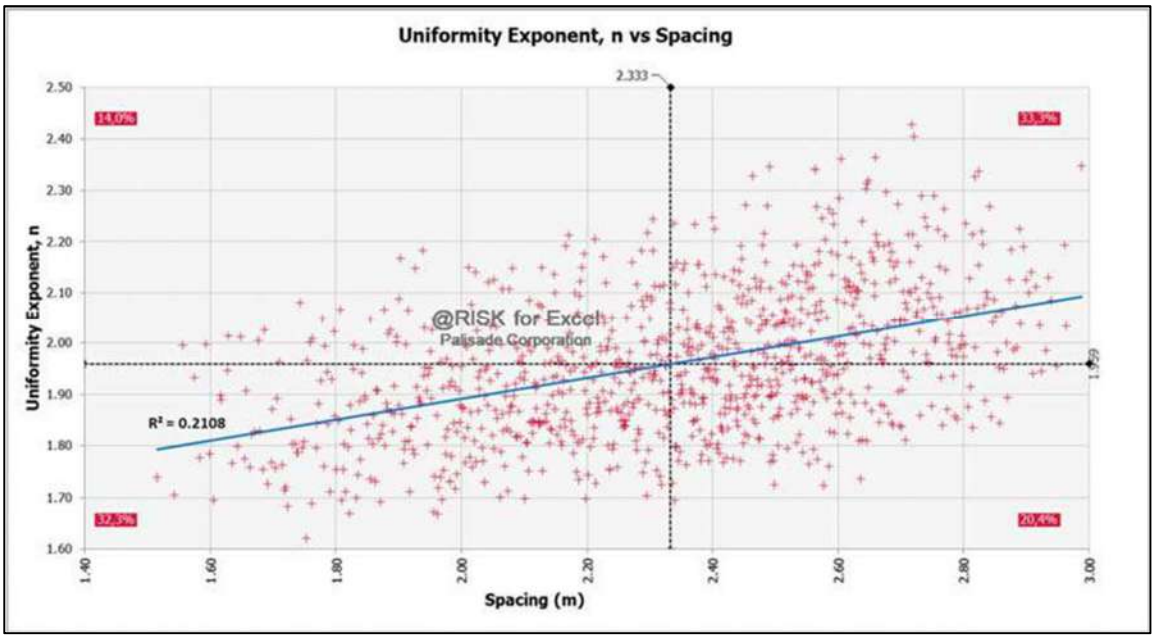

Figure 4.19: South-East Uniformity Index vs spacing

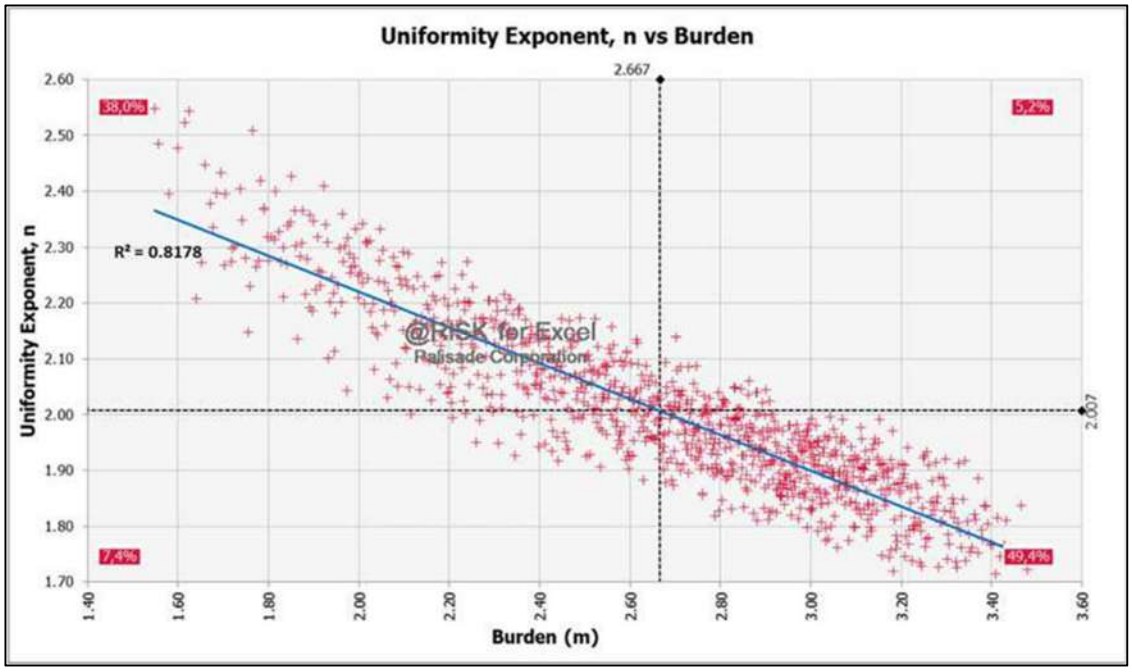

Figure 4.20: South Uniformity Index vs burden

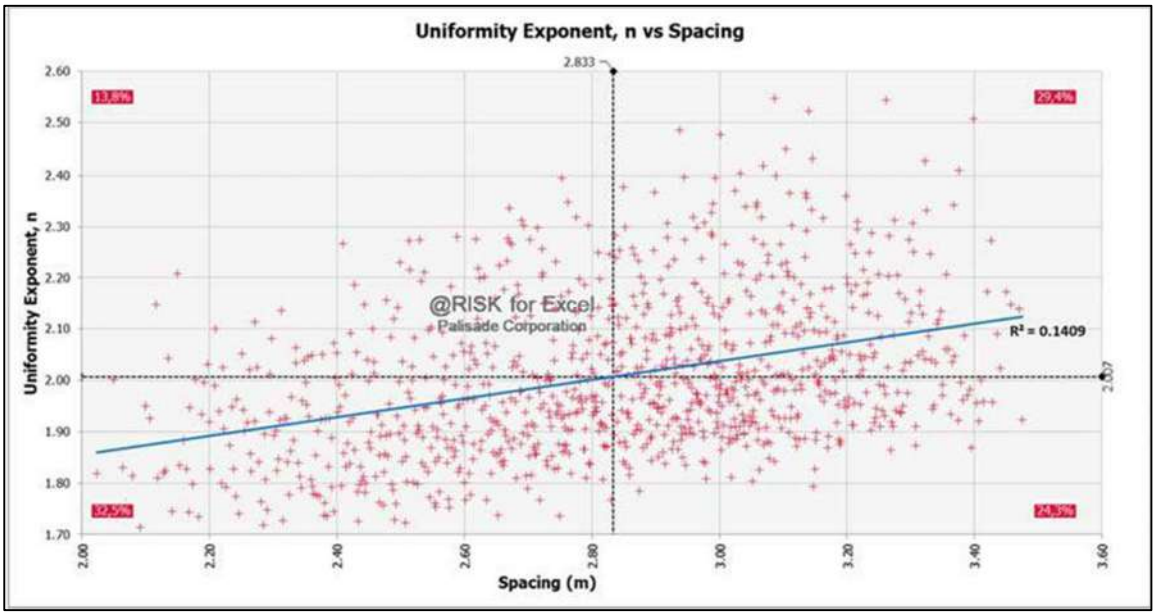

Figure 4.21: South Uniformity Index vs spacing

Figure 4.17 indicates that the Uniformity Index increases with an increase in stemming length. One could see from Figure 4.16 that in a constant burden and spacing scenario, the parameter with the most impact of the Uniformity index is the stemming length.

The results for South-East and South blasts (dynamic parameters) are presented in Figures 4.18 and 4.20, which show that there is an inverse relationship between the burden and the Uniformity Index. These graphs indicate that smaller burdens produce more uniform material than large burdens.

Figures 4.19 and 4.21 depict that the Uniformity Index has a positive relationship with the spacing. The Uniformity Index is expected to increase with the increase in the spacing. Also, when comparing the burden and spacing graphs with the Uniformity Index parameter, one can see that the burden has a much pronounced (higher Regression coefficient) influence compared to the spacing on the Index. The spacing to burden ratio is thus essential to ensure that the blast muckpile is uniform. Uniform muckpile promote efficient mining and crushing operations.

4.4 Mean Fragment Size Results

The factors that influenced the mean fragment results were the Blastability Index, powder factor, Uniformity Index, and the simulation conditions placed upon the blast areas. South-West area had its burden and spacing dynamic, and the powder factor was constant. The maximum powder factor of 0.30 kg/m^3 was used for the blast

simulation. South-East blast area, on the other hand, had all its parameters dynamic, from the geometric design elements to geotechnical parameters, and the powder factor used in the area was 0.65 kg/m^3.

South blast area had a dynamic powder factor with constant burden and spacing. For South areas, two powder factors values of 0.35 kg/m^3 and 0.65 kg/m^3 were used. The idea of using two powder factors was to determine which powder factor produced the best fragmentation size distribution results when compared against the actual fragmentation results (image analysis).

Section 4.4.1 presents the mean fragmentation size results achieved for the respective blast areas. Ruashi mine has the following size classification categories, undersize is material below 10cm, the optimal size is 30cm, and oversize material is above 50cm.

4.4.1 The Mean Fragment Size Frequency Distribution

The South-West blast fragmentation distribution results are presented in Figure 4.22.

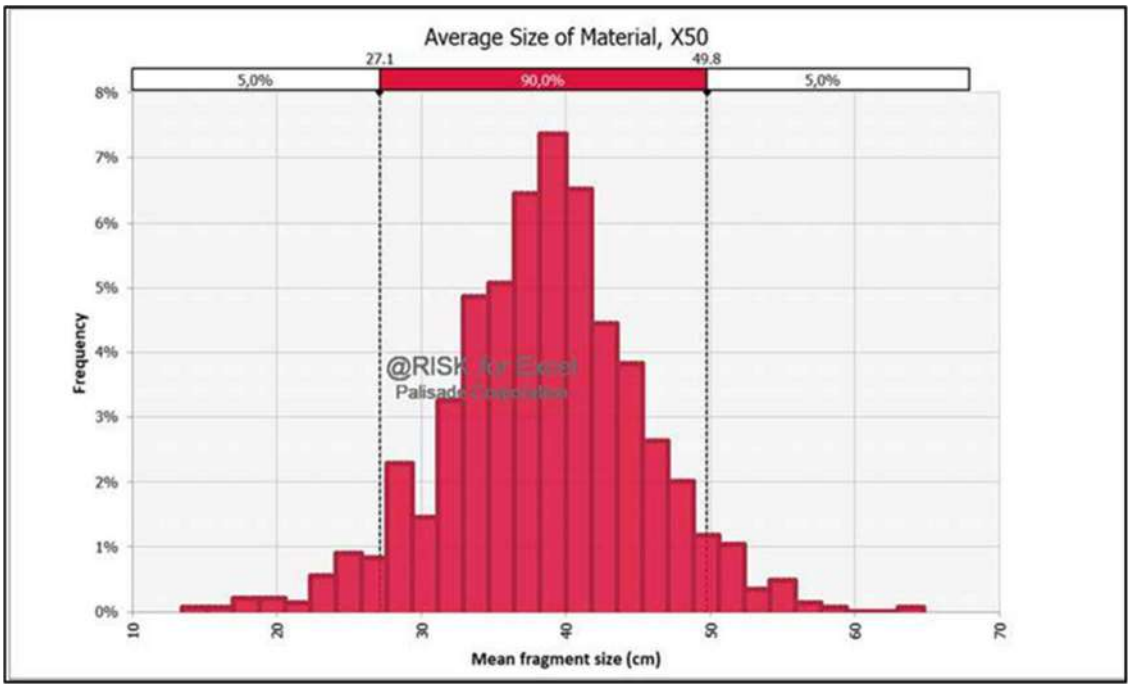

Figure 4.22: South-West mean fragment size distribution (PF = 0.30 kg/m^3)

The graph shows that 90% of the material is between 27cm and 49cm fragment size. The chart also shows that 50% of the material was below the mean fragment size of 39cm. Further, 45% of the blasted material was between 39cm and 49cm fragment size. Given the max fragment size of 50cm was desired, one can see that 95% of the

material was below the cutoff limit of 50cm. This might be an ideal situation. However, it would have to be mindful of the associated costs drilling and blasting to achieve this scenario

The South-East blast fragmentation distribution results are presented in Figure 4.23.

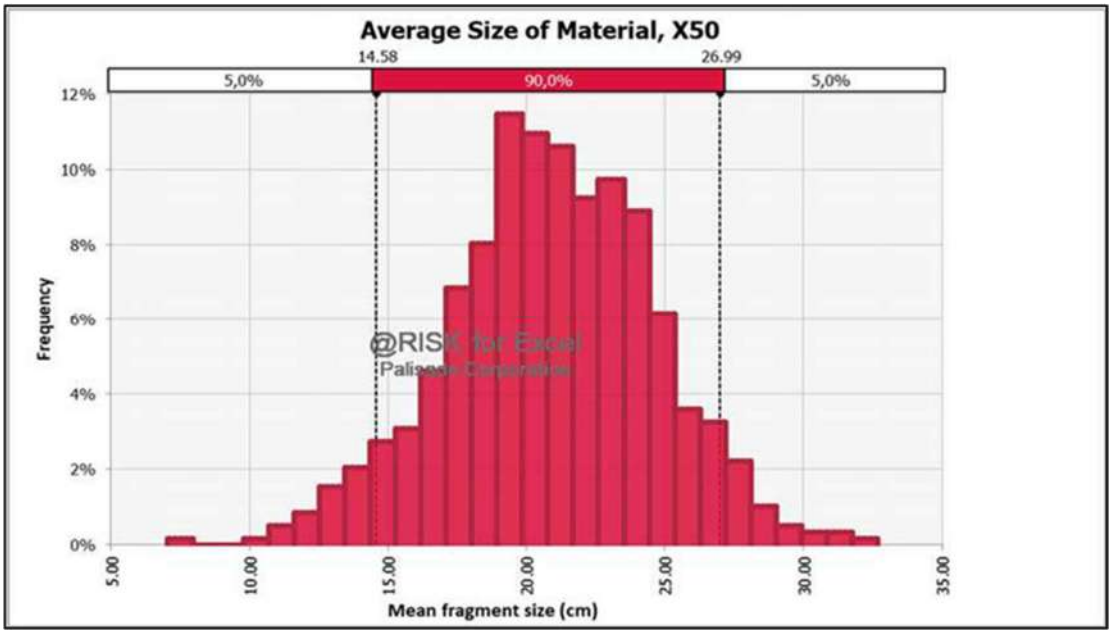

Figure 4.23: South-East mean fragment size distribution (PF = 0.65 kg/m^3)

Figure 4.23 depicts that in the South-East blast area (with all parameters dynamic and powder factor of 0.65 kg/m3), the size fragment distribution is between 14.58cm and 26.99cm. Half (50%) of the material was below the mean fragment size of 21cm with 45% of the material being between 21cm and 27cm. In this scenario, more than 97% of the blasted material was below the mine's mean fragment size of 30cm. The mine required particle size at 50% passing to be 30cm and 80% passing to be 50cm. with the results of this scenario, excessive amounts of explosives would be used. This is not an ideal situation for a mine that is less than 120m from residential areas. Figures 4.24 and 4.25 depict the results of obtained from the simulation of South blast area.

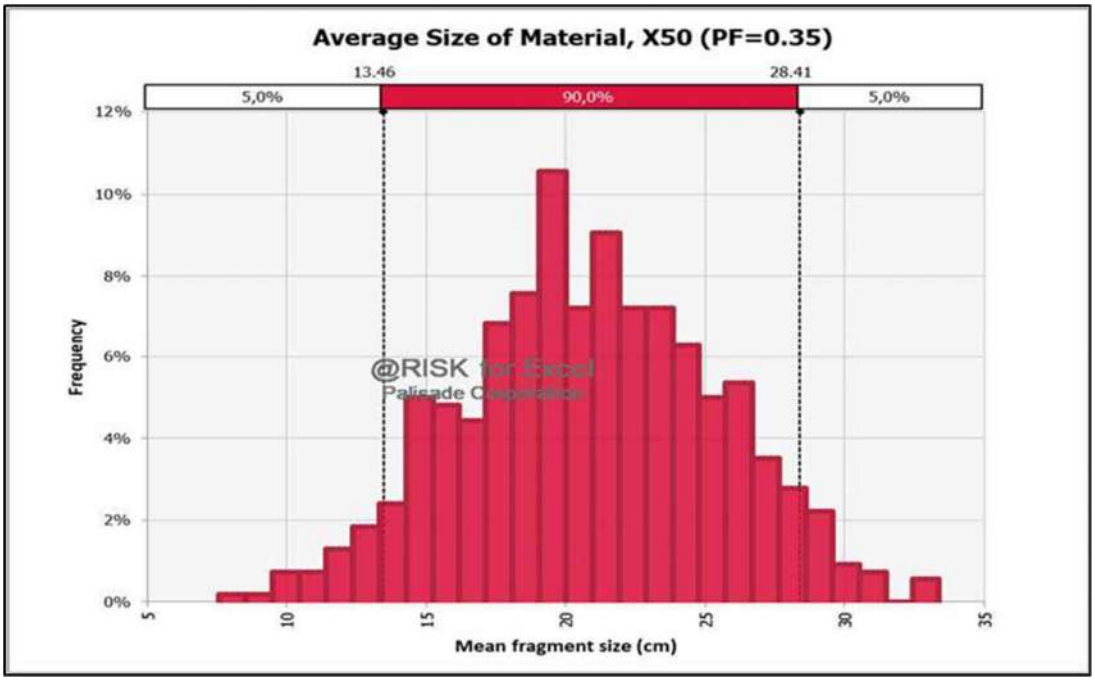

Figure 4.24: South mean fragment size distribution (PF = 0.35 kg/m^3)

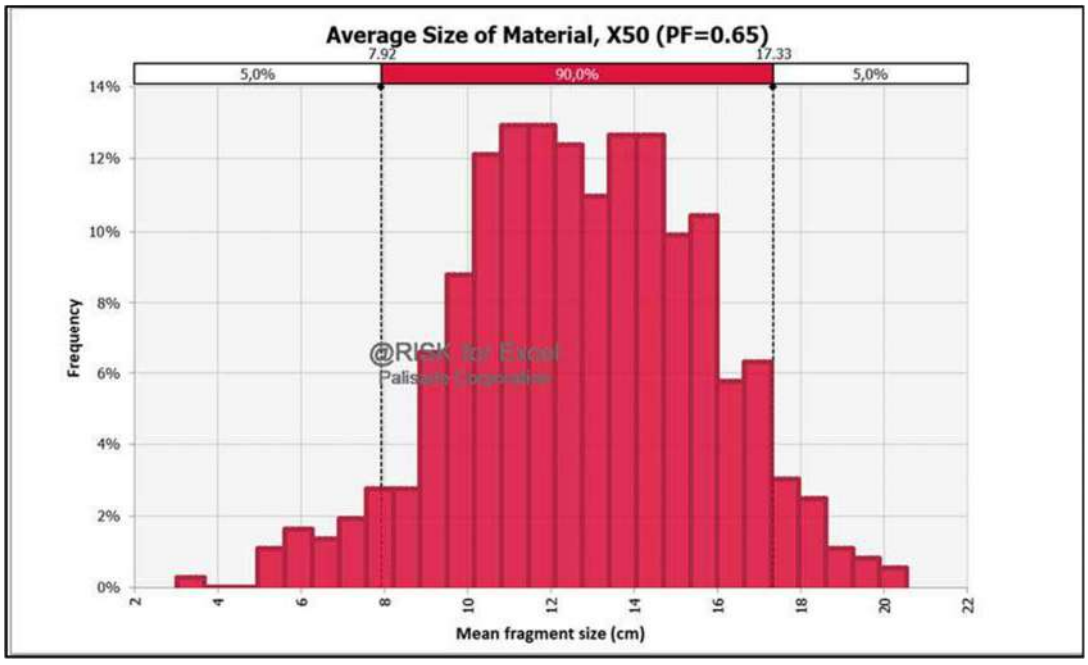

Figure 4.25: South mean fragment size distribution (PF = 0.65 kg/m^3)

For the South blast, Figure 4.24 and 4.25 results indicate that the size fragment distribution varies significantly between the two powder factors values with the high powder factor producing finer fragment size. The blast simulation results of areas with powder factor 0.35kg/m^3 produced results that are closer to the target mean fragment size of 30cm. However, those of a higher powder factor (0.65kg/m^3) produced

excessively finer fragment size that was below 20cm. This scenario was clearly not desired from a cost point of view.

Due to the higher powder factor (0.65kg/m^3) associated with the results of Figure 4.23 and 4.25, the following concerns were raised:

- The powder factor was too high for the type of rock encountered.
- The proximity of the mine to residential areas gave rise to incidents of fly-rocks reported by the community.
- Excessive ground vibration destroying houses and the mine was having to compensate the community.
- The higher powder factor would result in higher explosives consumption.

4.4.2 Mean Fragment Size Sensitivity

A sensitivity analysis was performed to identify parameters with the most significant influence on blast fragmentation size distribution. Given that different simulation conditions were placed upon each blast area, the results of the sensitivity analysis would indicate which parameters most influenced the blast fragmentation results under the set conditions per blast area. The South-West blast fragmentation sensitivity results are presented in Figure 4.26.

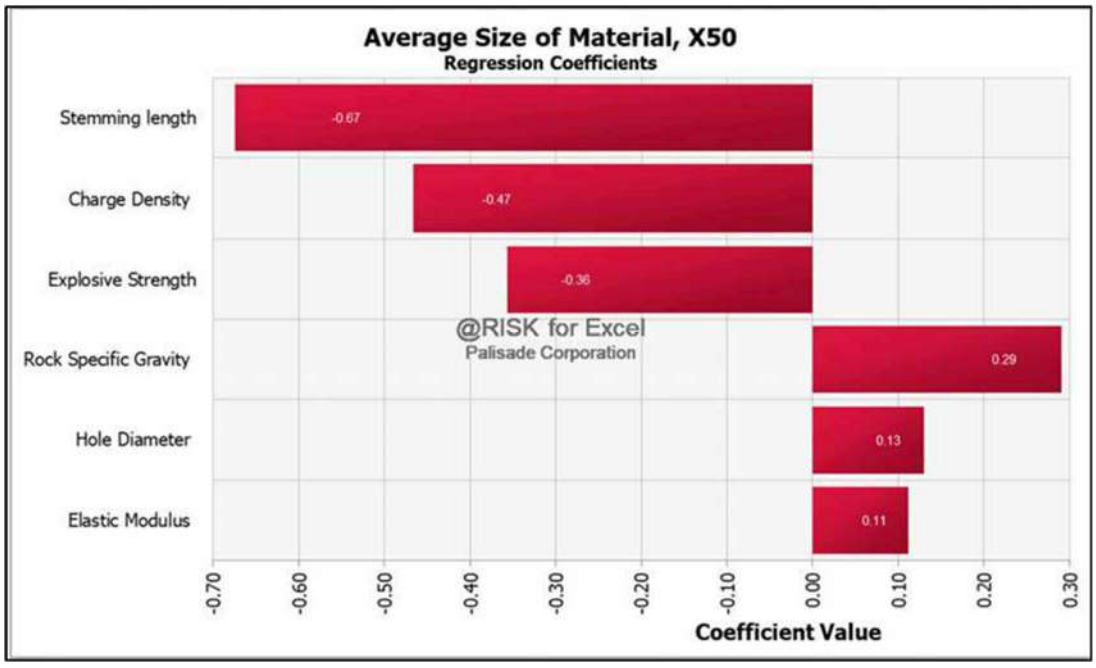

Figure 4.26: South-West mean fragment size sensitivity analysis

Figures 4.26 indicated that stemming length, charge density, and explosive strength had a significant influence on the fragmentation size distribution for the South-West blast. When one fixes the burden and spacing, the only factors that would likely affect the fragmentation are down the hole parameters as already expressed above.

The South-East blast fragmentation sensitivity results are presented in Figure 4.27.

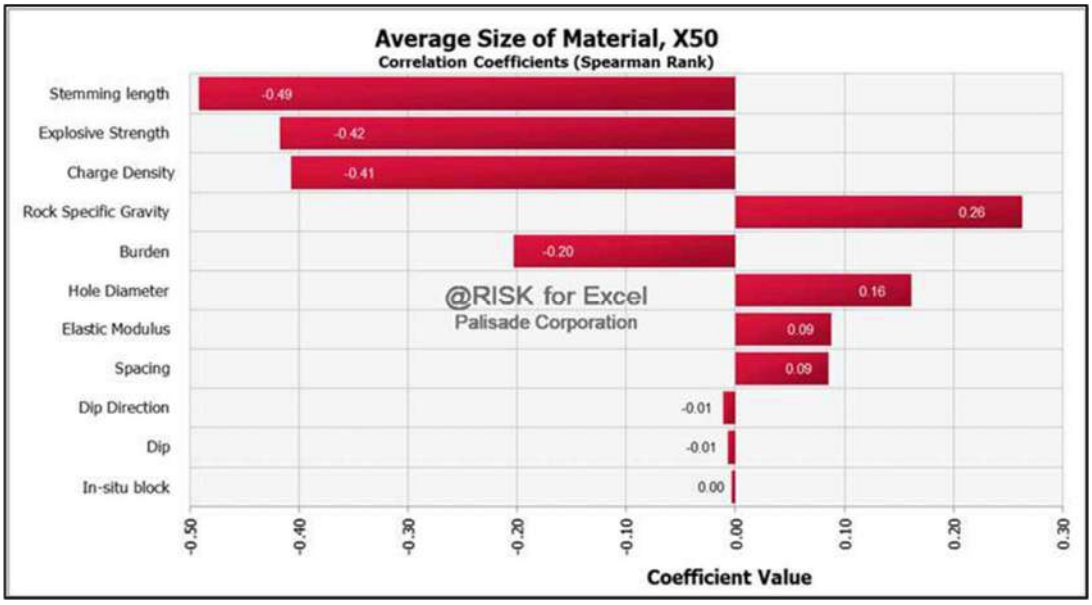

Figure 4.27: South-East mean fragment size sensitivity analysis

In the South-East blast (Figure 4.27), all the blast design parameters were dynamic. In this case, the stemming length, explosive strength, and charge density are the major influencers. When studying results for South-East and South-West blasts, one can see that the factors with the most influence on mean fragment size are the same for fixed burden and spacing pattern and dynamic burden and spacing pattern.

Figure 4.28 depicts the parameters that influenced the blast results achieved from the South blast area, where the powder factor was constant. In this case, joint dip angle, stemming length, and rock density were influential parameters.

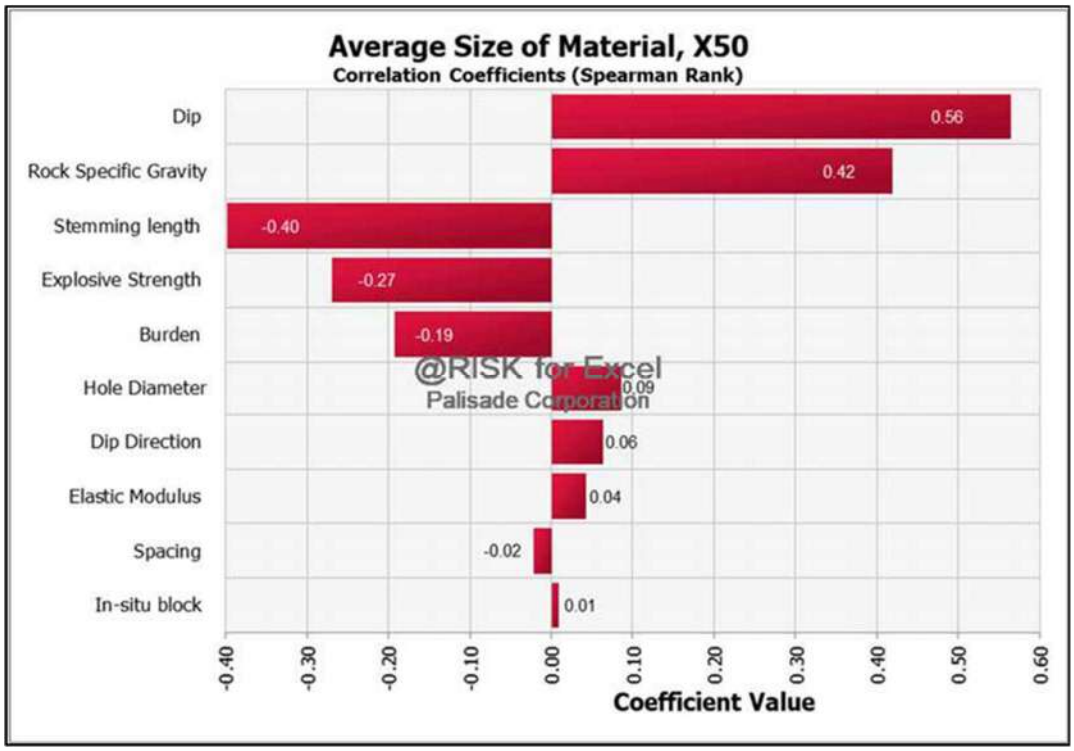

Figure 4.28: South mean fragment size sensitivity analysis

4.4.3 Mean Fragment Size Scatter Plots

The degree of influence on fragmentation size was driven by the Blastability Index of each area and blast design pattern. The relationship for the most influential parameters, which are parameters with a correlation coefficient above 0.4, are presented in this section. The 0.4 correlation coefficient was chosen as the lower limit to determine parameters with a moderate to strong correlation.

The majority of parameters selected to have an influence (those with correlation coefficient 0.4 and above) on the mean fragment size had a moderate to weak linear relationship with the mean fragment size. Their regression coefficient values were between 14% and 48%. Figure 4.29 depicts the relationship between the mean fragment size and stemming length for the South-West blast.

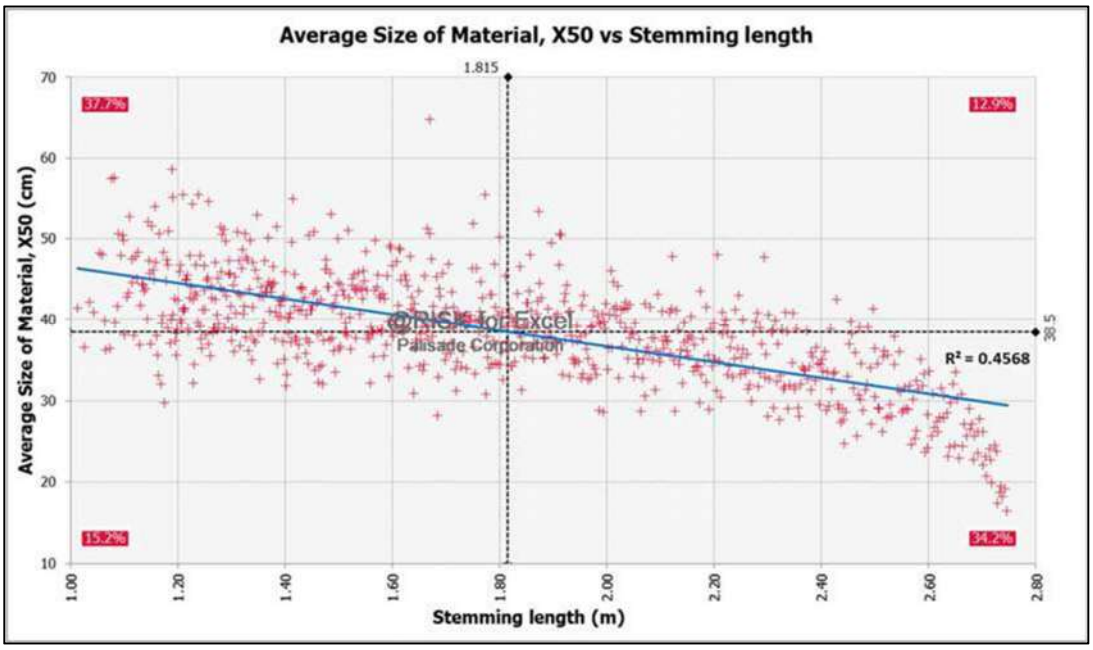

Figure 4.29: South-West mean fragment size vs stemming

The graph showed that the greater the stemming length, the smaller the fragmentation size gets. This is because the higher the stemming length (Including the quality of the stemming material in terms of its interlocking properties), the more time the explosive energy will have in interacting with the rockmass thus producing the desired fragment size.

The stemming was very important to determine the fragment size achieved, given that the burden and spacing, and the powder factor were already preselected. The longer the stemming length, the charge density remained more stable within the 0.30 kg/Bcm and 0.4 kg/Bcm. This could be as a result of the dynamic hole diameter in the simulation run.

Figure 4.30 depicts the relationship between the mean fragment size and charge density for the South-West blast.

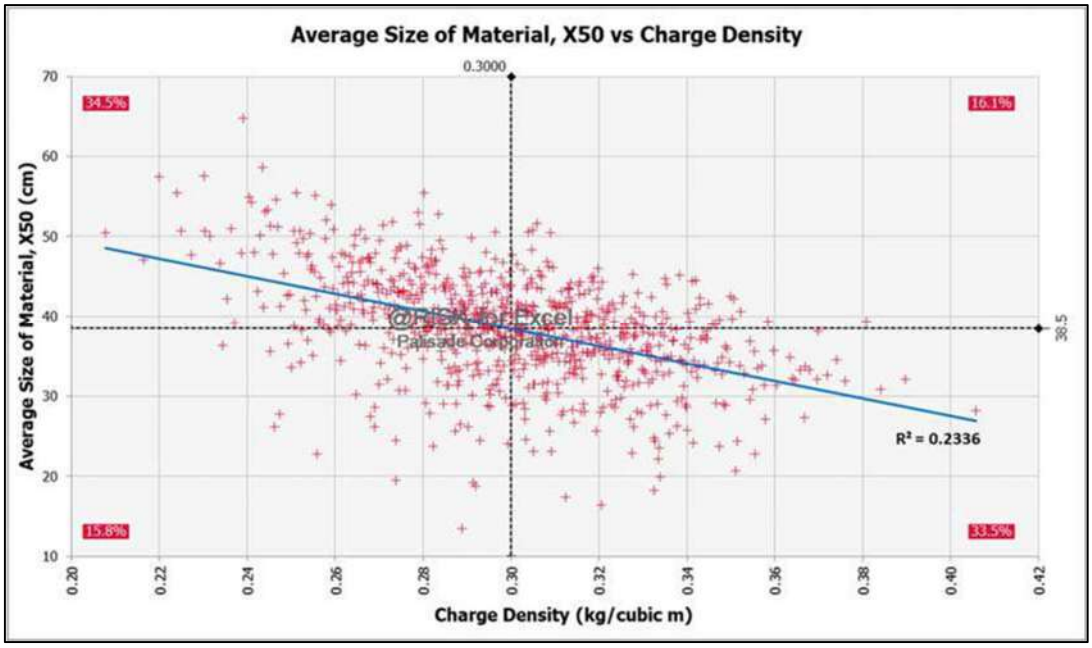

Figure 4.30: South-West mean fragment size vs charge density

The higher the charge density, the smaller the average fragment size. To achieve a finer fragmentation size, the powder factor (charge density) must increase. The charge per hole is another significant factor in determining the fragment size achieved. Given that both the stemming length and charge density affected the fragment size, it was interesting to compare the two variables against each other to test their relationship. There was no clear trend between the charge density and the stemming length, as depicted in Figure 4.31.

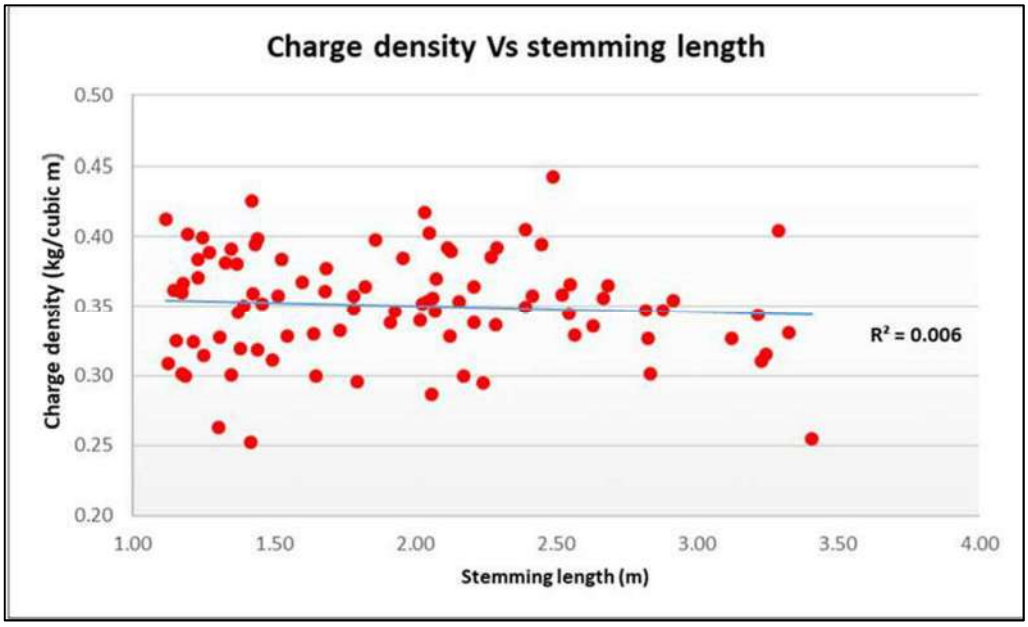

Figure 4.31: South-West charge density vs stemming length

Figure 4.32 depicts the relationship between the mean fragment size and the stemming length for the South-East blast.

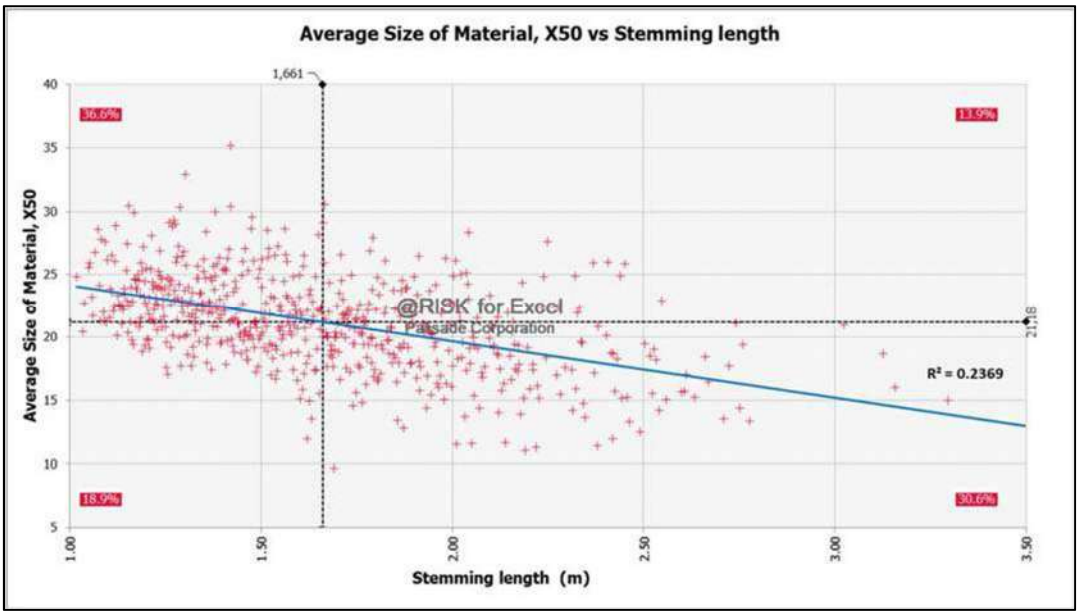

Figure 4.32: South-East mean fragment size vs stemming length

The graph depicts that, the longer the stemming length, the smaller the fragmentation size material. However, this must be counterbalanced with the explosive column charge to ensure good fragmentation.

Figure 4.33 depicts the relationship between the mean fragment size and explosives strength for the South-East blast. The stronger the explosive, the smaller the average material size achieved.

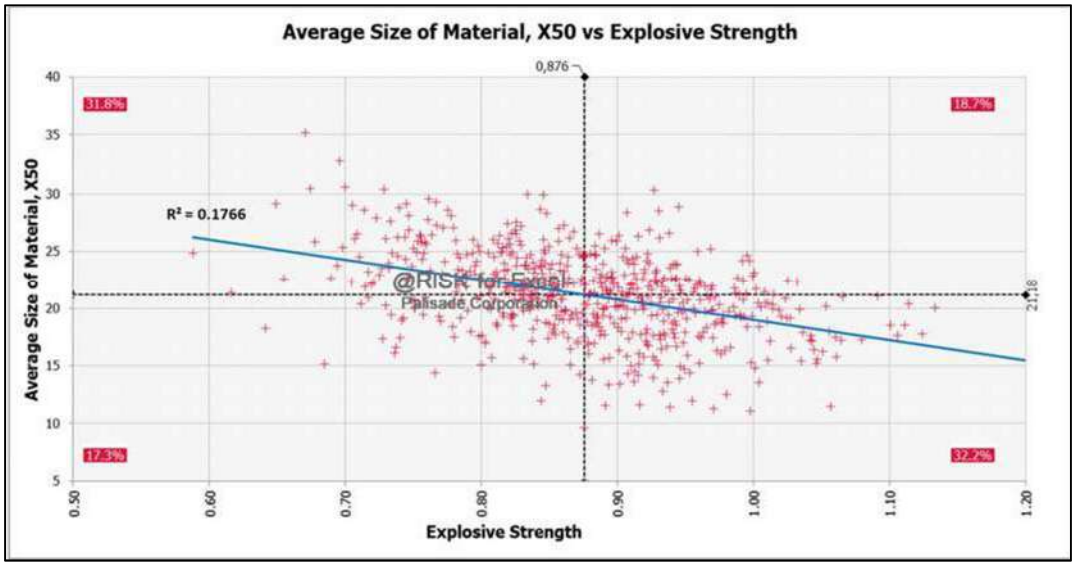

Figure 4.33: South-East mean fragment size vs explosives strength

Figure 4.34 depicts the relationship between the mean fragment size and dip angle for the South blast

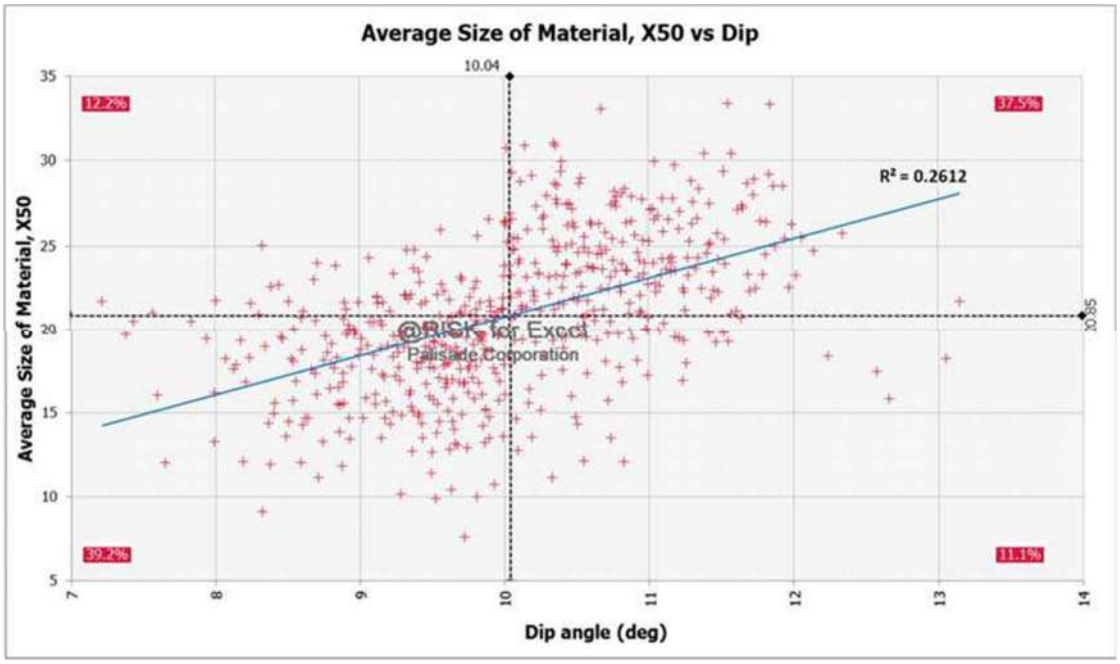

Figure 4.34: South mean fragment size vs dip angle

The graph shows that the shallower the joint dip angle, the finer the fragmentation size will be. However, the strength of the relationship between the two variables is not that strong.

Figure 4.35 depicts the relationship between the mean fragment size and rock specific gravity for the South blast.

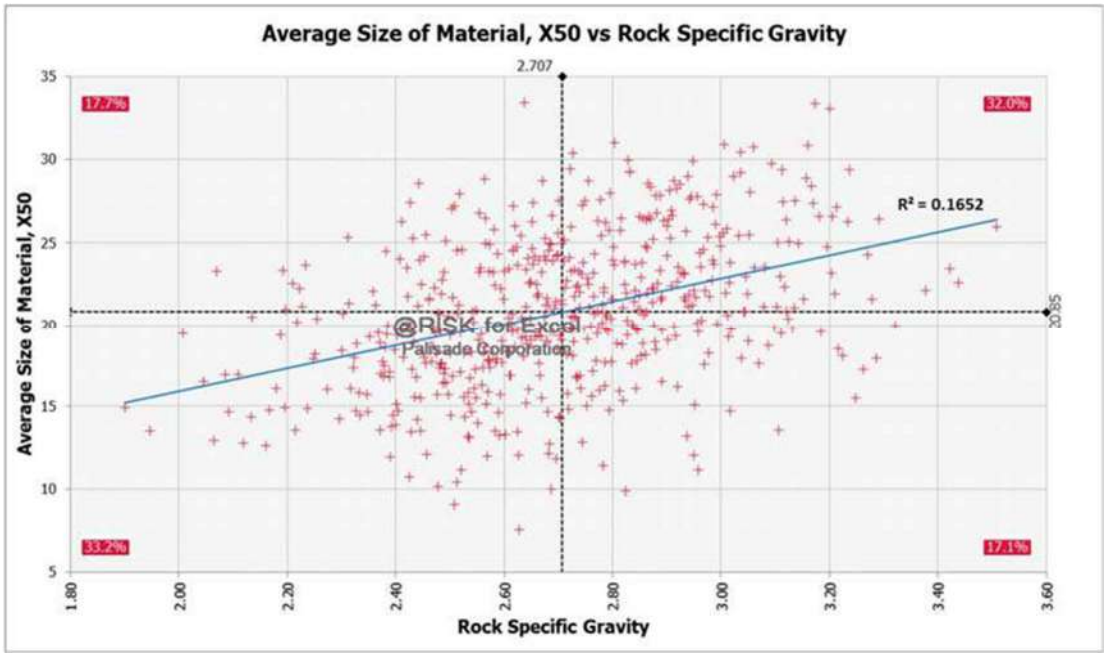

Figure 4.35: South mean fragment size vs rock specific gravity

Figure 4.35 shows that if the rock material being blasted has a lower rock density, finer fragmentation size materials is achievable. Figure 4.36 depicts the relationship between the mean fragment size and stemming length for the South blast.

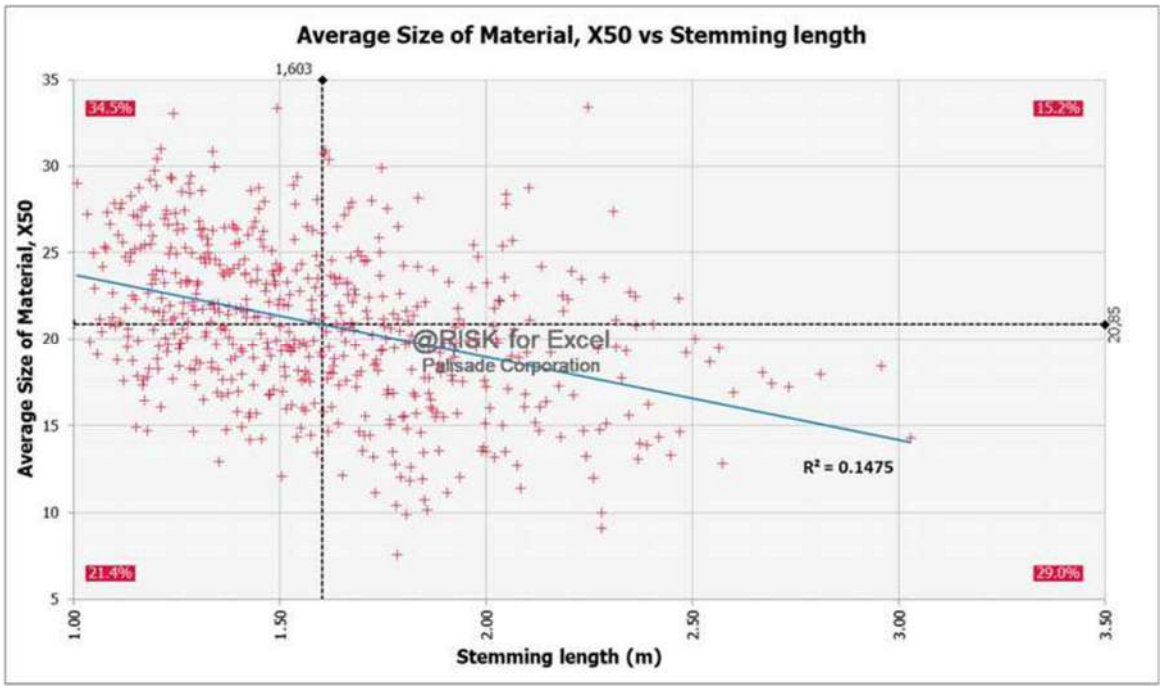

Figure 4.36: South mean fragment size vs stemming length

The same conclusion is reached as in Figure 4.32 in that, the longer the stemming length, the smaller the fragmentation size material achieved

4.5 Fragment Size Distribution from Simulation

Given the differences that existed between the three blasted areas in terms of their geotechnical characteristics, geometric blast parameters and the simulation conditions, the fragmentation distribution graphs for these blast areas were always going to differ. Figures 4.37 to 4.43 depict a series of fragmentation size distributions achieved from the simulation studies of the blasted areas. Figure 4.37 shows the single fragment size distribution for South-East blast.

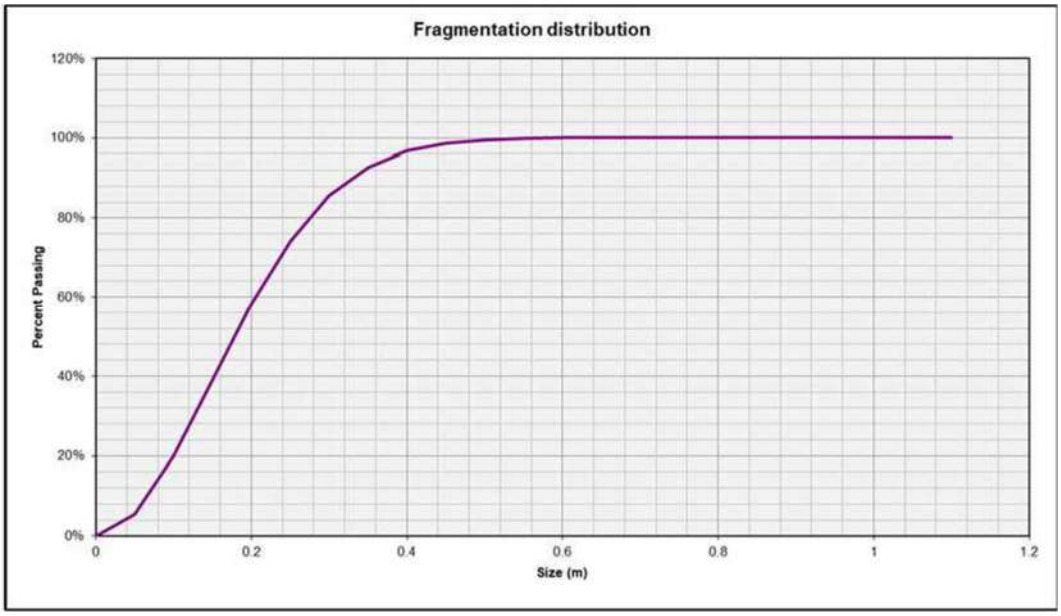

Figure 4.37: South-East blast fragmentation distribution (PF = 0.65 kg/m^3)

This single particle size graph shows that at 50% passing, the particle size was about 18cm while at the 80% passing mark, the fragmentation size was around 28cm. For 100% of the material passing, the fragmentation size was below 44cm. These results were within the required targets of the mine. However, the associated high powder of 0.65kg/Bcm required to achieve this result was not acceptable as per the reasons explained in Section 4.4.1 concerning Figures 4.23 and 4.25. Figure 4.38 shows multiple simulation results not shown in Figure 4.37.

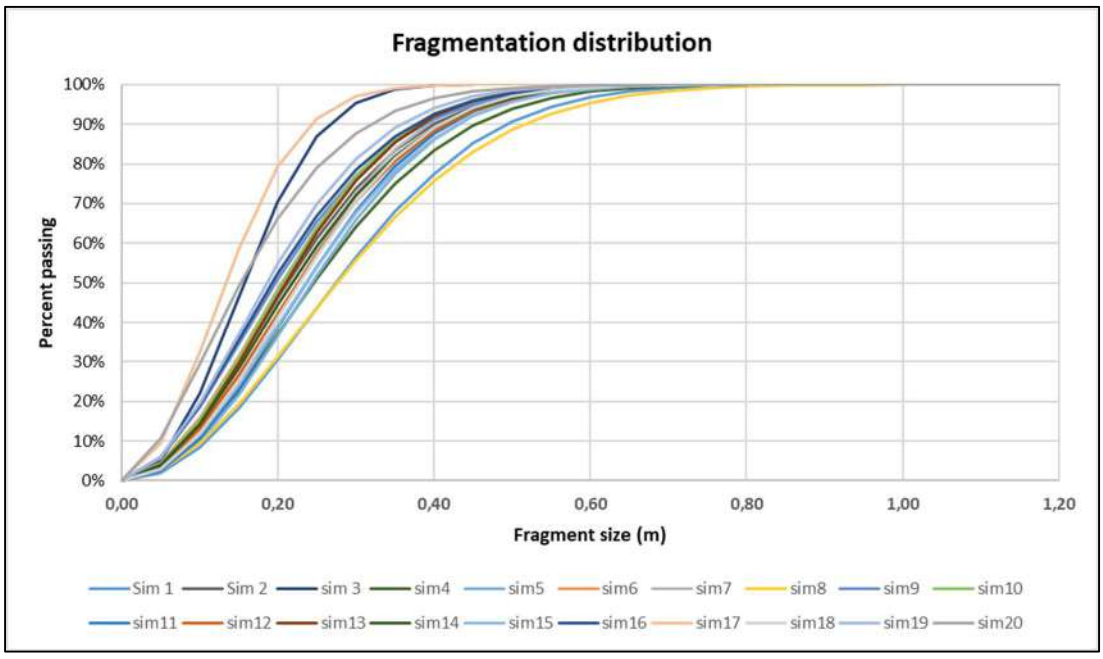

Figure 4.38: South-East simulation output results (PF = 0.65 kg/m^3)

The simulation results used to produce Figure 4.38 are contained in Appendix D15. Figure 4.39 shows the single fragment size distribution for South-West blast (powder factor 0.30 kg/m^3).

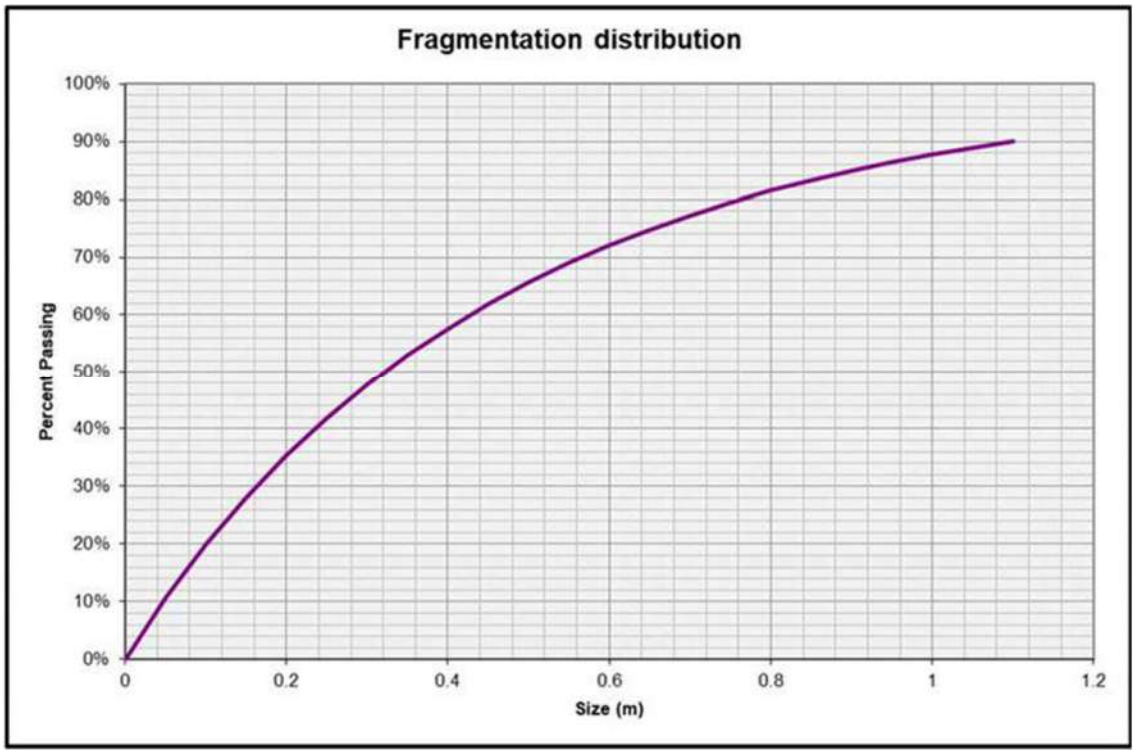

Figure 4.39: South-West blast fragmentation distribution (PF = 0.30 kg/m^3)

Figure 4.39 shows that at 50% passing, the fragment size was 35cm and 80% passing the fragment size was 76cm. The pattern of 2m by 2m with a powder factor of 0.30kg/Bcm was not able to meet the target fragmentation size requirements. However, this was due to a shorter stemming length. From the simulation results contained in Appendix D16, one can see that when the stemming length continues to increase, the fragment size improved dramatically. This points to the fact that, in a small drill and blast pattern, to get effective fragmentation size, one must be able to contain the explosive energy within the blast hole for longer. Figure 4.40 shows the other simulation results achieved for the fixed powder factor of 0.30kg/Bcm in the south-west blast.

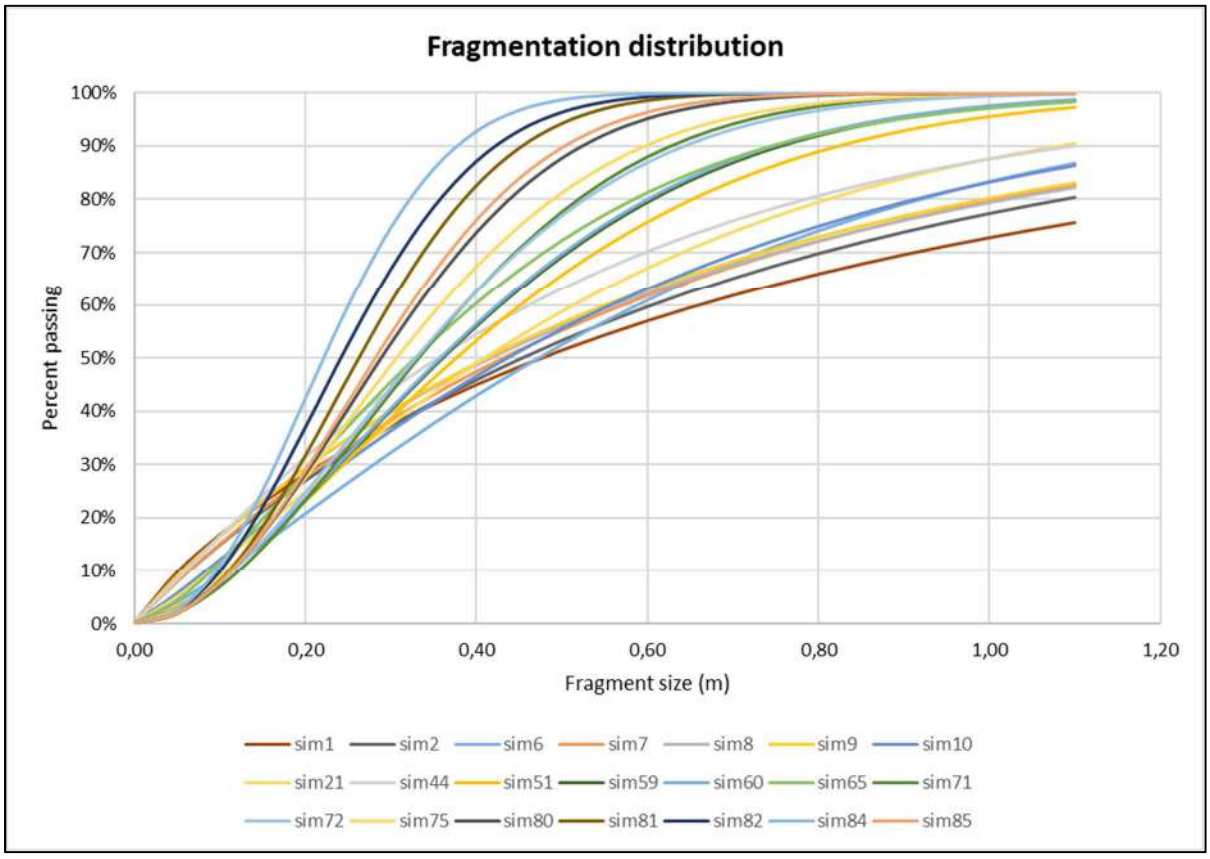

Figure 4.40: South-West simulation output results (PF = 0.30 kg/m^3)

The sim80 results shows fragment size (30cm) passing at 53% and 88% of the fragment size spectrum up to top size (50cm) passing. This was achieved when the burden was 2.16m and spacing was 1,97m, while the stemming length was 2.37m with a fixed powder factor of 0.30kg/Bcm. Sim85 shows fragment size of 30cm passing at 55% and 50cm fragment size at 90%, when burden was 2.10m and spacing was 1.96m, stemming was 2.59m with powder factor of 0.30kg/Bcm. Therefore, in a blocky ground conditions, it is imperative to contain the explosive energy in the blast hole to get good fragmentation. Figure 4.41 shows a single fragment size distribution for South blast for powder factor 0.35 kg/m^3.

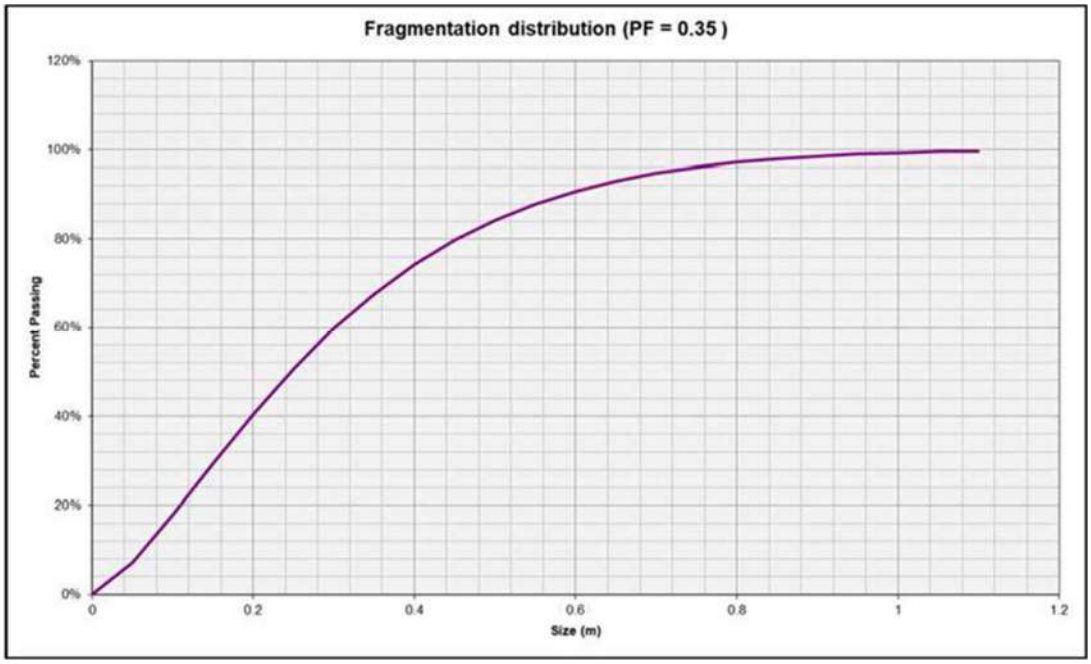

Figure 4.41: South blast fragmentation distribution (PF = 0.35 kg/m^3)

Figure 4.41 shows that at 50% passing the average fragment size was 24cm while at 80% passing the fragment size was about 42cm. This scenario offered possibilities to refine the blast results due to the fragment sizes being closer to the target fragment size requirements. Figure 4.42 shows the multiple simulation results for the south blast.

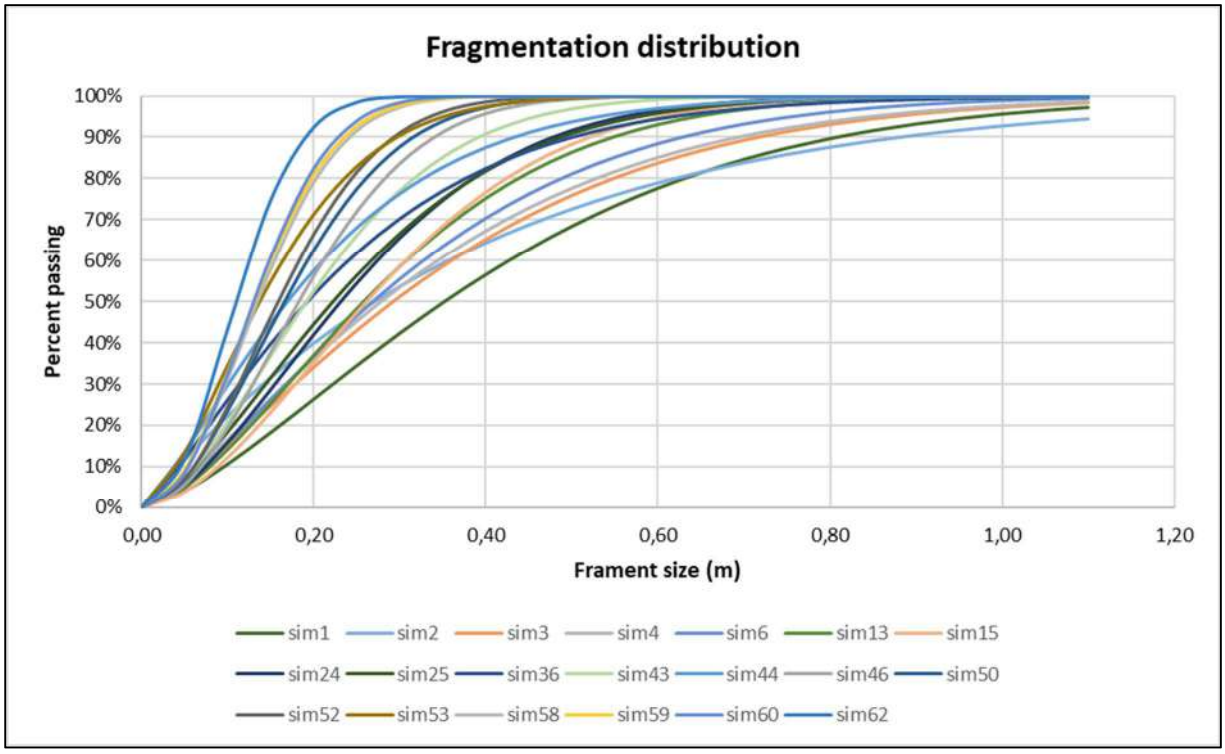

Figure 4.42: South simulation output results (PF = 0.35 kg/m^3)

Sim13 shows that when the burden and spacing are held constant at 2.5m by 2.5m, the stemming being 1.6m, 59% of the fragment size of 30cm would pass and 86% of fragment size of 50cm would pass. However, one gets to see also (Appendix D17) from the results of sim62 that when you increase the stemming and powder factor, 100% of particle size 30cm gets to pass. Therefore, it is sensible to choose the right stemming length to ensure that you don't create too much fine fragment size material than necessary. Figure 4.43 shows the fragment size distribution for South blast with a powder factor of 0.65 kg/m^3. The other simulation results of powder factor 0.65kg/Bcm are not shown as they were too excessive as per reasons advanced in Section 4.4.1.

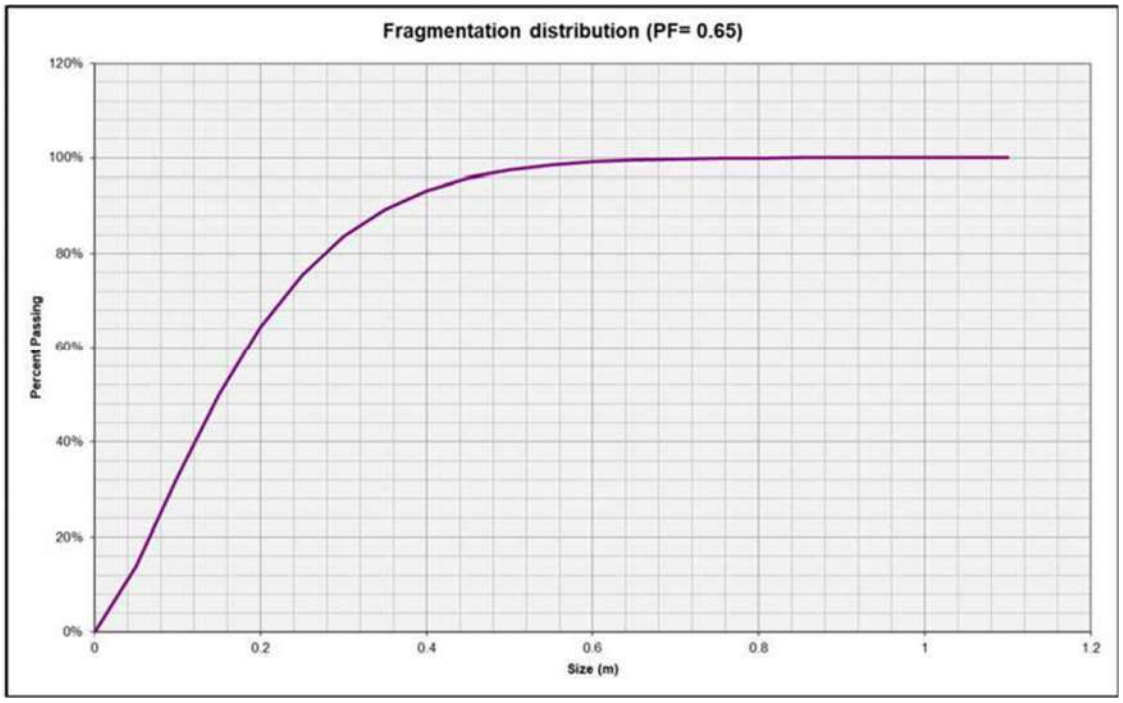

Figure 4.43: South blast fragmentation distribution (PF = 0.65 kg/m^3)

The results of Figure 4.43 indicate that the powder factor of 0.65 kg/m^3 was way too much for the rock-type encountered and does not meet the mine requirements of ensuring mean fragment of 30cm at 50% passing and 50cm at 80% passing, in this case, at 50% passing the fragment size was 18cm and at 80% passing the fragment size was 28cm.

4.6 Fragmentation Size Distribution Results from Image Analysis

Each blast area image results were obtained by combining a minimum of three image analysis taken at different positions to get a more accurate result of the blast. Figures

4.44 to 4.46 depicts the results achieved from the actual blasts in the respective blast areas.

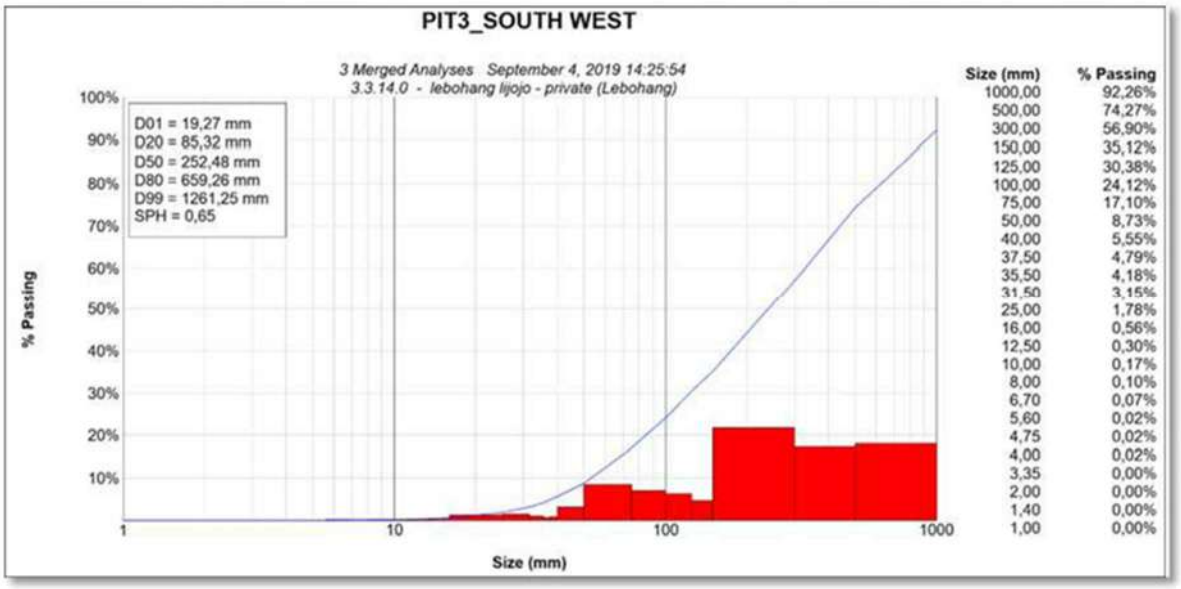

Figure 4.44: South-West blast fragmentation distribution

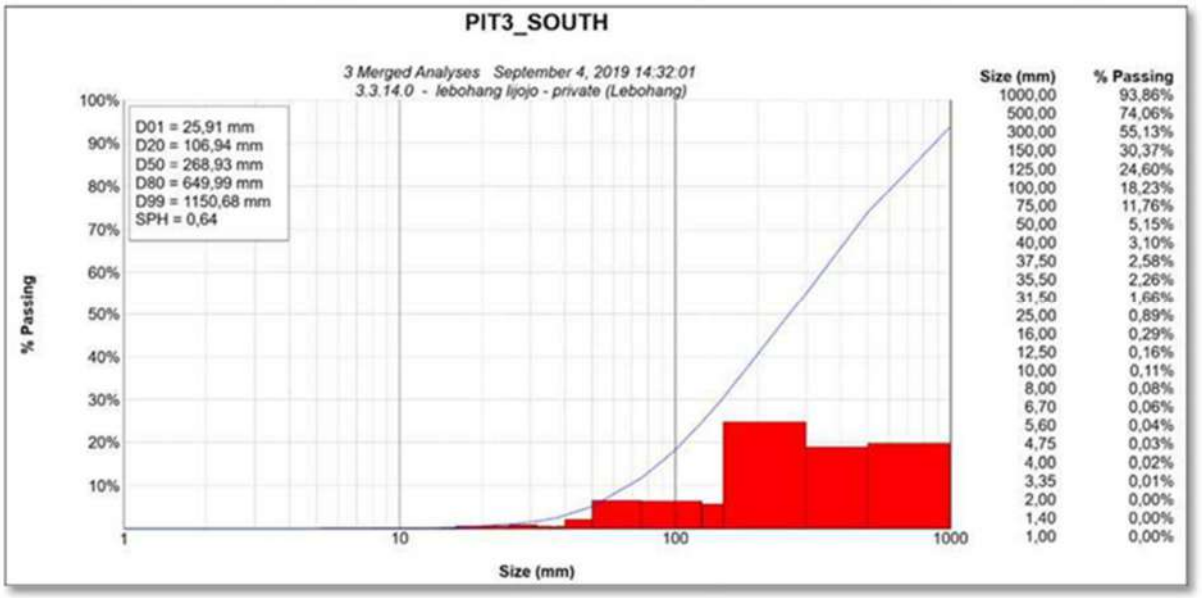

Figure 4.45: South blast fragmentation distribution

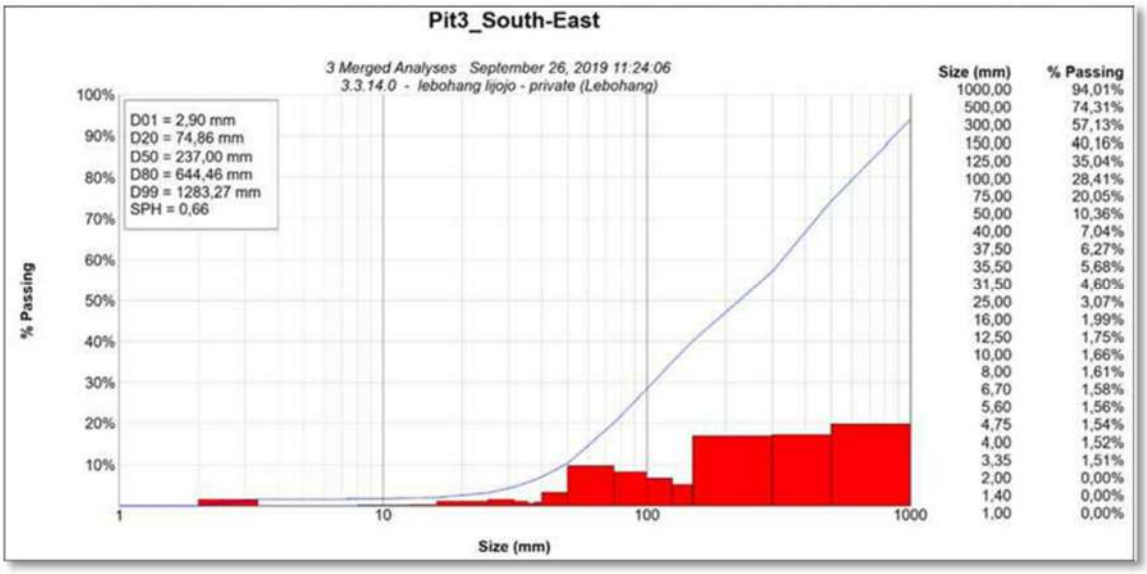

Figure 4.46: South-East blast fragmentation distribution

4.7 Results Comparison for Single Particle Size Distributions

The image analysis results (actual fragmentation results) were compared with the simulation results of each blast area to assess the accuracy of the simulation results. The blast areas where the variance between the actual results and the predicted results was less than 10% were considered accurate, and no further work was required. Blast areas where the variance was between 10% and 20% were deemed to be reasonable. However, parameters such as the powder factor, Blastability Index and the Uniformity Index would have to be adjusted. Results of areas with errors of more than 20% were declared invalid.

Figures 4.47 to 4.50 depict the comparison of the simulated fragmentation and the achieved results from the image analysis. Table 4.1 outlines the errors achieved at 50% of the material passing through the screen. The simulation results that were outside the limits of tolerance were adjusted. The adjustment was done by altering either the powder factor or the burden and spacing. In the South-East blast, the original powder factor of 0.65 kg/Bcm was reduced to 0.35 kg/Bcm the blast pattern was reduced to 2.5m by 2.5m.

Table 4.1: Blasting Efficiency using single particle size distribution

Blasts	Mean (x_{50})	Predicted (cm)	Actual (cm)	Error (%)
South-East	Mean (x_{50})	18	22	+ 22
South-East (Adjusted PF 0.35)	Mean (x_{50})	27	22	-18
South (PF 0.35)	Mean (x_{50})	24	26	+ 8.3
South (PF 0.65)	Mean (x_{50})	15	26	+ 73
South West	Mean (x_{50})	32	24	-25
South West (Adjusted PF 0.35)	Mean (x_{50})	28	24	-14

The results of the South-West blast are depicted in Figure 4.47 and they show that the predicted fragmentation distribution was higher than the actual results achieved from the blast. The error achieved between the actual and predicted was -25%, as shown in Table 4.1.

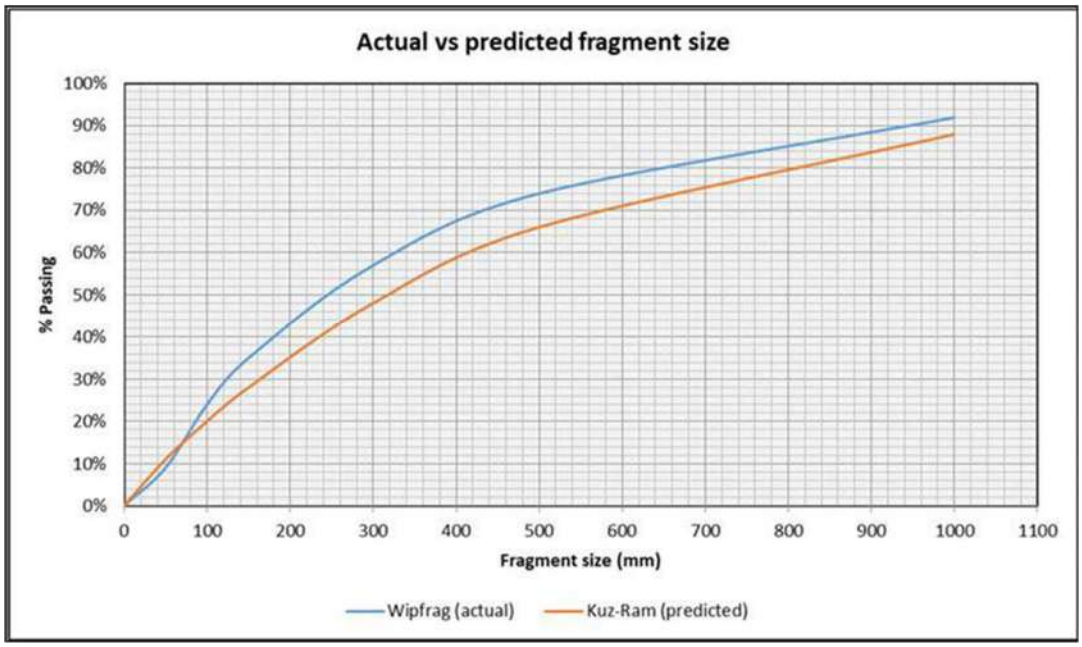

Figure 4.47: South-West blast actual fragmentation vs predicted

The graph depicts the simulation results (orange line) compared with the actual results (blue line) when the initial powder factor of 0.30kg/Bcm. The lower the fragment size, the easier the loading, hauling and crushing. However, the blasting costs need to be

monitored closely to ensure that excessive spending is curbed by not blasting more finer fragment size than required. The initial simulation conditions were adjusted from 0.30 kg/Bcm powder factor to 0.35 kg/Bcm. The burden and spacing of 2m x 2m was changed to 2.5m by 2.5m to correct the -25% error to get it within the 20% (acceptable range). The powder factor was further increased to 0.4 Kg/Bcm to get mean fragment size (30cm) at 58% and max fragment (50cm) at 80%. Figure 4.48 depicts the adjusted Kuz-Ram results compared with the actual results and the initial simulation results.

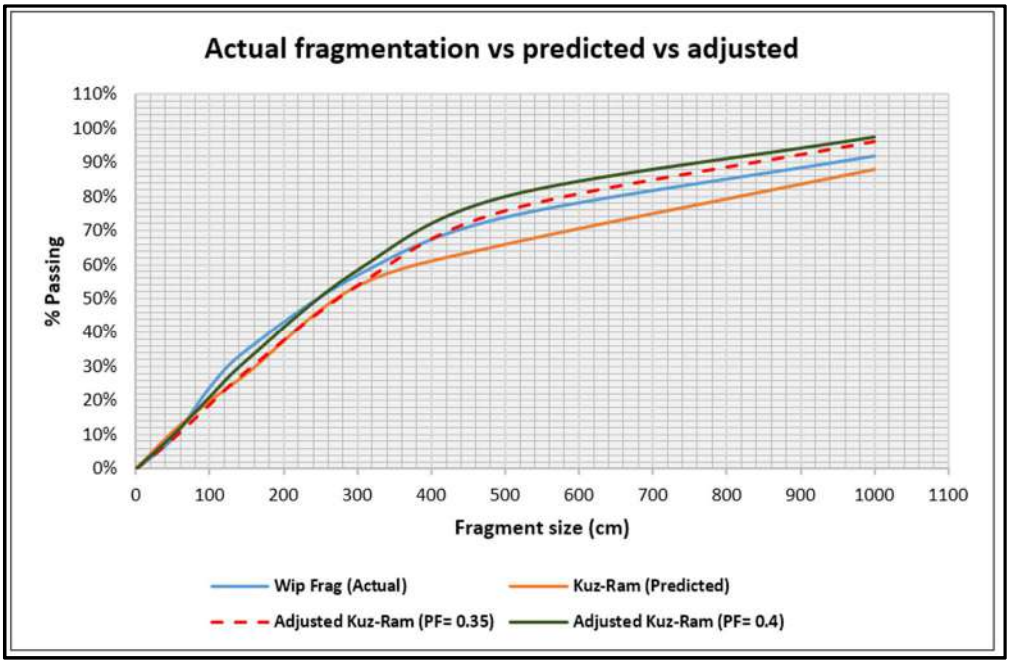

Figure 4.48: South-West blast actual fragmentation vs predicted vs adjusted

Figure 4.49 depicts the simulation and actual fragmentation results for the South blast

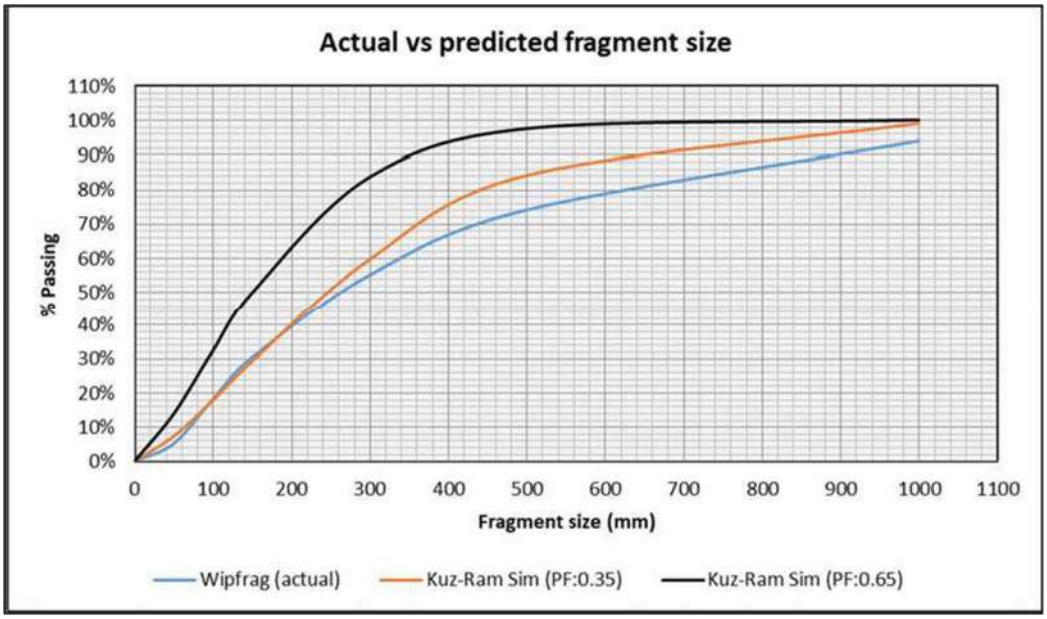

Figure 4.49: South blast actual fragmentation vs predicted

Figure 4.49 indicates that the results of the South blast simulation, where the powder factor of 0.65 kg/Bcm was used were completely unreliable. The gap between the actual fragment results (blue line) and the 0.65 kg/Bcm powder factor results (black line) was excessive. The 0.65Kg/Bcm powder factor produced excessive finer fragment size material than required and would result in higher quantities of explosives used. The powder factor of 0.35 kg/Bcm in this area proved accurate when the burden and spacing were constant at 2.5m by 2.5m. The error between the actual and predicted fragmentation distribution for the powder factor of 0.35 kg/Bcm was 8%, as seen in Table 4.1. Figure 4.50 depicts the simulation and actual fragmentation size results for the South-East blast

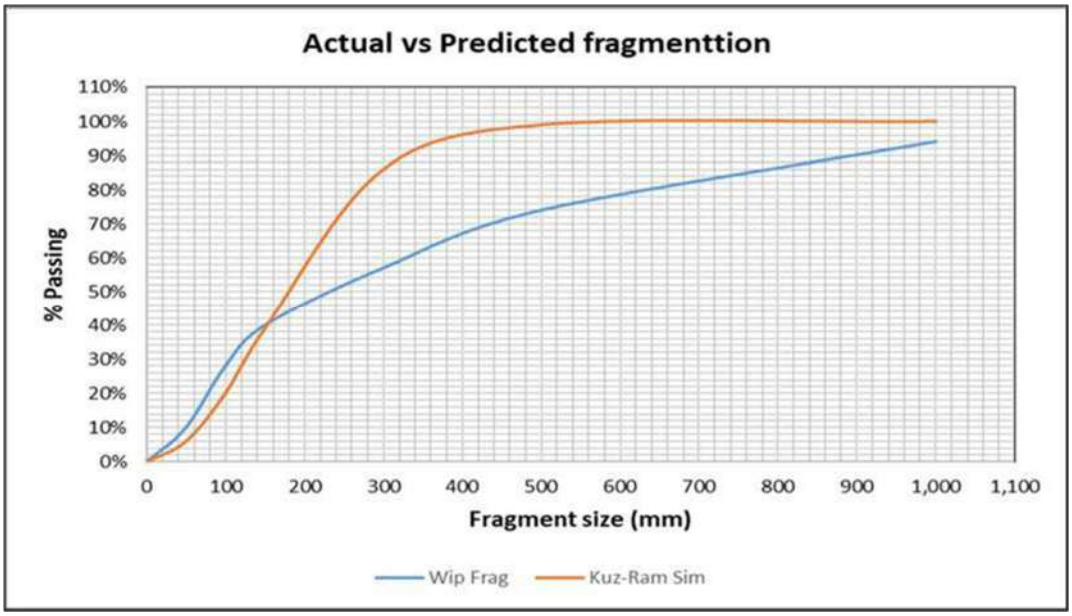

Figure 4.50: South-East blast actual fragmentation vs predicted

Figure 4.50 indicates that at 100% of the material passing, the fragment size would be below 40cm. This result is also achieved with a higher powder factor of 0.65 kg/Bcm. The simulation results for the South-East polygon, as shown in Figure 4.50 indicate that at 50% material passing, the blasting efficiency (error) was closer to the acceptable error region of 20%. However, beyond this point, the gap between the actual and simulated fragmentation size was significant.

Having a dynamic burden and spacing with a dynamic powder factor of 0.65 kg/Bcm was not producing acceptable results. However, when adjusting the powder factor to 0.35 kg/Bcm, the results were within the margin of error of 18%. When adjusting the powder factor further to 0.4 kg/Bcm, mean fragment size (30cm) was 51.6% while max fragment size (50cm) was 86.4%, as shown in Figure 4.51.

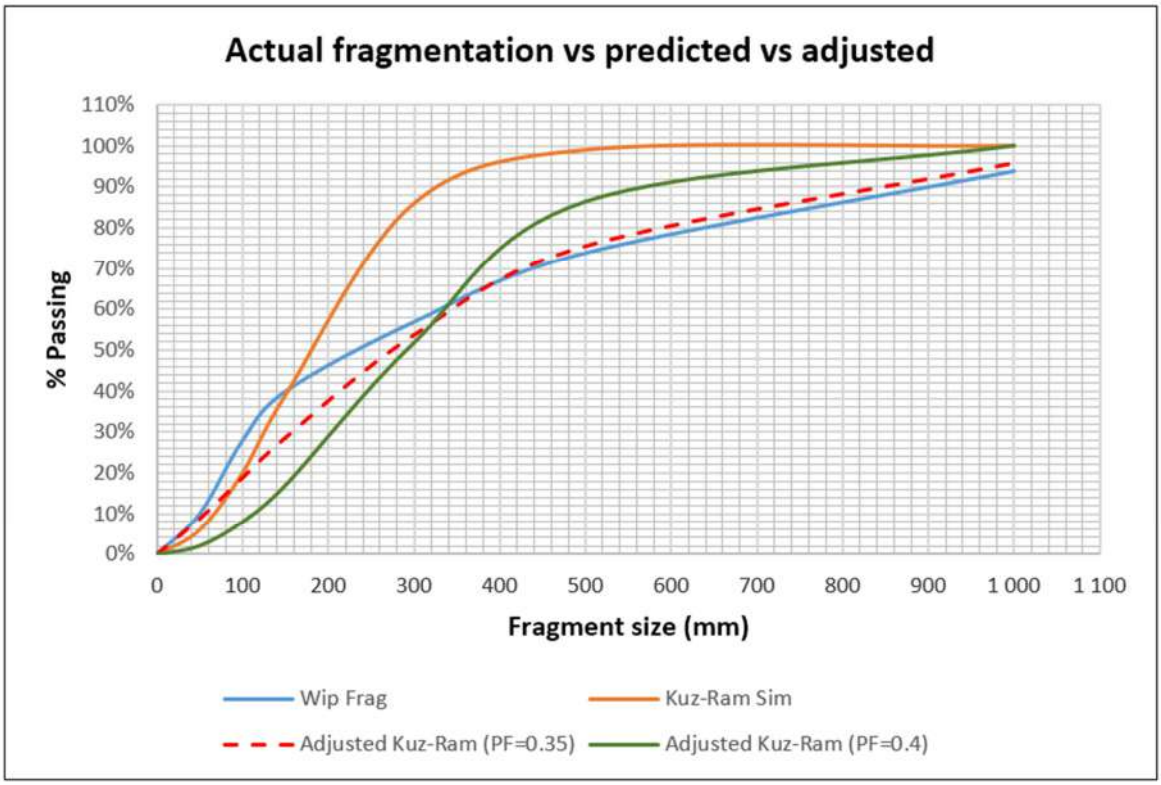

Figure 4.51: South-East blast actual fragmentation vs predicted vs adjusted

It was thus clear that the general blast pattern that produced reliable results in all the blast areas was the burden and spacing of 2.5m by 2.5m with a powder factor between 0.35 kg/Bcm and 0.4kg/Bcm. The mine resolved to use two blasting patterns for ore and waste. The main blast pattern for ore will be 2m x 2m, and the waste pattern will be 2.5m by 2.5m with both materials using a powder factor of 0.35 kg/Bcm or 0.4 kg/Bcm depending on the rockmass characteristics encountered. The idea for the smaller drill and blast pattern for the ore was to increase the proportion of blasted ore fragment of below 50cm passing to above 80%.However, this pattern will also depend on rock characteristics.

4.8 Blasting Costs

The costs studies were conducted after having adopted the drill and blast pattern of 2m by 2m and 2.5m by 2.5m. The preferred drill bit sizes were 105mm and 127mm, and the acceptable powder factor range was between 0.3 kg/Bcm and 0.4 kg/Bcm. The cost analysis for these patterns were conducted using the parameters and simulation conditions set for Pit3_South blast (constant burden and spacing, constant drill hole diameter and variable powder factor).

The constant parameters meant that the costs for the drilling were constant as the drilled or blasted volume was constant. Thus, the total drilling and blasting costs were only affected by the amount of explosives and the number of holes blasted. Figure 4.52 depicts the unit drilling and explosive costs range from the simulation.

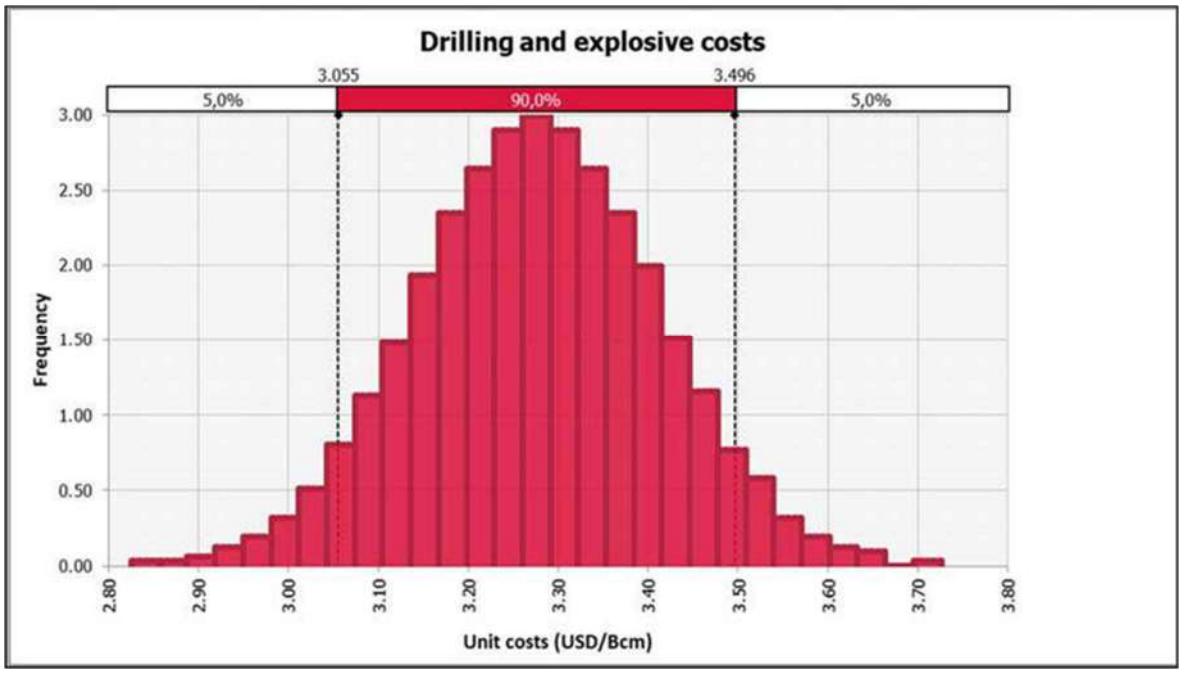

Figure 4.52: Unit drilling and blasting costs

Figure 4.53 depicts the expected absolute drilling and blasting costs range for 400 holes.

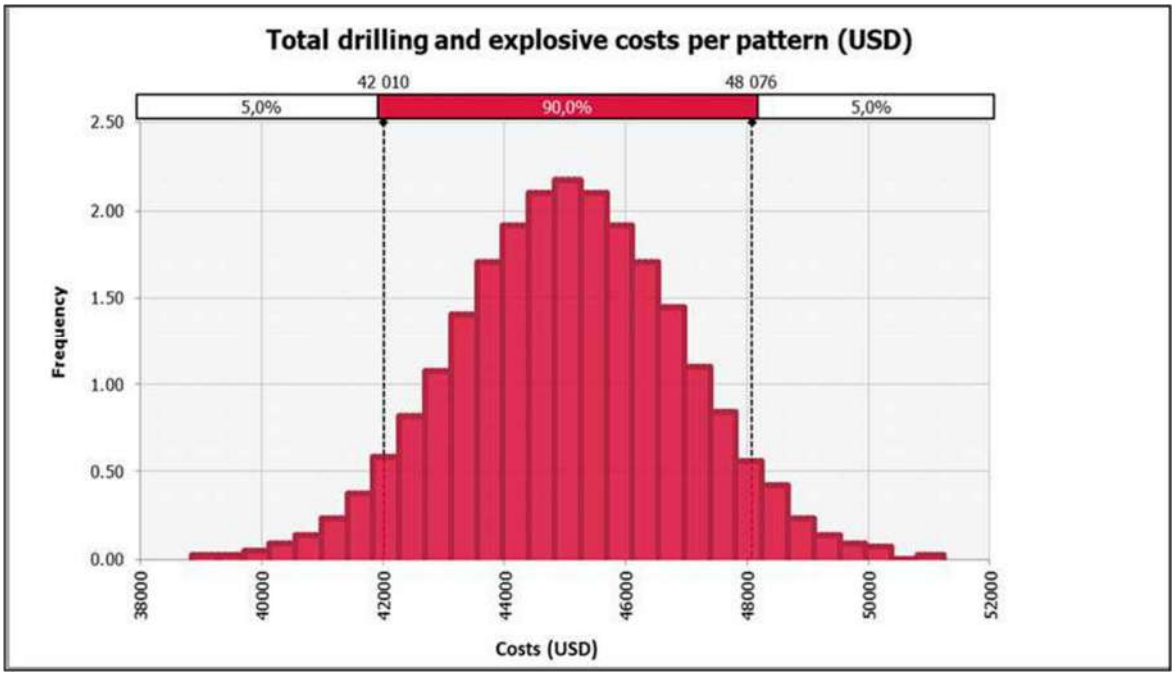

Figure 4.53: Total drilling and blasting costs for 400 blast holes

The average total costs were expected to be USD 45000 per blast with a maximum cost of USD 48000. The simulated cost (cost per Bcm) results were compared with the actual costs (cost per Bcm) for the ten blasts that were conducted, as depicted in Figure 4.54.

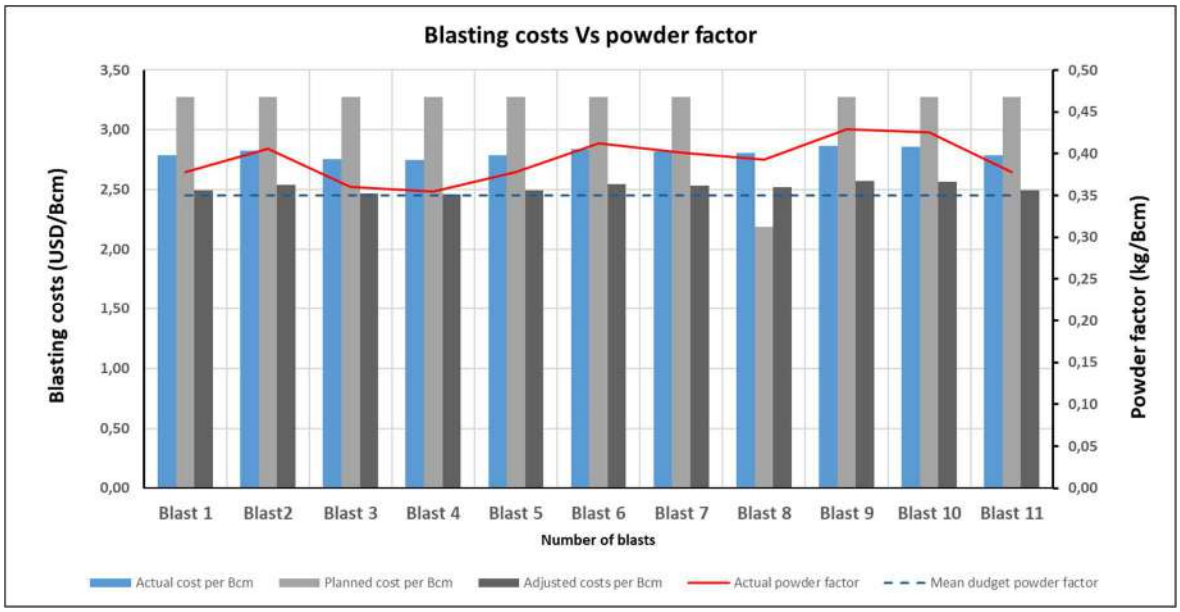

Figure 4.54: Comparison of actual costs vs planned costs

Figure 4.54 shows that the planned drilling and blasting costs were higher than the actual costs before the adjustment. There were two major contributing factors for the lower actual costs. First, it was the explosive price adjustment factor and second, the reduced unit drilling costs realized after the renegotiation and conclusion of the new mining contract. The cost of emulsion explosive decreased from 1614 USD/tonne to 1545 USD/tonne, while the unit drilling costs decreased by 15% from figures stated in Table 3.6. The adjusted costs show that actual costs were slightly higher, with an increase of about 0.3 USD/Bcm over the adjusted costs. Figure 4.55 depicts the relationship between the powder factor and the fragment size achieved.

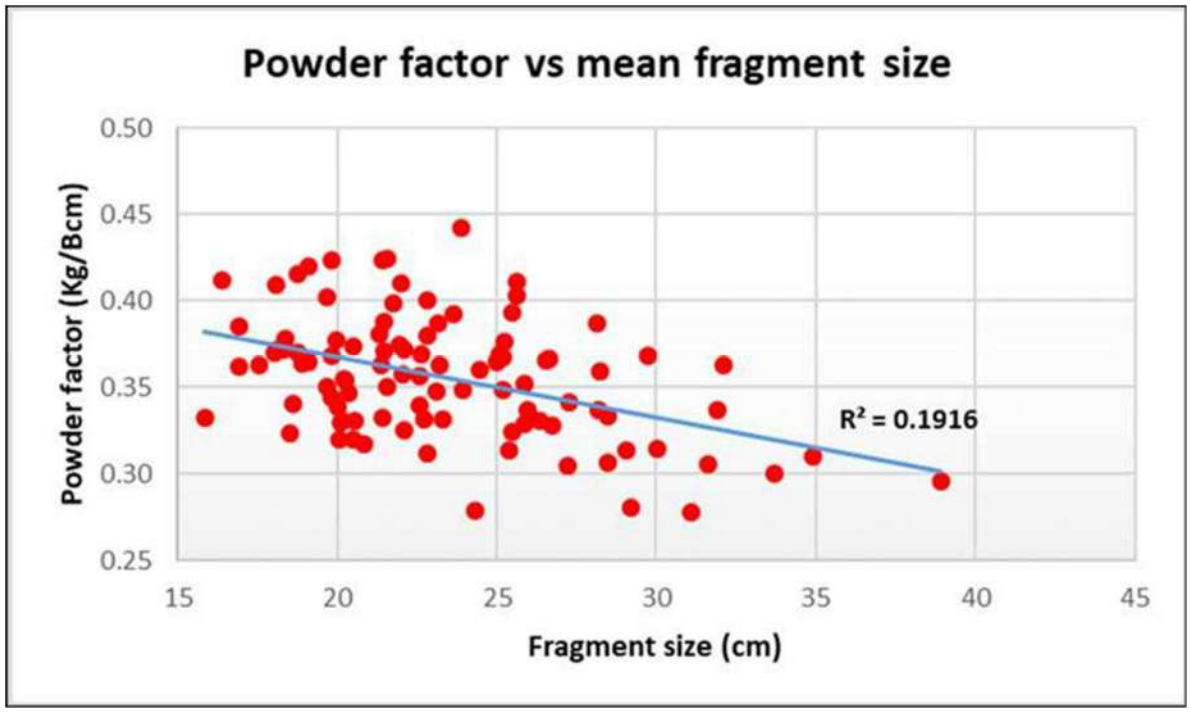

Figure 4.55: Powder factor and the fragment size

When studying the actual costs against the actual powder factor results in Figure 4.54, one notices that the powder factor was generally between the ranges 0.35kg/Bcm and 0.45 kg/Bcm. When comparing this powder factor against the fragment size in Figure 4.55, one realizes that the expected fragment would be between 15cm and 30cm, which was in line with the mine's target of a mean fragment size of 30cm.

Figure 4.17 showed that for a constant burden and spacing, the Uniformity Index was only affected by stemming length and similarly Figure 4.26 depicted that the key parameters that affected the mean fragment results were the stemming and charge density. It was thus essential to draw the relationship between the unit drill and blast costs and the stemming length and the charge length. Figure 4.56 depicts the relationship between unit drilling and blasting costs and charge length.

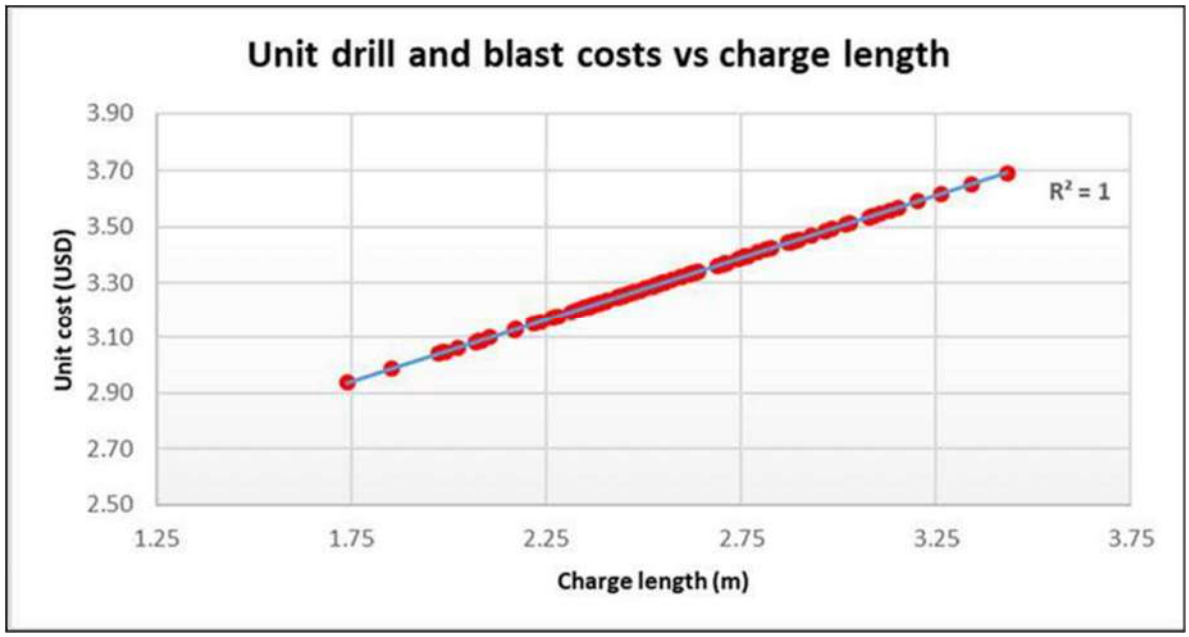

Figure 4.56: Unit drill and blast costs vs charge length

There is a direct linear relationship between the charge length and unit drilling and blasting costs. It is also essential to mention that when the drilling costs are constant given that the blasting pattern is fixed together with the hole diameter, thus the parameter contributing to the increase in the cost is the quantity of explosives or charge per hole. The converse is true that when the stemming length increases, the charge per hole required will decrease and thus, the unit costs will decrease.

Figure 4.57 depicts that the unit drilling and blasting cost will decrease with an increase in the stemming length, while Figure 4.58 shows that the powder factor will increase with the increase in the charge per hole.

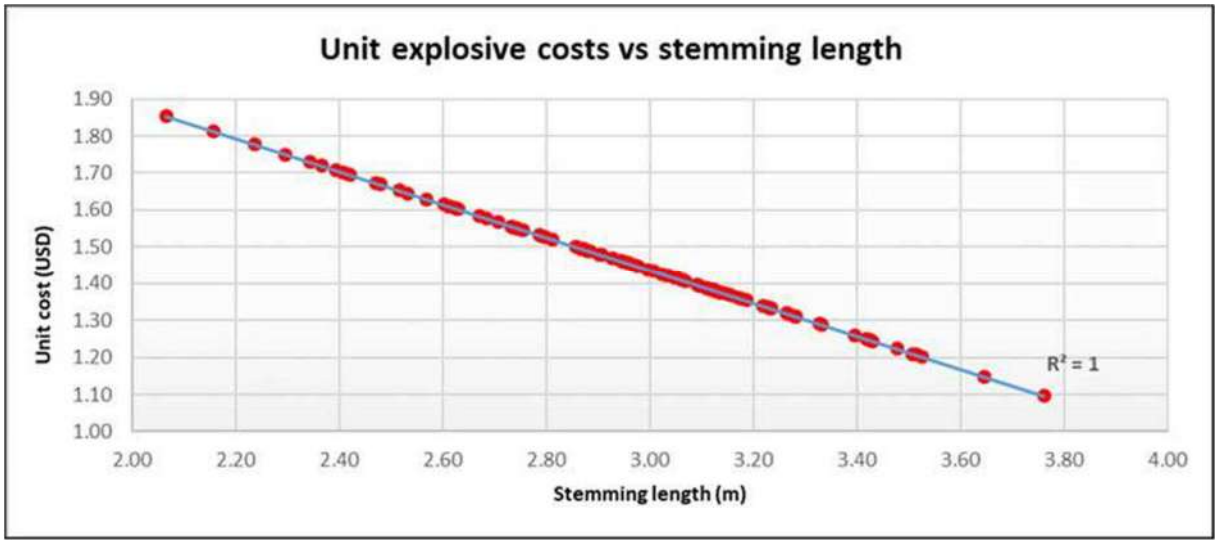

Figure 4.57: Unit costs vs stemming length

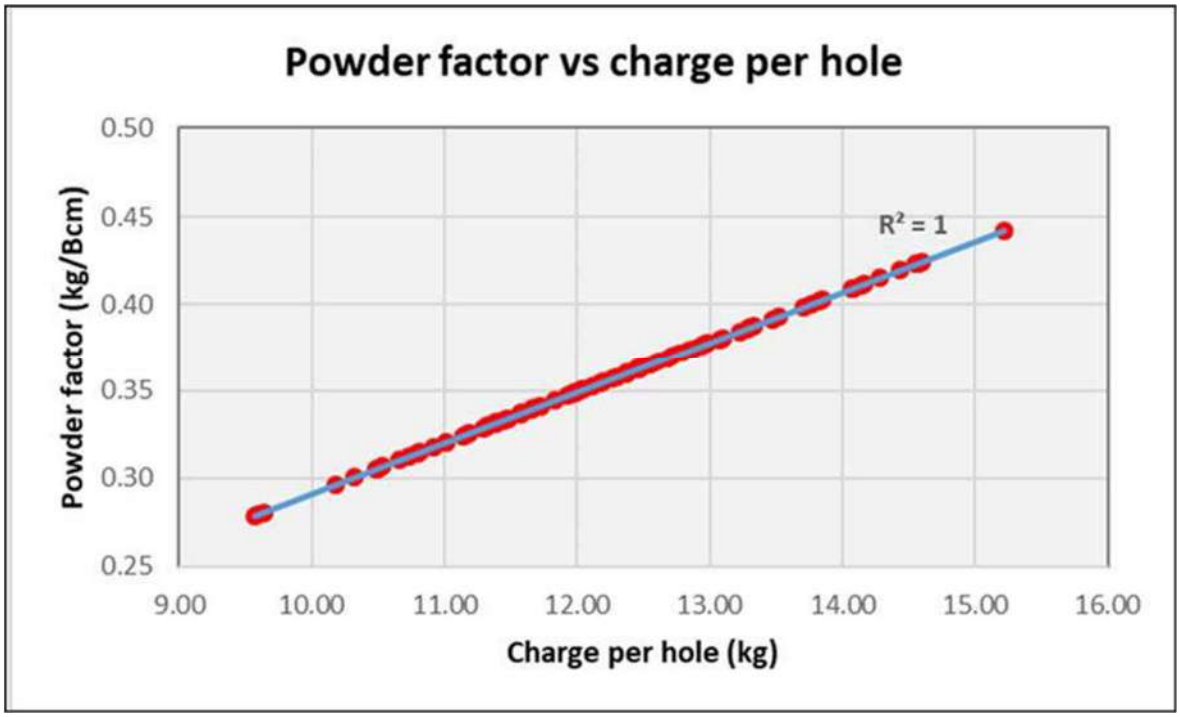

Figure 4.58: Powder factor vs charge per hole.

The higher the powder factor, the finer the fragment size; thus, the higher the blasting costs. Finer fragmentation size leads to higher crusher productivity and lower mechanical energy input in downstream processing units resulting in a net reduction in the operations costs. However, there is a delicate balance that has to be struck between fragment size required and blasting costs to achieve optimal blasting costs.

It was also essential to relate the rockmass conditions and the costs incurred in blasting a block of ground. The Blastability Index as a factor that represents the rockmass condition was plotted against the cost as depicted in Figure 4.59.

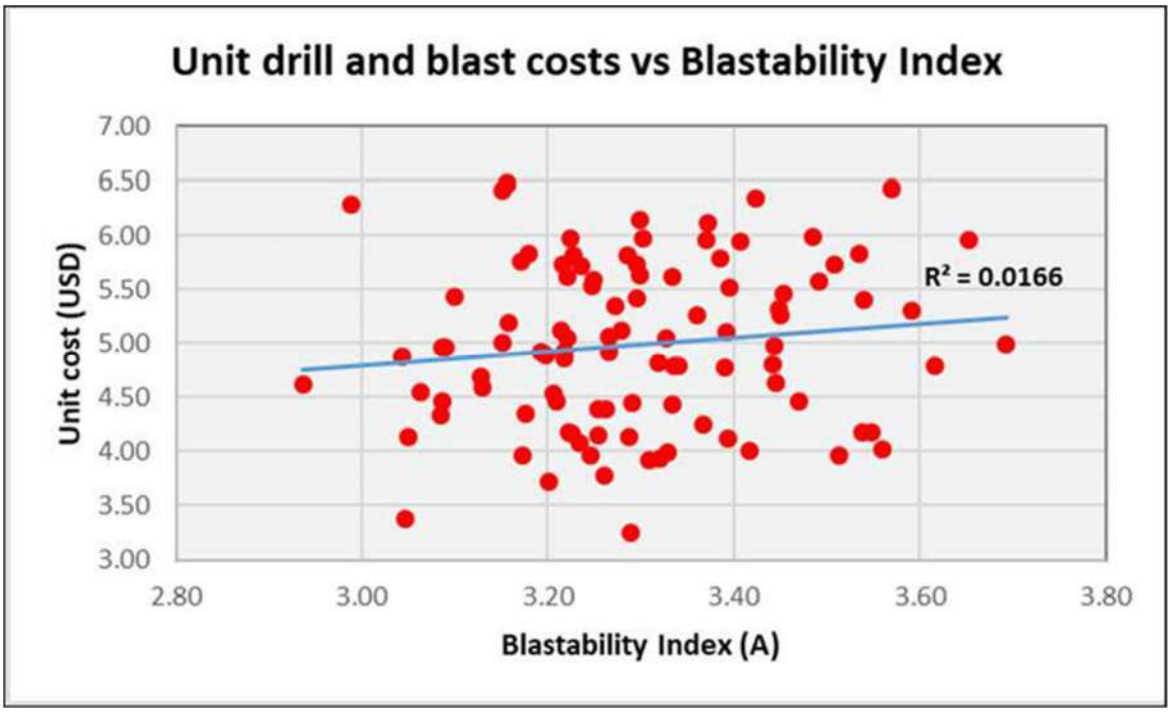

Figure 4.59: Unit costs and Blastability Index

There exists a positive relationship between the unit drill and blast costs and Blastability Index — the more competent the rockmass, the higher the unit drill and blast costs. Though the graph indicates a weak correlation, more data points would be required to conclude the causal relationship definitively. Figure 4.60 shows the Uniformity Index against the unit drill and blast costs.

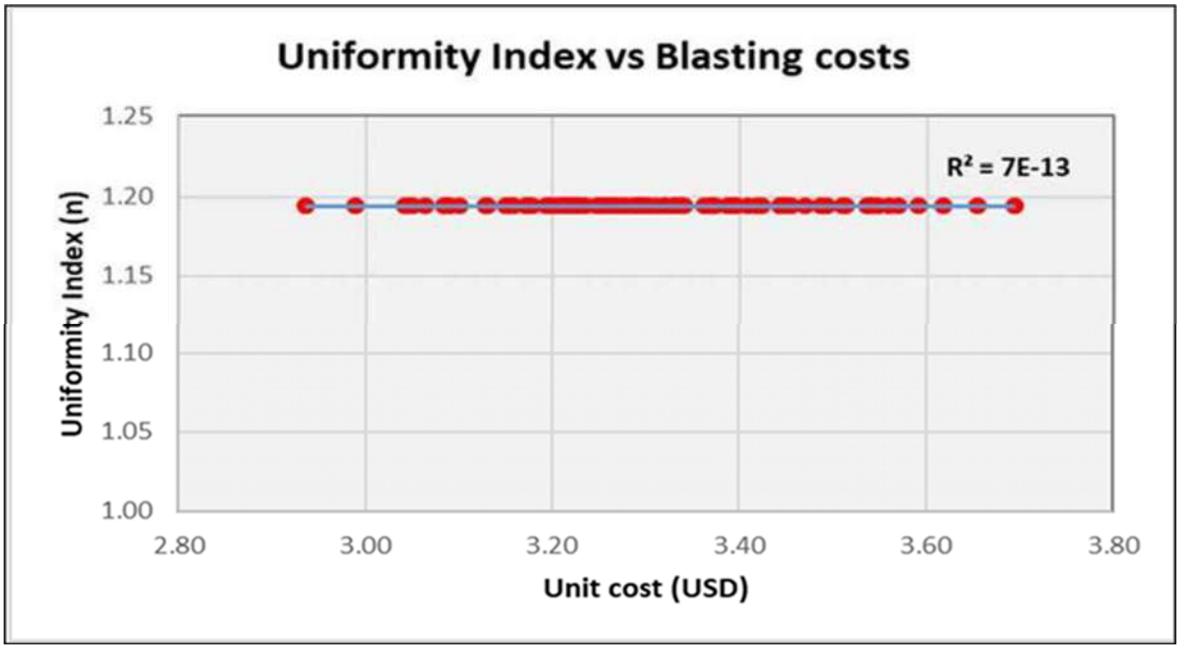

Figure 4.60: Uniformity Index and unit costs

In a fixed burden, spacing and drill hole diameter, the Uniformity Index value remained constant regardless of the changes in the unit drill and blast cost. The Uniformity Index of the muckpile is not affected by the decrease or increase in input costs.

4.9 Chapter Summary

This section of the report highlighted the results achieved from the three blast areas that were studied. The chapter further outlines the relationship between the different parameters that make up the Kuz-Ram model and the associated drilling and blasting costs. Some of the findings from this section were:

- The Blastability Index for the South blast areas (more competent and less fractured rockmass) ranged between 7 and 9 and was higher than the Blastability Index of both the South-West and South-East blast areas which ranged between 4 and 6.
- Parameters that had a stronger influence on the Blastability Index were the rock specific gravity and joint dip angle.
- The Uniformity Index results for all the blast areas were low, ranging between0.9 and 3, indicating that less uniform muck piles prevailed.
- The Uniformity Index results were mainly influenced by the burden, spacing, and the stemming length.
- The mean fragment size for constant burden, constant spacing, and a powder factor of 0.35 kg/Bcm produced fragment size results that were in line with the specified mean fragment size.
- The main parameters that influenced the mean fragment size were stemming length, powder factor, joint dip angle and rock specific gravity.
- The simulated drilling and blasting costs for 400 blast holes per pattern ranged between USD 42,000 and USD 48,000. The actual costs for the ten test blast were lower than the simulated cost peaking at USD 38,000 with the exception of one blast where an extra 200 holes were blasted. The cost per Bcm difference between the actual blast and the adjusted (budget) cost was 0.3 USD/Bcm with the adjusted cost peaking at 2.5 USD/Bcm.
- The unit drilling and blasting cost decreased with an increase in stemming length, and the converse was true for the charging length.

CHAPTER 5

Conclusions and Recommendations

5.1 Introduction

Blast rock fragmentation size plays a vital role in the mining value chain. Often poor blast results or sub-optimal blast fragment size negatively affects the downstream mining operation by reducing the productivity of the units and increasing their associated unit costs. Blasting operations as the first stage in the size reduction process thus form an integral part in the mine to mill optimization philosophy. The increase in the operational costs and reduced productivity can be correlated to the blast fragment size handled by the units. The research objectives of the study were:

RO1: To explore the role of rockmass conditions on blast rock fragmentation size.

RO2: To explore the role of blast design parameters on blast rock fragmentation size

RO3: To determine a drill and blast pattern that will produce optimal fragmentation size at the lowest cost possible.

To answer the research questions posed in Chapter 1, the Kuz-Ram model was chosen as the preferred empirical model. The Kuz-Ram model has been used for years in the mining industry to predict the blast fragment size distribution. Parameters that make up the Kuznetsov function and Rosin-Ramler function; both functions that make up the Kuz-Ram model, were simulated to study their influence on blast fragment size. These parameters were the Blastability Index, Uniformity Index and the explosive parameters in the mean fragment size.

Microsoft Excel, Palisade @Risk and Wipfrag were used in the study to perform the simulations and the image analysis of the fragment size achieved from the blast. Sensitivity analysis studies were then performed to identify the Kuz-Ram model parameters with significant impact on the fragment size. The relationships of the different parameters were plotted to study the nature of their relationship.

5.2 Conclusions

From the analysis, several findings were observed from the three test site. The results are discussed in the following sub-sectionsns.

5.2.1 Blastability Index

The Blastability Index is concerned with the classification of the rockmass quality by incorporating parameters such as rock density, rock strength, elasticity and fractures. The index describes the ease of blasting the rock by assigning a value to the block of ground. Values less than 8 indicate medium to hard rock conditions, 8 to 10 hard highly fractured rock and 10 to 13 indicate hard competent rock.

South blast had an index value ranging from 3.9 to 6.1. In this area, the rock was less fractured with steep joints and consisted predominately of dolomite. The parameters with significant influence on the index were the joint dip angle and rock density.

South-West blast had an index value ranging from 7.0 to 8.4. The rockmass in this area was fractured with horizontal joints and made up of black shale and breccia material. In this case, the parameter with the most influence on the index was the rock density.

South-East blast had index values between 7.4 and 8.8. The rockmass in the area was made up of sandstone and dolomite. The influential parameter on the index value was the rock density.

In general, the rock type encountered in Ruashi mine can be classified as easy to blast with some areas having a fractured rockmass. The leading influential parameter on the Blastability Index was the rock density parameter. The Blastability Index and the rock density had a positive direct relationship meaning an increase in the rock density would result in a corresponding increase in the Blastability Index value.

5.2.2 Uniformity Index

The Uniformity Index describes the uniform nature of the muckpile. The Uniformity Index is primarily influenced by the blast design pattern. Higher values of the Uniformity Index indicate uniform muckpile. Typical values of the index are between

0.6, and 2.2. Index values between 0.6 and 1.0 indicate less uniform muck piles characterised by boulders and a high degree of fines. While values between 1.0 and 1.5 indicate fines and oversize muckpile. Uniformity Index values between 1.5 and 2.2 are generally associated with a uniform muckpile and typically indicate competent rockmass conditions.

South blast Uniformity Index ranged between 1.7 and 2.2 with a slight positive skew distribution. These values were expected given that the rockmass in this area was relatively more competent. Also, the burden, spacing and drill hole diameter were constant in this test site, which meant that the only parameter that would influence the Uniformity Index values was the stemming length. The stemming length and the Uniformity Index had an inverse relationship, meaning an increase in the stemming length resulted in a decrease in the Uniformity Index value.

South-West blast Uniformity Index ranged between 0.9 and 2.7 with a positive skew distribution. The rockmass in this area was relatively weak and fractured, and the burden and spacing parameters were dynamic. The Uniformity Index results in this area, thus provided an opportunity for optimising the blast design pattern to get a more uniform blast fragment size. The influential parameters on the index results were the burden and spacing.

South-East blast Uniformity Index ranged between 1.1 and 3.2 with a positive skew distribution. The majority of the index results were leaning towards lower values in the range of 1.0 and 1.5, and this meant that the muckpile in this area was characterized by oversize to fine fragment size material. The rockmass in this area was moderately competent with fewer fractures, and all the blast design parameters were dynamic during the simulation runs. The primary influencers on the Uniformity Index value were the burden and spacing.

In general, in the South-East and South-West blasts, the primary influencer on the Uniformity Index value was the burden and spacing, while with the South Blast the stemming length was the influential parameters on the Uniformity Index value. The burden had an inverse relationship with the Uniformity Index, while the spacing had a direct relationship with the Uniformity Index. The burden to spacing ratio, whether one chooses a square or staggered pattern, influences the Uniformity Index value.

5.2.3 Mean Fragment Size

South blast had two powder factors assigned, namely the 0.35 kg/Bcm and 0.65 kg/Bcm. Results for the 0.35 kg/Bcm powder factor indicated that the mean fragment size range was between 13cm and 28cm. The majority of the fragment size (95%) material was below the mean fragment size of 30cm. The blasting efficiency for 0.35 kg/Bcm powder factor was 8% (Table 4.1).

Despite the lower error or blasting efficiency margin, the concern was that higher blasting costs could be realized due to tighter burden and spacing that resulted in the majority of the fragment size being below the required mean fragment size of 30cm. An increase in the burden and spacing to move the size distribution closer to the required mean fragment size of 30cm would be required while keeping the same powder factor.

The powder factor of 0.65 kg/Bcm was too excessive, with 100% of the fragment size distribution below the 21cm fragment size. The simulation results were rejected in totality. The influential primary parameters on the mean fragment size results for this test site were joint dip angle, rock density, and stemming length.

South-West blast fragment size distribution ranged between 27cm and 49cm, which was between the required mean fragment size of 30cm and the oversize fragment size of 50cm. The blasting efficiency for this blast was -25% which meant that the predicted fragmentation was higher than the actual fragmentation achieved. The influential parameters for the mean fragment size results were the stemming length and powder factor.

South-East blast fragment size distribution ranged between 14cm and 26cm, with 97% of the material size below 30cm for a powder factor of 0.65 kg/Bcm. The blasting efficiency measured at 50% of the material passing was +22%. The higher powder factor of 0.65 kg/Bcm meant that the simulation results could not be accepted. In order to correct the fragment size distribution, the powder factor was adjusted down to between 0.3 kg/Bcm and 0.4 kg/Bcm. The influential parameters in this blast area were the stemming length, explosive strength, and powder factor.

The stemming length and powder factor were the most prevalent influential parameters across all the mean fragment size results for the three test sites. Both

parameters had an inverse relationship with the fragment size. An increase in the powder factor resulted in a decrease in the fragment size while reduced stemming length resulted in an increase in the fragment size.

5.2.4 Suggested Blast Pattern

From the comparison of the results in Section 4.7, it was clear that the blast pattern which produced the most reliable results when compared with the actual fragmentation results was the 2.5m by 2.5m burden and spacing with powder factor values between 0.3 kg/Bcm and 0.4 kg/Bcm. This pattern was adopted as a general pattern blast pattern for mine.

5.2.5 Blasting Costs

The simulated cost for 400 holes was slightly higher than the actual cost incurred for the ten blasts conducted using the recommended pattern. The blasting costs ranged between USD 42,000 and USD 48,000 as compared to the maximum actual costs of USD 40,000. The actual powder factor range was between 0.35 kg/Bcm and 0.4 kg/Bcm as compared to the preferred range of 0.3 kg/Bcm and 0.4 kg/Bcm. In general, the adopted pattern performed very well, and the fragment size distribution was in line with the stipulated requirements.

There was a direct relationship between the charge length and the unit drill and blast cost. The increase in the charge length meant that there was an increase in the amount of explosives per hole, which in turn meant that there was an increase in the unit drill and blast costs. The converse was true that the increase in the stemming length resulted in decreased unit drill and blast costs. The more competent the rockmass was, the higher the unit drill and blast costs. However, the uniform nature of the muckpile after blast did not have any effect on blasting costs.

5.3 Recommendations

Given that the study only concentrated on the drilling and blasting operations, and did not consider the effects of blasting operations on hauling, crushing, and grinding operations, its impact was limited. The following recommendations are made:

- A comprehensive mine to the mill optimization study should be undertaken on the entire value chain to achieve a net positive value.

- The mining department should recruit blasting engineers and providing them with the necessary tools and equipment to do their jobs in an effort to establish a functional blasting department.
- Blast performance monitoring system should be established to proactively manage blast results and carry out continuous improvements on the blasts.
- Relocation of nearby residents should be considered to reduce the risks posed by blasting operations to the community.

REFERENCES

Adebayo, B. and Umeh, E., 2007. Influence of Some Rock Properties on Blasting Performance - A Case Study. *Journal of Engineering and Applied Science,* Volume 2, pp. 41- 44.

Anon, 2018. What are the Main Methods of Calculating Business Costs? *Investopedia.*

[Online] Available at: https://www.investopedia.com/ask/answers/101314/what-are-main-methods-calculating-business-costs.asp
[Accessed 08 October 2018].

Ash, R. L., 1963. The Mechanics of the Rock Blasting. In *Pit and Quarry.* Volume 56, Number 2, pp. 98 - 100.

Ash, R. L., 1968. The Design of Blasting Rounds. In: E.P. Pfleider, ed., *Surface Mining*, New York: AIME, pp. 373 - 397.

Babbie, E.R. 2004. The practice of social research. 10th ed. Belmont, USA: Thomson/Wadsworth.

Chatziangelou, M. and Christaras, B., 2017. A New Development of BQS (Blastability Quality System) for Closely Spaced Formations. *Journal of Geological Resource and Engineering,* Volume 1, pp. 24-37.

Chung, H. S., and Katsabanis, P.D, 2000, “Fragmentation prediction using improved engineering formulae,“ International Journal of Blasting and Fragmentation, Vol. 4, Issue 3-4, pp. 198-207.

Clark, G., 1987. *Principles of Rock Fragmentation*. New York, John Wiley and Sons pp. 432-442.

Cunningham, C., 2005. The Kuz-Ram Fragmentation Model - 20 Years On. *In Brighton Conference Proceedings.* Edition. R. Holmberg

Cunningham, C. V., 1983. The Kuz-Ram Model for Prediction of Fragmentation from Blasting*. In Proceedings of the First International Symposium on Rock Fragmentation by Blasting.* Lulea, Sweden. pp. 439-454.

Cunningham, C. V., 1987. Fragmentation Estimation and the Kuz-Ram Model-Four Years On*. In Proceedings of the Second International Symposium on Rock Fragmentation by Blasting.* Keystone, Colorado. pp. 475-487.

Davis, D. 2004. Business research for decision making. 6th ed. South-Western College Publishing.

Doucet, C., 1995. *The Effects of Geology on Fragmentation in Small Development Headings,* Montreal: The Department of Mining and Metallurgical Engineering, M.Sc. Thesis. McGill University.

Djordjevic, N., (1998). Two-component Blast Fragmentation Model. JKMRC Internal Report

Eloranta, J., 1997. The Efficiency of Blasting versus Crushing and Grinding. *The Journal of Explosives Engineering.* September/October*,* pp.12-14.

Fernberg, H., 2005, "Surface drilling," in Quarrying and Open Pit Mining, M.Smith, ed., Atlas Copco, Orebro, Sweden, pp. 37-40.

Fishman, G. S., 1966. *Monte Carlo,* Second Edition, P.78. Berlin: Springer.

Gheibie, S., Aghababaei, H., Hoseinie, S. and Pourrahimian, Y., 2009. Modified Kuz-Ram Fragmentation Model and its use at the Sungun Copper Mine. *International Journal of Rock Mechanics and Mining Sciences,* Volume 46, pp. 967- 973.

Hustrulid, W., 1999. Blasting Principles for Open Pit Mining. Volume 1 (Chapter-7), Balkema, Rotterdam, p.382.

Jimeno, C. L., Jimeno, E. L. and Carcedo, F. J. A., 1995. Drilling and Blasting of Rocks. London and New York: Taylor and Francis.

Kanchibotla, S.S., Morrell, S., Valery, W., and O'Laughlin, P., 1998, "Exploring the effect of blast design on SAG mill throughput at KCGM." Proceedings of the Mine to Mill Conference, The Australian Institute of Mining and Metallurgy, Brisbane, Australia, pp. 153-162.

Kanchibotla, S.S., Valery, W., and Morrell, S., 1999. Modeling fines in blast fragmentation and its impact on crushing and grinding. Julius Kruttschnitt Mineral Research Centre. The University of Queensland

Kanchibotla, S., 2001. Optimum Blast? Is it Minimum Cost per Broken Rock or Maximum Value per Broken Rock? *In Explo 2001 Hunter Valley*. NSW, Australia. 28-31 October, pp. 35-40.

Kecojevic, V., and Komljenovic, D., 2016. Impact of burden and spacing on fragment size distribution and total cost in quarry mining. *Society for Mining, Metallurgy, and Exploration.* Vol. 320, pp.133-141

Kojovic, T., Michaux, S., and Mackenzie, C., 1995, Impact of blast fragmentation on crushing and screening operations in quarrying, Proceedings of the Mine to Mill Conference, The Australian Institute of Mining and Metallurgy, Brisbane, Sept, pp. 427-436.

Konya, C. J., and Walter, E. J., 1991. *Rock Blasting and Overbreak Control.* Montville: National Highway Institute.

Kulula, M. I., Nashongo, M. N. and Akande, J. M., 2017. Influence of Blasting Parameters and Density of Rock on Blast Performance at Tschudi Mine, Tsumeb, Namibia. *Journal of Minerals and Materials Characterization and Engineering,* Volume 5, pp. 339 - 352.

Kulula, M. I., Nashongo, M. N. and Akande, J. M., 2017. Influence of Blasting Parameters and Density of Rocks on Blast Performance at Tschudi Mine, Tsumeb, Namibia. *Journal of Minerals and Material Characterization and Engineering,* Volume 5, pp. 335-352.

Kuznetsov, V. M., 1973. The Mean Diameter of Fragments Formed by Blasting Rock. Soviet Mining Science (in Russsian), Volume 9, pp.144-148.

Leedy, P. D., Ormrod, J. E., 2015. Practical Research: Planning and Design, Global Edition, 11th Edition

Lilly, P. A., 1986. An Empirical Method of Assessing Rock Mass Blastability. *In Proceedings of Large Open Pit Planning Conference. The Australian Institute of Mining and Metallurgy,* October. Parkville, Victoria. pp. 89-92.

Lizotte, C., 1990. Empirical Procedures for Prediction of Rock Fragmentation by Blasting. *CANMET-MRL Report,90-06, 59p-Quebec,* pp.2-26.

Mackenzie, A. S., 1966. Cost of Explosives - Do you Evaluate it Properly?. *Mining Congress Journal.* Volume 52, Number 5, pp. 32-41.

Mackenzie, A. S., 1967. Optimum Blasting; 28th Annual Mining Symposium and 40th Annual Meeting of the Minnesota Section, AIME. pp. 181-188.

McFarlane, A., 2015. Ruashi Mine Life of Mine Planning 2015-2022 Report. Available from: Ruashi Mine.

McKee, D.J., Chitombo, G.P. and Morell, S. (1995). The relationship between fragmentation in mining and comminution circuit throughput, Minerals Engineering, 8, (11): 1265 – 1274.

McKee, D. J., 2013. *Understanding Mine to Mill.* St Lucia, Brisbane: The Cooperative Research Centre for Optimising Resource Extraction (CRC ORE).

Mishra, A., 2009. *Design of Surface Blast - A Computational Approach*. Rourkela, India: Department of Mining Engineering, B.Sc. Thesis. National Institute of Technology.

Moody, L., Cunninghamm, C., and Lourens, H., 1996, "Measuring the effect of blasting fragmentation on hard rock quarrying operations," Proceedings of the of FRAGBLAST 5, Fragmentation by Blasting, Montreal, Quebec, Canada, pp. 269-277.

Morin, M. A. and Ficarazzo, F., 2006. Monte Carlo Simulation as a Tool to Predict Blasting Fragmentation Based on the Kuz-Ram Model. *Computers and Geoscience,* Volume 32, pp. 352 - 359.

Noy, M. J., 1997. 2D vs 3D Fragmentation Analysis; Preliminary Findings. *13th Annual Symposium on Explosives and Blasting Research*, 2-5 February, Las Vegas, Nevada, USA, pp. 181-190.

Outcherlony, F., Olsson, M., Nyberg, U., Anderson, P. and Gustavsson, L., 2006. Construction of Fragment Size Distribution of Bench Blasting Round, Using the New Swebrec Function. *Fragblast 8, Proceedings of 8th International Symposium on Rock Fragmentation by Blasting*, Editec, Santiago, pp. 332-334.

Rai, P., Abhai, K. R. and B, S., 2005. Optimizing Fragmentation. QMJ Group, February, pp. 33-37.

Rajpot, M., 2009. *The Effects of Fragmentation Specification on Blasting Cost,* Kingston, Ontario: The Department of Mining Engineering, M.Sc. Thesis. Queen's University.

Rensburg, J. v., Joubert, Pellissier, Stack., 2017. *Economic and Management Research.* Vasco Boulevard, Goodwood, N1 City, Cape Town, South Africa. Oxford University Press Southern Africa (Pty) Ltd

Rosin, R. and Rammler, E., 1933. Laws Governing the Fineness of Powdered Coal. Journal Institute of Fuels, Volume 7, pp. 29-36.

Roy, M., Paswan, R., Sarim, M., Jha, R., Kumar, S. and Singh, P., 2016. Rock Fragmentation by Blasting- A Review. *Journal of Mines, Metals and Fuels.* Volume 64, Issue 9, pp. 424-431.

Ruashi, 2018. *Ruashi Mine Explosive Prices for 2018 Report,* Lubumbashi: Ruashi Mining.

Ruashi, 2015. *Competent Persons Report*, Lubumbashi: Ruashi Mining.

Ruashi, 2016. *Ruashi Mining Contract,* Lubumbashi: Ruashi Mining.

Scott, A., Cocker, A., Djordjevic, N., Higgins, M., La Rosa, D., Sarma, K. and Wiedmaier, R., 2009. *Open Pit Blast Design, Analysis and Optimisation.* Isles Road, Indooroopilly, Queensland 4068, Australia: Julius Kruttschnitt Mineral Research Centre.

Scott, G., 2015. *Fragmentation Management for the Downstream Value Chain*. Quarry Academy, pp. 1-32.

School of Mining, 2019. *Unit 6: Blast Design for Surface Mine*s, Lecture Notes, Explosives Engineering for Surface and Underground Mines Minn140, University of the Witwatersrand, Johannesburg, South Africa, Delivered 25th - 29th March 2019.

Singh, P., Roy, M., Drebenstedt, C. and Prasad, B., 24-25 August 2015. Blast Design Parameters and Their Impact on Rock Fragmentation. *International Symposium on Rock Fragmentation by Blasting,* Volume 11, pp. 755 - 762.

Solomon, A. T., 2015. *An Evaluation of the Effects of Blast-Generated Fragment size Distribution on the Unit Costs of a Mining Operation, using Modelling and Simulation Techniques,* M.Sc. Thesis. Utah: The University of Utah.

Strelec, S., Gazdek, M. and Mesec, J., 2011. *Blasting Design For Obtaining Desired Fragmentation.*, Technical Gazette 18. Volume 1, pp. 79-86.

Thornton, D., Kanchibotla, S. S. and Brunton, I., 2001. Modelling the Impact of Rockmass and Blast Design Variation on Blast Fragmentation. *EXPLO 2001,* October, pp. 28 - 31.

APPENDICES

Appendix A

Table A1: Ruashi Explosive Prices for January 2018

Initiation Systems				
Item	Units/Box	USD/Unit	Cost/Unit or kg	Cost/Unit or kg
Cordtex 10 gm/m (2 x 350m)	700	690.00	0.99	0.99
Explosives				
Item	Units	Kg/Unit	USD/Unit	USD/kg
Anfex	Bags	25	71.66	2.87
P100 Emulsion	Bags	1000	1614.66	1.62
Pentolite Booster 150gm	Pack	120	642.95	5.36
Detonators				
Item	Units/Box	USD/Box	Cost/Unit	Cost/Unit or kg
Benchmaster 7.5m-500ms	150	735.36	4.90	4.90
Handite 7.5m-0ms	150	735.36	4.90	4.90
Handite 7.5m-17ms	150	735.36	4.90	4.90
Handite 7.5m-25ms	150	735.36	4.90	4.90
Handite 7.5m-42ms	150	735.36	4.90	4.90
IED	1000	1243.00	1.24	1.24

Appendix B

Table B 1: Rock Mass Classification from the Core in Pit 3

Borehole	From	To	Length	Elevation	Lithology Rock Type	Stratigraphy	RQD (%)	Weathering	Jn	Jr	Ja	Jw	SRF	Q	Is	RQD	Js	Jc	Jw	RMR
RGT6	69.75	73	3.25	1214	Breccia	RAT	7.1	W4	4	3	8	0.66	10	0.0	2	3	8	0	10	23
RGT6	79	85	6	1205	Siltstone	RAT	27.2	W4	6	3	8	0.66	10	0.1	2	8	8	0	10	28
RGT6	85	89.5	4.5	1201	Dolomite	RAT	19.1	W3	4	1.5	6	0.66	10	0.1	7	3	8	0	10	28
RGT6	89.5	91	1.5	1200	Dolomite	RAT	0.0	W4	2	3	8	0.66	10	0.0	4	3	5	0	10	22
RGT6	91	96.7	5.7	1196	Dolomite	RAT	80.2	W1	4	1	1	1	10	2.0	12	17	10	25	10	74
RGT6	96.7	98.9	2.2	1194	Breccia	RAT	58.6	W3	2	3	8	0.66	10	0.7	7	13	10	0	10	40
RGT6	98.9	100	1.1	1193	Dolomite	RAT	70.9	W2	2	3	8	0.66	10	0.9	12	13	8	0	10	43
RGT7	33	39.5	6.5	1240	Dolomite	RAT	54.2	W4	4	3	8	0.66	1	3.4	2	13	10	0	10	35
RGT7	39.5	45.6	6.1	1236	Dolomite	RAT	50.7	W3	4	2	6	0.66	10	0.3	7	13	10	0	10	40
RGT7	45.6	51.5	5.9	1231	Dolomite	RAT	76.4	W3	6	2	6	0.66	10	0.3	7	17	10	0	10	44
RGT7A	34.17	40.34	6.17	1230	Dolomite	RAT	29.3	W4	4	3	8	0.66	10	0.2	2	8	10	0	10	30
RGT7A	40.34	41.37	1.03	1229	Breccia	RAT	56.3	W3	3	3	5	0.66	2.5	3.0	2	13	8	25	10	58
RGT7A	41.37	50.16	8.79	1220	Breccia	RAT	82.8	W2	4	3	1	0.66	1	41.0	7	17	10	0	10	44
RGT7A	50.16	58.5	8.34	1212	Breccia	RAT	80.5	W1	4	2	1	0.66	1	26.6	12	17	10	0	10	49
RGT7A	58.5	60	1.5	1210	Dolomite	RAT	100.0	W1	2	2	1	0.66	1	66.0	12	20	10	0	10	52
RGT8	75.6	81.5	5.9	1208	Breccia	RAT	37.6	W3	6	3	6	0.66	10	0.2	4	8	8	10	10	40
RGT8	81.5	87.5	6	1204	Breccia	RAT	59.3	W3	4	3	6	0.66	10	0.5	4	13	8	10	10	45
RGT8	87.5	93.5	6	1199	Breccia	RAT	35.5	W3	6	3	6	0.66	10	0.2	4	8	8	10	10	40
RGT8	93.5	101.8	8.3	1193	Breccia	RAT	13.9	W3	6	3	6	0.66	10	0.1	4	3	8	10	10	35
RGT9	58.06	64.15	6.09	1222	Breccia	RAT	17.4	W4	6	3	8	0.66	10	0.1	2	3	8	20	10	43
RGT9	64.15	69.5	5.35	1218	Breccia	RAT	28.0	W3	12	3	6	0.66	10	0.1	4	8	8	0	10	30
RGT9	69.5	73.49	3.99	1215	Breccia	RAT	27.6	W4	6	3	6	0.66	10	0.2	4	8	8	20	10	50
RGT9	73.49	81.5	8.01	1209	Dolomite	RAT	54.4	W1	4	2	6	0.66	10	0.3	12	13	8	0	10	43
		Total	118.22																Average	41
																			Std Dev	11.7

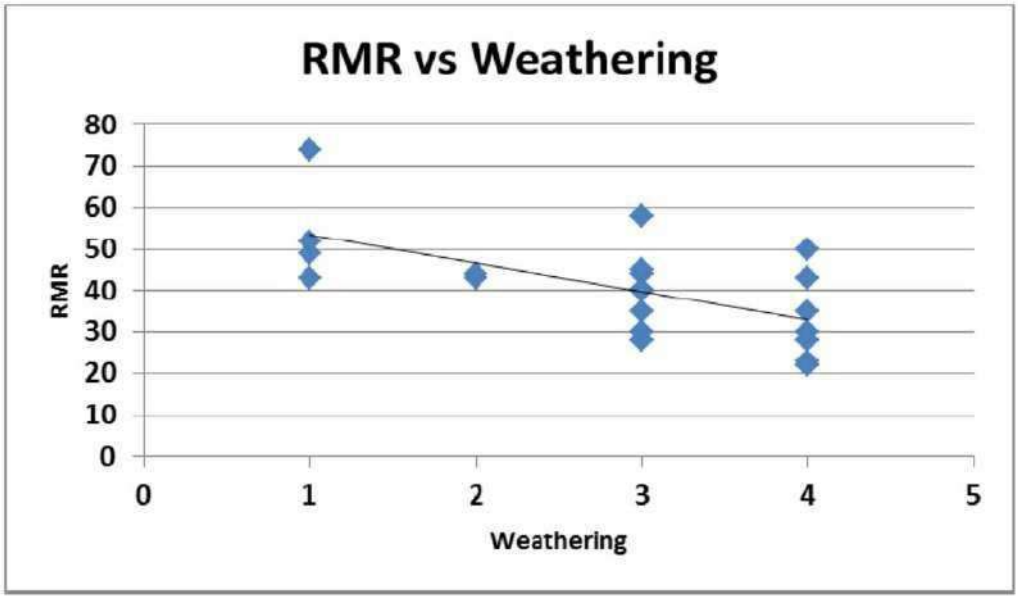

Figure B 1: Relationship between Weathering and RMR

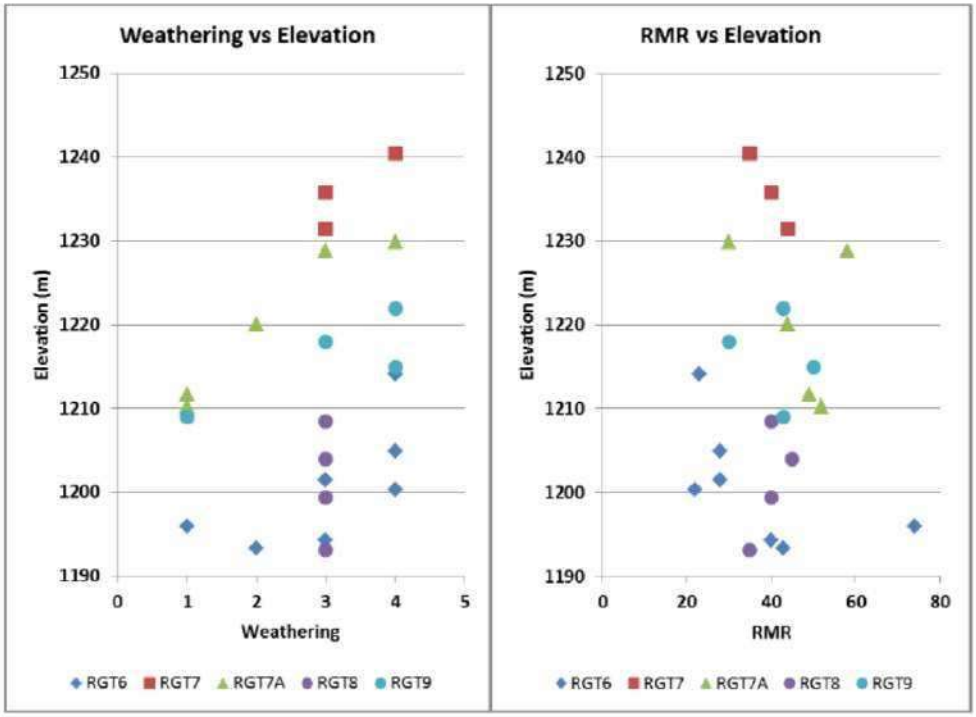

Figure B 2: Weathering vs Elevation and RMR vs Elevation

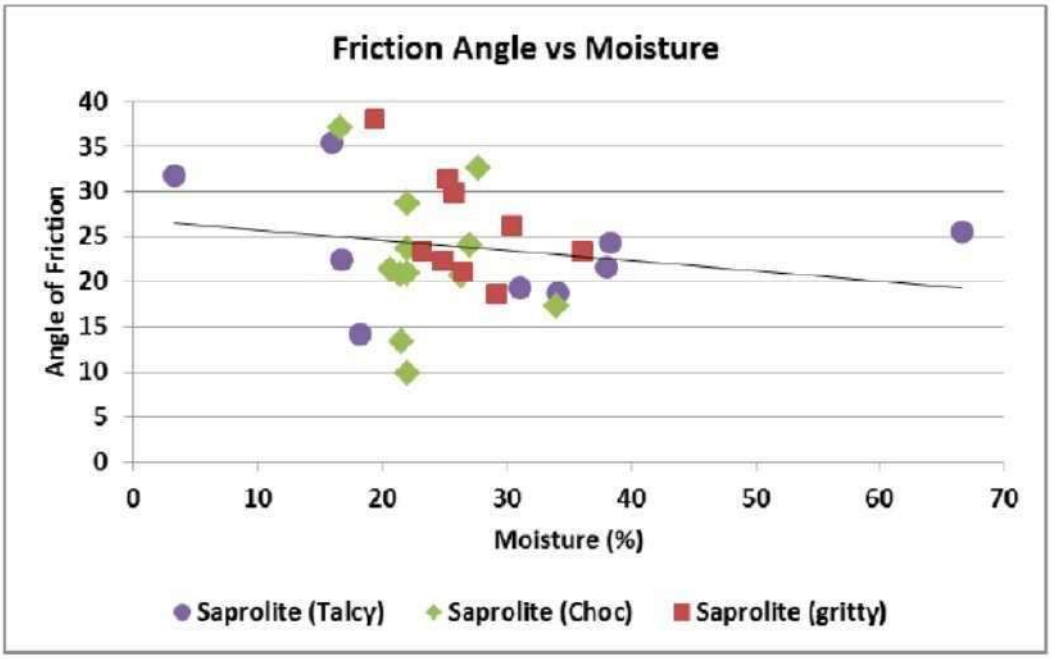

Figure B 3: Friction Angle vs Moisture

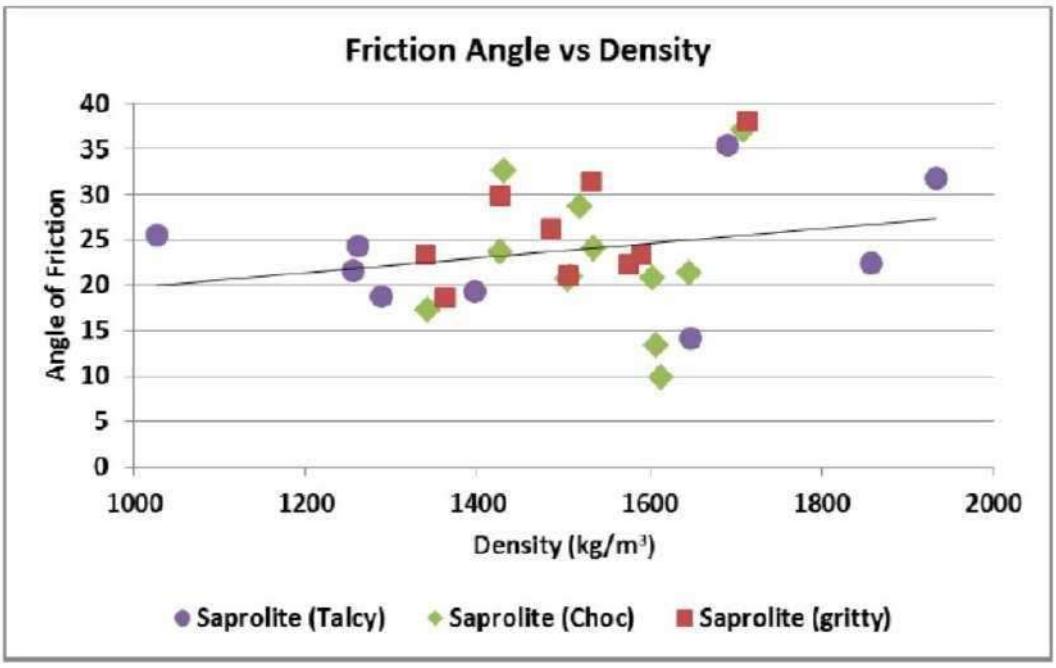

Figure B 4: Friction Angle vs Density

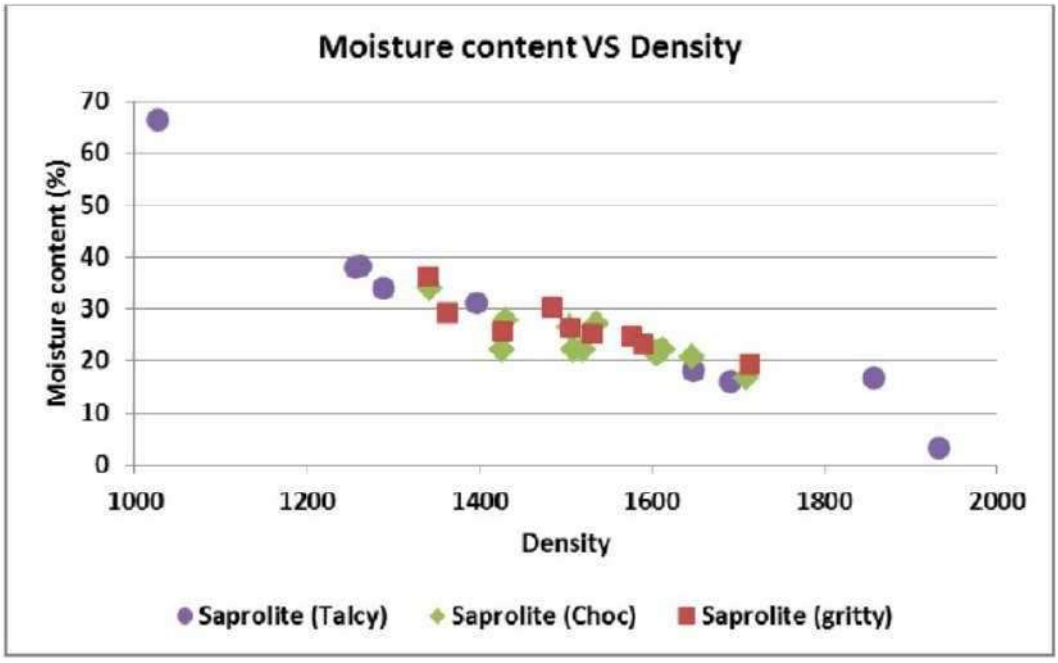

Figure B 5: Moisture Content vs Density

Table B 2: Triaxial Strength Test Database

SPECIMEN PARTICULARS							SPECIMEN DIMENSIONS					SPECIMEN TEST RESULTS			
Rocklab Specimen No 4259-	Borehole ID	Sample No	Depth From.. To..	Rock Type	Eletvation	Stratigraphy	Diameter mm	Height mm	Ratio of Height to Diameter	Mass g	Density g/cm³	Confining Pressure δ_3 MPa	Failure Load P kN	Strength (TCS) δ_1 MPa	Failure Mode
TCS-07A-04A	RGT7A	RGT7A-04	44.55 - 45.00	Breccia	1225.22	RAT	47.45	96.2	2.0	434.1	2.55	2.5	52.1	29.5	XA
TCS-07A-04B	RGT7A	RGT7A-04	44.55 - 45.00	Breccia	1225.22	RAT	47.32	96.3	2.0	433.2	2.56	5.0	67.8	38.5	XA
TCS-07A-04C	RGT7A	RGT7A-04	44.55 - 45.00	Breccia	1225.22	RAT	47.68	93.5	2.0	426.7	2.56	10.0	99.8	55.9	XA
TCS-07A-05A	RGT7A	RGT7A-05	47.29 - 47.73	Breccia	1222.49	RAT	47.82	85.2	1.8	376.0	2.46	2.5	66.1	36.8	XA
TCS-07A-05B	RGT7A	RGT7A-05	47.29 - 47.73	Breccia	1222.49	RAT	47.68	92.4	1.9	390.7	2.37	5.0	68.2	38.2	5B
TCS-07A-05C	RGT7A	RGT7A-05	47.29 - 47.73	Breccia	1222.49	RAT	60.84	121.3	2.0	836.1	2.37	10.0	157.3	54.1	XA
TCS-07A-06A	RGT7A	RGT-07A-06	55.5 - 56.05	Breccia	1214.17	RAT	60.56	104.8	1.7	842.8	2.79	2.5	202.8	70.4	XA
TCS-07A-06B	RGT7A	RGT-07A-06	55.5 - 56.05	Breccia	1214.17	RAT	47.69	97.4	2.0	472.9	2.72	5.0	160.8	90.0	XA
TCS-07A-06C	RGT7A	RGT-07A-06	55.5 - 56.05	Breccia	1214.17	RAT	47.81	92.0	1.9	450.4	2.73	10.0	170.5	95.0	XA
TCS-07A-07A	RGT7A	RGT-07A-07	56.37 - 56.74	Breccia	1213.48	RAT	47.86	81.5	1.7	388.4	2.65	2.5	65.2	36.2	XA
TCS-07A-07B	RGT7A	RGT-07A-07	56.37 - 56.74	Breccia	1213.48	RAT	47.80	81.7	1.7	390.8	2.66	5.0	81.4	45.4	5B
TCS-07A-07C	RGT7A	RGT-07A-07	56.37 - 56.74	Breccia	1213.48	RAT	47.76	87.4	1.8	432.2	2.76	10.0	160.5	89.6	XA
TCS-12A	RGT2	RGT2-10	113.33 - 113.81	Dolomite	1201.72	RAT	60.78	120.7	2.0	950.4	2.71	1.0	134.5	46.4	5B
TCS-12B	RGT2	RGT2-10	113.33 - 113.81	Dolomite	1201.72	RAT	60.78	120.4	2.0	984.6	2.82	2.0	139.9	48.2	3B
TCS-12C	RGT2	RGT2-10	113.33 - 113.81	Dolomite	1201.72	RAT	60.72	118.2	1.9	996.8	2.91	5.0	308.9	106.7	XA
TCS-07A-08A	RGT7A	RGT-07A-08	58.67- 58.9	Dolomite	1211.32	RAT	47.68	45.9	1.0	232.1	2.83	2.5	51.4	28.8	5B
TCS-07A-08B	RGT7A	RGT-07A-08	58.67- 58.9	Dolomite	1211.32	RAT	47.83	53.6	1.1	278.3	2.89	5.0	201.6	112.2	XA
TCS-07A-08C	RGT7A	RGT-07A-08	58.67- 58.9	Dolomite	1211.32	RAT	47.85	67.1	1.4	340.3	2.82	10.0	100.7	56.0	XA
TCS-07A-09A	RGT7A	RGT-07A-09	59.51 - 59.74	Dolomite	1210.48	RAT	47.79	71.5	1.5	374.7	2.92	2.5	102.9	57.3	XA
TCS-07A-09B	RGT7A	RGT-07A-09	59.51 - 59.74	Dolomite	1210.48	RAT	47.87	67.7	1.4	357.7	2.94	5.0	210.6	117.0	XA
TCS-07A-09C	RGT7A	RGT-07A-09	59.51 - 59.74	Dolomite	1210.48	RAT	47.74	62.4	1.3	319.2	2.86	10.0	161.1	90.0	7B
TCS-07A-10A	RGT7A	RGT-07A-10	59.07 - 59.32	Dolomite	1210.90	RAT	47.73	46.1	1.0	228.0	2.76	2.5	74.5	41.6	XA
TCS-07A-10B	RGT7A	RGT-07A-10	59.07 - 59.32	Dolomite	1210.90	RAT	47.74	46.6	1.0	233.0	2.80	5.0	104.6	58.4	4B
TCS-07A-10C	RGT7A	RGT-07A-10	59.07 - 59.32	Dolomite	1210.90	RAT	47.76	53.1	1.1	264.7	2.78	10.0	182.6	101.9	XA
TCS-09-18A	RGT9	RGT9-18	78.93 - 79.21	Dolomite	1210.68	RAT	35.41	40.0	1.1	110.5	2.81	2.5	24.1	24.4	5B
TCS-09-18B	RGT9	RGT9-18	78.93 - 79.21	Dolomite	1210.68	RAT	35.39	45.0	1.3	123.7	2.79	5.0	33.9	34.4	5B
TCS-09-19A	RGT9	RGT9-19	79.47 - 79.72	Dolomite	1210.29	RAT	35.47	52.2	1.5	148.4	2.88	2.5	42.6	43.1	XA
TCS-09-19B	RGT9	RGT9-19	79.47 - 79.72	Dolomite	1210.29	RAT	47.79	69.3	1.4	357.6	2.88	5.0	135.2	75.4	XA
TCS-09-19C	RGT9	RGT9-19	79.47 - 79.72	Dolomite	1210.29	RAT	47.80	62.5	1.3	322.6	2.88	10.0	119.7	66.7	5B
TCS-09-20A	RGT9	RGT9-20	80.56 - 80.98	Dolomite	1209.35	RAT	47.71	57.7	1.2	297.5	2.89	2.5	62.7	35.1	XA
TCS-09-20B	RGT9	RGT9-20	80.56 - 80.98	Dolomite	1209.35	RAT	48.29	45.2	0.9	238.1	2.87	5.0	94.3	51.5	5B
TCS-09-20C	RGT9	RGT9-20	80.56 - 80.98	Dolomite	1209.35	RAT	47.78	84.3	1.8	433.7	2.87	10.0	159.6	89.0	XA
TCS-11C	RGT2	RGT2-9	94.9 - 95.43	Shale	1214.71	RAT	60.63	106.5	1.8	877.6	2.86	5.0	331.5	114.8	5B
TCS-28A	RGT3	RGT3-15	105.33 - 105.58	Siltstone	1203.96	RAT	48.72	81.5	1.7	422.7	2.78	1.0	87.2	46.8	XA
TCS-28B	RGT3	RGT3-15	105.33 - 105.58	Siltstone	1203.96	RAT	48.78	59.2	1.2	301.0	2.72	5.0	84.0	44.9	4B
TCS-29A	RGT3	RGT3-15	105.33 - 105.58	Siltstone	1203.96	RAT	48.72	89.1	1.8	459.0	2.76	1.0	61.4	32.9	XA
TCS-29B	RGT3	RGT3-16	105.97 - 106.32	Siltstone	1203.42	RAT	48.72	67.9	1.4	352.3	2.78	2.0	127.0	68.1	7B
TCS-29C	RGT3	RGT3-16	105.97 - 106.32	Siltstone	1203.42	RAT	48.79	76.1	1.6	392.2	2.76	5.0	102.2	54.7	3B
TCS-30A	RGT3	RGT3-17	106.32 - 106.62	Siltstone	1203.20	RAT	48.69	88.5	1.8	452.1	2.74	1.0	68.9	37.0	4B
TCS-30B	RGT3	RGT3-17	106.32 - 106.62	Siltstone	1203.20	RAT	48.69	85.5	1.8	446.1	2.80	2.0	142.1	76.3	2B
TCS-30C	RGT3	RGT3-17	106.32 - 106.62	Siltstone	1203.20	RAT	48.70	82.7	1.7	429.5	2.79	5.0	187.3	100.5	XA

Appendix C

Table C 1: Drill and Blast Costs

Blast	Drilled meters	Cost of Drilling ($)	Explosive Quantity (Tonnes)	Bcm/Blast	Explosives Costs ($)	Blasting Costs ($)	Cost/Bcm	Powder Factor	Blasted Tonnage	Cost/Tonne
1	2200	24200	5,20	13750	13925,33	38125,33	1,01	0,38	27500	0,51
2	2200	24200	5,58	13750	14519,81	38719,81	1,06	0,41	27500	0,53
3	2200	24200	4,95	13750	13533,76	37733,76	0,98	0,36	27500	0,49
4	2200	24200	4,88	13750	13410,11	37610,11	0,98	0,35	27500	0,49
5	2200	24200	5,20	13750	13925,33	38125,33	1,01	0,38	27500	0,51
6	2200	24200	5,67	13750	14670,41	38870,41	1,07	0,41	27500	0,53
7	2200	24200	5,52	13750	14432,62	38632,62	1,05	0,40	27500	0,52
8	3300	36300	8,10	20625	21355,65	57655,65	1,04	0,39	41250	0,52
9	2200	24200	5,90	13750	15035,03	39235,03	1,09	0,43	27500	0,55
10	2200	24200	5,85	13750	14957,35	39157,35	1,09	0,43	27500	0,54
11	2200	24200	5,20	13750	13925,33	38125,33	1,01	0,38	27500	0,51
Total	25300	278300	62	158125	163690,71	441990,71	1,04	0,39	316250	0,52

Appendix D

Table D 1: South-West Kuz-Ram Model

KUZ-RAM FRAGMENTATION ANALYSIS

Project:	Pit3_South_West			
Rock Type	Dolomite	Sandstone	Breccia	Average
Specific Gravity	2,71	2,73	2,42	2,62
Elastic Modulus	53	88	53	64,67
UCS	79	88	79	82,00

1. Intact Rock Properties		
Rock Factor		
Rock Type	Dolomite,Sandstone and Breccia	
Rock Specific Gravity	2,62	SG
Elastic Modulus	64,67	GPa
UCS	82,00	MPa
2. Jointing		
Spacing	0,10	m
Dip	67	deg
Dip Direction	92	deg
In-situ block	0,2	m
3. Explosives		
Density	1,1	SG
RWS	100%	(% ANFO)
Nominal VOD	4800	m/s
Effective VOD	4600	m/s
Explosive Strength	0,88	0,88
4. Pattern Design		
Staggered or square	1,10	
Hole Diameter	102,00	mm
Charge Length	3,10	m
Burden	2,00	m
Spacing	2,00	m
Drill Accuracy SD	0,10	m
Bench Height	5,00	m
Face Dip Direction	0,00	deg
Stemming length	2,40	m
Mass per Meter	8,99	Kg/m
Broken Volume	22,00	m^3
Powder Factor	0,30	kg/tonne
Charge Density	0,30	kg/m^3
Charge Weight per hole	27,87	kg/hole
5. Kuz_Ram Model		
Blastability Index, A	5,8434	
Average Size of Material, X50	32	cm
Uniformity Exponent, n	0,98	
Characteristic Size, Xc	0,47	m
6. Fragmentation Target Parameters		
Oversize	0,5	m
Optimum	0,25	m
Undersize	0,1	m
7. Predicted Fragmentation		
Percent Oversize	34,4%	
Percent In Range	45,7%	
Percent Undersize	19,9%	

Fragment Size Distribution	
Percent Passing	Size (m)
0,0%	0
10,7%	0,05
19,9%	0,10
28,1%	0,15
35,4%	0,20
41,9%	0,25
47,7%	0,30
52,9%	0,35
57,6%	0,40
61,8%	0,45
65,6%	0,50
69,0%	0,55
72,0%	0,60
74,8%	0,65
77,3%	0,70
79,5%	0,75
81,5%	0,80
83,3%	0,85
84,9%	0,90
86,4%	0,95
87,7%	1,00
88,9%	1,05
90,0%	1,10

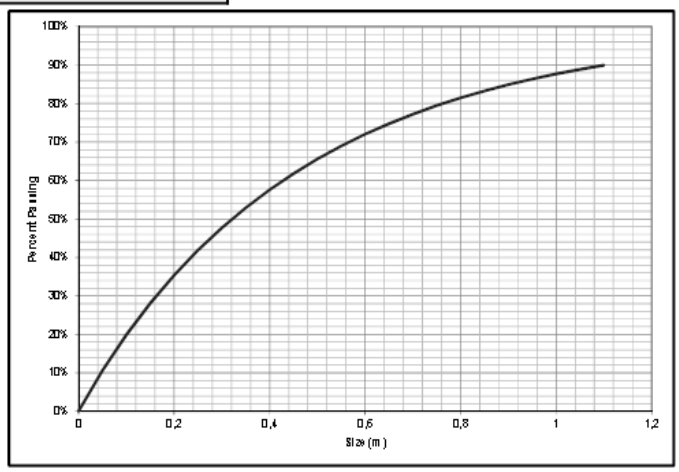

@RISK Output Report for Blastability Index, A B42

Performed By: Lijojo

Date: Monday, 16 September 2019 14:14:04

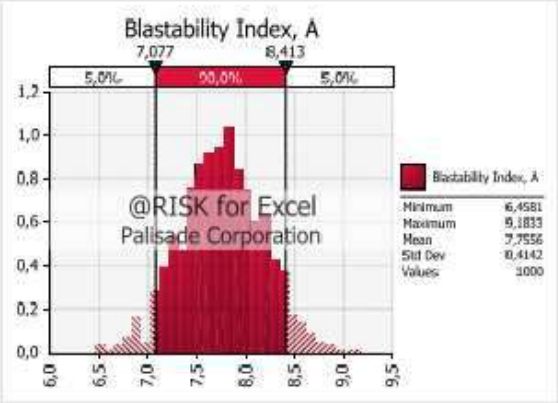



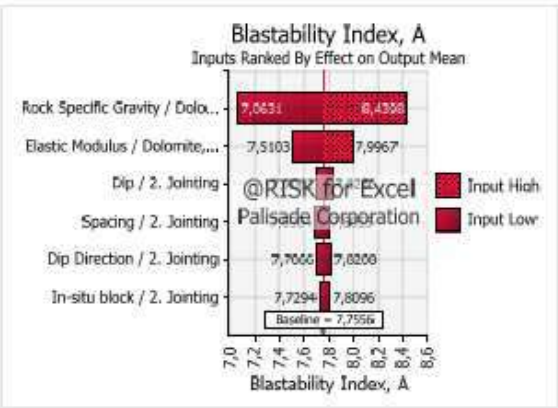

Simulation Summary Information	
Workbook Name	Pit3_south west.xlsx
Number of Simulations	1
Number of Iterations	1000
Number of Inputs	11
Number of Outputs	4
Sampling Type	Latin Hypercube
Simulation Start Time	2019/09/16 14:13
Simulation Duration	00:00:03
Random # Generator	Mersenne Twister
Random Seed	1372988118

Summary Statistics for Blastability Index, A			
Statistics		Percentile	
Minimum	6,468142408	5%	7,07747625
Maximum	9,183251936	10%	7,21220273
Mean	7,75558951		7,31536443
Std Dev	0,414197862	20%	7,41520909
Variance	0,171559869	25%	7,48156549
Skewness	-0,021607431	30%	7,54607725
Kurtosis	2,979734687	35%	7,59399822
Median	7,75602638	40%	7,65735124
Mode	7,733328468	45%	7,70663352
Left X	7,077476246	50%	7,75602638
Left P	5%	55%	7,80459675
Right X	8,412867115	60%	7,85066785
Right P	95%	65%	7,90539407
Diff X	1,335390869	70%	7,97049542
Diff P	90%	75%	8,03349659
#Errors	0	80%	8,1135618
Filter Min	Off	85%	8,18520411
Filter Max	Off	90%	8,29278341
#Filtered	0	95%	8,41286712

Change in Output Statistic for Blastability In			
Rank	Name	Lower	Upper
1	Rock Specific Gr	7,06312852	8,4398334
2	Elastic Modulus /	7,5103086	7,99672439
3	Dip / 2. Jointing	7,70618174	7,82659382
4	Spacing / 2. Joint	7,69037389	7,80563567
5	Dip Direction / 2.	7,70655669	7,82083136
6	In-situ block / 2.	7,72936101	7,80962898

Figure D 1: South-West Blastability Index Report

@RISK Output Report for Uniformity Exponent, n B44

Performed By: Lijojo

Date: Monday, 16 September 2019 14:14:17

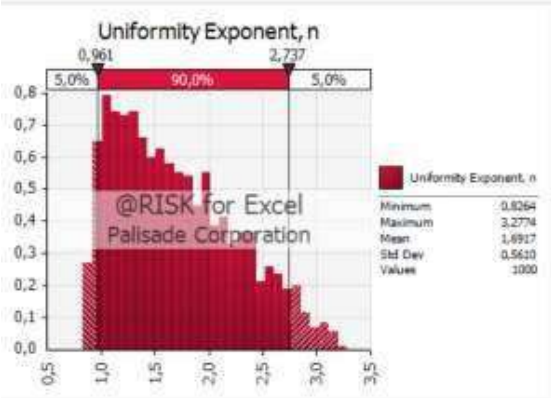

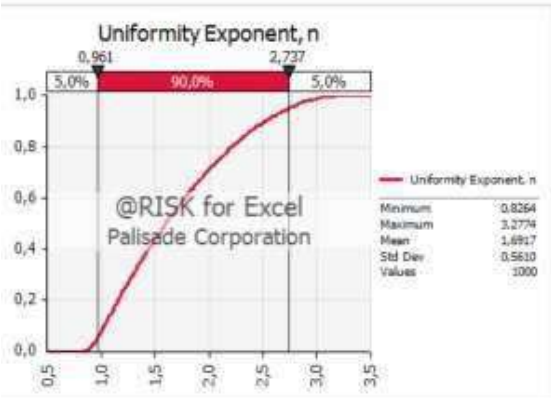

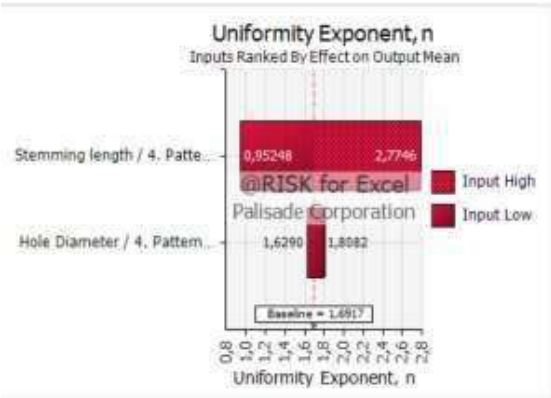

Simulation Summary Information	
Workbook Name	Pit3_south west.xlsx
Number of Simulations	1
Number of Iterations	1000
Number of Inputs	11
Number of Outputs	4
Sampling Type	Latin Hypercube
Simulation Start Time	2019/09/16 14:13
Simulation Duration	00:00:03
Random # Generator	Mersenne Twister
Random Seed	1372988118

Summary Statistics for Uniformity Exponent			
Statistics		Percentile	
Minimum	0,83	5%	0,96
Maximum	3,28	10%	1,02
Mean	1,69		1,09
Std Dev	0,56	20%	1,15
Variance	0,314723884	25%	1,22
Skewness	0,557256763	30%	1,29
Kurtosis	2,405562847	35%	1,36
Median	1,59	40%	1,43
Mode	1,40	45%	1,52
Left X	0,96	50%	1,59
Left P	5%	55%	1,68
Right X	2,74	60%	1,77
Right P	95%	65%	1,87
Diff X	1,78	70%	1,97
Diff P	90%	75%	2,09
#Errors	0	80%	2,21
Filter Min	Off	85%	2,35
Filter Max	Off	90%	2,52
#Filtered	0	95%	2,74

Change in Output Statistic for Uniformity Ex			
Rank	Name	Lower	Upper
1	Stemming length	0,95	2,77
2	Hole Diameter / 4	1,63	1,81

Figure D 2: South-West Uniformity Index Report

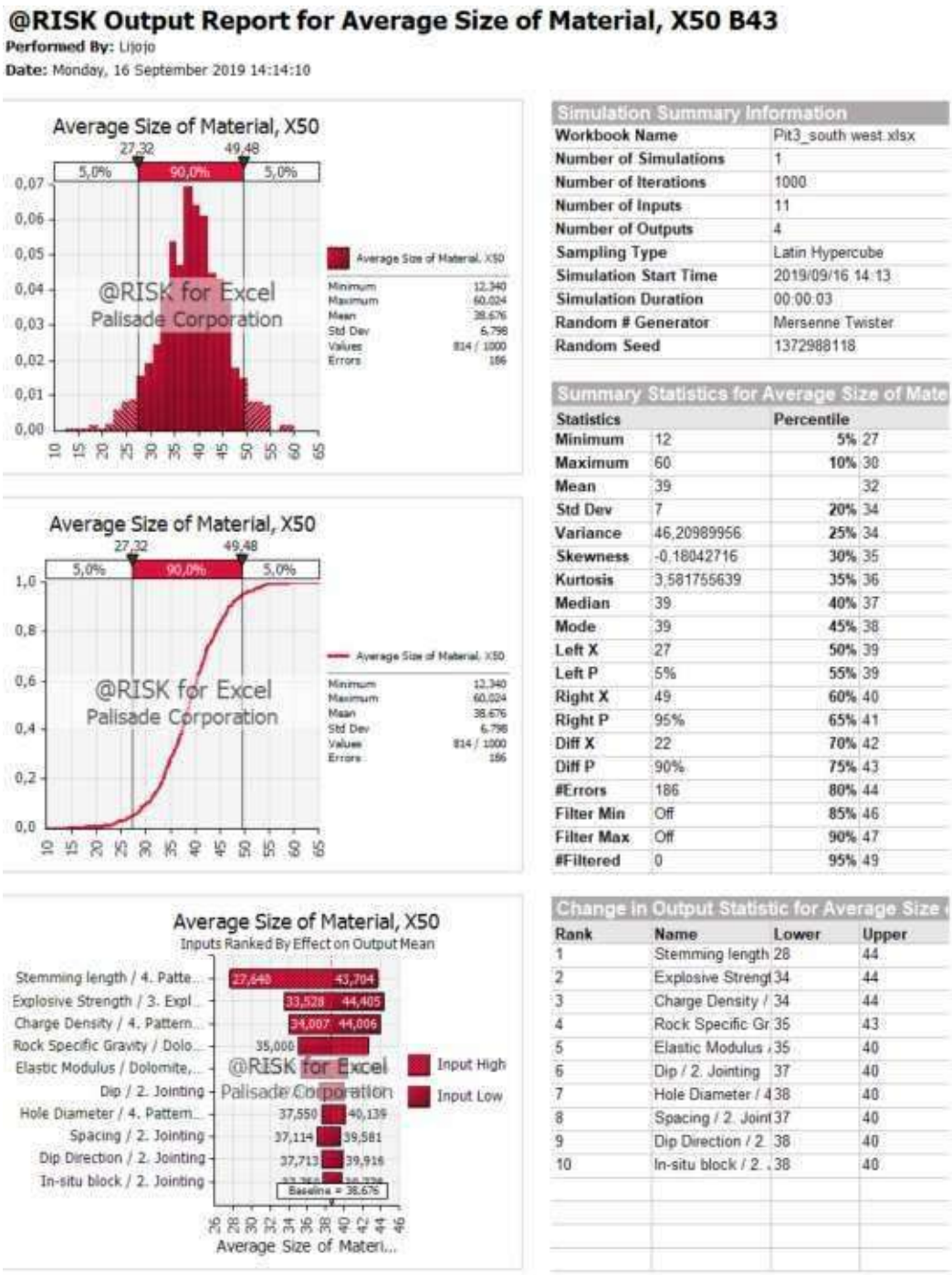

Figure D 3: South-West Mean Fragment Size Report



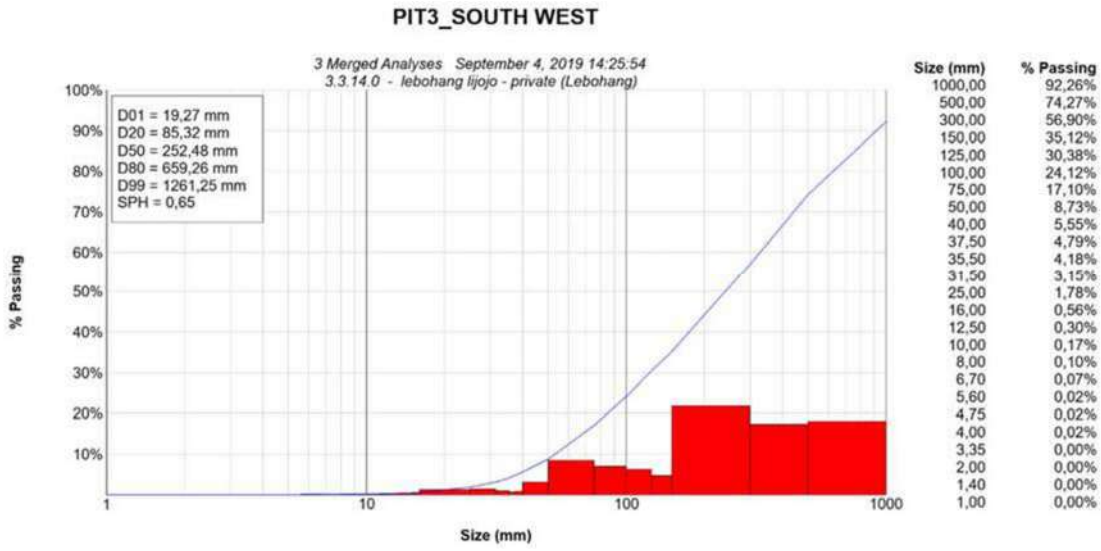

Figure D 4: South-West Actual Fragment Report (image analysis)

Table D 2: South-East Kuz-Ram Model

KUZ-RAM FRAGMENTATION ANALYSIS

Project:	Pit3_South	
Rock Type	Dolomite	
Specific Gravity	2.71	
Elastic Modulus	53	
UCS	79	

1. Intact Rock Properties		
Rock Factor		
Rock Type	Dolomite	
Rock Specific Gravity	2.71	SG
Elastic Modulus	53.00	GPa
UCS	79.00	MPa
2. Jointing		
Spacing	0.05	m
Dip	10	deg
Dip Direction	207	deg
Insitu block	0.7	m
3. Explosives		
Density	1.1	SG
RWS	100%	(% ANFO)
Nominal VOD	4800	m/s
Effective VOD	4500	m/s
Explosive Strength	0.88	0.88
4. Pattern Design		
Staggered or square	1.10	
Hole Diameter	105.00	mm
Charge Length	1.90	m
Burden	3.00	m
Spacing	3.00	m
Drill Accuracy SD	0.10	m
Bench Height	5.00	m
Face Dip Direction	0.00	deg
Stemming length	3.60	m
Mass per Meter	9.53	Kg/m
Broken Volume	49.50	m^3
Powder Factor	0.35	kg/tonne
Charge Density	0.35	kg/m^3
Charge Weight per hole	18.10	kg/hole
6. Kuz_Ram Model		
Blastability Index, A	5.55	
Average Size of Material, Xso	25	cm
Uniformity Exponent, n	1.39	
Characteristic Size, Xc	0.32	m
8. Fragmentation Target Parameters		
Oversize	0.5	m
Optimum	0.3	m
Undersize	0.1	m
7. Predicted Fragmentation		
Percent Oversize	15.7%	
Percent In Range	66.4%	
Percent Undersize	17.9%	

Fragment Size Distribution	
Percent Passing	Size (m)
0.0%	0
7.3%	0.05
17.9%	0.10
29.3%	0.15
40.4%	0.20
50.7%	0.25
59.8%	0.30
67.6%	0.35
74.3%	0.40
79.8%	0.45
84.3%	0.50
88.0%	0.55
90.8%	0.60
93.1%	0.65
94.8%	0.70
96.2%	0.75
97.2%	0.80
97.9%	0.85
98.5%	0.90
98.9%	0.95
99.2%	1.00
99.5%	1.05
99.6%	1.10
Calculated Pf	0.37

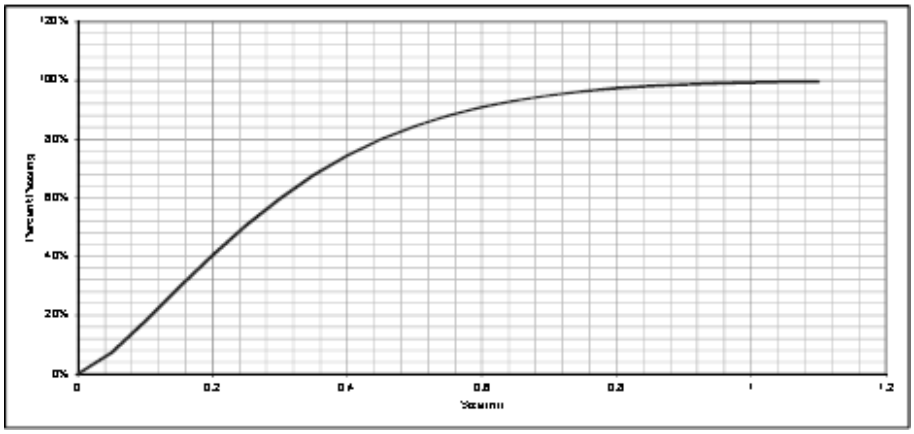

@RISK Output Report for Blastability Index, A B42

Performed By: Lijojo

Date: Tuesday, 03 September 2019 15:24:23

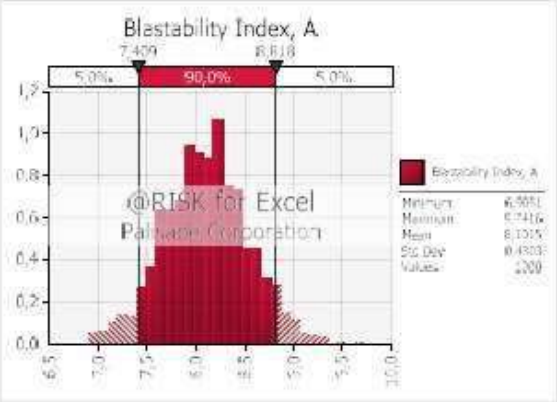

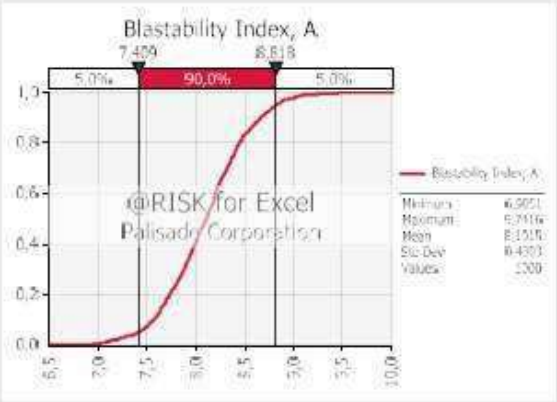

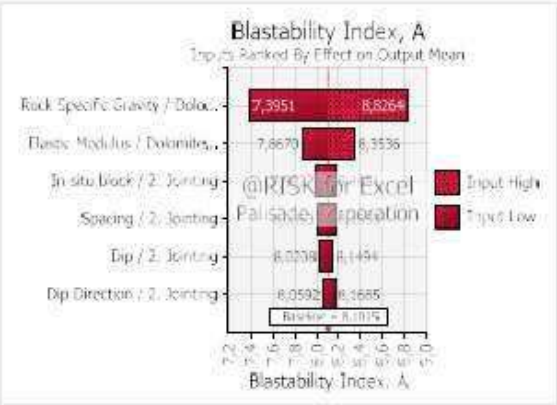

Simulation Summary Information	
Workbook Name	pit3-south_east.xlsx
Number of Simulations	1
Number of Iterations	1000
Number of Inputs	13
Number of Outputs	4
Sampling Type	Latin Hypercube
Simulation Start Time	2019/09/03 14:00
Simulation Duration	00:00:03
Random # Generator	Mersenne Twister
Random Seed	753820258

Summary Statistics for Blastability Index, A			
Statistics		Percentile	
Minimum	6,91	5%	7,41
Maximum	9,74	10%	7,57
Mean	8,10	15%	7,65
Std Dev	0,43	20%	7,73
Variance	0,185191773	25%	7,81
Skewness	0,077721614	30%	7,88
Kurtosis	3,092629752	35%	7,93
Median	8,11	40%	7,99
Mode	7,69	45%	8,04
Left X	7,41	50%	8,11
Left P	5%	55%	8,16
Right X	8,82	60%	8,20
Right P	95%	65%	8,25
Diff X	1,41	70%	8,32
Diff P	90%	75%	8,39
#Errors	0	80%	8,44
Filter Min	Off	85%	8,54
Filter Max	Off	90%	8,66
#Filtered	0	95%	8,82

Change in Output Statistic for Blastability In			
Rank	Name	Lower	Upper
1	Rock Specific Gr	7,40	8,83
2	Elastic Modulus /	7,87	8,35
3	In-situ block / 2. J	7,99	8,17
4	Spacing / 2. Joint	8,01	8,16
5	Dip / 2. Jointing	8,02	8,15
6	Dip Direction / 2.	8,06	8,17

Figure D 5: South-East Blastability Index Report

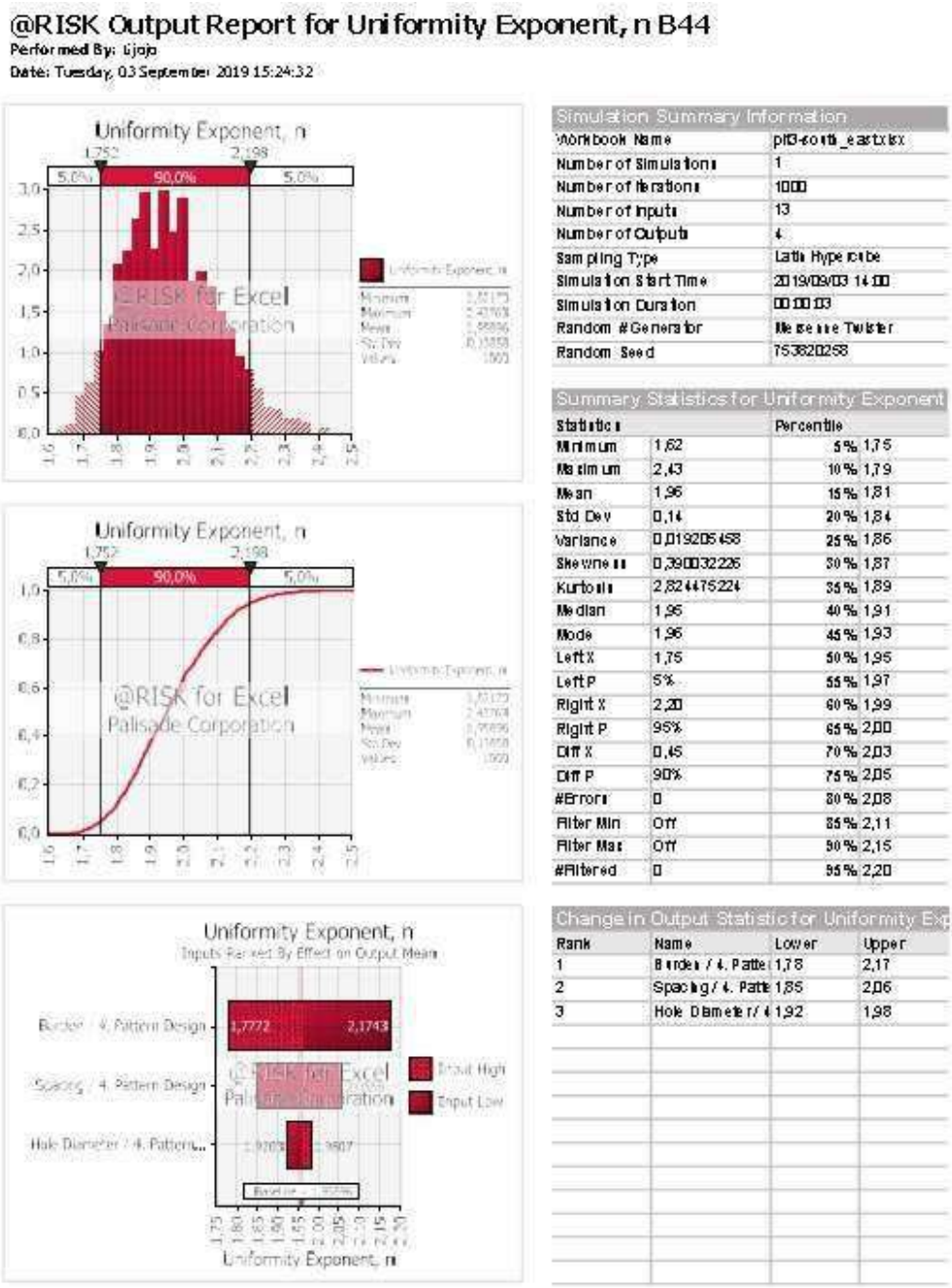

Figure D 6: South-East Uniformity Index Report

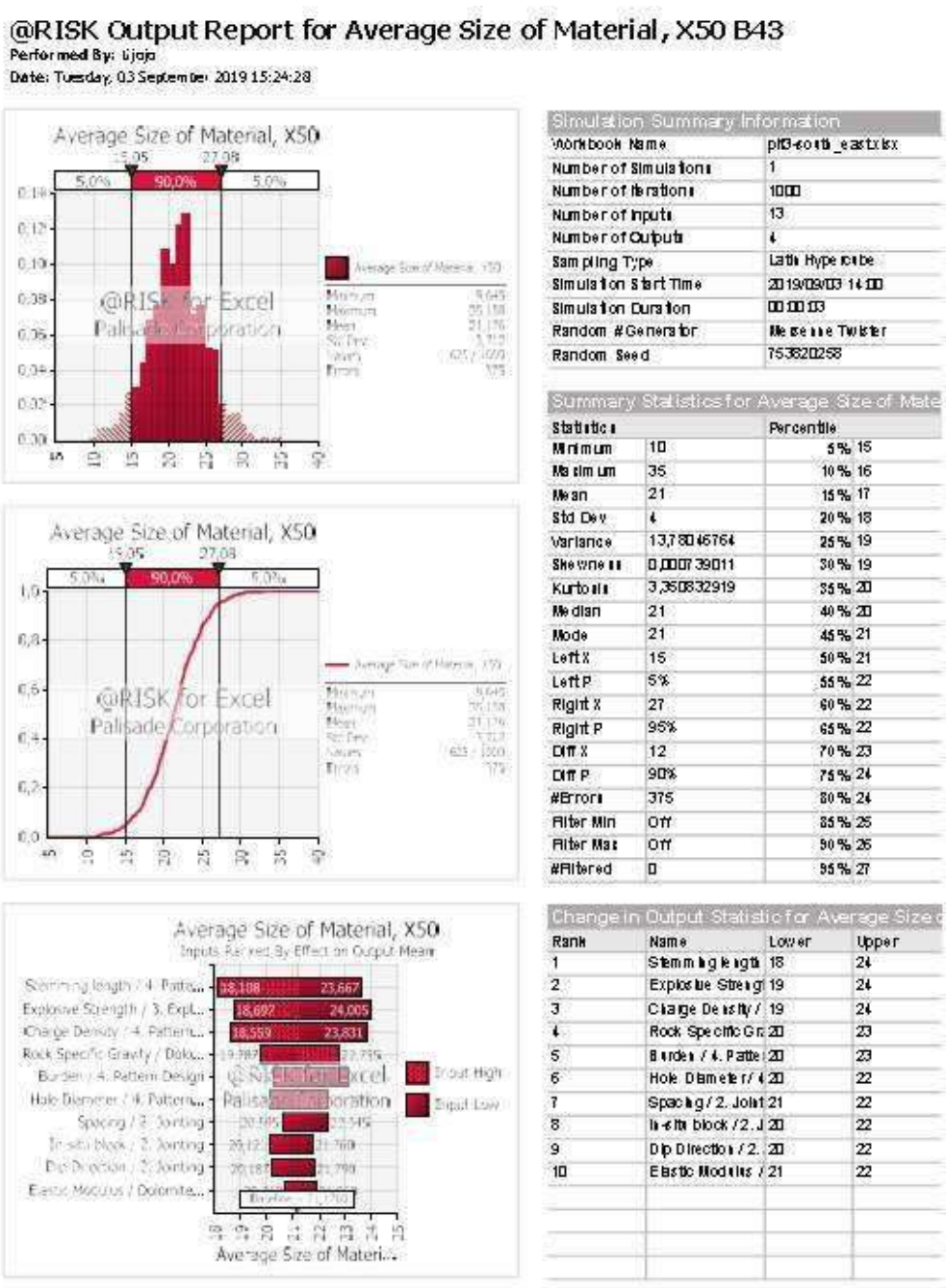

Figure D 7: South-East Mean Fragment Size Report

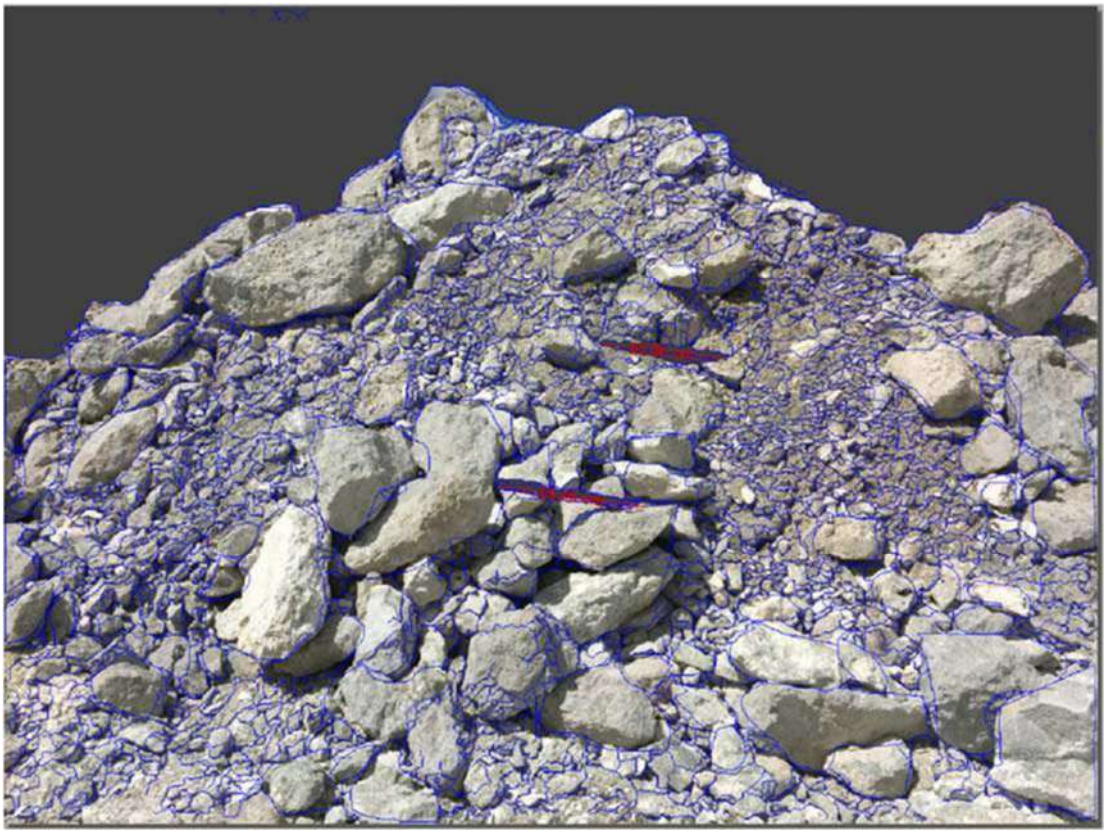

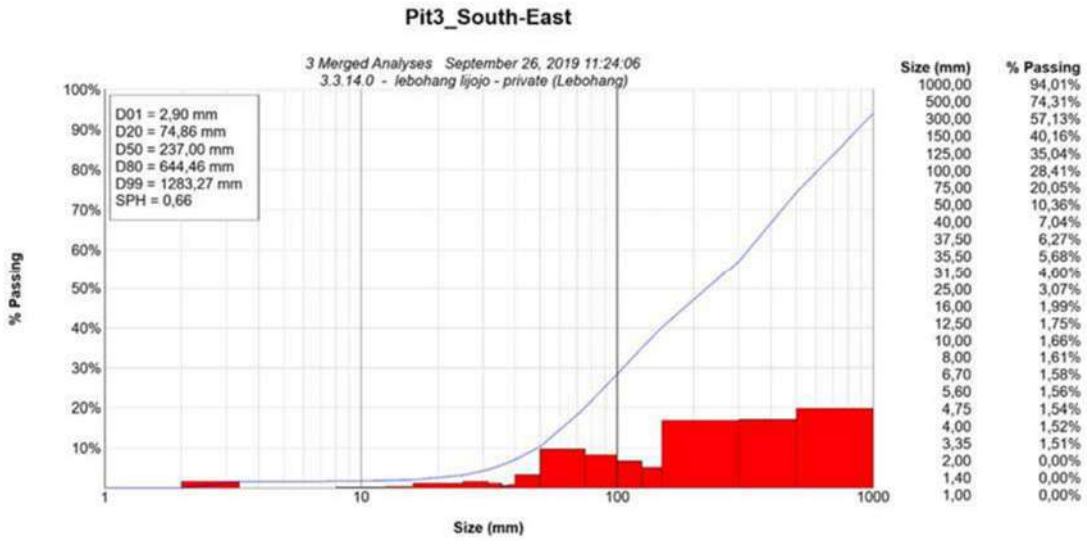

Figure D 8: South-East Actual Fragment Report (image analysis)

Table D 3: South Kuz-Ram Model

KUZ-RAM FRAGMENTATION ANALYSIS

Project:	PIT3_South	
Rock Type	Dolomite	
Specific Gravity	2,71	
Elastic Modulus	53	
UCS	79	

1. Intact Rock Properties			
Rock Factor			
Rock Type	Dolomite		
Rock Specific Gravity	2,71	SG	
Elastic Modulus	53,00	GPa	
UCS	79,00	MPa	
2. Jointing			
Spacing	0,05	m	
Dip	10	deg	
Dip Direction	207	deg	
In-situ block	0,7	m	
3. Explosives			
Density	1,1	SG	
RWS	100%	(% ANFO)	
Nominal VOD	4800	m/s	
Effective VOD	4500	m/s	
Explosive Strength	0,88		0,88
4. Pattern Design			
Staggered or square	1,10		
Hole Diameter	105,00	mm	
Charge Length	2,50	m	
Burden	2,50	m	
Spacing	2,50	m	
Drill Accuracy SD	0,10	m	
Bench Height	5,00	m	
Face Dip Direction	0,00	deg	
Stemming length	3,00		3,00
Mass per Meter	9,53	Kg/m	
Broken Volume	34,38	m^3	
Powder Factor	0,35	kg/tonne	
Charge Density	0,35	kg/m^3	
Charge Weight per hole	23,82		23,82
5. Kuz_Ram Model			
Blastability Index, A	5,55		
Average Size of Material, Xao	26	cm	
Uniformity Exponent, n	1,19		
Characteristic Size, Xc	0,35	m	
6. Fragmentation Target Parameters			
Oversize	0,5	m	
Optimum	0,3	m	
Undersize	0,1	m	
7. Predicted Fragmentation			
Percent Oversize	21,7%		
Percent In Range	58,3%		
Percent Undersize	20,0%		
Drilling Costs			
Bcm Blasted per hole (m)	34,375		
Metres drilled per hole (m)	5,50		
Metres drilled per Bcm (m/Bcm)	0,16		
Drilling Rate (USD/m) 105 diameter	11,5		
Total drilling costs per Bcm (USD/Bcm)	1,84		
Blasting Costs			
Hole Diameter (mm)	105,00		
Stemming length (m)	3		3,00
Charging length (m)	2,5		2,50
Density of explosives	1,1		
Charging per metre (kg/m)	9,53		9,53
Charge per hole (Kg)	23,82		23,82
Powder Factor (Kg/Bcm)	0,51		0,69
Emulsion bulk explosives costs (USD/Kg)	1,61		
Emulsion bulk explosives costs per hole (USD)	38,35		
Initiation system cost per hole (USD)	11,04		
Total blasting cost per hole (USD)	49,39		
Total blasting cost per Bcm (USD)	1,44		
Total drilling and Blasting Costs (USD/Bcm)	3,28		
Volume blasted per 400 hole pattern	13750		400
Total drilling and blasting costs per pattern (USD)	45054,00		

Fragment Size Distribution	
Percent Passing	Size (m)
0,0%	0
9,3%	0,05
20,0%	0,10
30,4%	0,15
40,0%	0,20
48,7%	0,25
56,4%	0,30
63,1%	0,35
68,9%	0,40
74,0%	0,45
78,3%	0,50
81,9%	0,55
85,0%	0,60
87,6%	0,65
89,8%	0,70
91,6%	0,75
93,1%	0,80
94,4%	0,85
95,4%	0,90
96,3%	0,95
97,0%	1,00
97,5%	1,05
98,0%	1,10
Calculated Pf	0,69

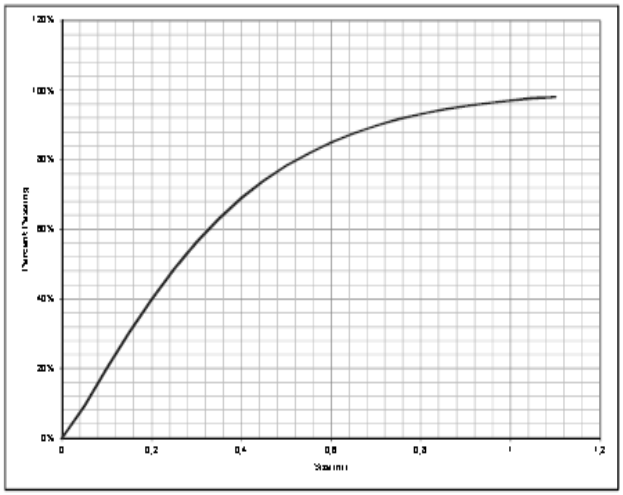

@RISK Output Report for Blastability Index, A B42

Performed By: Lijojo

Date: Wednesday, 04 September 2019 13:09:40

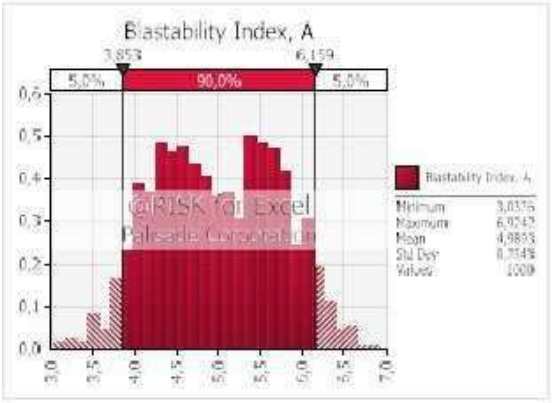



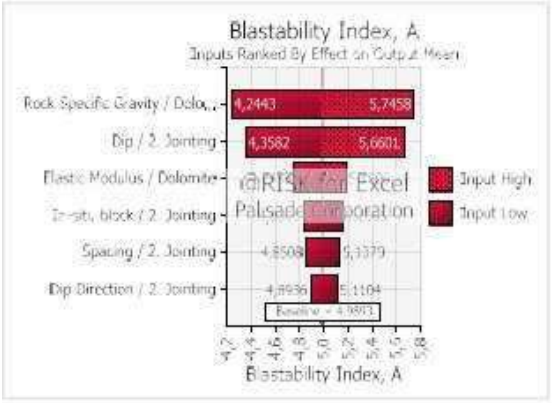

Simulation Summary Information	
Workbook Name	Book1.xlsx
Number of Simulations	1
Number of Iterations	1000
Number of Inputs	24
Number of Outputs	8
Sampling Type	Latin Hypercube
Simulation Start Time	2019/09/04 11:01
Simulation Duration	00:00:02
Random # Generator	Mersenne Twister
Random Seed	810617637

Summary Statistics for Blastability Index, A			
Statistics		Percentile	
Minimum	3,04	5%	3,85
Maximum	6,92	10%	4,05
Mean	4,99	15%	4,16
Std Dev	0,73	20%	4,30
Variance	0,539224821	25%	4,40
Skewness	0,010081258	30%	4,50
Kurtosis	2,171034476	35%	4,61
Median	4,98	40%	4,73
Mode	5,55	45%	4,81
Left X	3,85	50%	4,98
Left P	5%	55%	5,11
Right X	6,16	60%	5,24
Right P	95%	65%	5,37
Diff X	2,31	70%	5,48
Diff P	90%	75%	5,58
#Errors	0	80%	5,70
Filter Min	Off	85%	5,78
Filter Max	Off	90%	5,97
#Filtered	0	95%	6,16

Change in Output Statistic for Blastability In			
Rank	Name	Lower	Upper
1	Rock Specific Gra	4,24	5,75
2	Dip /2. Jointing	4,36	5,66
3	Elastic Modulus /	4,75	5,18
4	In-situ block / 2. J	4,83	5,16
5	Spacing / 2. Joint	4,85	5,14
6	Dip Direction / 2.	4,89	5,11

Figure D 9: South Blastability Index Report

@RISK Output Report for Uniformity Exponent, n B44

Performed By: Lijojo

Date: Wednesday, 04 September 2019 13:09:50

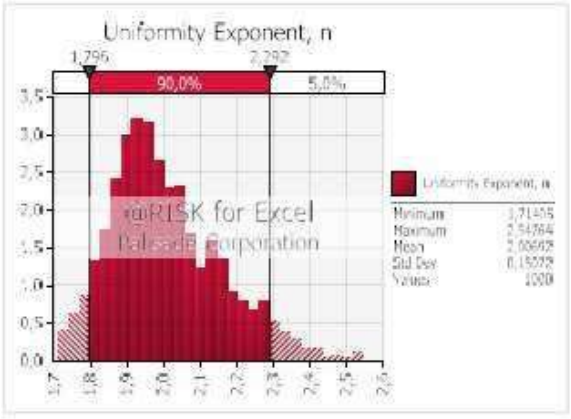



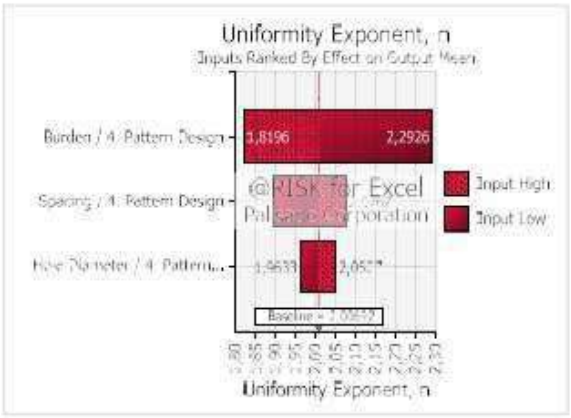

Simulation Summary Information	
Workbook Name	Book1.xlsx
Number of Simulations	1
Number of Iterations	1000
Number of Inputs	24
Number of Outputs	8
Sampling Type	Latin Hypercube
Simulation Start Time	2019/09/04 11:01
Simulation Duration	00:00:02
Random # Generator	Mersenne Twister
Random Seed	810617637

Summary Statistics for Uniformity Exponent			
Statistics		Percentile	
Minimum	1,71	5%	1,80
Maximum	2,55	10%	1,83
Mean	2,01	15%	1,86
Std Dev	0,15	20%	1,88
Variance	0,022715149	25%	1,90
Skewness	0,698228312	30%	1,92
Kurtosis	3,264743569	35%	1,93
Median	1,98	40%	1,95
Mode	1,93	45%	1,96
Left X	1,80	50%	1,98
Left P	5%	55%	2,00
Right X	2,29	60%	2,02
Right P	95%	65%	2,04
Diff X	0,50	70%	2,07
Diff P	90%	75%	2,10
#Errors	0	80%	2,13
Filter Min	Off	85%	2,17
Filter Max	Off	90%	2,22
#Filtered	0	95%	2,29

Change in Output Statistic for Uniformity Ex			
Rank	Name	Lower	Upper
1	Burden / 4. Patter	1,82	2,29
2	Spacing / 4. Patte	1,90	2,08
3	Hole Diameter / 4	1,96	2,05

Figure D 10: South Uniformity Index Report (Pf 0.35 kg/Bcm)

@RISK Output Report for Uniformity Exponent, n B44

Performed By: Lijojo

Date: Wednesday, 04 September 2019 13:10:10

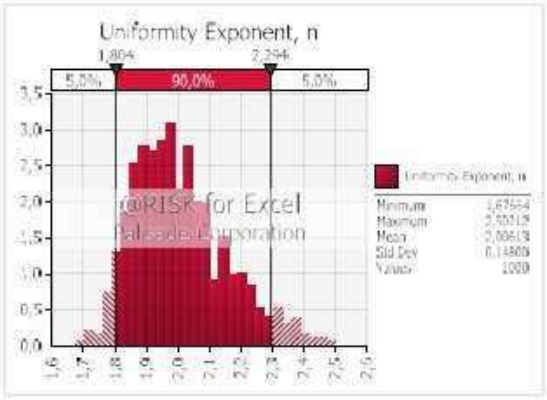

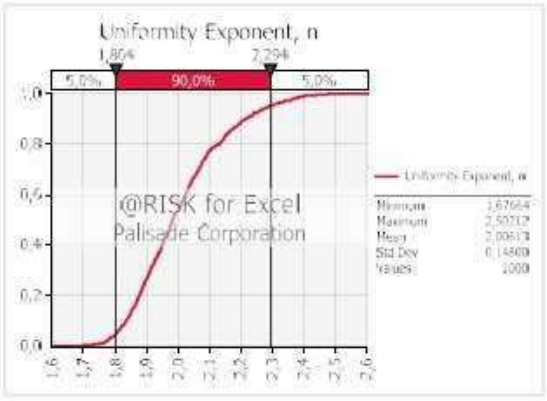

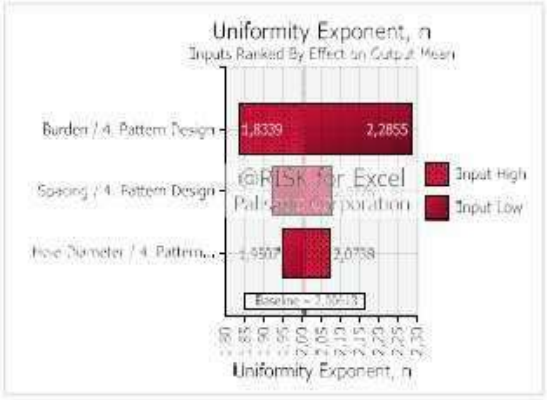

Simulation Summary Information	
Workbook Name	Book1.xlsx
Number of Simulations	1
Number of Iterations	1000
Number of Inputs	24
Number of Outputs	8
Sampling Type	Latin Hypercube
Simulation Start Time	2019/09/04 11:01
Simulation Duration	00:00:02
Random # Generator	Mersenne Twister
Random Seed	810617637

Summary Statistics for Uniformity Exponent			
Statistics		Percentile	
Minimum	1,68	5%	1,80
Maximum	2,50	10%	1,83
Mean	2,01	15%	1,86
Std Dev	0,15	20%	1,88
Variance	0,021904948	25%	1,89
Skewness	0,873325315	30%	1,91
Kurtosis	3,128990963	35%	1,93
Median	1,98	40%	1,95
Mode	1,98	45%	1,97
Left X	1,80	50%	1,98
Left P	5%	55%	2,00
Right X	2,29	60%	2,02
Right P	95%	65%	2,04
Diff X	0,49	70%	2,07
Diff P	90%	75%	2,09
#Errors	0	80%	2,13
Filter Min	Off	85%	2,17
Filter Max	Off	90%	2,21
#Filtered	0	95%	2,29

Change in Output Statistic for Uniformity Ex			
Rank	Name	Lower	Upper
1	Burden / 4. Patter	1,83	2,29
2	Spacing / 4. Patte	1,92	2,08
3	Hole Diameter / 4	1,95	2,07

Figure D 11: South Uniformity Index Report (Pf 0.65 kg/Bcm)

@RISK Output Report for Average Size of Material, X50 B43

Performed By: Lijojo

Date: Wednesday, 04 September 2019 13:09:46

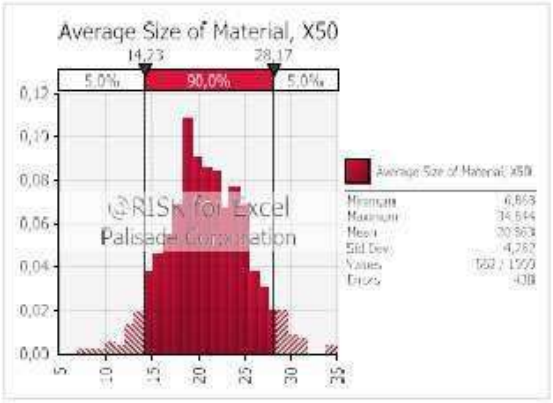

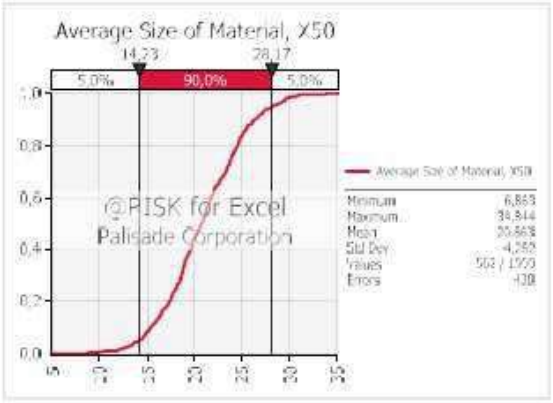



Simulation Summary Information	
Workbook Name	Book1.xlsx
Number of Simulations	1
Number of Iterations	1000
Number of Inputs	24
Number of Outputs	8
Sampling Type	Latin Hypercube
Simulation Start Time	2019/09/04 11:01
Simulation Duration	00:00:02
Random # Generator	Mersenne Twister
Random Seed	810617637

Summary Statistics for Average Size of Mate			
Statistics		Percentile	
Minimum	7	5%	14
Maximum	35	10%	15
Mean	21	15%	16
Std Dev	4	20%	17
Variance	18,33553015	25%	18
Skewness	0,081153228	30%	19
Kurtosis	3,011381201	35%	19
Median	21	40%	20
Mode	22	45%	20
Left X	14	50%	21
Left P	5%	55%	21
Right X	28	60%	22
Right P	95%	65%	22
Diff X	14	70%	23
Diff P	90%	75%	24
#Errors	438	80%	25
Filter Min	Off	85%	25
Filter Max	Off	90%	26
#Filtered	0	95%	28

Change in Output Statistic for Average Size			
Rank	Name	Lower	Upper
1	Dip /2. Jointing	18	24
2	Explosive Strengt	18	23
3	Rock Specific Gra	18	23
4	Stemming length	18	23
5	Elastic Modulus /	19	22
6	Burden /4. Patter	20	22
7	In-situ block /2. J	20	22
8	Hole Diameter /4	20	22
9	Dip Direction /2.	20	22
10	Spacing /2. Joint	20	21

Figure D 12: South Mean Fragment Size Report (Pf 0.35 kg/Bcm)

@RISK Output Report for Average Size of Material, X50 B43

Performed By: Lijojo

Date: Wednesday, 04 September 2019 13:10:06

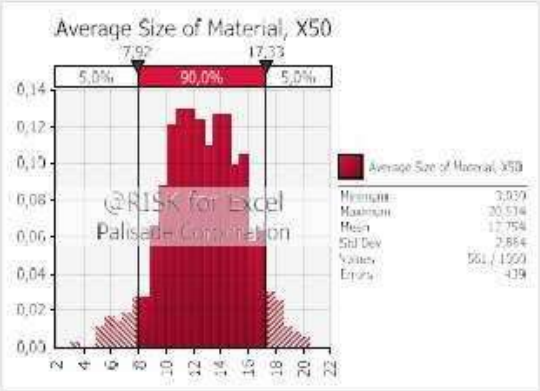

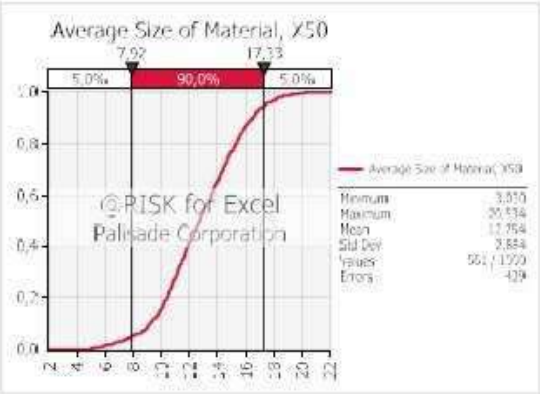

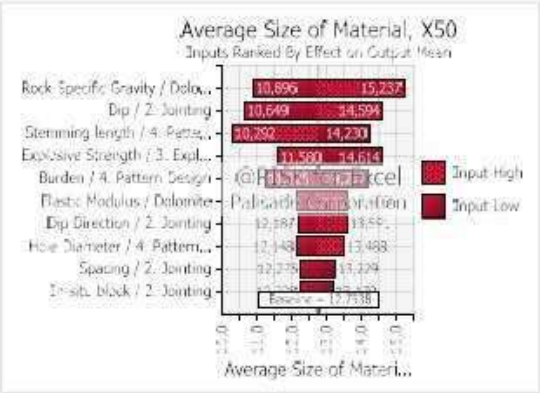

Simulation Summary Information	
Workbook Name	Book1.xlsx
Number of Simulations	1
Number of Iterations	1000
Number of Inputs	24
Number of Outputs	8
Sampling Type	Latin Hypercube
Simulation Start Time	2019/09/04 11:01
Simulation Duration	00:00:02
Random # Generator	Mersenne Twister
Random Seed	810617637

Summary Statistics for Average Size of Mate			
Statistics		Percentile	
Minimum	3	5%	8
Maximum	21	10%	9
Mean	13	15%	10
Std Dev	3	20%	10
Variance	8,317632234	25%	11
Skewness	-0,109578875	30%	11
Kurtosis	2,914440788	35%	12
Median	13	40%	12
Mode	13	45%	12
Left X	8	50%	13
Left P	5%	55%	13
Right X	17	60%	14
Right P	95%	65%	14
Diff X	9	70%	14
Diff P	90%	75%	15
#Errors	439	80%	15
Filter Min	Off	85%	16
Filter Max	Off	90%	16
#Filtered	0	95%	17

Change in Output Statistic for Average Size			
Rank	Name	Lower	Upper
1	Rock Specific Gra	11	15
2	Dip /2. Jointing	11	15
3	Stemming length	10	14
4	Explosive Strengt	12	15
5	Burden /4. Patter	11	14
6	Elastic Modulus /	12	14
7	Dip Direction /2.	12	14
8	Hole Diameter /4	12	13
9	Spacing /2. Joint	12	13
10	In-situ block /2. J	12	13

Figure D 13: South Mean Fragment Size Report (Pf 0.65 kg/Bcm)



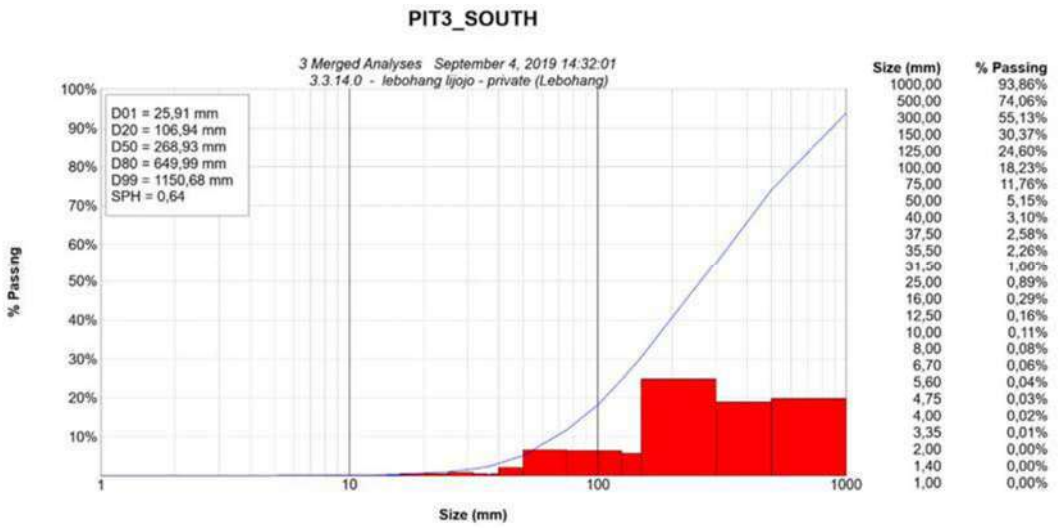

Figure D 14: South Actual Fragment Report (image analysis)

Burden (m)	2,16	2,34	1,83	2,33	1,95	2,73	2,03	2,22	3,25	2,51	2,27	2,76	2,72	2,36	2,57	3,20	1,85	2,29	3,11	3,35
Spacing (m)	2,26	1,87	2,75	2,37	2,18	2,59	2,70	1,91	2,58	2,32	2,91	2,87	2,97	2,07	2,81	2,44	1,65	2,47	2,83	1,82
Stemming (m)	1,24	1,89	2,86	1,19	2,25	1,49	1,95	1,05	1,35	1,67	1,65	1,27	1,70	1,74	1,43	1,33	2,93	1,97	1,19	1,54
Powder factor 9kg/Bcm)	0,50	0,56	0,57	0,58	0,58	0,59	0,59	0,60	0,60	0,60	0,60	0,60	0,64	0,65	0,65	0,68	0,70	0,70	0,71	0,72
N	2,05	1,91	2,30	1,98	2,12	1,94	2,20	1,92	1,79	1,98	2,10	1,97	2,02	1,93	2,01	1,81	2,00	2,07	1,85	1,63
Xc (m)	0,33	0,26	0,18	0,30	0,29	0,25	0,27	0,33	0,24	0,25	0,28	0,27	0,25	0,26	0,28	0,24	0,16	0,27	0,23	0,19
Size (m)	Sim 1	Sim 2	sim 3	sim4	sim5	sim6	sim7	sim8	sim9	sim10	sim11	sim12	sim13	sim14	sim15	sim16	sim17	sim18	sim19	sim20
0,00	0%	0%	0%	0%	0%	0%	0%	0%	0%	0%	0%	0%	0%	0%	0%	0%	0%	0%	0%	0%
0,05	2%	4%	5%	3%	2%	4%	2%	3%	6%	4%	3%	3%	4%	4%	3%	6%	9%	3%	6%	11%
0,10	8%	15%	22%	11%	10%	16%	11%	9%	19%	15%	11%	13%	14%	14%	12%	19%	32%	12%	20%	30%
0,15	18%	30%	47%	23%	22%	31%	24%	19%	35%	31%	23%	27%	30%	29%	24%	36%	59%	25%	37%	49%
0,20	30%	46%	70%	37%	37%	48%	41%	31%	51%	48%	39%	42%	47%	44%	39%	52%	79%	41%	55%	66%
0,25	44%	61%	87%	51%	52%	64%	58%	44%	65%	64%	54%	57%	63%	59%	54%	67%	91%	57%	70%	79%
0,30	56%	74%	95%	64%	66%	76%	72%	56%	77%	77%	68%	70%	76%	72%	68%	79%	97%	71%	81%	88%
0,35	68%	83%	99%	75%	77%	86%	84%	67%	86%	86%	79%	81%	86%	82%	78%	87%	99%	81%	89%	93%
0,40	78%	90%	100%	84%	86%	92%	91%	76%	91%	93%	88%	88%	92%	89%	87%	93%	100%	89%	94%	97%
0,45	85%	95%	100%	90%	92%	96%	96%	83%	95%	96%	93%	93%	96%	94%	92%	96%	100%	94%	97%	98%
0,50	91%	97%	100%	94%	96%	98%	98%	89%	97%	98%	96%	96%	98%	97%	96%	98%	100%	97%	99%	99%
0,55	94%	99%	100%	97%	98%	99%	99%	93%	99%	99%	98%	98%	99%	98%	98%	99%	100%	99%	99%	100%
0,60	97%	99%	100%	98%	99%	100%	100%	95%	99%	100%	99%	99%	100%	99%	99%	100%	100%	99%	100%	100%
0,65	98%	100%	100%	99%	100%	100%	100%	97%	100%	100%	100%	100%	100%	100%	100%	100%	100%	100%	100%	100%
0,70	99%	100%	100%	100%	100%	100%	100%	98%	100%	100%	100%	100%	100%	100%	100%	100%	100%	100%	100%	100%
0,75	100%	100%	100%	100%	100%	100%	100%	99%	100%	100%	100%	100%	100%	100%	100%	100%	100%	100%	100%	100%
0,80	100%	100%	100%	100%	100%	100%	100%	100%	100%	100%	100%	100%	100%	100%	100%	100%	100%	100%	100%	100%
0,85	100%	100%	100%	100%	100%	100%	100%	100%	100%	100%	100%	100%	100%	100%	100%	100%	100%	100%	100%	100%
0,90	100%	100%	100%	100%	100%	100%	100%	100%	100%	100%	100%	100%	100%	100%	100%	100%	100%	100%	100%	100%
0,95	100%	100%	100%	100%	100%	100%	100%	100%	100%	100%	100%	100%	100%	100%	100%	100%	100%	100%	100%	100%
1,00	100%	100%	100%	100%	100%	100%	100%	100%	100%	100%	100%	100%	100%	100%	100%	100%	100%	100%	100%	100%
1,05	100%	100%	100%	100%	100%	100%	100%	100%	100%	100%	100%	100%	100%	100%	100%	100%	100%	100%	100%	100%
1,10	100%	100%	100%	100%	100%	100%	100%	100%	100%	100%	100%	100%	100%	100%	100%	100%	100%	100%	100%	100%
1,15	100%	100%	100%	100%	100%	100%	100%	100%	100%	100%	100%	100%	100%	100%	100%	100%	100%	100%	100%	100%
1,20	100%	100%	100%	100%	100%	100%	100%	100%	100%	100%	100%	100%	100%	100%	100%	100%	100%	100%	100%	100%

Appendix D15: South-East blast simulation results (PF=0.65kg/Bcm)

Burden (m)	2,04	1,68	1,99	1,98	1,80	1,64	1,90	2,07	2,40	2,32	2,08	2,23	2,20	2,02	2,10	2,30	2,16	1,91	2,11	1,53	2,10
Spacing (m)	2,05	1,72	1,93	1,75	1,87	1,97	1,71	2,30	2,26	2,28	2,14	2,05	2,18	1,64	2,00	1,85	1,97	2,25	2,03	1,65	1,96
Stemming (m)	1,03	1,39	1,59	1,27	1,27	1,36	1,52	1,44	1,13	1,66	1,92	1,86	1,66	2,42	2,14	2,06	2,37	2,71	2,55	3,51	2,59
Powder factor (kg/Bcm)	0,30	0,30	0,30	0,30	0,30	0,30	0,30	0,30	0,30	0,30	0,30	0,30	0,30	0,30	0,30	0,30	0,30	0,30	0,30	0,30	0,30
N	0,85	0,97	1,27	0,99	0,94	0,96	1,15	1,24	1,07	1,54	1,63	1,63	1,47	1,89	1,80	1,80	2,02	2,20	2,16	2,26	2,08
Xc	0,73	0,66	0,63	0,63	0,62	0,61	0,60	0,55	0,50	0,48	0,45	0,45	0,42	0,40	0,40	0,38	0,35	0,31	0,29	0,26	0,34
Size (m)	sim1	sim2	sim6	sim7	sim8	sim9	sim10	sim21	sim44	sim51	sim59	sim60	sim65	sim71	sim72	sim75	sim80	sim81	sim82	sim84	sim85
0,00	0%	0%	0%	0%	0%	0%	0%	0%	0%	0%	0%	0%	0%	0%	0%	0%	0%	0%	0%	0%	0%
0,05	10%	8%	4%	8%	9%	9%	6%	5%	8%	3%	3%	3%	4%	2%	2%	3%	2%	2%	2%	2%	2%
0,10	17%	15%	9%	15%	16%	16%	12%	11%	16%	9%	8%	8%	11%	7%	8%	9%	8%	8%	10%	11%	8%
0,15	23%	21%	15%	22%	23%	23%	18%	18%	24%	15%	15%	15%	20%	14%	16%	17%	17%	18%	22%	25%	17%
0,20	28%	27%	21%	28%	29%	29%	25%	25%	31%	23%	23%	23%	28%	23%	25%	27%	28%	32%	37%	42%	29%
0,25	33%	32%	27%	33%	35%	35%	31%	31%	38%	31%	32%	32%	37%	33%	34%	38%	40%	46%	53%	60%	42%
0,30	37%	37%	32%	38%	40%	40%	36%	37%	44%	39%	40%	40%	45%	43%	44%	49%	53%	60%	67%	75%	55%
0,35	41%	42%	38%	43%	44%	45%	42%	43%	49%	46%	48%	49%	53%	53%	54%	58%	64%	73%	79%	86%	66%
0,40	45%	46%	43%	47%	49%	49%	47%	49%	54%	53%	56%	56%	60%	62%	63%	67%	74%	83%	87%	93%	76%
0,45	48%	50%	48%	51%	52%	53%	51%	54%	59%	60%	63%	63%	67%	71%	70%	75%	82%	90%	93%	97%	84%
0,50	51%	53%	52%	55%	56%	56%	56%	59%	63%	66%	69%	70%	72%	78%	77%	81%	88%	94%	96%	99%	90%
0,55	54%	57%	57%	59%	59%	60%	59%	63%	67%	71%	75%	75%	77%	83%	82%	86%	92%	97%	98%	100%	94%
0,60	57%	60%	61%	62%	62%	63%	63%	67%	70%	76%	80%	80%	81%	88%	87%	90%	95%	99%	99%	100%	96%
0,65	59%	62%	65%	65%	65%	66%	67%	71%	73%	80%	84%	84%	85%	91%	90%	93%	97%	99%	100%	100%	98%
0,70	62%	65%	68%	67%	68%	68%	70%	74%	76%	83%	87%	87%	88%	94%	93%	95%	98%	100%	100%	100%	99%
0,75	64%	68%	71%	70%	70%	71%	72%	77%	78%	86%	90%	90%	90%	96%	95%	97%	99%	100%	100%	100%	99%
0,80	66%	70%	74%	72%	72%	73%	75%	79%	81%	89%	92%	92%	92%	97%	97%	98%	100%	100%	100%	100%	100%
0,85	68%	72%	77%	74%	74%	75%	77%	82%	83%	91%	94%	94%	94%	98%	98%	99%	100%	100%	100%	100%	100%
0,90	70%	74%	79%	76%	76%	77%	80%	84%	84%	93%	95%	96%	95%	99%	99%	99%	100%	100%	100%	100%	100%
0,95	71%	76%	81%	78%	78%	79%	82%	86%	86%	94%	96%	97%	96%	99%	99%	100%	100%	100%	100%	100%	100%
1,00	73%	77%	83%	80%	79%	80%	83%	88%	88%	95%	97%	98%	97%	100%	99%	100%	100%	100%	100%	100%	100%
1,05	74%	79%	85%	81%	81%	82%	85%	89%	89%	96%	98%	98%	98%	100%	100%	100%	100%	100%	100%	100%	100%
1,10	76%	80%	87%	83%	82%	83%	86%	90%	90%	97%	99%	99%	98%	100%	100%	100%	100%	100%	100%	100%	100%

Appendix D16: South-West blast simulation results (PF=0.30kg/Bcm)

Burden (m)	2,50	2,50	2,50	2,50	2,50	2,50	2,50	2,50	2,50	2,50	2,50	2,50	2,50	2,50	2,50	2,50	2,50	2,50	2,50	2,50
Spacing (m)	2,50	2,50	2,50	2,50	2,50	2,50	2,50	2,50	2,50	2,50	2,50	2,50	2,50	2,50	2,50	2,50	2,50	2,50	2,50	2,50
Stemming (m)	1,46	1,02	1,35	1,32	1,42	1,60	1,75	1,66	1,54	1,26	1,69	1,28	1,94	1,88	1,97	1,56	2,07	2,06	2,15	2,19
Powder factor (kg/Bcm	0,28	0,32	0,29	0,36	0,35	0,37	0,31	0,29	0,38	0,36	0,34	0,39	0,41	0,38	0,37	0,33	0,28	0,36	0,36	0,40
N	1,45	1,02	1,34	1,31	1,41	1,59	1,74	1,66	1,53	1,26	1,68	1,28	1,93	1,87	1,96	1,56	2,06	2,05	2,14	2,18
Xc	0,45	0,39	0,38	0,37	0,35	0,33	0,32	0,29	0,28	0,26	0,24	0,23	0,22	0,20	0,19	0,17	0,16	0,16	0,15	0,13
Size (m)	sim1	sim2	sim3	sim4	sim6	sim13	sim15	sim24	sim25	sim36	sim43	sim44	sim46	sim50	sim52	sim53	sim58	sim59	sim60	sim62
0,00	0%	0%	0%	0%	0%	0%	0%	0%	0%	0%	0%	0%	0%	0%	0%	0%	0%	0%	0%	0%
0,05	4%	12%	6%	7%	6%	5%	4%	5%	7%	12%	7%	14%	6%	7%	7%	13%	9%	9%	9%	12%
0,10	11%	22%	15%	17%	16%	14%	12%	16%	18%	26%	21%	30%	19%	24%	25%	35%	31%	33%	33%	43%
0,15	18%	32%	25%	26%	26%	25%	23%	29%	32%	40%	37%	45%	38%	44%	46%	55%	58%	60%	61%	75%
0,20	26%	40%	34%	36%	37%	37%	35%	42%	45%	52%	53%	58%	56%	63%	66%	71%	79%	81%	82%	92%
0,25	34%	47%	43%	45%	46%	48%	47%	54%	56%	62%	66%	68%	72%	77%	82%	83%	92%	93%	94%	99%
0,30	42%	54%	51%	53%	55%	59%	59%	66%	67%	70%	77%	76%	84%	88%	91%	90%	97%	98%	98%	100%
0,35	50%	59%	59%	61%	63%	68%	68%	75%	75%	77%	85%	83%	91%	94%	96%	95%	99%	99%	100%	100%
0,40	57%	64%	65%	67%	70%	75%	77%	82%	82%	82%	91%	87%	96%	97%	99%	97%	100%	100%	100%	100%
0,45	63%	69%	71%	73%	76%	81%	83%	88%	87%	87%	95%	91%	98%	99%	100%	99%	100%	100%	100%	100%
0,50	68%	73%	76%	78%	81%	86%	88%	92%	91%	90%	97%	94%	99%	100%	100%	99%	100%	100%	100%	100%
0,55	73%	76%	80%	82%	85%	90%	92%	95%	94%	93%	98%	96%	100%	100%	100%	100%	100%	100%	100%	100%
0,60	78%	79%	84%	85%	88%	93%	95%	97%	96%	95%	99%	97%	100%	100%	100%	100%	100%	100%	100%	100%
0,65	81%	82%	87%	88%	91%	95%	97%	98%	97%	96%	100%	98%	100%	100%	100%	100%	100%	100%	100%	100%
0,70	85%	84%	89%	90%	93%	97%	98%	99%	98%	97%	100%	99%	100%	100%	100%	100%	100%	100%	100%	100%
0,75	87%	86%	91%	92%	95%	98%	99%	99%	99%	98%	100%	99%	100%	100%	100%	100%	100%	100%	100%	100%
0,80	90%	88%	93%	94%	96%	99%	99%	100%	99%	98%	100%	99%	100%	100%	100%	100%	100%	100%	100%	100%
0,85	92%	89%	94%	95%	97%	99%	100%	100%	100%	99%	100%	100%	100%	100%	100%	100%	100%	100%	100%	100%
0,90	93%	90%	96%	96%	98%	99%	100%	100%	100%	99%	100%	100%	100%	100%	100%	100%	100%	100%	100%	100%
0,95	95%	92%	97%	97%	98%	100%	100%	100%	100%	99%	100%	100%	100%	100%	100%	100%	100%	100%	100%	100%
1,00	96%	93%	97%	98%	99%	100%	100%	100%	100%	100%	100%	100%	100%	100%	100%	100%	100%	100%	100%	100%
1,05	97%	94%	98%	98%	99%	100%	100%	100%	100%	100%	100%	100%	100%	100%	100%	100%	100%	100%	100%	100%
1,10	97%	94%	98%	99%	99%	100%	100%	100%	100%	100%	100%	100%	100%	100%	100%	100%	100%	100%	100%	100%

Appendix D17: South blast simulation results (PF=0.35kg/Bcm)